Temporal and Spatial Variability of Transport and Mixing Mechanisms Using Heat and Salt in the Duplin River, Georgia

by

James Paul McKay

(Under the direction of Daniela Di Iorio)

Abstract

A study of the Duplin River, a shallow, sinuous, tidal creek which connects the salt marshes of Sapelo Island, on the central Georgia coast, with the waters of Doboy Sound and the coastal Atlantic Ocean, was conducted to quantify the physical processes which regulate the flux and zonation of heat and salt throughout the creek system.

Three water masses are identified with differing temperature and salinity regimes. Hourly scale heat budgets are constructed for the upper (warmer) and lower (cooler) areas of the Duplin River showing the diminishing importance of tidal advection away from the mouth of the creek along with the concomitant increase in the importance of both direct atmospheric fluxes and of interactions with the marsh and side creeks. The heat budget is re-examined on daily averaged scales revealing the decreased importance of advective fluxes relative to direct atmospheric fluxes on this scale but the constant importance of marsh/creek interactions regardless of time scale or season.

Tidally averaged along channel salt fluxes are calculated and a contrast is drawn between the lower and the upper Duplin. The main channel of the lower Duplin is bordered by creekless marsh, marsh hammocks and hard upland and salt fluxes are largely constrained to the main channel with salinity in the lower Duplin closely tracking observed salt fluxes. The upper Duplin is isolated from the lower Duplin by a sinuous channel and is subject to significant local fresh groundwater input. The upper Duplin acts as a reversing estuary on a fortnightly time scale. Salt fluxes are not constrained to the main channel but show a significant influence of the marsh.

Vertical mixing is shown to be modulated on both M4 and fortnightly frequencies with turbulent stresses being generated near the bed and propagating into the water column on periods of max flood and ebb and being significantly greater on spring tide than on neap. Horizontal mixing is driven by tidal dispersion, which is modulated by the fortnightly spring/neap cycle. Net export of salt from the lower Duplin is shown to be due to residual advection modified by upstream tidal pumping which, in the absence of external forcing, exhibits a pulsating character with net export taking place for a short period on spring tide followed by a longer period of net import of salt.

A box model is developed to explore subtidal inputs of groundwater and salt into the three water masses of the Duplin River. The results of this model are examined to draw insights into the magnitude and spatial distribution of these processes and their effect on the Duplin River water masses.

Index words: estuary, salt marsh, tidal creek, tides, heat budget, salt flux, reversing estuary, groundwater, vertical mixing, turbulence, dispersion, tidal pumping, Kx, Kz, marsh-creek interaction, box model, Duplin River, Sapelo Island, Georgia, U.S.

Temporal and Spatial Variability of Transport and Mixing Mechanisms Using Heat and Salt in the Duplin River, Georgia

by

James Paul McKay

B.A.E., Georgia Institute of Technology, 1994

M.S., North Carolina State University, 1996

A Dissertation Submitted to the Graduate Faculty

of The University of Georgia in Partial Fulfillment

of the

Requirements for the Degree

Doctor of Philosophy

Athens, Georgia

2008

Temporal and Spatial Variability of Transport and Mixing Mechanisms Using Heat and Salt in the Duplin River, Georgia

by

James Paul McKay

Approved:

Major Professor: Daniela Di Iorio

Committee: Jackson O. Blanton
Adrian B. Burd
Christof Meile
David E. Stooksbury

Electronic Version Approved:

Maureen Grasso
Dean of the Graduate School
The University of Georgia
August 2008

Dedication

This dissertation is dedicated to my mother, Beverly Jane McKay, whose love of nature and of the ocean has served as a continuing inspiration. Rest in Peace.

And the sea lends large, as the marsh: lo, out of his plenty the sea
Pours fast: full soon the time of the flood tide must be:
Look how the grace of the sea doth go
About and about through the intricate channels that flow
Here and there,
Everywhere,
Till his waters have flooded the uttermost creeks and the low-lying lanes,
And the marsh is meshed with a million veins,
That like as with rosy and silvery essences flow
In the rose-and-silver evening glow.
Farewell, my lord Sun!
The creeks overflow: a thousand rivulets run
'Twixt the roots of the sod; the blades of the marsh-grass stir;
Passeth a hurrying sound of wings that westward whirr;
Passeth, and all is still; and the currents cease to run;
And the sea and the marsh are one.

— Sidney Lanier, 'The Marshes of Glynn' (lines 79–94)

Acknowledgments

I owe a great deal of thanks to my adviser, colleague and friend Daniela Di Iorio for accepting me into her lab and providing the right mix of guidance and freedom to allow me to pursue this goal of mine despite my numerous outside commitments. Not many professors would have been so accommodating or encouraging and I can not imagine having found a better mentor, adviser, teacher or friend.

Thanks also go to Jack Blanton for his insightful comments and questions and for his central role in initiating the Duplin River study. I would like to thank Adrian Burd for agreeing to sit on my committee at the last moment and for his comments, which have greatly improved this manuscript. I owe thanks to Christof Meile who played an invaluable role in my education as an oceanographer by making me realize that it is not enough to understand the physics of how things move in tidal creeks if you do not also understand what is being moved and why it is important. And thanks go to David Stooksbury for his insight into the parallels between oceanography and meteorology, especially in shallow water coastal systems.

This work would not have been possible without the efforts of the captain and crew of the R/V Savannah (Captain Raymond Sweatte, First Mate Michael Richter, Second Mate Todd Recicar, Engineer Raymond Thomas and Marine Technician Bryan Lincoln) and of Julie Amft and Trent Moore of the Skidaway Institute of Oceanography. Special thanks go to Ken Helm, recently of the University of Georgia Marine Institute, for his assistance during many long days on the water and our always interesting conversations.

I appreciate all of my friends and colleagues in the department including Marcia Hsu, Matt Erickson, Kate Doyle, KiRyong Kang, Lisa Pfau, Erin Jane Biers and Justin Hartman.

I would like to thank John Knox for our many conversations and for his ready willingness to lend a hand whenever asked.

Finally I owe my utmost thanks to my friends and family who have provided support and encouragement despite my frequent neglect of them over the past five years. Special thanks go to my wife Jennifer, who is both my friend and my family, who has accepted being a Ph.D. widow so that I could pursue this goal.

This work was supported by the NSF (OCE-9982133 and 0670959) as part of the Georgia Coastal Ecosystems - Long Term Ecological Research (GCE-LTER) project with Tim Hollibaugh and Meryl Alber as Principal Investigators).

Table of Contents

List of Figures

Chapter 1

Introduction and Literature Review

1.1 Salt Marsh Tidal Creeks

Intertidal salt marshes are among the most productive and economically valuable ecosystems on the planet (Reimold et al., 1975). Through their regular flooding and draining by the tides they interact with the coastal ocean to serve as both a source and a sink of sediment, capturing sediment from the mainland to build the marsh and exporting sediment to build barrier islands and offshore deposits (Childers and Day, 1990a; Cavatorta et al., 2003). They serve both to fix inorganic carbon from the atmosphere and to export inorganic and organic carbon to the atmosphere and ocean (Wolaver and Spurrier, 1988; Cai et al., 2003; Wang and Cai, 2004). They sequester inorganic nutrients such as nitrogen and phosphorus in their sediment and export organic nutrients, derived from the marsh vegetation, to the coastal ocean (Childers and Day, 1990b; Teal and Howes, 2002). By absorbing tidal energy they serve as a vital barrier to dissipate storm surge and protect coastal structures (Moeller et al., 2001).

The primary linkage between the salt marsh and the coastal ocean occurs through the network of tidal creeks, which cut through the marsh and provide a direct conduit to the neighboring sounds and to the coastal ocean. These creeks provide ideal habitat for many species of fish, shellfish, crabs, shrimp and other organisms during some or all of their life (Boesch and Turner, 1984; Minello et al., 2003). The quality of these creeks as habitat is strongly regulated by the physical properties of the water, especially the distribution and variability of temperature and salinity, and by the rate at which nutrients and larvae are mixed, dispersed and advected through the system and exported to the coastal ocean.

The role of seasonal and annual scale temperature variation in regulating the biological productivity of salt marsh creeks has long been recognized (see, for example, Pomeroy, 1959; Vernberg, 1993), however recent work has begun to explore the role of smaller, short period temperature variation in regulating biological productivity and activity. Perez-Domingues and Holt (2001) have described how the relative magnitude of small diurnal temperature fluctuations in seagrass beds, on the order of $\pm$ 1–3 °C, affects the hardiness and survival rate of red drum fish larvae while Newman et al. (2006) showed how similar fluctuations affect the growth and development rate of South African prawn larvae. Both Jorgensen (1990) and Bernard et al. (1988) have shown how short term reductions in temperature due to local weather or coastal upwelling can alter the behavior of estuarine filter feeders or even lead to significant mortality for creatures with a short larval period.

Most studies of the temperature cycle in coastal waters have concentrated on the shelf and near shore regions examining them on seasonal or annual time scales (see, for example, Prandle and Lane, 1995; Na et al., 1999; Bignami and Hopkins, 2002; Wilkin, 2006), though recently Kaplan et al. (2003) examined the role of solar and wind forcing in generating large diurnal fluctuations in the temperature off the central and northern coast of Chile.

Several studies have been published describing the temperature cycle and distribution in tidal creeks (see, for example, Ragotzkie and Bryson, 1955; Hackney et al., 1976; Schwing and Kjerfve, 1980; Uncles and Stephens, 2001; Vaz et al., 2005), but most have either been conducted over short periods or else have focused on long term trends. Smith (1983) described both high and low frequency temperature variations in a shallow lagoon during both summer and winter conditions, while Hoguane et al. (1999) described the diurnal and semi-diurnal temperature variability in a mangrove swamp controlled by the interactions between solar heating, tidal advection of heat and bathymetry. Heat budgets, with attempts to reconcile the observed temperature variability with measured atmospheric and tidal heat fluxes, are rare in estuarine waters due to the difficulty of constraining the fluxes through the intertidal areas. Smith (1981) and Smith and Kierspe (1981) observed the heat budget in a shallow estuary on the Texas Gulf coast showing that the difference between latent and sensible heat fluxes closely matched observed changes in heat storage in those waters.

The presence of extensive intertidal marshes and mud flats can greatly affect the temperature cycle in a tidal creek. Thin sheets of water are spread across the marsh at high tide, where heat can be readily exchanged with the atmosphere and sediment, only to return, less water loss to evaporation, on ebb tide. Crabtree and Kjerfve (1978) investigated the radiation balance over a South Carolina marsh vegetated with *Spartina alterniflora* , showing the relation of net and reflected radiation with the amount of vegetation while Heilman et al. (2000) showed the dependence of radiative heat fluxes on the percent inundation of a similar marsh in Texas. Harrison and Phzacklea (1985) showed how the interaction between tidal and solar frequencies causes complex patterns in the storage of heat in an intertidal mud flat in an estuary in Scotland. Vugts and Zimmerman (1985) observed similar patterns in mud flats on the North Sea. Matsunaga and Kodama (2000) showed the importance of transfer between the sediment of a mud flat and the overlying water to the local heat budget and speculated that the large lateral heat gradient across the flat could be a significant term in the heat budget of the adjacent water.

Like temperature, the distribution and variation of salinity within a tidal creek acts to strongly regulate local productivity (Hackney et al., 1976; Underwood et al., 1998; Islam et al., 2006). Given the lack of surface freshwater runoff into most tidal creeks, the distribution of salt within the creek is tied primarily to the input of fresh groundwater, which tends to dilute the salt and, by driving the mean outflow, to export it from the creek, and to the action of the tides which tend to pump salt into the creek (Lewis, 1997; Dyer, 1997). Advective fluxes in the creek channel are due to the residual export of fresh groundwater, which flows into the creek, changes in storage volume, tied to meteorological forcing caused by local and offshore winds, and runoff due to precipitation.

The action of tides in the creek causes a net tidal dispersive flux which was described by Fischer et al. (1979). This dispersive flux is generally decomposed into terms referred to as tidal pumping, tidal trapping and shear dispersion terms. Tidal pumping is the along channel dispersion of salt due to correlations between the tidally varying depth, velocity and salinity in the creek. It generally results in a net influx of salt, which varies strongly with the spring/neap cycle. Tidal trapping refers to the along channel dispersion of salt caused by the temporary diversion of water into small side creeks and embayments, and onto the intertidal marsh areas, on flood, which then mixes back into a potentially dissimilar water mass in the main channel on ebb, causing an effective along channel dispersion of salt. This term is highly variable with tidal height and the spring/neap cycle and can result in either a net influx or outflux of salt. Shear dispersion refers to the net along channel dispersion of salt caused by vertical or lateral shear in the flow acting on a vertical or lateral salinity gradient respectively. This term has components tied to both tidal flows and the residual flows due to the estuarine circulation.

Neglecting tidal trapping, which is highly dependent on bathymetry and thus difficult to calculate, the tidal dispersive terms due to tidal pumping and shear dispersion are generally quantified through a process of decomposition. Building on the work by Taylor (1953) and Taylor (1954), Bowden (1965) was the first to consider the along channel dispersion of salt related to the action of stratification on shear in both the mean and the tidally varying flow. Hansen (1965) proposed a decomposition which expressed the estuarine salt flux in terms of vertical and lateral variability in flow and properties; Fischer (1972) proposed a decomposition which allowed the vertical and lateral shear processes to be separated, but which did not account for tidal variations in depth, which can be important in shallow estuaries with large tidal ranges. Kjerfve (1986) modified the work of Hansen (1965) and Bowden (1965) to account for tidal variations of depth in a shallow estuary.

Measuring these fluxes can be a difficult task. The measurement of the residual advection is complicated when the net discharge is low and unknown, as it generally is in a tidal creek, as it is the result of the small difference between two much larger quantities (flood and ebb tidal velocities) making this measurement particularly sensitive to errors related to instrument bias and placement (Lane et al., 1997; Simpson et al., 2001). Despite the fact that lateral variability can be of the same order of magnitude as vertical variability (Dyer, 1974), most salt flux measurements neglect the lateral terms, out of concern for the logistical problems of sampling for lateral variability, concentrating only on the center channel salt fluxes. This simplification can be justified in areas where a regular channel geometry and small scale reduce the lateral variability in flow and salt. Rattray and Dworski (1980) showed that for many cases, lateral variability is indeed small compared to vertical variability. The presence of secondary flows due to curvature in the channel (Dyer, 1974; Chant, 2002) and density driven flows (Turrell et al., 1996), caused by the uneven distribution of salt due to Coriolis or bathymetric effects, can further complicate issues by introducing localized lateral flows which may be significant to the local salt flux. When these areas of curvature or density gradients occur with a separation distance less than or equal to, the tidal excursion distance, locally enhanced salt fluxes and mixing can occur (Geyer and Signell, 1992).

The classical salt budget techniques are formulated assuming that the estuary is in quasi-steady state and that upstream salt fluxes generally balance downstream export (Dyer, 1997), but this is often not the case as changes in freshwater flushing, storage volume and oceanic forcing can radically alter this balance. Much current interest is focused on understanding salt fluxes in these unsteady estuaries. Bowen and Geyer (2003) have reported that during low outflow conditions in the Hudson River, salt entered the estuary primarily in monthly pulses tied to the apogean neap tide causing the salt content of the lower tidal prism to fluctuate by 10% as the salinity increased rapidly and then recovered. Banas et al. (2004) reported on a highly unsteady estuary in Washington State and derived a modification to the classic estuarine classification scheme of Hansen and Rattray (1965) by introducing an 'unsteadiness' parameter accounting for the highly variable oceanic and river forcing.

When steady state can be assumed, some progress has been made toward crafting a theoretical framework for estimating salt fluxes and tidal dispersion from basic geometry and flow. MacCready (2004) developed a method using a first order ordinary differential equation to describe sectionally averaged salinity distributions in simple estuarine geometries which encompasses and extends the small body of earlier work on estuarine prediction (see Hansen and Rattray, 1965; Chatwin, 1976).

Vertical mixing has long been appreciated as an important control on the flux of dissolved or suspended substances (such as sediment, salt, nutrients and larvae) and fluid properties (such as temperature) through the estuarine environment through its action on stratification (see, for example, Pritchard, 1952, 1954; Hansen and Rattray, 1965). Increased mixing decreases stratification and thus decreases the magnitude of shear dispersion. Unlike on the larger horizontal scales in an estuary, where tidal dispersive forces dominate mixing, on the smaller vertical length scale, where vertical velocity is very low, turbulence, the highly irregular and diffusive small scale fluctuations of the velocity field, is the primary physical driver of vertical mixing (Tennekes and Lumley, 1999).

In a sheared flow, bounded at the bottom by the bed and the top by the atmosphere, turbulence is primarily generated by tidal friction at the bottom boundary. Wind stress on the top boundary, surface stress as water heats and cools due to atmospheric effects, thus changing its buoyancy, and internally generated turbulence caused by shear through the water column are also contributors. This mixing is opposed by stratification, which serves to damp and dissipate the mixing stresses. Where mixing is vigorous, stratification will be low or non-existent, and dissolved substances and fluid properties will mix freely through the water column. Where mixing is low, and stratification is high, these substances and properties will not move as freely through the water column.

In a tidal creek, with its low freshwater input, stratification is mainly due to the interaction of tidal flows with the along channel salinity gradient. This causes an intermittent stratification referred to as strain induced periodic stratification or SIPS (Simpson et al., 1990, 2005). With stress in the water column primarily being generated through bottom boundary friction, except at times near slack water when the lower levels caused by internally generated turbulence dominate (Abraham, 1980), and with stratification often variable between flood and ebb tide, vertical mixing generally shows tidal periodicity. The fortnightly spring/neap cycle, with its attendant modulation of tidal velocities, also exerts a strong control on vertical mixing (see, for example, Peters, 1997; Chant et al., 2002; Simpson et al., 2005; Chant et al., 2007).

It is often difficult to measure turbulent processes due to the wide range of length and time scales they span, from microscopic fluctuations which take fractions of a second, to eddy sizes of greater than a meter with a correspondingly longer time scale (Kantha and Clayson, 2000). With the development of four beam, high frequency acoustic Doppler current profilers in the 1990s, it became possible to expand upon the work of Lohrman et al. (1990), who used a single beam pulse-to-pulse coherent SONAR to measure turbulent fluctuations, and techniques were developed to estimate the vertical profile of the Reynolds stress, $\tau_x/\rho = -\langle u'w' \rangle$, throughout the water column (see, for example, Stacey et al., 1999; Lu and Lueck, 1999). Since then, many studies of estuarine and shallow water ocean turbulence have been undertaken with an aim of understanding the relationship between tidal and spring/neap forcing on vertical mixing, stratification and horizontal transport in shallow coastal waters (see, for example, Lueck et al., 1997; Stacey et al., 1998; Rippeth et al., 2002, 2003; Simpson et al., 2005)

1.2 The Georgia Coast and the Duplin River study area

The Georgia coast is characterized by shallow continental shelf waters bordered by a collection of barrier islands (see Figure 1.1). A network of sounds, creeks and the Intracoastal Waterway interlace the coast, allowing water to circulate between the various river systems, which supply the coast with freshwater outflow. Connecting the islands to the mainland are intertidal salt marshes, which are drained by a network of tidal creeks of varying sizes, from hundreds of meters across to less than one meter.

The study site chosen for this research is a small tidal creek in the marsh on Sapelo Island, on the central Georgia coast, known as the Duplin River. Running, as it does, through the marshes of the Sapelo Island National Estuarine Research Reserve (SINERR), and bordering the University of Georgia Marine Institute (UGAMI), the Duplin has been reported on many times over the years (see, for example, Ragotzkie and Bryson, 1955; Kjerfve, 1973; Imberger et al., 1983).

The Duplin winds through extensive intertidal marshes, composed mainly of mud flats vegetated primarily with *Spartina alterniflora* and drained by a complex dendritic network of side creeks and channels of varying sizes. The main channel of the Duplin River runs

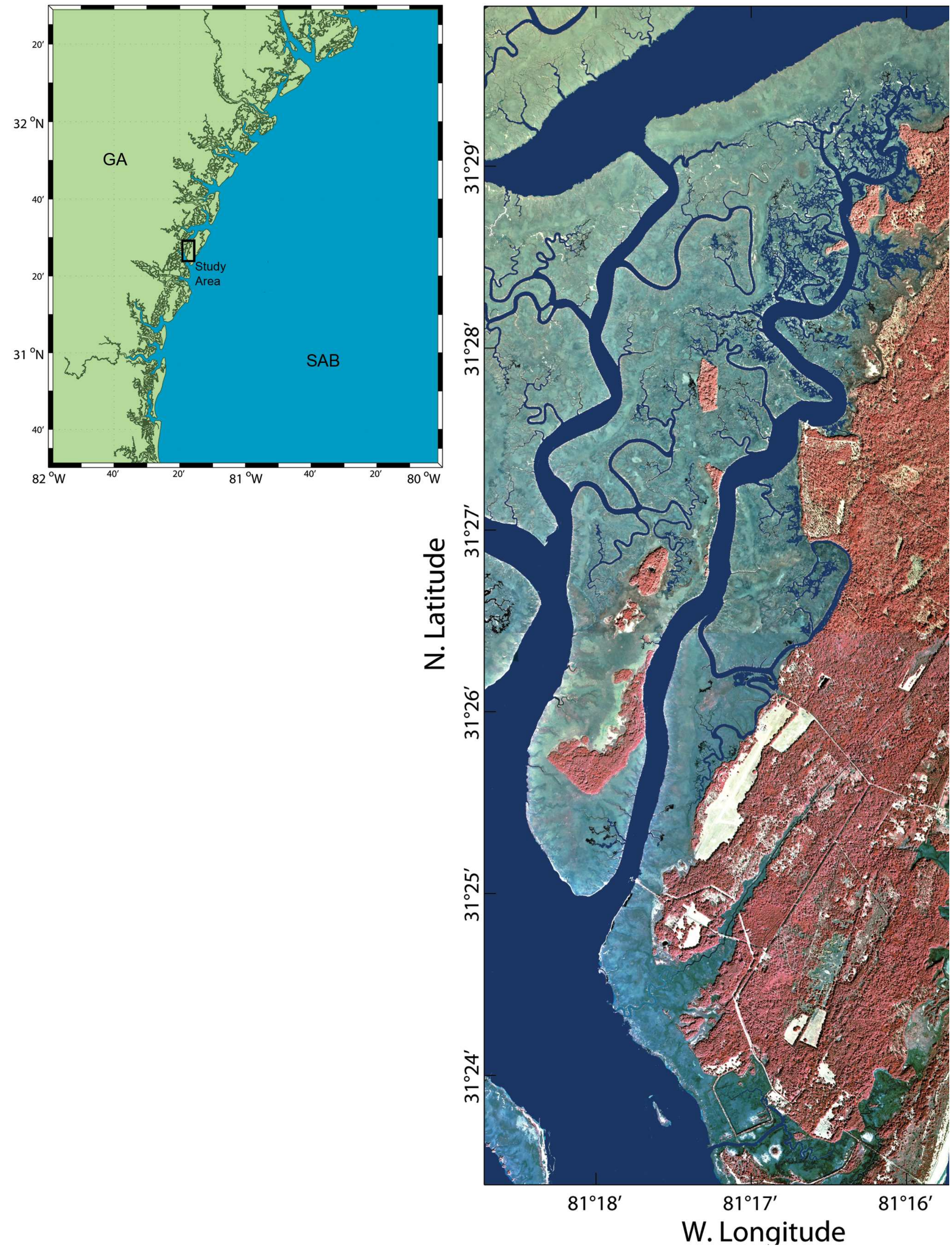

Figure 1.1: A map of the Georgia coast with the Duplin River study area highlighted as an infrared photograph.

approximately 13 km from its mouth at the connection with Doboy Sound to its head in the marsh. Based on the measured tidal excursion in the lower Duplin of approximately 4 km, it is believed to have three tidal prisms (Ragotzkie and Bryson, 1955).

The mean depth along the thalweg is approximately 6.5 meters though there are several deeper holes in regions of curvature or near large side creeks. Tides are predominantly semi-diurnal and vary from 1 to 3 m on neap and spring tide respectively. Figure 1.2 shows bottom bathymetry measured by the R/V Gannet's echosounder as it traversed the creek during the flooding tide so as to gain access to the major creek channels. Tidal flows exhibit the ebb dominance of velocity which is a common characteristic of this class of salt marsh estuary (Dronkers, 1986; Dyer, 1997; Blanton et al., 2002), which is due to interactions between the main channel and the intertidal areas causing frictional distortion of the tide.

The lower reaches of the Duplin border Doboy Sound and enjoy easy communication with the waters of the sound and thus the coastal Atlantic Ocean. These lower Duplin waters are generally cool and salty and tend to be vertically and laterally well mixed at most times. Intermittent periods of short-lived stratification have been observed and are believed to be related to changes in groundwater input, meteorological forcing and the influence of the Altamaha River input into Doboy Sound through the Intracoastal Waterway. There is a strong along channel salinity gradient between the saltier waters of Doboy Sound and the fresher waters of the upper and middle Duplin, presumably influenced by fresh groundwater discharge in that region. The channel in the lower reaches (see Figure 1.1) is generally straight, wide and of regular cross- section and cuts through an area of generally creekless marsh bordered by hard upland and marsh hammocks (isolated areas of upland surrounded by marsh).

By contrast, the upper Duplin is isolated from the lower Duplin and Doboy Sound, by the sinuous nature of its winding channel (see Figure 1.1). The channel of the upper Duplin is much narrower than the lower Duplin and is bordered by marsh with an extensive network of small side creeks on the western side and by Moses hammock and Sapelo Island on the

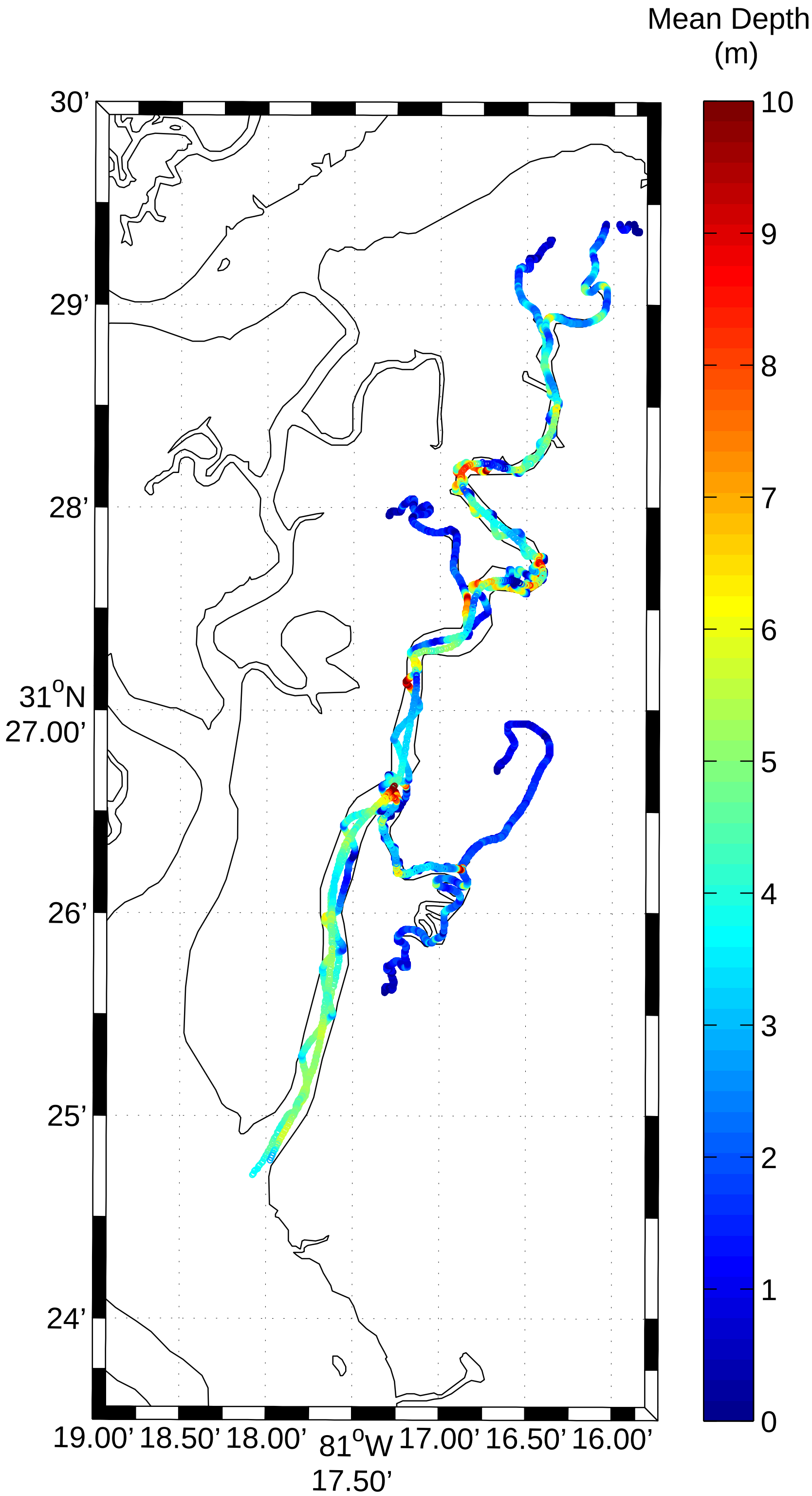

Figure 1.2: Bathymetry of the Duplin River study area as measured by the R/V Gannet's echosounder during a flooding tide.

eastern side. These upper Duplin waters are generally fresher than those of the lower Duplin, reflecting the groundwater (and occasional surface water) input into this region. The water is well mixed both vertically and laterally and shows only a low and variable along channel salinity gradient.

1.3 Objectives

Despite many years of study of their biological and biogeochemical properties, the physical processes, which regulate shallow tidal creeks, are still poorly understood. In large part this is due to the difficulty inherent in maintaining long term measurement stations in these shallow, turbid areas of high biological productivity, with the attendant problem of bio-fouling of sensors. Measurements are further complicated by the poorly understood nature of what are believed to be significant linkages between the creek channels and the intertidal marsh (Peterson and Howarth, 1987). However, any hope to understand the biological and biogeochemical dynamics of this class of creek must necessarily require an understanding of the physical processes which control the mixing, dispersion and transport of salt, heat, sediment, dissolved nutrients and larvae through the creek system and which control the export of the same to the coastal ocean. This study is designed to answer questions in three broad areas of concern.

The first question concerns the structure of the water masses in the Duplin and the zonation of temperature through the creek system. The temperature and salinity of the creek waters are regulated by the input of salt and heat from Doboy Sound, atmospheric fluxes, advection and dispersion through the main channel, diluting nature of groundwater input and by linkages with the intertidal marsh, which can serve both as a source and a sink of salt and heat. As most of these processes are also the routes by which many nutrients and larvae enter the Duplin, it is reasonable to expect that they will show a similar spatial and temporal distribution. Hanson and Snyder (1980) showed that glucose, derived from plant matter both in the main channel of the Duplin and in the marsh showed a similar zonation to that observed for heat and salt in the Duplin. Thus the first objective is to determine the water mass structure of the Duplin as well as the relative importance of residual and tidal advection, tidal dispersion, shear, groundwater, and linkages with the marsh to defining that water mass structure.

The second question concerns the nature of mixing in the creek. Vertical mixing, driven largely by bottom boundary stress, either allows or destroys vertical stratification in the Duplin depending on its intensity. The saltier water, which enters the Duplin on flood, is denser than the fresher water already in the creek. Due to this the Duplin water's natural tendency would be to form a layer toward the bottom creating a stratified system. If it does not, it is the result of vigorous vertical mixing which overcomes this stratifying tendency. Similarly, substances may enter the Duplin from the sediment and, in the absence of vertical mixing, would be expected to only slowly diffuse through the water column. The same vertical mixing which reduces salinity stratification also mixes nutrients, as well as passively floating larvae, through the water column. The interaction between residual advection and tidal dispersion in the creek channel controls how dissolved and suspended substances and fluid properties move from the upper to the lower Duplin and then are exported to Doboy Sound and the coastal ocean. As tidal creeks are the primary conduits through which the highly biologically productive intertidal marshes export sediment, carbon and nutrients to the coastal ocean (see, for example, Wolaver and Spurrier, 1988; Childers and Day, 1990a,b; Cai et al., 2003; Wang and Cai, 2004), an understanding of the temporal dynamics of salt import and export, especially on the spring/neap scale, will inform a much greater understanding of the role of tidal creeks in influencing the characteristics of the coastal ocean.

The final question concerns the linkages between the creek channel and the intertidal marsh. A large volume of water, in the form of a sheet, moves onto the intertidal marsh with each flood tide and drains on each ebb. The volume of water involved is controlled by the tidal range, largely determined by the spring/neap cycle, and the mean water depth, influenced by local winds as water is forced into or out of the creek or transported into and out by coastal up- or downwelling favorable winds. While on the marsh, the water can change temperature and salinity and then bring that new heat and salt content back into the main channel on ebb, thus affecting the properties of the main channel. Similarly it can pick up sediment and nutrients, which it will also bring back into the main channel. By attempting to understand the relative importance of linkages with the marsh on the physical properties of the main channel of the Duplin, a better understanding will also be developed of the relative freedom with which marsh generated nutrients are transferred to the main channel.

The goal of this study then is to develop a better understanding of the physical processes of mixing, dispersion and advection, which control the physical properties of temperature and salinity in the main channel of the Duplin. With this knowledge it will be possible to better understand the way in which these same physical processes influence the flux of biological and biogeochemical substances through the same system and into the coastal ocean.

1.4 Overview of the Dissertation

This dissertation reports on the results of a series of experiments that were conducted in the Duplin River from 2003 to 2005 as part of the Georgia Coastal Ecosystems - Long Term Ecological Research program. These experiments were designed both to measure the tidal transport in the upper and lower Duplin and to measure the spatial and temporal changes in heat and salt content along the Duplin River. This information is then used to estimate the importance of mixing and of marsh interactions to maintaining the physical characteristics of the Duplin, concentrating on variability on tidal, meteorological event and fortnightly time scales. Two of the chapters are papers, which have been either accepted or submitted for publication in scientific journals while the others serve to tie those two together.

Chapter two reports on Lagrangian observations of flow using a series of drifter experiments in 2005 and 2006. The nature of the flow in the upper and lower Duplin as well as export from the lower Duplin to Doboy Sound and the coastal Atlantic Ocean is observed from the drifter tracks. In addition, surveying of the current over a tidal period will show cross sectional characteristics.

Chapter three, which is currently in press for *Continental Shelf Research*, examines the heat budget of the Duplin River in order to explore the mechanisms which regulate the temperature of the water in the main channel of the creek. Data from several days of intensive temperature and salinity surveys along the axis of the Duplin on a spring and neap tide in August of 2003, allow the Duplin to be characterized by water mass. Month long temperature and flow moorings allow the temporal variability in the local heat budget to be explored for the upper and the lower Duplin. The influence of the marsh on the local heat budget is explored as a function of the ease of communication between the channel and the marsh. The tidally varying heat budget for the lower Duplin is compared to a tidally averaged heat budget constructed from a three month long measurement of temperature and flow at the same location from March through May of 2004, establishing the importance of the marsh to local properties regardless of season or timescale.

Chapter four examines the salt budget in the Duplin River, concentrating on the upper and lower Duplin at the same moorings used for the heat budget in chapter two. Instantaneous along channel salt fluxes are decomposed to separate the contributions due to residual transport and tidal dispersion; the physical meaning of the various tidal correlation terms is then explored and correlated to observed changes in the physical properties of the water. The upper Duplin is shown to act as a reversing estuary on a fortnightly time scale, due to the interplay between tidal energy and fresh groundwater discharge into the middle region of the creek. The concentration and dilution of salt due to evaporation and precipitation is shown to be small. The salinity of the lower Duplin is shown to be largely controlled by direct along channel advection and dispersion of salt tied to groundwater export, offshore forcing and tidal pumping. In the upper Duplin, the salinity is shown not to be controlled by along channel salt fluxes but is hypothesized to be more closely tied to along channel dispersive transport due to tidal trapping and to the flux of salt across the lateral boundaries, both of which are tied to interactions with the intertidal marsh.

Chapter five then combines salt flux measurements taken in the lower Duplin, in October of 2005, along with high frequency acoustic measurements of the flow to explore the vertical and along channel horizontal mixing mechanisms. Tidal and fortnightly variations in turbulent stresses and vertical mixing are explored as is the fortnightly variation of the residual and tidal salt flux tied to changes in tidal energy and groundwater input. Parallels are drawn to examine the export of carbon, nutrients and larvae to the coastal ocean.

The final chapter then ties this all together into an overall theme addressing fortnightly variability and the importance of poorly constrained marsh processes to the physical processes which regulate water properties and transport mechanisms. Future research is suggested which will allow a more thorough investigation of these marsh/creek interactions.

Bibliography

Abraham, G. (1980). On internally generated estuarine turbulence. In Carstens, T. and McClimans, T., editors, *Second international symposium on stratified flows*, pages 344–363. AIHR.

Banas, N., Hickey, B., and MacCready, P. (2004). Dynamics of Willapa Bay, Washington: A highly unsteady, partially mixed estuary. *Journal of Physical Oceanography*, 24:2413–2427.

Bernard, R., Davies, B., and Hodgson, A. (1988). Reproduction in a brackish-water mytilid: gametogenesis and embryonic development. *The Veliger*, 30:278–290.

Bignami, F. and Hopkins, T. (2002). Salt and heat trends in the shelf waters of the southern Middle-Atlantic Bight. *Continental Shelf Research*, 23:647–667.

Blanton, J., Lin, G., and Elston, S. (2002). Tidal current asymmetry in shallow estuaries and tidal creeks. *Continental Shelf Research*, 22:1731–1743.

Boesch, D. and Turner, E. (1984). Dependence of fishery species on salt marshes: The role of food and refuge. *Estuaries*, 17(4):460–468.

Bowden, K. (1965). Horizontal mixing in the sea due to a shearing current. *Journal of Fluid Mechanics*, 21(2):83–95.

Bowen, M. and Geyer, R. (2003). Salt transport and the time dependent salt balance of a partially stratified estuary. *Journal of Geophysical Research*, 108:27:1–15.

Cai, W.-J., Wang, Z., and Wang, Y. (2003). The role of marsh-dominated heterotrophic continental margins in transport of CO2 between the atmosphere, the land-sea interface and the ocean. *Geophysical Research Letters*, 30(16):1849–1853.

Cavatorta, J., 2and C. Hopkinson, M. J., and Valentine, V. (2003). Patterns of sedimentation in a salt marsh-dominated estuary. *The Biological Buletin*, 205:239–241.

Chant, R. (2002). Secondary circulation in a region of flow curvature: Relationship with tidal forcing and river discharge. *Journal of Geophysical Research*, 107(C9):3131–3142.

Chant, R., Geyer, R., Houghton, R., and Hunter, E. (2002). A lagrangian view of the estuarine neap/spring transition. *AGU Fall Meeting Abstracts*, pages B265+.

Chant, R., Geyer, R., Houghton, R., Hunter, E., and Lerczak, J. (2007). Estuarine boundary layer mixing processes: Insights from dye experiments. *Journal of Physical Oceanography*, 25:1859–1877.

Chatwin, P. (1976). Some remarks on the maintenance of the salinity distribution in estuaries. *Estuarine and Coastal Marine Science*, 4:555–566.

Childers, D. and Day, J. (1990a). Marsh-water column interactions in two Louisiana estuaries, I. Sediment dynamics. *Estuaries*, 13(4):393–403.

Childers, D. and Day, J. (1990b). Marsh-water column interactions in two Louisiana estuaries, II. Nutrient dynamics. *Estuaries*, 13(4):404–417.

Crabtree, S. and Kjerfve, B. (1978). Radiation balance over a salt marsh. *Boundary-Layer Meteorology*, 14:59–66.

Dronkers, J. (1986). Tidal asymmetry and estuarine morphology. *Netherlands Journal of Sea Research*, 20:117–131.

Dyer, K. (1974). The salt balance in stratified estuaries. *Estuarine and Coastal Marine Science*, 2:273–281.

Dyer, K. R. (1997). *Estuaries: A Physical Introduction*. John Wiley and Sons.

Fischer, H. (1972). Mass transport mechanisms in partially stratified estuaries. *Journal of Fluid Mechanics*, 53:671–687.

Fischer, H., List, E., Koh, R., Imberger, J., and Brooks, N. (1979). *Mixing in Inland and Coastal Waters*. Academic Press, Inc.

Geyer, W. and Signell, R. (1992). A reassessment of the role of tidal dispersion in estuaries and bays. *Estuaries*, 15(2):97–108.

Hackney, C., Burbanck, W., and Hackney, O. (1976). Biological and physical dynamics of a Georgia tidal creek. *Chesapeake Science*, 17(4):271–280.

Hansen, D. (1965). Currents and mixing in the Columbia River estuary. In *Transaction of the Joint Conference of the Marine Technologocal Society and the American Society of Limnology and Oceanography*, pages 943–955.

Hansen, D. and Rattray, M. (1965). Gravitational circulation in straits and estuaries. *Journal of Marine Research*, 23:104–122.

Hanson, R. and Snyder, J. (1980). Glucose exchanges in a salt-marsh estuary: Biological activity and chemical measurements. *Limnology and Oceanography*, 25(4):633–642.

Harrison, S. and Phzacklea, P. (1985). Seasonal changes in heat flux and heat storage in the intertidal mudflat of the Forth Estuary, Scotland. *Journal of Climatology*, 5:473–485.

Heilman, J., Heinsch, F., Cobos, D., and McInnes, K. (2000). Energy balance of a high marsh on the Texas Gulf Coast: Effect of water availability. *Journal of Geophysical Research*, 105(D17):22,371–22,377.

Hoguane, A., Hill, A., Simpson, J., and Bowers, D. (1999). Diurnal and tidal variations of temperature and salinity in the Ponta Rosa mangrove swamp, Mozambique. *Estuarine, Coastal and Shelf Science*, 49:251–264.

Imberger, J., Berman, T., Christian, R., Sherr, E., Whitney, D., Pomeroy, L., Wiegert, R., and Wiebe, W. (1983). The influence of water motion on the distribution and transport of materials in a salt marsh estuary. *Limnology and Oceanography*, 28(2):201–214.

Islam, M., Hibino, M., and Tanaka, M. (2006). Distribution and diets of larval and juvenile fishes : Influence of salinity gradient and turbidity maximum in a temperate estuary in upper Ariake Bay, Japan. *Estuarine, Coastal and Shelf Science*, 68(1-2):62–74.

Jorgensen, C. (1990). *Bivalve Filter Feeding: hydrodynamics, bioenergetics, physiology and ecology*. Olsen and Olsen.

Kantha, L. and Clayson, C. (2000). *Small scale processes in geophysical fluid flows*. Academic Press.

Kaplan, D., Largier, J., Navarette, S., Guinez, R., and J, C. (2003). Large diurnal temperature fluctuations in the nearshore water column. *Estuarine, Coastal and Shelf Science*, 57:385–398.

Kjerfve, B. (1973). Volume Transport, Salinity Distribution and Net Circulation in the Duplin Estuary, Georgia. Technical report, ERC-0273 Marine Institute, University of Georgia, Sapelo Island, Georgia.

Kjerfve, B. (1986). Circulation and salt flux in a well mixed estuary. In van de Kreeke, J., editor, *Physcis of Shallow Estuaries and Bays*, pages 22–29. Springer Verlag: Berlin.

Lane, A., Prandle, D., A.J. Harrison, P. J., and Jarvis, C. (1997). Measuring fluxes in tidal estuaries: Sensitivity to instrumentation and associated data analyses. *Estuarine, Coastal and Shelf Science*, 45:433–451.

Lewis, R. (1997). *Dispersion in Estuaries and Coastal Waters*. John Wiley and Sons.

Lohrman, A., Hackett, B., and Roed, L. (1990). High resolution measurements of turbulence, velocity, and stress uding a pulse-to-pulse coherent SONAR. *Journal of Atmospheric and Oceanic Technology*, 7:19–37.

Lu, Y. and Lueck, R. (1999). Using a broadband ADCP in a tidal channel. Part II:Turbulence. *Journal of Atmospheric and Oceanic Technology*, 16:1568–1579.

Lueck, R., Huang, D., D.Newman, and Box, J. (1997). Turbulence measurement with a moored instrument. *Journal of Atmospheric and Oceanic Technology*, 14:142–151.

MacCready, P. (2004). Toward a unified theory of tidally-averaged estuarine salinity structure. *Estuaries*, 27(4):561–570.

Matsunaga, M. and Kodama, M. (2000). Thermal environment properties on a tidal flat. In *Proceedings of the 4th International Conference of Hydro-Science and Engineering (CD)*. Korean Water Resources Association.

Minello, T., Able, K., Weinstein, M., and Hays, C. (2003). Salt marshes as nurseries for nekton: Testing hypothesis on density, growth and survival through meta-analysis. *Marine Ecology Progress Series*, 249:39–59.

Moeller, I., Spencer, T., French, J., Leggett, D., and Dixon, M. (2001). The sea-defense value of salt marshes: Field evidence from north norfolk. *Water and Environment*, 15(2):109–116.

Na, J., Seo, J., and Lie, H. (1999). Annual and seasonal variations of the sea surface heat fluxes in the east asian marginal seas. *Journal of Oceanography*, 55:257–270.

Newman, B., Papadopolous, I., Vorsatz, J., and Wooldridge, T. (2006). Influence of temperature on the larval development of Upogebia africana and U. capensis (Decapoda: Thalassinidae: Upogebiidae) in the laboratory. *Marine Ecology Progress Series*, 325:165–180.

Perez-Domingues, R. and Holt, G. (2001). Effects of nursery environmental cycles on larval red drum (sciaenops ocellatus) growth and survival. *Fisheries Science*, 68(1):186–189.

Peters, H. (1997). Observations of stratified turbulent mixing in an estuary: Neap-to-spring variations during high river flow. *Estuarine, Coastal and Shelf Science*, 45:69–88.

Peterson, B. and Howarth, R. (1987). Sulfur, carbon and nitrogen isotopes used to trace organic matter flow in the salt-marsh estuaries of sapelo island, georgia. *Limnology and Oceanography*, 32:1195–1213.

Pomeroy, L. (1959). Algal productivity in salt marshes of Georgia. *Limnology and Oceanography*, 4(4):386–397.

Prandle, D. and Lane, A. (1995). The annual temperature cycle in shelf seas. *Continental Shelf Research*, 15(6):681–704.

Pritchard, D. (1952). Estuarine hydrography. *Advances in Geophysics*, 1:242–280.

Pritchard, D. (1954). A study of the salt balance in a coastal plain estuary. *Journal of Marine Research*, 13:133–144.

Ragotzkie, R. and Bryson, R. (1955). Hydrography of the Duplin River, Sapelo Island, Georgia. *Bulletin of Marine Science of the Gulf and Caribbean*, 5:297–314.

Rattray, M. and Dworski, J. (1980). Comparison of methods for analysis of the transverse and vertical contributions to the longitudinal advective salt flux in estuaries. *Estuarine and Coastal Marine Science*, 11:515–536.

Reimold, R., Gallagher, J., Linthurst, R., and Pfeiffer, W. (1975). Detritus production in coastal Georgia salt marshes. In Cronin, L., editor, *Estuarine Research I*, pages 217–220. Academic Press.

Rippeth, T., Simpson, J., Williams, E., and Simpson, J. (2003). Measurement of the rates of production and dissipation of turbulent kinetic energy in an energetic tidal flow: Red Warf Bay revisited. *Journal of Physical Oceanography*, 33:1889–1901.

Rippeth, T., Williams, E., and Simpson, J. (2002). Reynolds stress and turbulent energy production in a tidal channel. *Journal of Physical Oceanography*, 32:1242–1251.

Schwing, F. and Kjerfve, B. (1980). Longitudinal characterization of a tidal marsh creek separating two hydrographically distinct estuaries. *Estuaries*, 3(4):236–241.

Simpson, J., Brown, J., Matthews, J., and Allen, G. (1990). Tidal straining, density currents, and stirring in the control of estuarine stratification. *Estuaries*, 13:125–132.

Simpson, J., Vennell, R., and Souza, A. (2001). The salt fluxes in a tidally energetic estuary. *Estuarine, Coastal and Shelf Science*, 52:131–142.

Simpson, J., Williams, E., Brasseur, L., and Brubaker, J. (2005). The impact of tidal straining on the cycle of turbulence in a partially stratified estuary. *Continental Shelf Research*, 25:51–64.

Smith, N. (1981). Energy balance in a shallow seagrass flat under winter conditions. *Limnology and Oceanography*, 26:482–491.

Smith, N. (1983). A comparison of winter and summer temperature variations in a shallow bar-built estuary. *Estuaries*, 6(1):2–9.

Smith, N. and Kierspe, G. (1981). Local energy exchanges in a shallow, coastal lagoon:Winter conditions. *Estuarine and Coastal Marine Science*, 13:159–167.

Stacey, M., Monismith, S., and Burau, J. (1998). Observations of turbulence in a partially stratified estuary. *Journal of Physical Oceanography*, 29:1950–1970.

Stacey, M., Monismith, S., and Burau, J. (1999). Measurements of Reynolds stress profiles in unstratified tidal flow. *Journal of Geophysical Research*, 104:10933–10949.

Taylor, G. (1953). Dispersion of soluble matter in solvent flowing slowly through a tube. *Philosophical Proceedings of the Royal Society of London*, A219:186.

Taylor, G. (1954). The dispersion of matter in turbulent flow through a pipe. *Philosophical Proceedings of the Royal Society of London*, A223:446.

Teal, J. and Howes, B. (2002). Salt marsh values: Retrospection from the end of the century. In *Concepts and Controversies in Tidal Marsh Ecology*, pages 9–19. Springer Netherlands.

Tennekes, H. and Lumley, J. (1999). *A First Course in Turbulence*. MIT Press.

Turrell, W., Brown, J., and Simpson, J. (1996). Salt intrusion and secondary flow in a shallow, well-mixed estuary. *Estuarine, Coastal and Shelf Science*, 42:153–169.

Uncles, R. and Stephens, J. (2001). The annual cycle of temperature in a temperate estuary and associated heat fluxes to the coastal zone. *Journal of Sea Research*, 46(2):143–159.

Underwood, G., Phillips, J., and Saunders, K. (1998). Distribution of estuarine benthic diatom species along salinity and nutrient gradients. *European Journal of Phycology*, 33:173–183.

Vaz, N., Dias, J., Leitao, P., and Martins, I. (2005). Horizontal patterns of water temperature and salinity in an estuarine tidal channel: Rio de Aveiro. *Ocean Dynamics*, 55:416–429.

Vernberg, F. (1993). Salt-marsh processes: A review. *Environmental Toxicology and Chemistry*, 12(12):2167–2193.

Vugts, H. and Zimmerman, J. (1985). Heat balance of a tidal flat area. *Netherlands Journal of Sea Research*, 19:1–14.

Wang, Z. and Cai, W.-J. (2004). Carbon dioxide degassing and inorganic carbon export from a marsh dominated estuary (the Duplin River): A marsh CO2 pump. *Limnology and Oceanography*, 49(2):341–352.

Wilkin, J. (2006). The summertime heat budget and circulation of Southeast New England shelf waters. *Journal of Physical Oceanography*, 36:1997–2011.

Wolaver, T. and Spurrier, J. (1988). Carbon transport between a euhaline vegetated marsh in South Carolina and the adjacent tidal creek: contributions via tidal inundation, runoff and seepage. *Marine Ecology Progress Series*, 42:53–62.

Chapter 2

Tidal Flow and Lateral Variability in the Duplin River

2.1 Introduction

Salt marsh creeks and estuaries are defined by their tides. The twice daily rise and fall of the tide floods and drains the intertidal marsh allowing it to exchange heat, salt, sediment and nutrients with the main channel. The tides create currents which advect these properties and substances, as well as suspended larvae, through the creek channel, alternately augmenting and opposing the mean advection caused by fresh water export, and eventually driving export to the coastal ocean. Stress generated by tidal currents flowing over the bottom causes vertical mixing, which controls the distribution of substances through the water column. Acting on longitudinal salinity and temperature gradients, tidal currents cause regular fluctuations in the properties, which strongly regulate productivity in estuarine waters. Secondary flows generated by tidal currents flowing through a curved or irregular channel can cause cross-channel variations in flow or fluid properties. When averaged over long periods, small tidal asymmetries, due to correlations between tidally varying depth, current and scalar properties, can result in significant dispersive fluxes along the axis of the creek or estuary.

Most studies of estuarine transport and dispersion emphasize subtidal, long term averaged processes as these are often the dominant drivers defining estuarine structure and circulation. However it is also important to understand tidal transport and velocity as these affect the environment in which biological organisms exist and drive the movement of water borne substances and changes in water properties. The purpose of this study is to examine tidal transport and dispersion in the upper and lower sections of the Duplin River and to investigate tidal export to the coastal ocean as well as to investigate cross- channel variability in along channel tidal velocity in a straight sided region of the upper Duplin. Section 2.2 will describe the custom built Lagrangian surface drifters used to investigate tidal flows at the creek surface. Section 2.3 will describe the drifter experiments while Section 2.4 will present the results of the cross-channel velocity surveys. Finally, section 2.5 will discuss the importance of these results to understanding tidal processes in the Duplin River.

2.2 Drifters

Horizontal transport and dispersion/diffusion is difficult to measure using Eulerian moorings, involving assumptions about uniformity of flow and integration of point measured velocities (Winant, 1983; Dame et al., 1986; Winant and de Velasco, 2003). Lagrangian techniques, involving groups of drifting floats (Tseng, 2002; Stocker and Imberger, 2003; Johnson et al., 2003; Austin and Atkinson, 2004) or dye patches (Elliott et al., 1997; Vallino and Hopkinson, 1998), allow researchers to follow the flow and directly measure advective transport and apparent horizontal dispersion and, in the case of dye studies, vertical and horizontal eddy diffusion.

Drifters have a long history of use in the open ocean (Davis, 1991), but have found limited use in coastal and estuarine environments, due to the high cost and large size of drifters designed for the open ocean, as well as the shallow nature of these waters and the tendency of the drifters to ground on beaches, mudflats and marsh areas. Recently, however, some progress has been made in modifying open ocean drifters to work in shallow water environments (Davis, 1983; List et al., 1990; George and Largier, 1996; Johnson et al., 2003; Austin and Atkinson, 2004). Early attempts to develop small and inexpensive drifters have resulted in drifters which are either visually tracked (Johnson et al., 2003) and thus subject to loss or are limited by battery life and radio range (Austin and Atkinson, 2004). However the recent introduction of inexpensive commercially available Global Positioning System (GPS) satellite receiver combined with General Mobile Radio Spectrum (GMRS) radio transmitter units with PC connections, such as the Garmin Rino 130, and the easing of FCC rules to allow high powered data transmissions on GMRS frequencies (Federal Communication Commission, 2005), makes it possible to develop small and inexpensive drifters capable of internally logging their position and transmitting it back at regular intervals to a remote base station for real time tracking.

2.2.1 Design and Construction

A set of six Davis style surface drifters was designed and constructed based on the earlier work of Austin and Atkinson (2004), with upgraded electronics, removable wings (for improved storage capability and transport efficiency) and an upgraded software suite for real time tracking. The drifters (see Figure 2.1) were constructed of schedule 4 PVC plumbing pipe material, 4 inch inside diameter (ID), with a main body length of 30 inches. One end is fitted with a standard plumbing end cap and the other with a screw-in clean out fitting. Inside of each is 6 ounces of lead fishing weights, for ballast, topped by a length of closed cell foam flotation and a Garmin RINO 130 GPS receiver/GMRS transmitter encased in a sealed plastic bag, with the antenna above the waterline in the relieved handle area of the clean out plug end cap. Arrayed around the outside of the case are four screw-in wings constructed of 1/2 inch ID PVC tubing spanned by Plexiglas sheets. A GMRS receiver unit is connected via an RS-232 cable to a Windows laptop running the shareware Ozi- Explorer mapping software which displays a periodically updated plot of each drifter's location on a hydrographic chart of the region. The drifters float in the surface layer of the water column with approximately 5 cm exposed above the waterline to allow radio transmissions. GMRS frequencies work via line of sight and the units have a transmission range of approximately 1 km with this antenna height.

2.2.2 Theory

Following the methods described by Okubo and Ebbesmeyer (1976), a group of at least four drifters were deployed and tracked continuously; the greater the number of drifters the smaller the standard error of the measurement. From the recorded drifter paths the centroid of a group of N drifters at time i is given as,

$$\overline{x_i} = \frac{1}{N}\sum_{j=1}^{N} x_{ij} \qquad \overline{y_i} = \frac{1}{N}\sum_{j=1}^{N} y_{ij} \tag{2.1}$$

Figure 2.1: Davis style surface drifter deployed in the Duplin River

where x and y are the along and cross channel coordinates respectively. The variance in the drifter position is then

$$\sigma_{x_i}^2 = \frac{1}{N-1}\sum_{j=1}^{N}(x_{ij} - \overline{x_i})^2 \qquad \sigma_{y_i}^2 = \frac{1}{N-1}\sum_{j=1}^{N}(y_{ij} - \overline{y_i})^2 \tag{2.2}$$

with the total variance,

$$\sigma_i^2 = \frac{1}{2}(\sigma_{x_i}^2 + \sigma_{y_i}^2) \tag{2.3}$$

given as the average of the along and cross-channel variance assuming that they are independent in this class of a narrow channel.

The time rate of change of these variances gives the relative dispersion coefficients (K)

$$K_x(t_i) = \frac{1}{2}\frac{d\sigma_{x_i}^2}{dt} \qquad K_y(t_i) = \frac{1}{2}\frac{d\sigma_{y_i}^2}{dt} \qquad K(t_i) = \frac{1}{2}\frac{d\sigma_i^2}{dt} \tag{2.4}$$

where a negative K implies convergence, K_x is the along channel dispersion coefficient and K_y the cross channel dispersion coefficient and K the average of the along and cross-channel dispersion coefficients.

2.3 Drifter Experiments

A series of drifter experiments was run in the upper and lower Duplin and Doboy Sound on a spring and neap tide in September and October of 2005 and again in July of 2006 for a total of eight deployments. While afternoon thunderstorms generally terminated the experiments prematurely, one entire ebb/flood cycle was captured in the upper Duplin on 1 October 2005, shortly before spring tide. That was the only entire tidal cycle captured for all of the deployments and was a result of the sheltered nature of those waters. Several partial tidal cycles were observed in the lower Duplin and Doboy Sound and all showed similar behavior. Presented here are the results of a deployment in the lower Duplin on ebb and flood tide on 30 September 2005 as well as one upper Duplin deployment on 1 October 2005, both shortly before spring tide.

2.3.1 Lower Duplin Experiments

Five drifters were deployed from the research vessel Salty Dawg at 0700 EDT, at slack water, near the junction of Barn Creek with the Duplin River. This was approximately 3 km from the mouth of the Duplin, which has an estimated tidal excursion distance of 4 km (Ragotzkie and Bryson, 1955), and the location was chosen such that the drifters would enter Doboy Sound before the end of the ebb. The drifters stayed together as a coherent group and followed the path of the thalweg through the lower Duplin. They showed no apparent dispersion, either cross-channel or along channel, and generally arrayed themselves in a straight line along the channel and followed very similar tracks. Their tracks are shown in Figure 2.2(a). The drifters grounded and fouled in the marsh at the channel edge several times during the experiment and we were forced to retrieve them and relocate them in the center of the channel.

The drifters exited the Duplin and entered Doboy Sound approximately 3-1/2 hours after the start of ebb tide. On reaching the foam line, which defines the edge of the influence of the Duplin on ebb, the drifters converged into a group, hesitated, and then crossed the foam line, turned left and proceeded down the axis of Doboy Sound. A little less than 4-1/2 hours after the start of the ebb tide the drifters were nearing the mouth of Doboy Sound, and thus the Atlantic Ocean, and a decision was made to terminate the experiment.

Figure 2.2(b) shows the dispersion coefficients calculated from the drifter tracks during the experiment. While in the Duplin channel the along and cross channel dispersion coefficients are close to zero at all times except when the drifters were being relocated after fouling in the marsh. On nearing the mouth of the Duplin the drifters show some along channel dispersion before converging again at the foam line, which marks the end of the influence of the Duplin. After entering Doboy sound the drifters show more pronounced dispersion (and convergence) along channel and slightly more cross channel though the value remains small, compared to the horizontal scale, and the drifters stay in a coherent formation at all times. It is apparent, both from direct observation of drifter behavior and calculations of dispersion

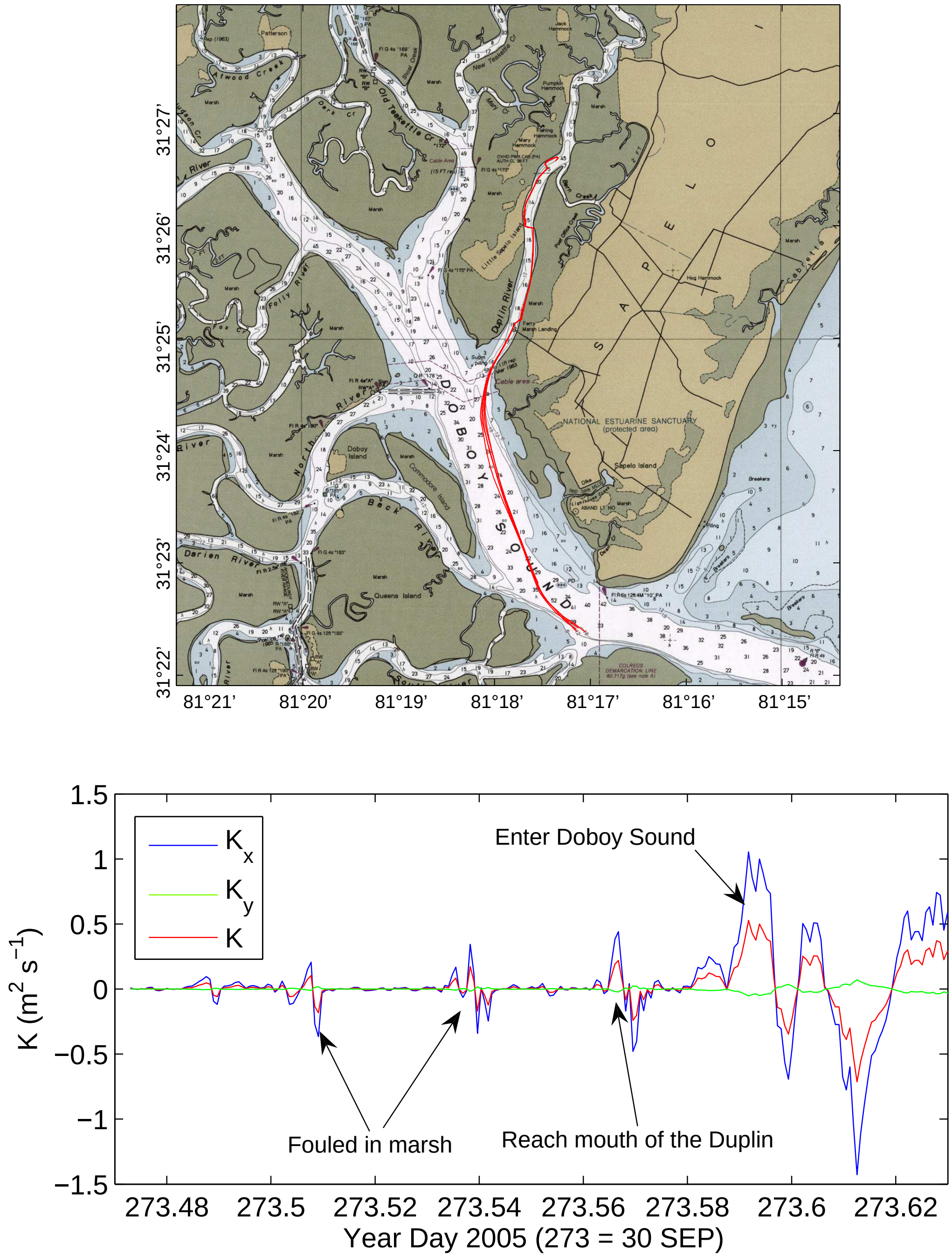

(a)

(b)

Figure 2.2: (a) Drifter tracks on the ebb tide of 30 September 2005 in the lower Duplin and Doboy Sound and (b) along channel (K_x), cross channel(K_y) and total (K) dispersion coefficients calculated from the drifter tracks.

coefficients, that there is essentially no along or cross channel dispersion in the Duplin or Doboy Sound on a tidal time scale. Transport is almost purely advective. Later deployments, which repeated this experiments on both spring and neap tide showed very similar behavior and similarly low values for K.

After recovery, the drifters were checked and then redeployed (less one which was slightly damaged during recovery) inside of the mouth of the Duplin around 1300 EDT to capture the flooding tide. These tracks are shown as the thin red lines in Figure 2.3. In order to avoid ferry and barge traffic the drifters were released approximately 700 m inside of the mouth of the Duplin. The drifters were deployed in a group spaced along and across the channel in a square formation approximately 100 m on each side. They quickly converged into a group lined up along the axis of the creek, and stayed together in an approximately 50 m long line, showing essentially no along or cross-channel dispersion and behaving very similar to their behavior on ebb. The drifters fouled in the marsh several times and had to be repositioned out into the channel. At approximately 5 hours after the start of the flood the drifters had reached the vicinity of Pumpkin Hammock and flood velocities had decreased such that drifter movement was minimal. Some dispersion was noted in this area as local wind generated currents began to overwhelm the tidal flows. The drifters continued for another hour until they reached the midpoint of Pumpkin Hammock around slack water. The total distance of travel was just over 4 km, thus appearing to confirm the generally accepted tidal excursion distance in the lower Duplin of 4 km as stated by Ragotzkie and Bryson (1955). As this experiment, and all subsequent drifter experiments in the Duplin, showed essentially no tidal scale dispersion, no further plots of K will be presented.

Follow-up flood tide experiments were conducted to look at return flow from Doboy Sound into the Duplin River. The approximate location of the foam line which divides the influence of the Duplin and Doboy on ebb is indicated by the thick blue line on Figure 2.3. On several occasions drifters were deployed both inside and outside of that line during the slack before flood. In all cases none of the drifters entered the Duplin but instead flooded up

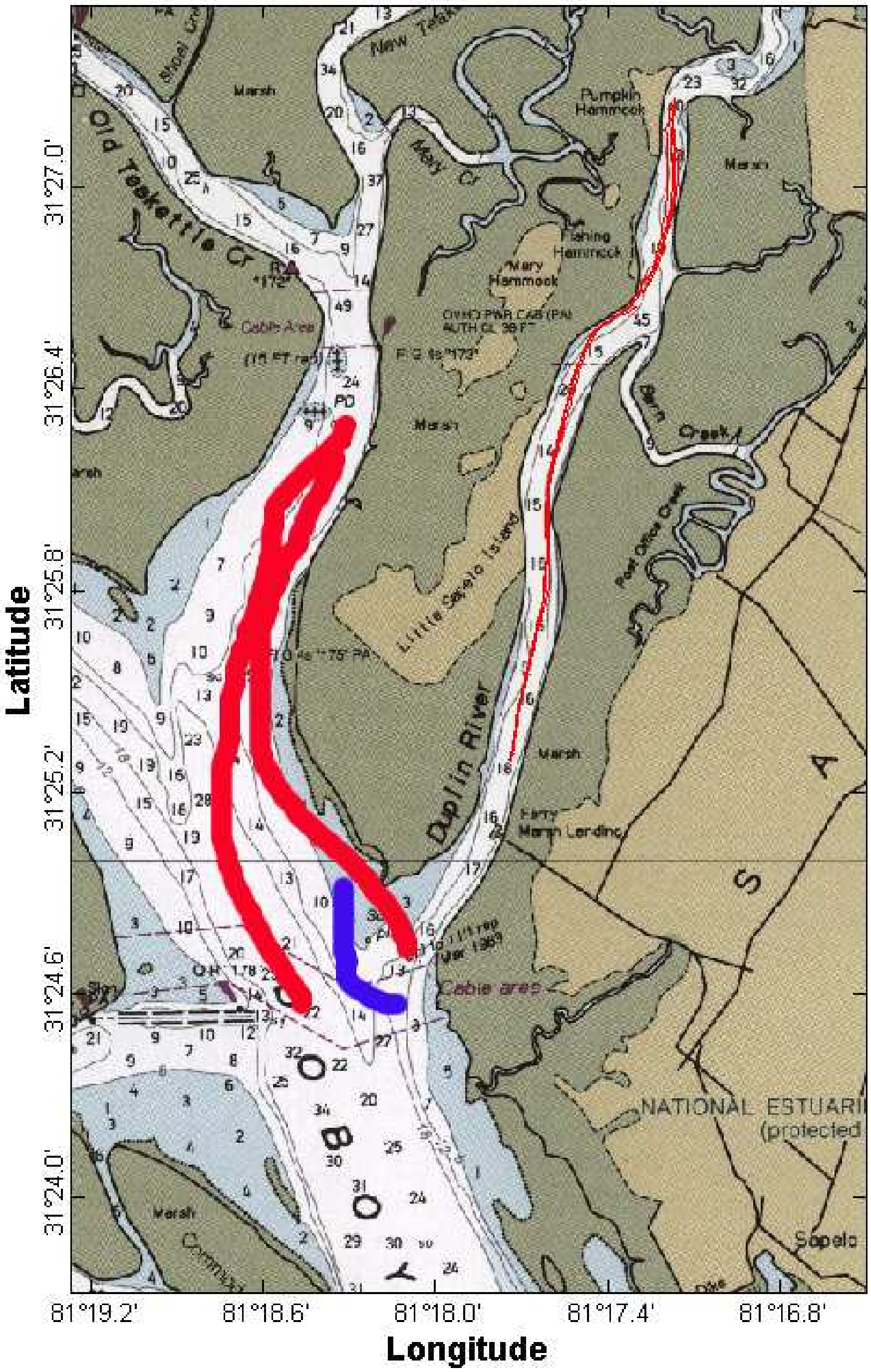

Figure 2.3: Drifter tracks on the flood tide of 30 September 2005 in the lower Duplin (thin red lines) along with the approximate location of the dividing line between the Duplin and Doboy Sound waters (thick blue line) and the general track of drifters released outside of the mouth of the Duplin on flood (thick red lines)

Doboy sound ending up in Old Teakettle Creek, New Teakettle Creek or Mary's Creek; their general track is indicated by the thick red lines. It is hypothesized that the water, which enters the Duplin on flood, comes from the shoaling region just south of the creek mouth where the drifters could not be deployed.

2.3.2 Upper Duplin Experiment

On the following day, 1 October 2005, the five drifters were deployed in the right fork of the upper Duplin, downstream of Flume Dock, shortly after the beginning of ebb at 0800 EDT. Their tracks are shown in Figure 2.4. While in the right fork, the drifters stayed in a coherent group showing no along or cross-channel dispersion but only tidal advection. On entering the main channel of the upper Duplin they began to foul in the marsh at the creek edge and had to be repeatedly relocated into the creek channel, this is evident in Figure 2.4. By six hours after the start of the ebb, at slack water, the drifters had traveled less than 1 km but it is not known if this truly represents the tidal excursion distance here or if it is related more to the amount of time the drifters spent fouled in the marsh and thus not moving. During slack water one drifter was lost as it disappeared from view and ceased to respond to requests for its position. It has never been recovered.

As the tide turned to flood, the remaining four drifters moved back into the upper Duplin. Three drifters returned to the right fork where they shortly became thoroughly fouled in the marsh requiring the boat to be grounded and the drifters recovered. The fourth drifter entered the left fork where it proceeded until entering a small side channel whereupon it was recovered to prevent it from entering an unnavigable area of the marsh. Due to the amount of time the drifters spent fouled in the marsh and the frequency with which they had to be relocated calculation of K from the drifter tracks is nearly meaningless as any real dispersion will be overwhelmed by the effect of relocating the drifters.

Due to the tendency of the drifters to foul in the marsh no further deployments were carried out in the upper Duplin and none at all in the more sinuous middle Duplin region.

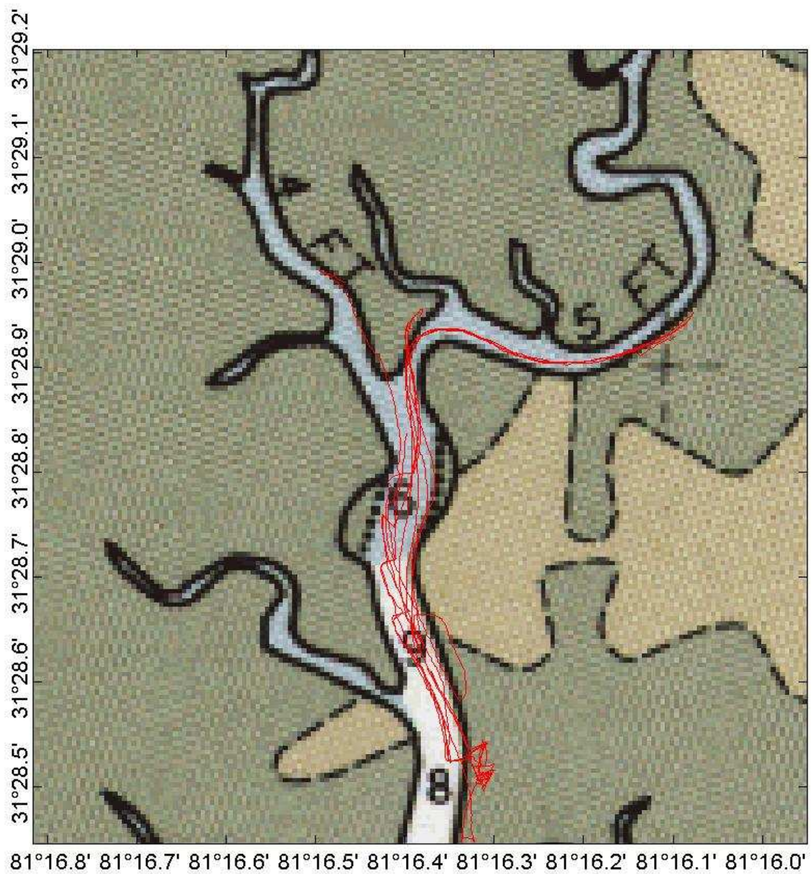

Figure 2.4: Drifter tracks for a complete tide on 1 October 2005 in the upper Duplin

2.3.3 GPS Accuracy

Global Positioning System location fixes do have some inherent error associated with them tied to the number and strength of the satellite signals received, atmospheric effects which can delay the timing signal and the use, or lack thereof, of Differential GPS (DGPS) or Wide Area Augmentation System (WAAS) technologies to improve accuracy. Many GPS receivers log statistics related to fluctuations in calculated position to give an estimate of position accuracy. The Garmin RINO series does not log this information so there is no way to estimate the true position accuracy during the deployments. However the systems indicated that six satellites were fixed with 80% or better signal strength at the start of each deployment and WAAS was active thus, according to information provided by Garmin, each unit should have achieved an average accuracy of 2 m or better. As the primary sources of error, satellite signal strength and atmospheric effects, were the same for every receiver unit, errors in position should have been uniform for all receivers. In this case the error in the variance calculated from Equation (2.2) is minimal.

To test this, a group of four different, but identical, Garmin RINO 130 units was placed outdoors on 5 July 2008 in a three meter spread square and set to log position every 30 s for six hours. Each unit showed a similar satellite fix to what was achieved with the drifters, reading six satellites at 80% or better signal strength. The mean standard deviation of the logged position fluctuations was 1.6 m and the position fluctuations for each unit were strongly correlated with the fluctuations of the other units. The calculated distance of each unit from the centroid of the group was nearly constant, showing a mean RMS fluctuation of less than 0.2 m, indicating that each unit was affected by errors in the same way and thus showed similar bias in position.

Due to this, the errors in the calculated K values will be very small. The exact values cannot be calculated as the units did not log error information during the deployment and those values will be affected by satellite position and atmospheric conditions.

2.4 Cross-channel Surveys

As part of the DUPLEX experiment in August of 2003, the R/V Gannet made a pair of 13 hour tidal surveys on 14 August and 19 August, shortly after a spring tide and shortly before a neap tide respectively, in the upper Duplin. An RD Instruments (RDI) acoustic Doppler current profiler (ADCP) was mounted downward looking on a towed sled and pinged continuously, providing flow profiles during the entire survey period. A typical track is shown in Figure 2.5 with the three cross channel survey legs highlighted as Z1, Z2 and Z3. From the raw ADCP data each cross-channel transect was isolated and the flow profiles were binned into 5 m wide bins spanning the width of the transect. The channel varies between 10 and 15 meters wide resulting in two to three bins for each transect with the region near the bank, where the boat turned, neglected. The 5 m bin width was chosen to give a sufficient number of profiles in each bin to get a valid average velocity for the bin. All profiles in each bin were averaged, decomposed into their along and cross-channel components and then depth averaged to get the mean velocity in the bin as a function of time.

Figure 2.6 shows plots of the depth averaged axial velocity in each lateral bin of each transect through an entire tide. A pronounced tidal asymmetry is seen as a short, strong ebb tide (positive value), followed by a longer, weaker flood period. This is due to frictional distortion of the tide, caused by interactions between the shallow main channel and the intertidal areas, which can be expressed by the relationship between the M2 and M4 tidal constituents (Dyer, 1997), and which is a common characteristic of this class of salt marsh estuary (Dronkers, 1986; Blanton et al., 2002). Neap tide velocities are lower than spring tide velocities and velocities are attenuated further up into the Duplin as frictional effects dissipate the tidal energy. There is apparently some cross-channel variability in flow at the Z1 transect likely tied to the pronounced curvature of the channel at this location with higher velocities located on the outer edge of the bend. This variability is significantly reduced at the Z2 transect, where there is less curvature, and there appears to be no cross-channel variability of flow at Z3, where the channel runs nearly straight.

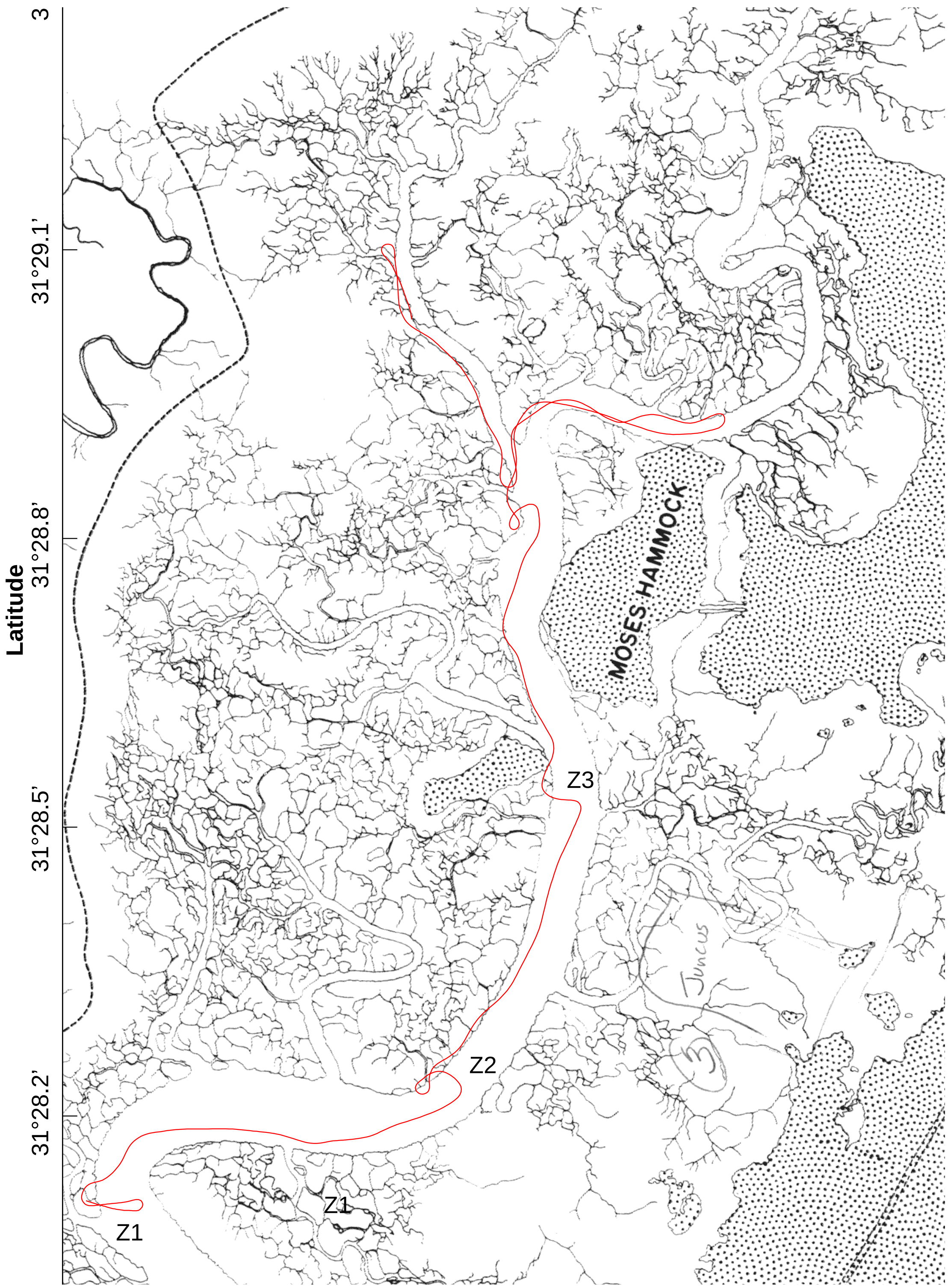

Figure 2.5: Track of the R/V Gannet on one upstream run on 14 August 2003 with cross-channel transects noted

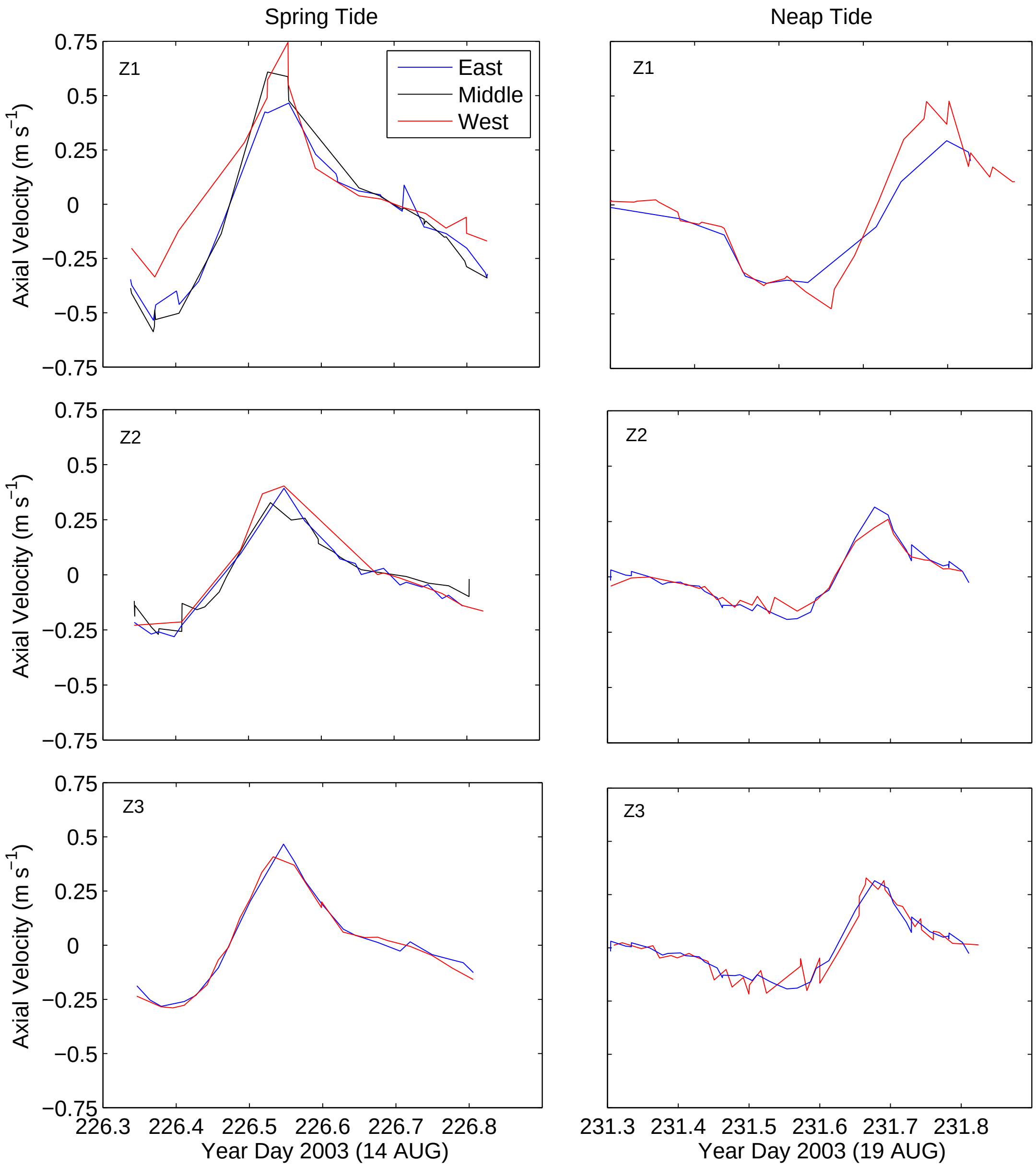

Figure 2.6: Cross-channel distribution of depth averaged axial velocity at Z1, Z2 and Z3 through one tidal cycle on spring and neap tide

2.5 Discussion and Conclusions

Results have been presented showing tidal scale transport and dispersion in the upper and lower Duplin River and Doboy Sound. Tidal transport in the surface waters is apparently purely advective and there is little to no dispersion on these time scales. The estimated lower Duplin tidal excursion distance of 4 km has been confirmed for a flooding spring tide. Ebb tides are stronger, though of a shorter duration, than flood tides with the result that much of the water of the lower tidal prism is exported to the coastal Atlantic Ocean on ebb to be replaced with water from Doboy Sound. There is likely to be little return flow. Tidal transport measurements in the upper Duplin are complicated by interference with the marsh in the narrow creek channel but as in the lower Duplin, little to no tidal scale dispersion is apparent using surface drifters, and flow here appears to be purely advective. The tidal excursion distance cannot be properly measured using surface drifters owing to interference from the marsh.

The scale of the Duplin River is such that the Coriolis effect never comes into play and cross-channel variability of flow is caused primarily by curvature in the channel. The waters of the Duplin are, as will be shown, generally well mixed for salt both vertically and laterally with the result that the Duplin can, in regions of low curvature, be regarded as sectionally homogeneous (Dyer, 1997).

2.6 Acknowledgments

This work was supported by the NSF (OCE-9982133) as part of the Georgia Coastal Ecosystems - Long Term Ecological Research (GCE-LTER) project (`http://gce-lter.marsci.uga.edu`). Thanks go to Julie Amft and Trent Moore of the Skidaway Institute of Oceanography for their assistance with the instrumentation and cross channel surveys and to Ken Helm of the UGA Marine Institute for his assistance with the drifter studies.

Bibliography

Austin, J. and Atkinson, S. (2004). The design and testing of small, low-cost GPS tracked surface drifters. *Estuaries*, 27(6):1026–1029.

Blanton, J., Lin, G., and Elston, S. (2002). Tidal current asymmetry in shallow estuaries and tidal creeks. *Continental Shelf Research*, 22:1731–1743.

Dame, R., Chrzanowski, T., Bildstein, K., Kjerfve, B., McKellar, H., Nelson, D., Spurrier, J., Stancyk, S., Stevenson, H., Nernberg, J., and Zingmark, R. (1986). The outwelling hypothesis and North Inlet, South Carolina. *Marine Ecology Progress Series*, 33:217–229.

Davis, R. (1983). Oceanic property transport: Lagrangian particle statistics and their prediction. *Journal of Marine Research*, 41:163–194.

Davis, R. (1991). Lagrangian ocean studies. *Annual Review of Fluid Mechanics*, 23:43–64.

Dronkers, J. (1986). Tidal asymmetry and estuarine morphology. *Netherlands Journal of Sea Research*, 20:117–131.

Dyer, K. R. (1997). *Estuaries: A Physical Introduction*. John Wiley and Sons.

Elliott, A., Barr, A., and Kennan, D. (1997). Diffusion in Irish coastal waters. *Estuarine, Coastal and Shelf Science*, 44(A):15–23.

Federal Communication Commission (2005). 2005 CFR Title 47, Volume 5, Part 95.

George, R. and Largier, J. (1996). Description and performance of finescale drifters for coastal and estuarine studies. *Journal of Atmospheric and Oceanic Technology*, 13:1322–1326.

Johnson, D., Stocker, R., Head, R., Imberger, J., and Pattiaratchi, C. (2003). A compact, low-cost GPS tracked drifter for use in the oceanic nearshore zone, lakes and estuaries. *Journal of Atmospheric and Oceanic Technology*, 13:1322–1326.

List, E., Gartrell, G., and Winant, C. (1990). Diffusion and dispersion in coastal waters. *Journal of Hydraulic Engineering*, 116:1158–1179.

Okubo, A. and Ebbesmeyer, C. (1976). Determination of vorticity, divergence and deformation rates from analysis of drogue observations. *Deep-Sea Research*, 23:369–352.

Ragotzkie, R. and Bryson, R. (1955). Hydrography of the Duplin River, Sapelo Island, Georgia. *Bulletin of Marine Science of the Gulf and Caribbean*, 5:297–314.

Stocker, R. and Imberger, J. (2003). Horizontal transport and dispersion in the surface layer of a medium sized lake. *Limnology and Oceanography*, 48(3):971–982.

Tseng, R. (2002). On the dispersion and diffusion near estuaries and around islands. *Estuarine, Coastal and Shelf Science*, 54:89–100.

Vallino, J. and Hopkinson, C. (1998). Estimation of dispersion and characteristic mixing times in Plum Island Sound Estuary. *Estuarine, Coastal and Shelf Science*, 46:333–350.

Winant, C. (1983). Longshore coherence of currents on the southern California shelf during the summer. *Journal of Physical Oceanography*, 13:54–64.

Winant, C. and de Velasco, G. (2003). Tidal dynamics and residual circulation in a well-mixed inverse estuary. *Journal of Physical Oceanography*, 33:1365–1379.

Chapter 3

Heat Budget for a Shallow, Sinuous Salt Marsh Estuary[1]

[1]Accepted by *Continental Shelf Research*. Reprinted here with permission of publisher, 6/5/2008

Abstract

An experimental study of temperature cycles and the heat budget in the Duplin River, a tidal creek bordered by extensive intertidal salt marshes, was carried out in late summer of 2003 and spring of 2004 near Sapelo Island on the central Georgia coast in the southeastern U.S. Three water masses are identified with differing temperature and salinity regimes, the characteristics of which are dictated by channel morphology, tidal communication with the neighboring sound, ground water hydrology, the extent of local intertidal salt marshes and side channels, and the spring-neap tidal cycle (which controls both energetic mixing and, presumably, ground water input). For the first experiment, heat budgets are constructed for the upper (warmer) and lower (cooler) areas of the Duplin River showing the diminishing importance of tidal advection away from the mouth of the creek along with the concomitant increase in the importance of both direct atmospheric fluxes and of interactions with the marsh and side creeks. The second experiment, in the spring of 2004, reexamines the heat budget on seasonal and daily averaged scales revealing the decreased importance of advective fluxes relative to direct atmospheric fluxes on this scale but the constant importance of marsh/creek interactions regardless of time scale or season. Short period temperature fluctuations, which affect larval development, are examined and analogies are drawn to use heat to understand the marsh as a source of sediment, carbon and other nutrients.

3.1 Introduction

Salt marsh ecosystems are among the most productive on the planet (Reimold et al., 1975) and their associated tidal creeks and channels provide ideal habitat for many species of fish and shellfish during some or all of their life (Boesch and Turner, 1984; Minello et al., 2003). With both primary productivity in the intertidal marsh region (Dai and Wiegert, 1996) and secondary productivity in the tidal creeks, which drain the marsh and serve as important conduits for nutrients (Odum and de la Cruz, 1967; Spurrier and Kjerfve, 1988) and larvae (Roegner, 2000), regulated by water temperature (Vernberg, 1993) it is important to understand the various factors which influence this temperature.

Temperatures in the tidal creeks are regulated by an interaction between atmospheric heat fluxes at the water surface (Wallace and Hobbes, 1977), the tidal advection and dispersion of heat through the creek channel, and the interactions between the main channel and the marsh and side creeks. Curvature in the main channel or irregularities in bathymetry can give rise to cross channel shear which locally modifies the along channel dispersion of heat (Rattray and Dworski, 1980). When the creek cuts through areas of intertidal marshes and mud flats, which are themselves often cut by small side creeks, along channel dispersive fluxes due to tidal trapping (Fischer et al., 1979) can become important. Atmospheric heat fluxes in the shallow side channels cause greater heating and cooling than in the main channel and this heat can be advected into and out of the main channel on tidal frequencies. Similarly atmospheric heat fluxes in the intertidal areas serve to warm or cool the sediment when the marsh is drained. This sediment then exchanges heat with the overlying water when the marsh is flooded, which is also affected by atmospheric influences, causing this water to mix into the main channel when the marsh again drains (Hackney et al., 1976). The resultant main channel temperature then exists as a complex signal which shows variability on diel, semi-diurnal and higher tidal harmonic and seasonal scales.

Most studies on the effect of changes in water temperature in estuarine and coastal environments generally concentrate on either long term seasonal temperature trends (see, for example, Uncles et al., 2000; Uncles and Stephens, 2001) or large temperature variations tied to seasonal upwelling events, both of which affect biological productivity in generally understood ways. However recent work shows that small diel and tidal frequency variations and meteorological event scale temperature fluctuations are also important to biological productivity and activity. While the larvae and fully developed organisms found in coastal and estuarine environments are generally tolerant of a large temperature range, small, 2-6 °C, fluctuations in water temperature on tidal and diel scales have been shown to affect the rate of development of prawn larvae (Newman et al., 2006) and the hardiness of fish larvae (Perez-Domingues and Holt, 2001). The internal circadian rhythm of adult zebrafish has been shown to be regulated by similar diel temperature cycles (Lahiri et al., 2005) in a way which expresses itself at a cellular level in their RNA. Larger short term temperature fluctuations on a meteorological event time scale, such as is caused by a storm event or upwelling favorable winds, can change the chemical and sediment load in the water column by affecting filter feeder behavior with the effect persisting days past the end of the event (Jorgensen, 1990). In the case of organisms with short larval periods, short term cooling events tied to coastal upwelling can severely disrupt their development and lead to significant mortality (Bernard et al., 1988).

Descriptive studies of temperature cycles and vertical and longitudinal temperature distributions in tidal creeks are not uncommon (see, for example, Ragotzkie and Bryson, 1955; Ayers, 1965; Hackney et al., 1976; Schwing and Kjerfve, 1980; Smith, 1983; Uncles and Stephens, 2001; Vaz et al., 2005). The temperature cycle in shallow and highly advective flows has been studied in rivers (Evans et al., 1998) and the effect of sills and constrictions on the balance between tidal advective and solar heating has been studied in mangrove swamps (Hoguane et al., 1999). The heating of water overlying intertidal marshes and mud flats has been studied as a function of solar and atmospheric input (see, for example, Crabtree and Kjerfve, 1978; Hughes et al., 2001), amount of inundation (Heilman et al., 2000), and the interaction between tidal inundation of the intertidal region and diurnal solar heating cycles (see, for example, Harrison and Phzacklea, 1985; Vugts and Zimmerman, 1985). However studies which tie together all of these inputs for shallow, sinuous marsh creeks have been lacking in the literature.

The study site presented here is the Duplin River which is a tidal creek located on Sapelo Island on the central Georgia coast (see Figure 3.1) which has been previously studied and reported on (see, for example, Ragotzkie and Bryson, 1955; Kjerfve, 1973; Imberger et al., 1983). The Duplin winds through extensive intertidal marshes characterized by mud flats vegetated with *Spartina alterniflora* and cut by a network of side creeks and channels of varying sizes. The greatest extent of both marsh and side channels is in the northern (upper) reaches of the Duplin while the southern (lower) reaches are bordered by more upland marsh, large marsh hammocks and creekless marsh as can be seen in Figure 3.1. With no source of freshwater input aside from precipitation and its associated runoff and an unmeasured groundwater input (Ragotzkie and Bryson, 1955) it is more properly a tidal creek but its geomorphology is suggestive of a river with a sinuous main channel and a network of dendritic feeder creeks. It is approximately 13 km long with a mean depth on the thalweg of approximately five meters but with several deeper holes associated with curvature or feeder creeks. Tidal range varies between two and three meters over a spring/neap cycle and there is significant tidal salinity variation in the lower reaches of the Duplin as water from Doboy Sound (influenced by the Altamaha River) is advected in (Kjerfve, 1973). The upper reaches are generally well mixed, both vertically and along channel, and are isolated from the sound by the sinuous nature of the channel. Temperatures in the upper region of the Duplin are warmer than in the lower region and increase toward the head. The maximum tidal excursion in the lower reaches is approximately 4 km and the creek is thought to have three tidal prisms (Ragotzkie and Bryson, 1955).

While previous studies in the Duplin have concentrated on hydrographic measurements of transport and horizontal mixing, the objective of the work presented here is to examine the heat budget in the Duplin and to quantify the effect on water column temperature of

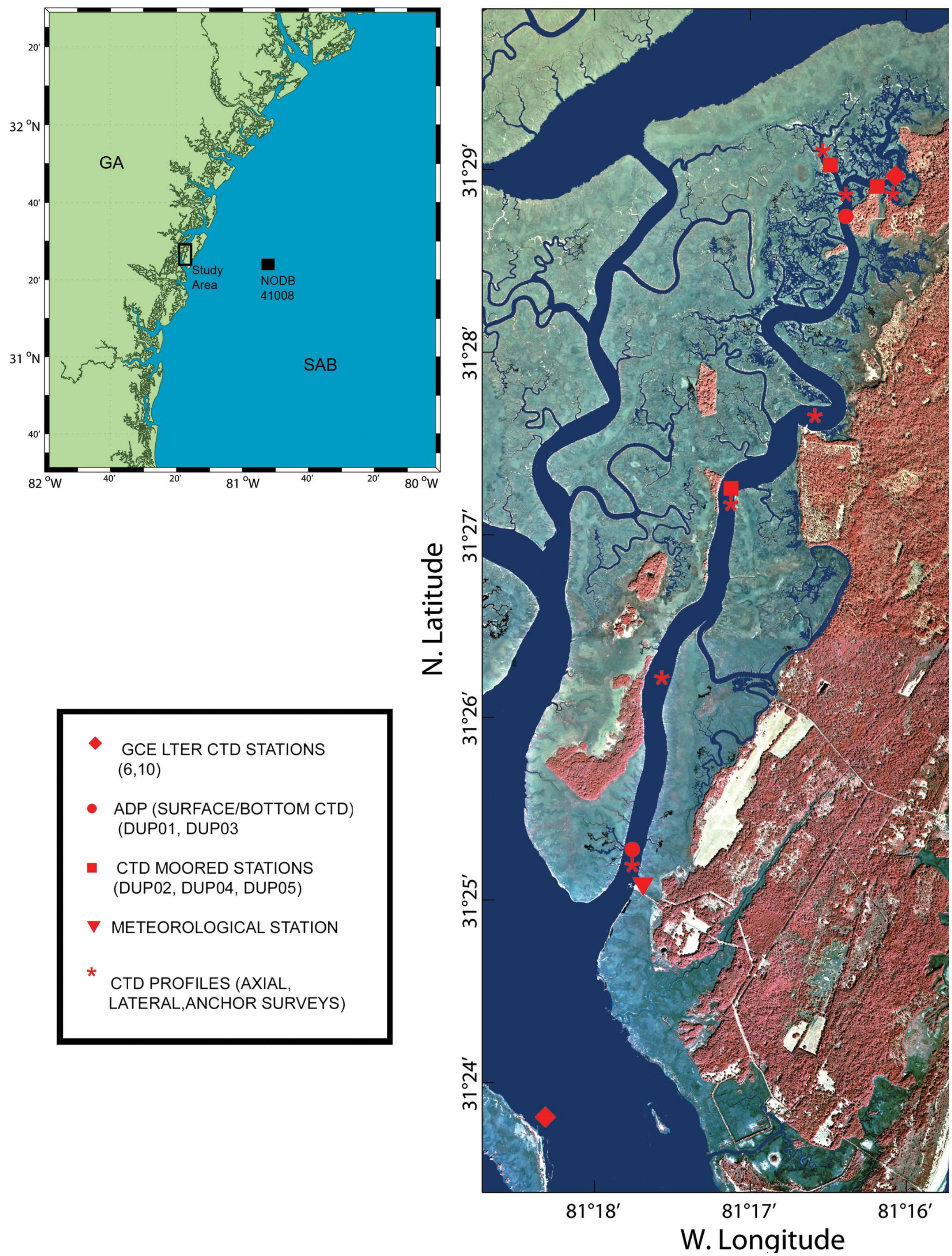

Figure 3.1: The Sapelo Island, GA study area highlighting mooring locations in the Duplin River and showing the offshore data buoy, NDBC 41006, at the Grays Reef National Marine Sanctuary.

the neighboring sound, the channel morphology and the extent of intertidal salt marshes and marsh creeks. The data presented here is based on two mooring experiments, designated DUPLEX I and II, during late summer 2003, over a 43 day deployment, and spring 2004, over a 79 day deployment, as will be described in Section 3.3. Section 3.2 details the various terms considered in constructing a heat budget for these waters along with their relative importance. Section 3.4 describes the two temperature regimes of the upper and lower Duplin River and examines the relative importance of direct, tidal and marsh heating on both hourly and daily averaged/seasonal scales. Finally Section 3.5 summarizes the findings and discusses implications for understanding the importance of marsh processes to a tidal creek.

3.2 Heat Budget Equation

The heat budget in estuarine waters is a balance between heat storage in the water column, advective heat fluxes, atmospheric heat fluxes and heat exchanges with the boundaries (Smith, 1983). Following the methods of Stevenson and Niller (1983), the vertically integrated heat content over the whole water column is,

$$\begin{aligned} h\frac{\partial T_a}{\partial t} + h\boldsymbol{v}_a \cdot \nabla T_a + \nabla \cdot \left(\int_{-h}^{0} \widehat{\boldsymbol{v}}\widehat{T} dz \right) \ldots \\ + (T_a - T_{-h}) \left(\frac{\partial h}{\partial t} - \boldsymbol{v}_{-h} \cdot \nabla h + w_{-h} \right) = \frac{Q_0 - Q_{-h}}{\rho C_p}, \end{aligned} \tag{3.1}$$

where molecular diffusion is neglected, h is the time varying water depth, $T_a = 1/h \int_{-h}^{0} T\ dz$ and $\boldsymbol{v_a} = 1/h \int_{-h}^{0} \boldsymbol{v}\ dz$ are depth averaged temperature and horizontal current respectively, $\widehat{T} = T - T_a$ and $\widehat{\boldsymbol{v}} = \boldsymbol{v} - \boldsymbol{v}_a$ are deviations from the depth averaged quantities, w is the vertical current and $\nabla \equiv (\partial/\partial x, \partial/\partial y)$ is the horizontal gradient. Our coordinate system adheres to the estuarine convention with the origin at the head of the Duplin where x is the along channel direction which is positive toward the mouth (South), y is the cross-channel direction, positive to the left of x (East), and z the vertical, which is positive up. The subscript 0 indicates a quantity at the surface and the subscript $-h$ indicates a quantity at the bottom. The vertical heat flux through the water surface is Q_0, the vertical heat flux through the sediment at the bottom is Q_{-h}, ρ is the water density and C_p is the specific heat of sea water, both calculated as a function of temperature and salinity.

Examining the terms of Equation (3.1) in order; on the left hand side the first term, $h\partial T_a/\partial t$, represents the rate of change of the depth integrated storage of heat in the water column and is our primary measured variable in the heat budget. The second term, $h\boldsymbol{v}_a \cdot \nabla T_a$, represents the depth integrated horizontal advective flux of heat past the mooring and is expected to be a major term in the heat budget. The third term, $\nabla \cdot \left(\int_{-h}^{0} \widehat{\boldsymbol{v}}\widehat{T} dz\right)$, represents the horizontal divergence of heat due to depth correlations between the vertical velocity and temperature profiles. The fourth term, $(T_a - T_{-h})(\partial h/\partial t - \boldsymbol{v}_{-h} \cdot \nabla h + w_{-h})$, represents the entrainment of heat across the bottom boundary of the system. The right hand side expresses the exchange at the boundaries where Q_0 is exchange between the water and the atmosphere and Q_{-h} is exchange between the water and the sediment.

The heat entrainment term may be simplified by noting that the no-slip boundary condition at the creek bed requires that the horizontal current at the bed, $\boldsymbol{v}_{-h}$, must be zero and the impermeable boundary condition at the bed requires that the normal velocity at the bed, w_{-h}, must be zero as well.

The atmospheric flux, Q_0, may be decomposed into fluxes caused by incoming solar (shortwave) radiation (Q_{sw}), net outgoing long wave radiation (Q_{lw}), latent heat exchange due to evaporation or condensation (Q_{lat}), sensible heat exchange at the surface (Q_{sen}) and heat exchange due to precipitation (Q_{rain}) (Hsu, 1988). These terms which comprise the net atmospheric heating and cooling term, Q_0, are difficult to measure directly but they may be computed from standard meteorological measurements using a number of bulk formulas as implemented in the MATLAB Air-Sea Toolbox (`www.sea-mat.whoi.edu`) developed by Bob Beardsley and Rich Pawlowicz (see Appendix A for details on the algorithms used).

Heat exchange with the sediment, Q_{-h}, has been shown to be important in rivers (Evans et al., 1998) where it accounted for approximately 15% of the observed energy exchange in a detailed study of the River Blithe, Staffordshire, UK. That study found that the majority of the measured bed heat flux was caused by short wave radiation penetrating the water column to the river bed which overwhelmed long wave radiation from the river bed, heat conduction, vertical convection and advection and frictional heating at the river bed as heat flux terms. Since the high turbidity and generally brown water color of the Duplin act to prevent short wave radiation from reaching the sediment, thus eliminating the dominant potential heating component of this term, we have chosen to neglect it in our calculations.

We can now write a simplified heat budget equation as,

$$h\frac{\partial T_a}{\partial t} + h\boldsymbol{v}_a \cdot \nabla T_a + \nabla \cdot \left(\int_{-h}^{0} \widehat{\boldsymbol{v}}\widehat{T} dz \right) + (T_a - T_{-h}) \left(\frac{\partial h}{\partial t} \right) = \frac{Q_0}{\rho C_p}, \tag{3.2}$$

and test the relative importance of each term. For computational purposes seawater density is calculated using the 1983 UNESCO formulation for the sea surface and the specific heat of sea water from the method of Millero et al. (1973), both as implemented in the MATLAB Air-Sea Toolbox.

3.3 Experimental Program

The first Duplin experiment (DUPLEX I), conducted from August 11 through September 23, 2003, involved physical, chemical and biological oceanographers from the University of Georgia and the Skidaway Institute of Oceanography and was designed to be an intensive study of processes in the Duplin during its most productive time. The physical oceanographic measurements described herein are summarized in Figure 3.1.

Two long term, multi-year, moorings of Seabird Microcat conductivity- temperature-depth (CTD) instruments are maintained in Doboy Sound, at Commodore Island, and in the upper Duplin, at Flume Dock, at the stations designated GCE-6 and 10 respectively, as part of the Georgia Coastal Ecosystems - Long Term Ecological Research (GCE-LTER) project. Data are logged every fifteen minutes and the instruments are rigorously maintained to limit biofouling.

Two Sontek acoustic Doppler profilers (ADPs) were deployed on bottom mount moorings, along with Seabird Microcats at the surface and bottom, at stations labeled DUP01 (at the mouth) and 03 (in the upper reaches). The surface Microcats were, however, not deployed until August 21 (YD 233), ten days after the bottom deployments. Bottom mounted Microcats were deployed at the stations DUP02 (in the lower Duplin) and 04 and 05 (both in the upper Duplin). The Microcats sampled every 12 minutes and the ADPs pinged continuously and logged averaged velocity profiles every 12 minutes.

Two thirteen hour anchor stations were occupied by the R/V Savannah, near DUP01 and 02, on the spring tide of August 14-15 and the neap tide of August 19-20, with hourly water column profiles taken with a Seabird 25 CTD profiler. During the first day of each of these anchor stations the R/V Gannet surveyed along the axis of the Duplin at both high and low water taking water column profiles with a Seabird 19 CTD profiler at the stations marked with an asterisk on Figure 3.1. On the second day the R/V Gannet completed a 13 hour survey of the upper Duplin taking water column profiles with the Seabird 19 CTD profiler at those stations marked with an asterisk on Figure 3.1 which lie between stations DUP02 and 04.

Meteorological data were measured at two locations during this study. The Campbell Scientific automatic weather station at Marsh Landing has been active since February of 2002 and conforms to LTER level two climate data standards, which are described at `http://intranet.lternet.edu/committees/climate/climstan/`. The station auto-harvests data every fifteen minutes and records wind speed and direction at 10 m, air temperature, relative humidity, barometric pressure, total solar radiation and precipitation, quantities that are used in estimating the atmospheric heat flux terms. The National Oceanic and Atmospheric Administration (NOAA) maintains the National Data Buoy Center (NDBC) 41008 buoy which is moored approximately 32 km offshore of Sapelo Island in the Gray's Reef National Marine Sanctuary (31.40 N, 81.87 W). This three meter discus buoy logs meteorological and hydrological measurements every ten minutes including wind speed and direction, taken 5 m

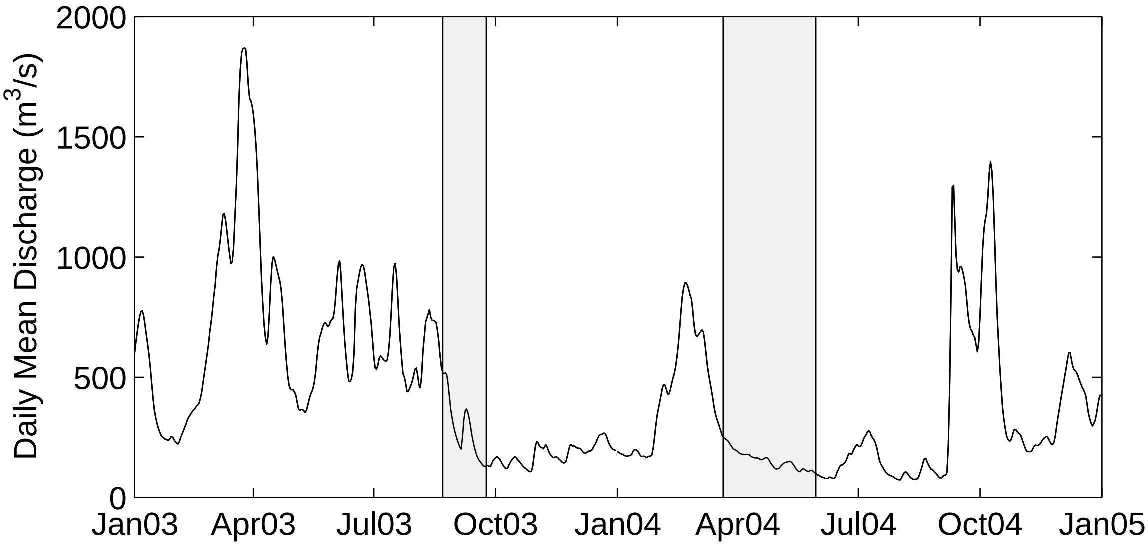

Figure 3.2: Daily mean Altamaha River discharge for the years 2003 and 2004 as measured at the USGS gaging station at Doctorstown, GA. The times of the DUPLEX I (2003) and DUPLEX II (2004) experiments are highlighted.

above sea level, which were used to quantify the estuarine response to coastal meteorological forcing as the Marsh Landing station was somewhat protected from the coastal environment.

A follow up study, designated DUPLEX II, was conducted from March 11 through May 27, 2004. Its purpose was to measure properties in the lower Duplin, around the DUP01 mooring, during the spring warming and when Altamaha River discharge is generally maximal, affecting the salinity and temperature of Doboy Sound as fresh water moves through the Intracoastal Waterway. As it happened river discharge during this study was greatly reduced due to an ongoing drought and was on par with that during the previous study (see Figure 3.2). This study uses data from a bottom mount mooring at DUP01 with an RDI ADCP programmed for 300 s, 2 Hz burst sampling every thirty minutes with Seabird Microcat CTDs at the surface and bottom sampling every 15 minutes.

Daily averaged meteorological measurements were obtained from the Marsh Landing weather station and flow and CTD data were 40 hour low pass filtered in order to study seasonal scale sub-tidal variations. During the period from April 8 through May 14, 2004 no air temperature or humidity data was available from the weather station due to instrument failure. The gap in the temperature record was filled with daily mean air temperature data from the National Weather Service co-op observer on Sapelo Island (Station ID: 097808). No similar backup data was available for humidity so this gap was filled using a linear interpolation of the available data.

The Marsh Landing weather station is located immediately adjacent to the DUP01 mooring site and as such its measurements may be taken as representative of conditions at that mooring. The station is located approximately 10 km from the upper Duplin mooring and that distance can result in some differences in conditions. However Smith (1985) showed that for distances on this scale, accumulated errors in radiation measurement become small over periods greater than three weeks and that the main source of error, differences in wind speed (see Appendix A and Figure A.2), becomes small when the wind is reasonably constant and there is no significant fetch at the remote site. Given that these conditions are met we believe that the Marsh Landing weather data is suitable for both of our mooring sites.

3.4 Results

The Duplin was essentially vertically well mixed for temperature for nearly the entire period of interest in the first Duplin experiment (DUPLEX I) with the exception of weak stratification only during the first two days of the measurements. After YD 235 there was intermittent weak stratification for less than half an hour during slack high and low water with this structure being destroyed once tidal flows recommenced. Because this temperature anomaly only occurred at slack water, when velocities were near zero through the entire water column, $\widehat{\boldsymbol{v}}$ and $\widehat{T}$ were out of phase and thus the third term on the left hand side of (3.2), the heat divergence term, was very small. Similarly the fourth term, the heat entrainment term, was also small since the surface to bottom temperature difference was out of phase with $\partial h/\partial t$ as stratification only occurred at slack water when $\partial h/\partial t = 0$.

Though the temperature profile at the DUP01 mooring is unknown during the period of our experiment hourly temperature profiles were taken in the lower Duplin near the mooring site through one complete tidal cycle on the spring tide of August 14 and the neap tide of August 19 immediately before the beginning of the experiment. These profiles showed low, but measurable, temperature stratification, strongest on the earlier spring tide, around times of slack high and low water with a profile which varied between being linear to being well mixed with an anomaly near the surface. Faced with a lack of measurements of this profile during our period of interest we have chosen to model the water column as two equal layers. While this is likely not physically correct it provides an upper bound to the heat divergence term as more realistic profiles result in a smaller value thus allowing us to state that the divergence term must be equal to or lower than our calculation. Figure 3.3 shows an estimate of the divergence term, separated into along (x) and cross (y) channel components (upper plot), during DUPLEX I made by assuming a two layer water column with properties of the layers given by the surface and bottom temperature sensors and averaged velocities through the layer. The horizontal gradient is estimated by the rate at which the term is advected past the mooring by the depth averaged velocity ($\partial/\partial(x,y) = (-1/(u_a,v_a))\partial/\partial t$).

The heat entrainment term shown in the lower plot of Figure 3.3 is calculated by multiplying the bottom temperature anomaly by the time rate of change of the water column depth. Both the heat divergence and entrainment terms are at least two orders of magnitude less (as will be shown) than the next smallest term in (3.2) and give the appearance of random noise. As such we will neglect both of them.

With these results, (3.2) may be rewritten, after dividing through by water depth, to express the heat budget in a shallow and vertically well mixed estuary as

$$\frac{\partial T_a}{\partial t} + u_a\frac{\partial T_a}{\partial x} + v_a\frac{\partial T_a}{\partial y} = \frac{Q_0}{\rho c_p h}, \tag{3.3}$$

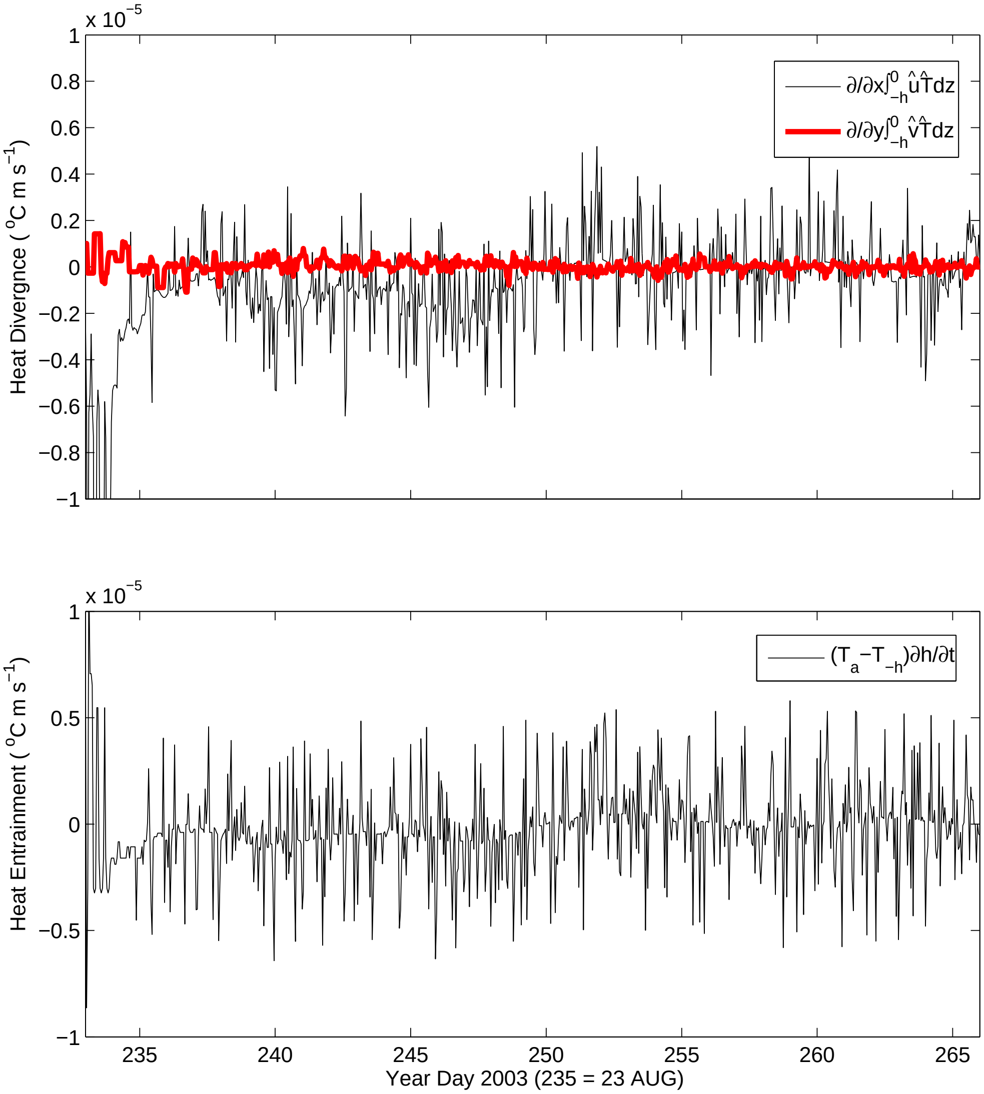

Figure 3.3: Divergence and entrainment of heat from Equation 3.2.

where u_a and v_a are the along and cross channel components of the depth averaged velocity $\boldsymbol{v}_a$ vector.

Lateral heat fluxes, expressed as the advective term $v_a \partial T_a / \partial y$, may result from the interaction between lateral temperature gradients in the main channel with secondary flows due to density gradients (Turrell et al., 1996) and curvature (Chant, 2002) as well as flow on and off the marsh, and through the side creeks, with an associated temperature gradient affected by heating and cooling in the adjacent salt marsh. These fluxes may be a significant factor in the local heat budget. The lateral heat fluxes can not be directly measured with the given instrument configuration but they may be estimated from the residual needed to close (3.3) after atmospheric and along channel advective fluxes have been accounted for.

3.4.1 Duplin River Water Masses

During the first spring and neap tides of the DUPLEX I experiment (August 14-15 (YD 226-227) and 19-20 (YD 231-232), 2003 respectively) extensive CTD profiles were taken along the axis of the Duplin and at anchor stations (see Figure 3.1 for locations identified as ★). Also seven time series moorings of Microcat CTD instruments (some of which were bottom mounted only) were in place (see Figure 3.1 for locations marked as ⧫, ● and ■). Temperature-salinity diagrams (see Figure 3.4) were constructed using these data and separated into upper and lower Duplin to show the structure of the water masses and their mixing characteristics as affected by the spring/neap cycle.

Three distinct water masses are apparent in the Duplin. The lower Duplin water at the bottom right of each T-S diagram is characteristically cool and salty and is influenced by Doboy Sound water advected in on the flood tide and upper/middle Duplin water mixed down on ebb tide. Upper Duplin water, in the top left of each T-S diagram, is warm and fresher reflecting the influence both of greater heating in the shallow upper waters and dilution, presumably due to ground water input into those waters. The middle region, in the vicinity of the vertex in the diagrams, is cool and fresh and shows high variability through the

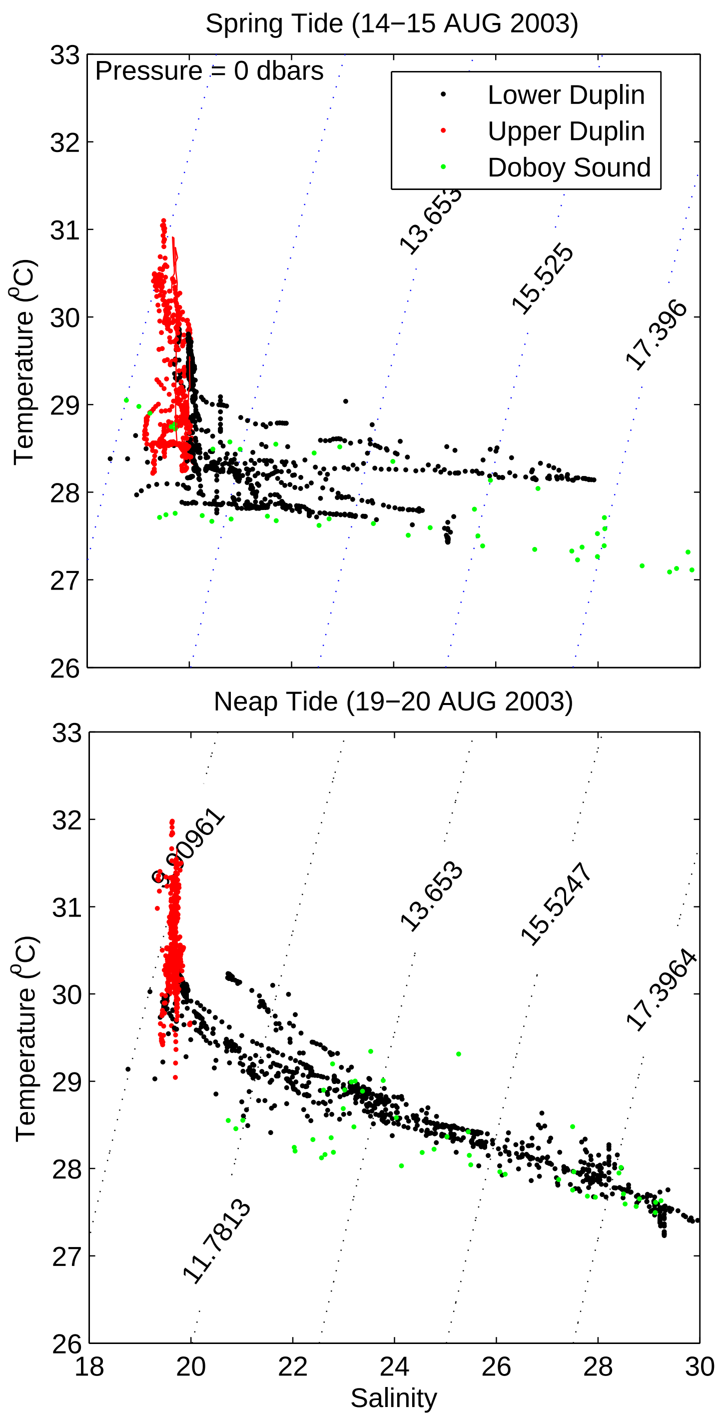

Figure 3.4: Temperature-salinity diagrams for the Duplin River and Doboy Sound at spring and neap tide at the start of the DUPLEX I experiment.

spring/neap cycle indicating the changing nature of the mixing between the water masses, being a time dependent interaction between tidal energy and ground water pumping. On the spring tide the Doboy Sound water mass (shown in green in the upper pane of Figure 3.4) shows a bifurcated pattern as Doboy Sound was warming during the two days of the spring tide survey (see the upper pane of Figure 3.5). The lack of a similar pattern on the neap tide survey indicates that this warming trend had abated.

From these diagrams, two characteristic regions are identified for further investigation: the lower Duplin, which is characterized by easy communication with Doboy Sound and limited tidal creek exchange with the upland marsh; and the upper Duplin, which is isolated from Doboy Sound and the lower Duplin by a winding and sinuous main channel and which is characterized by extensive intertidal marshes and creeks. These masses are sampled by the DUP01 and 03 moorings respectively (indicated as ● on Figure 3.1).

3.4.2 Tidal and Diel Variability (DUPLEX I)

Figure 3.5 shows a time series of temperature and mean (40 hour low pass filtered) depth at CGE6 in Doboy Sound, DUP01 in the lower Duplin and DUP03 in the upper Duplin. It is of note that while the DUPLEX I experiment started on YD 226 the records for DUP01 and 03 do not begin until YD 233 when the surface Microcats were deployed at these stations. Our heat budget analysis is thus limited to the fully instrumented time period after YD 233. All temperature measurements presented for DUP01 and 03 are depth averaged T_a, calculated as a direct average of the surface and bottom Microcat readings.

At all three moorings the water temperature can be seen to be increasing until near YD 248 (September 5) when temperatures drop approximately five degrees and stay low, with reduced tidal and diel variability, until both temperature and variability begin to increase again at all moorings near YD 255. Simultaneously, the mean water depth at all three moorings increases approximately half a meter and stays high for most of the rest of the

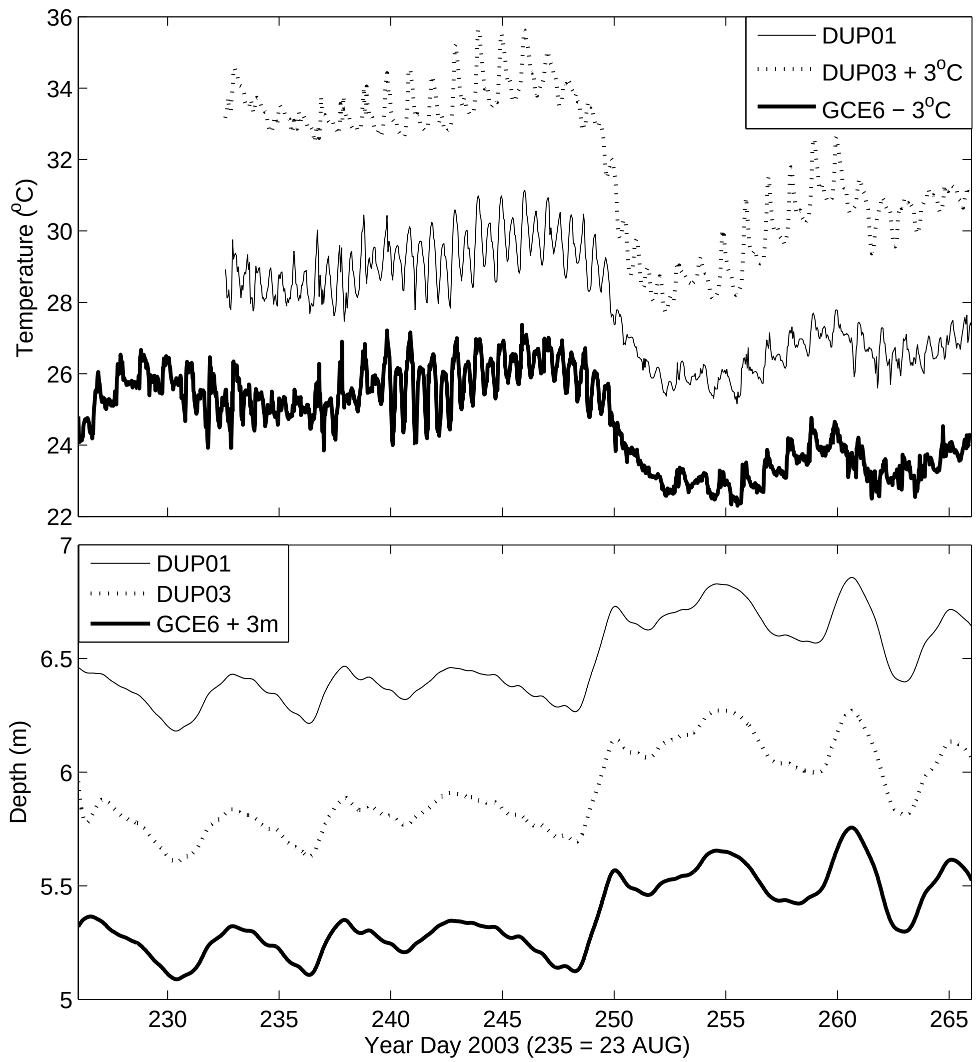

Figure 3.5: Depth averaged water temperature and 40 hour low pass filtered depth at the Doboy Sound (GCE-6), lower Duplin (DUP01) and upper Duplin (DUP03) moorings during the DUPLEX I experiment.

experiment. Close inspection of the temperature record shows a switch from predominately tidal to predominately diel variability between DUP01 and 03.

Plotting the time varying temperature signal at DUP01 and 03 as a variance preserving power spectral density plot (see Figure 3.6) reveals the dominant frequencies affecting the temperature in the Duplin. The temperature in the lower Duplin, at DUP01, is dominated by the primary semi-diurnal lunar (M2) frequency indicating that tidal advection dominates with a secondary peak at the primary solar diurnal (S1) frequency and tertiary peaks associated with higher shallow water tidal harmonics. In the upper Duplin, DUP03, the S1 peak is dominant over the M2, indicating that heating is largely solar in nature, and the shallow water harmonics are more pronounced as befits a region with more extensive intertidal marshes.

Atmospheric Effects and Fluxes in the Main Channel

Figure 3.7 shows meteorological measurements from the Marsh Landing weather station and the NDBC 41008 during DUPLEX I. The top pane shows a comparison between air temperature at Marsh Landing and sea surface temperature at DUP01 where it can be seen that except in the hottest part of the day water temperature is always warmer than air temperature and can be significantly so during the cool of the night. Wind stresses on the ocean surface in the second pane are calculated from wind speed and direction on the shelf as measured by the NDBC 41008 buoy and are plotted as along ($\tau_y = \rho_a C_D v|\boldsymbol{v}|$) and cross ($\tau_x = \rho_a C_D u|\boldsymbol{v}|$) shelf stresses using the air density ρ_a, a drag coefficient C_D and the wind velocity measured at 10 m height. Air density is calculated as a time varying quantity from temperature, relative humidity and atmospheric pressure using the standard CIPM 81/91 formula and has an average value of 1.18 kg/m^3. The drag coefficient is calculated using wind speed and air temperature following the method of Smith (1988) with an average value of 0.0013. Both of these functions are implemented in the Matlab Air-Sea Toolkit. The third pane shows scalar wind speed as measured at the Marsh Landing weather station; strong

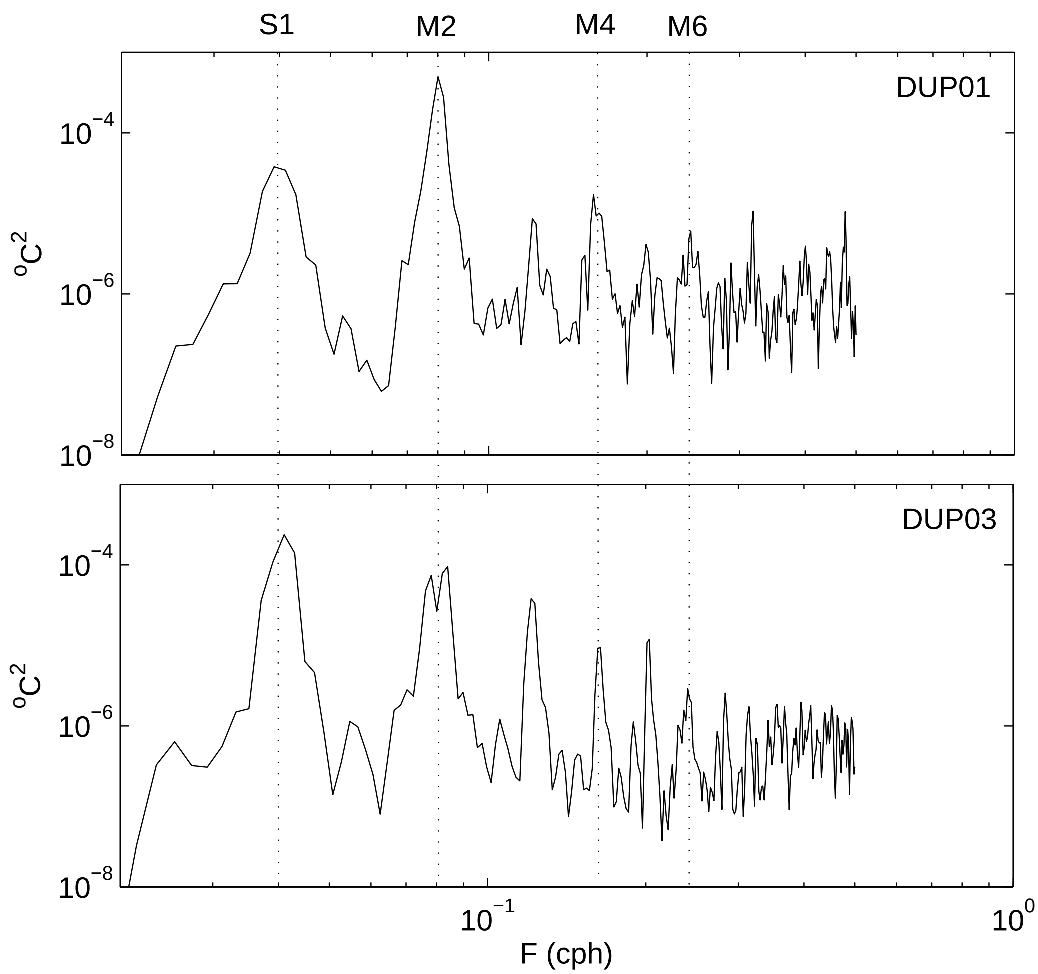

Figure 3.6: Variance preserving power spectral density plot for depth averaged temperature at the lower Duplin (DUP01) and upper Duplin (DUP03) moorings during the DUPLEX I experiment. The major astronomical (S1 and M2) and shallow water harmonic (M4 and M6) frequencies are indicated.

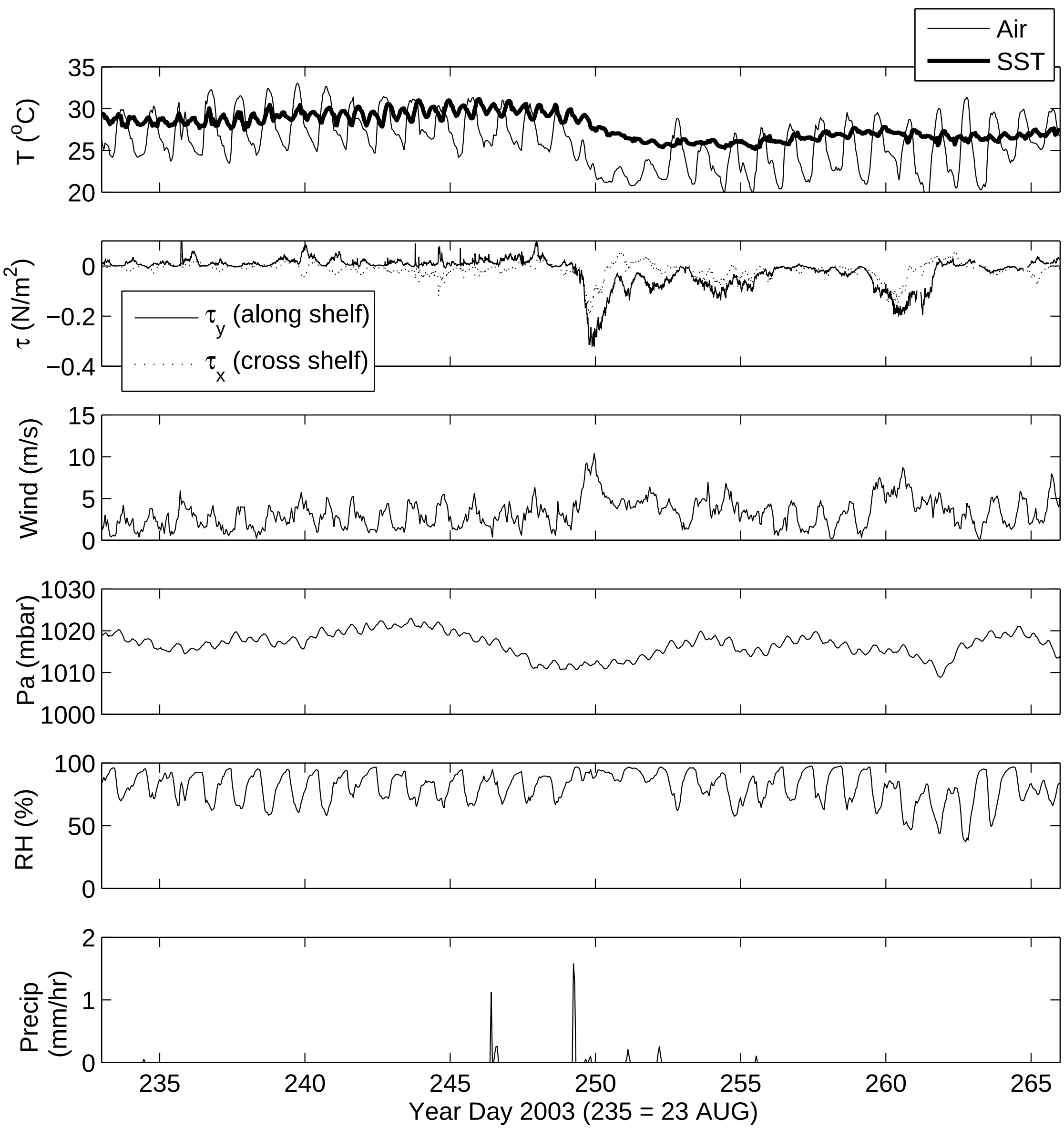

Figure 3.7: Atmospheric and oceanographic measurements from the Marsh Landing weather station showing air and sea surface temperature (from the DUP01 mooring), along (τ_y) and cross (τ_x) shelf surface wind stresses offshore at the NDBC 41008 buoy, inshore diurnal wind speed variations, atmospheric pressure, relative humidity and precipitation during the DUPLEX I experiment.

diurnal variability can be seen here which is associated with the sea breeze. The fourth, fifth and sixth panes show atmospheric pressure, relative humidity and precipitation, respectively, as measured at Marsh Landing.

Near YD 248 a pronounced change can be seen in all measured meteorological variables. Along shelf wind stress (τ_y) changes from a small positive to a large negative value while cross shelf stress (τ_x) stays negative and increases in magnitude. This indicates a change from gentle winds from the southeast to stronger winds from the northeast as the wind swings around and a Nor'Easter begins which induces Ekman transport onshore. Simultaneously, the wind speed at Marsh Landing increases as does humidity and precipitation while air and water temperature fall and barometric pressure is low. This Nor'Easter causes downwelling conditions on the coast which forces oceanic water inshore, which can be seen in Figure 3.5 as both a reduction in water temperature and an increase in mean water depth. Over the 10 km distance of the Duplin, the response is simultaneous throughout the domain as no time lags are measured from the mean water depth. After the Nor'Easter event the offshore winds calm but continue from the northeast showing the annual switch in the regional wind climatology from summer conditions to what has been designated as Mariner's Fall (Blanton et al., 1985). A similar, though smaller, event occurs again around YD 260 as northeasterly winds again increase and are associated with another increase in mean water depth and drop in water temperature.

Atmospheric heat fluxes into the Duplin were calculated using the bulk formulas implemented in the Air-Sea Toolbox and are shown in Figure 3.8. The top pane shows the short wave heat flux due to total solar radiation (Q_{sw}) that is the dominant atmospheric source term. The second pane shows the net long wave heat flux (Q_{lw}) due to reradiation. The latent heat flux (Q_{lat}) due to evaporation, which is primarily dependent on wind speed and humidity, is shown in the third pane and represents the largest heat loss term. The sensible heat flux (Q_{sens}), primarily dependent on wind speed and the air-sea temperature difference, is shown in the fourth pane. The fifth pane shows the minor cooling heat flux due to pre-

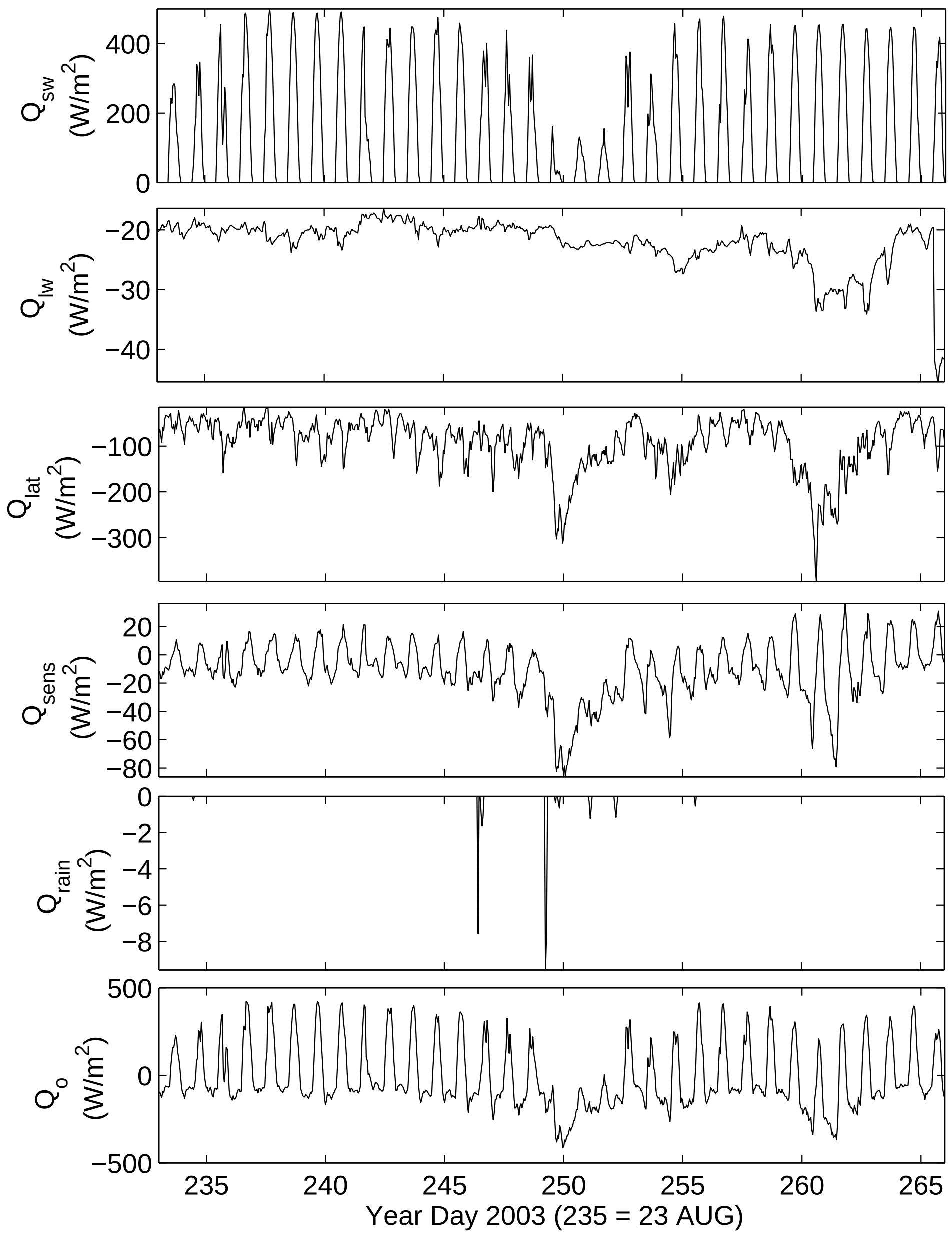

Figure 3.8: Calculated atmospheric heat fluxes at the Marsh Landing weather station comprising short wave, long wave, latent heat, sensible heat and rain heat fluxes into the water column during the DUPLEX I experiment. Net heating and cooling is shown as Q_0 in the bottom pane.

cipitation (Q_{rain}). The bottom pane then shows the net atmospheric heat flux (Q_0) for the Duplin. This net atmospheric heat flux switches sign between a net heat gain during the day and a smaller net loss at night with strong increases in heat flux out of the water column tied to the storm events starting on YD 248 and YD 260.

Heat Budgets

Figures 3.9 and 3.10 show the calculated heat budgets for the DUP01 and 03 moorings respectively. The uppermost pane in each figure shows the rate of heat storage, $\partial T_a/\partial t$, calculated as the time derivative of the depth averaged temperature signal. The second pane shows the along channel temperature gradient, $\partial T_a/\partial x$, calculated by approximating along channel advection as $\partial T_a/\partial x = (-1/u_a)\partial T_a/\partial t$. The heavy line shows the residual after a 40 hour low pass filter has been applied to eliminate the short period fluctuations due to tidal processes, cross channel processes and marsh interactions. With this is plotted the depth averaged along channel flow (u_a) with positive values corresponding to the ebb flow.

The instantaneous along channel temperature gradient in the Duplin is the sum of the residual temperature gradient due to the tidal dispersion of heat combined with the influence of the higher frequency heat fluxes due to atmospheric heating and marsh interactions. The direct computation of the heat gradient from the one dimensional advection of heat past the mooring will, as a matter of course, close the heat budget due to its inclusion of advective, solar and cross-channel effects in one term. Filtering with a 40 h low pass filter removes the higher frequency heating associated with solar and tidal inputs leaving only the tidally averaged gradient due to long term tidal dispersion. This residual gradient, multiplied by the tidal velocity, accounts for the along channel tidal advection of heat. The residual needed to close the heat budget accounts for both the atmospheric and lateral heat fluxes. As the direct atmospheric fluxes in the main channel may be calculated from meteorological measurements they can be removed leaving the residual to account mainly for cross-channel processes and marsh interactions.

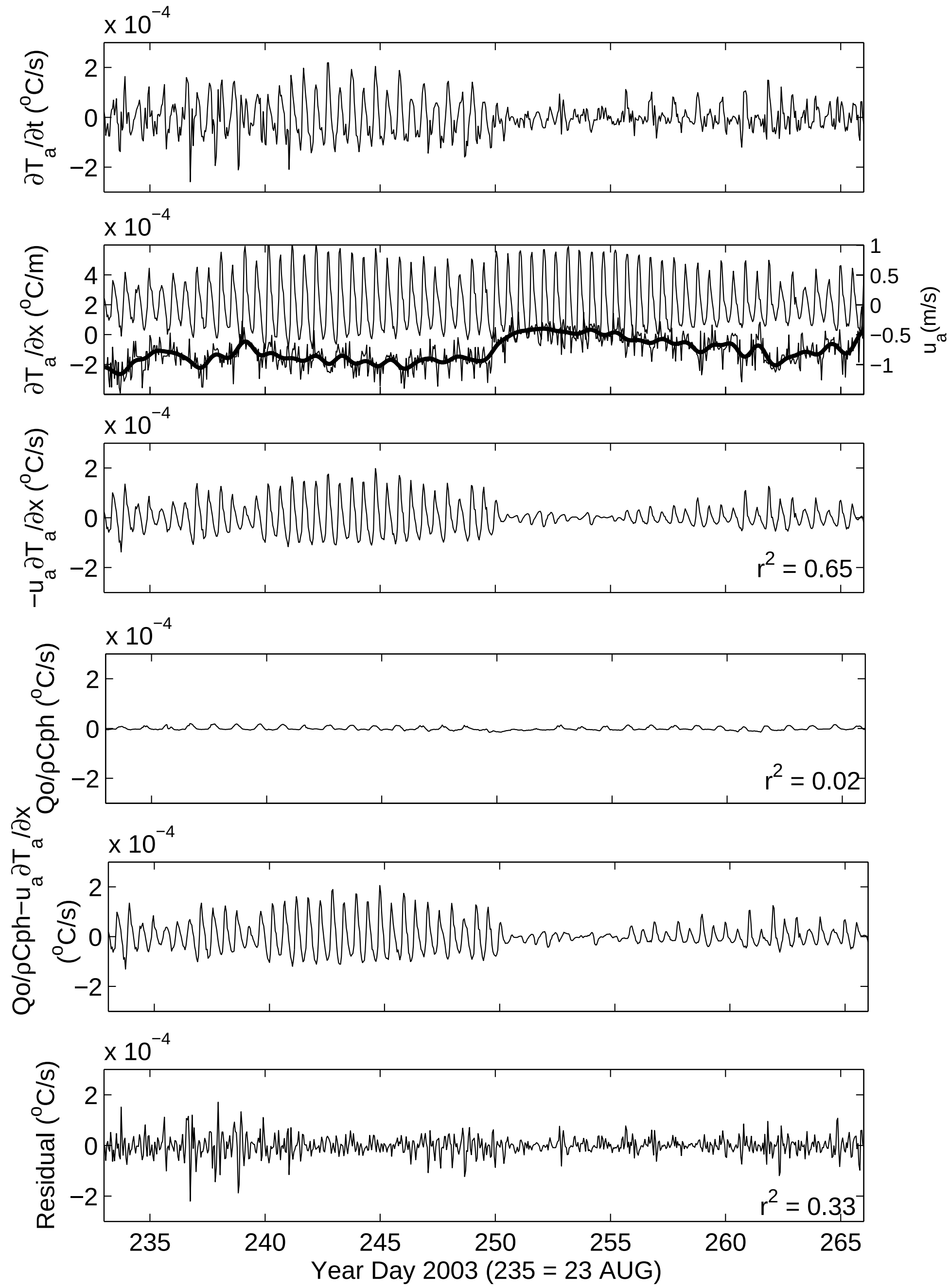

Figure 3.9: Heat storage components at the lower Duplin (DUP01) mooring during the DUPLEX I experiment showing the measured heat storage along with advective and atmospheric fluxes and the unmeasured residual. r^2 values show the percentage of the measured storage attributable to each term.

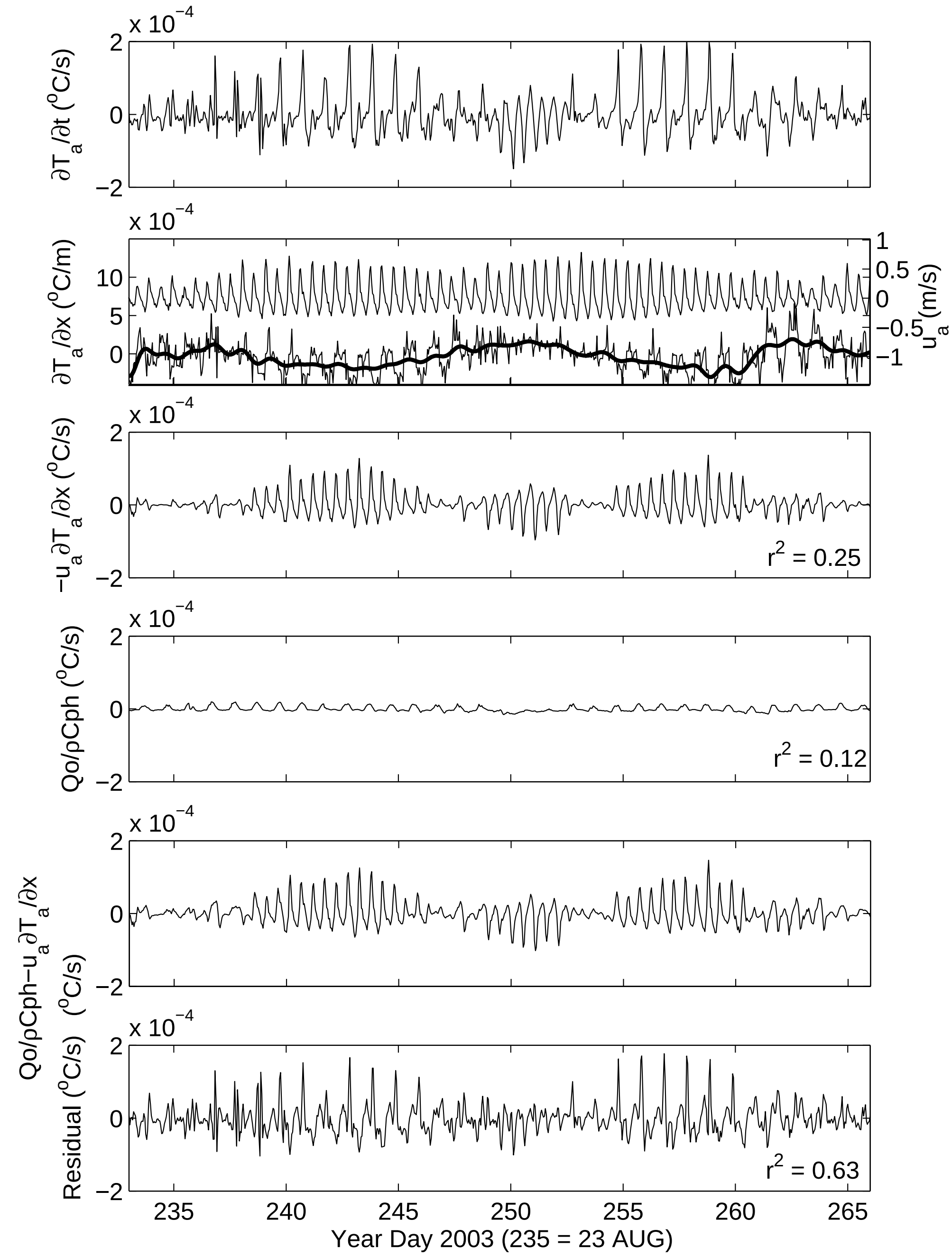

Figure 3.10: Heat storage components at the upper Duplin (DUP03) mooring during the DUPLEX I experiment showing the measured heat storage along with advective and atmospheric fluxes and the unmeasured residual. r^2 values show the percentage of the measured storage attributable to each term.

As expected, tidal velocities are greatest at the lower mooring (Dup01, shown in Figure 3.9) decreasing upstream in the shallower and more sinuous region of the Duplin (DUP03, shown in Figure 3.10). Both moorings show the pronounced ebb dominance of flow that is a common characteristic of this class of salt marsh estuary (Dronkers, 1986; Dyer, 1997; Blanton et al., 2002). Multiplying the low passed temperature gradient by the tidal velocity yields the along channel advective heat transport term, $-u_a \partial T_a / \partial x$, which is shown in the third pane. Dividing the Q_0 term from Figure 3.8 by the density, specific heat and depth of the water gives the total atmospheric heat input to the water column as shown in the fourth pane. The fifth pane then shows the rate of heat storage attributable to the sum of the along channel advective and atmospheric terms and the bottom pane shows the residual between this predicted storage rate and the actual rate as calculated from the temperature record. This residual contains terms which account for lateral advection of heat, neglected temperature shear terms and instrument noise.

Linear least squares regression analysis was performed comparing the advective, atmospheric and residual heat budget terms, in turn, to the measured heat storage to compute an r^2 value which expresses the percentage of the measured signal which is accounted for by each individual component. For this work, r^2 is considered as the multiple coefficient of determination defined as one minus the fraction of variance unexplained (FVU) such that

$$r^2 = 1 - \frac{SSerr}{SStot} \tag{3.4}$$

where

$$SSerr = \sum_i (y_i - f_i)^2 \tag{3.5}$$

$$SStot = \sum_i (y_i - \overline{y})^2 \tag{3.6}$$

where y is the observed signal and f the calculated signal. SSerr is the sum of the square of the errors and SStot the total sum of the squares, which is proportional to the signal variance (Mendenhall and Sincich, 1994). The r^2 value relates the fraction of the observed variance in heat storage which can be explained by the calculated heat flux component.

Figure 3.9 shows the r^2 analysis of the individual heating components against the measured heat storage. Tidal advection of the along channel temperature gradient dominates, accounting for 65% of observed heat in the lower Duplin. Direct atmospheric fluxes only account for 2% of the observed storage leaving 33% to be accounted for by unmeasured processes including marsh interactions, vertical temperature shear, ground water cooling and instrument noise.

The heat budget in the upper Duplin, at the DUP03 mooring, is shown in Figure 3.10. Here the influence of along channel tidal advection has decreased to 25%, reflecting the decreased tidal velocity, while direct atmospheric input has increased six fold to 12%. Unmeasured influences have increased nearly two fold to account for 63% of the observed temperature storage. This is expected as the DUP03 mooring is in a narrower channel and is bordered by much more extensive intertidal salt marshes and side creeks than is DUP01. While apparently direct tidal semi-diurnal heating is still twice as important as direct solar diurnal heating there is strong diurnal signal contained in the residual heating component which compensates for this and explains the dominance of the S1 signal in Figure 3.6.

Lateral Gradients

Previous work in 2003 and 2006 involving cross channel surveys of the Duplin with a towed CTD (upper and lower Duplin) and downward looking ADCP (upper Duplin) and moored Microcat CTDs (upper Duplin) has shown there to be very little cross channel variation in salinity or along channel flow and a low, but measurable, cross channel difference in temperature. The lack of a cross channel salinity gradient paired with a low cross channel temperature gradient reduces density driven cross channel secondary circulation to near zero but cross-channel barotropic pressure gradients may be important. The choice of mooring locations in areas of no curvature results in low cross channel secondary flows due to morphology and the scale of the Duplin is such that the Coriolis effect is not significant. While it is difficult to measure either the temperature gradient or the flow in the intertidal marsh proper, a follow up experiment in the summer of 2006 used two surface deployed Microcat CTDs to measure the temperature gradient between the main channel of the Duplin near the DUP03 mooring site and a location 250 meters up a small side creek, which cuts through the intertidal marsh, during the period from July 31 to August 29. The measured temperature gradient through this creek fluctuated on both tidal and subtidal time scales between ± 0.006 °C/m.

Assuming that the residuals shown in Figures 3.9 and 3.10 are dominated by lateral heat fluxes, as opposed to the presumably much smaller neglected shear terms from Equation (3.1), ground water cooling and instrument noise, an approximate cross channel temperature gradient, $\partial T_a/\partial y$, can be calculated by dividing the residual term by the depth averaged cross channel velocity, v_a. This is shown in Figure 3.11 for DUP01 and 03. The top panes show the depth averaged cross channel velocity at each mooring, notable here is the change seen in each plot at the start of the downwelling event around YD 248 with cross channel flows increasing at the lower mooring and simultaneously decreasing at the upper mooring both of which may be associated with a change in the percent inundation of the intertidal marsh with the change in mean water depth in the Duplin.

The calculated temperature gradient, which represents an average of the gradient through the marsh proper, the small side creeks and channels and across the main channel, varies on both tidal and subtidal scales generally between ± 0.002 - 0.005 °C/m. This is less than, but on the same order as, the measurement from 2006 indicating that the creeks are the more preferred path for heat fluxes as compared to the marsh itself.

3.4.3 Subtidal Variability (DUPLEX II)

Figure 3.12 shows 40 hour low pass filtered hydrographic measurements at DUP01 during the DUPLEX II experiment, which was designed to capture the spring warming during 2004. In the top pane a steady warming trend can be observed with water temperatures increasing from 17 to 27 °C over the duration of the experiment. In the bottom pane we can see fluctuations in the residual water depth.

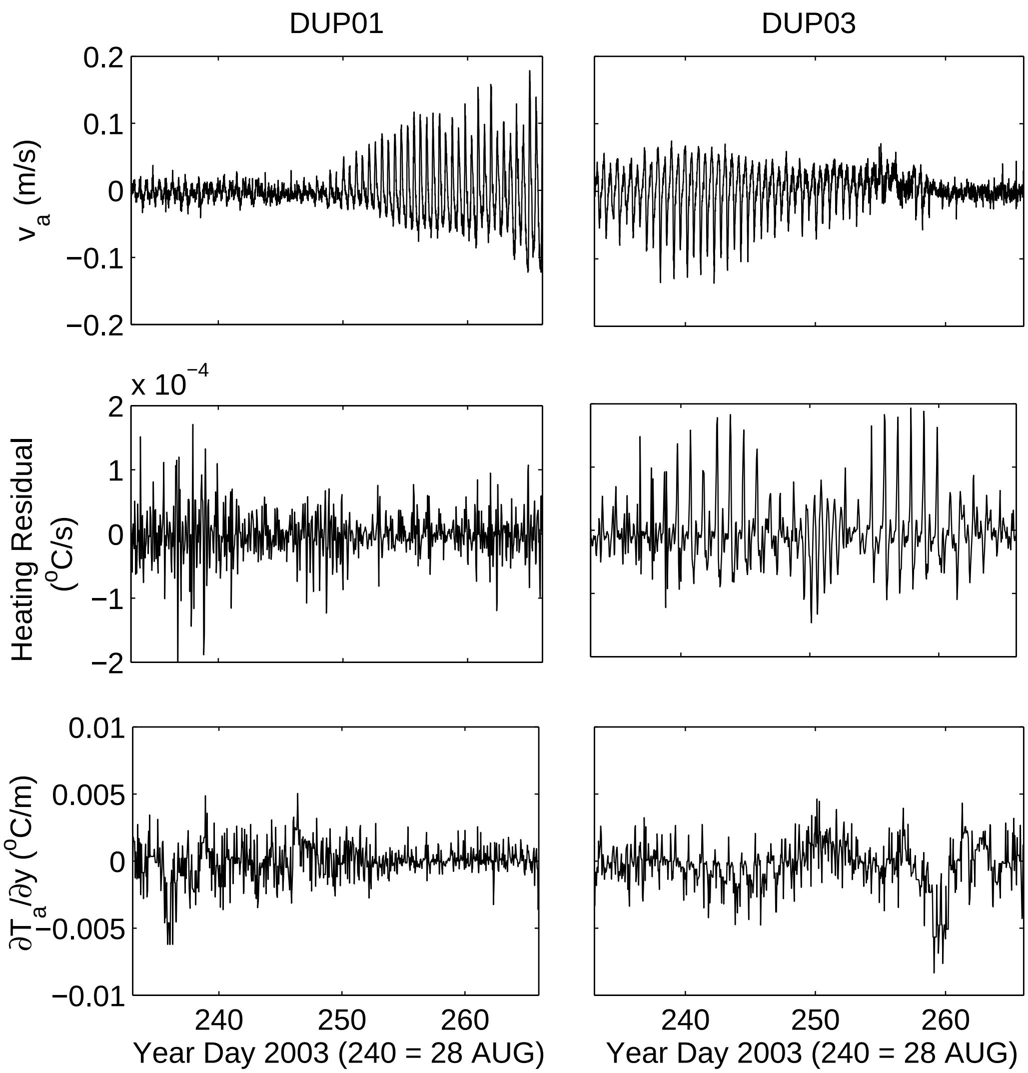

Figure 3.11: Depth averaged cross channel velocities at the lower Duplin (DUP01) and upper Duplin (DUP03) moorings during the DUPLEX I experiment. Heating residuals from figures 3.9 and 3.10 and the mean cross channel temperature gradient.

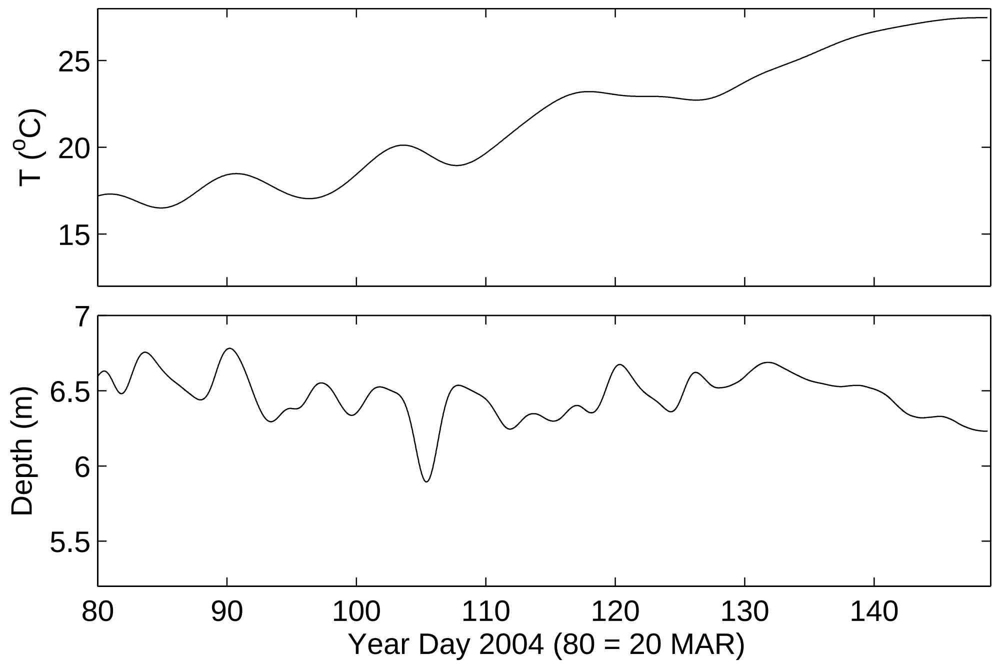

Figure 3.12: 40 hour low pass filtered water temperature and depth at the lower Duplin (DUP01) mooring during the DUPLEX II experiment.

Daily averaged meteorological measurements from the Marsh Landing weather station are shown in Figure 3.13. In the top pane it can be seen that mean water temperature is generally warmer than mean air temperature during the entire experiment. Daily averaged winds measured at the Marsh Landing weather station, in the second pane, are generally less than 5 m/s except around YD 105 when they increase to 10 m/s and accompany a short lived 0.5 m drop in mean sea surface height. A drop in mean barometric pressure prior to this indicates the passing of a storm system. There is a significant gap in the humidity data in pane four due to an instrument failure on the Marsh Landing weather station. For computational purposes this has been filled with a simple linear interpolation of the available data. Daily total precipitation is shown in the bottom pane. Off shore wind stress

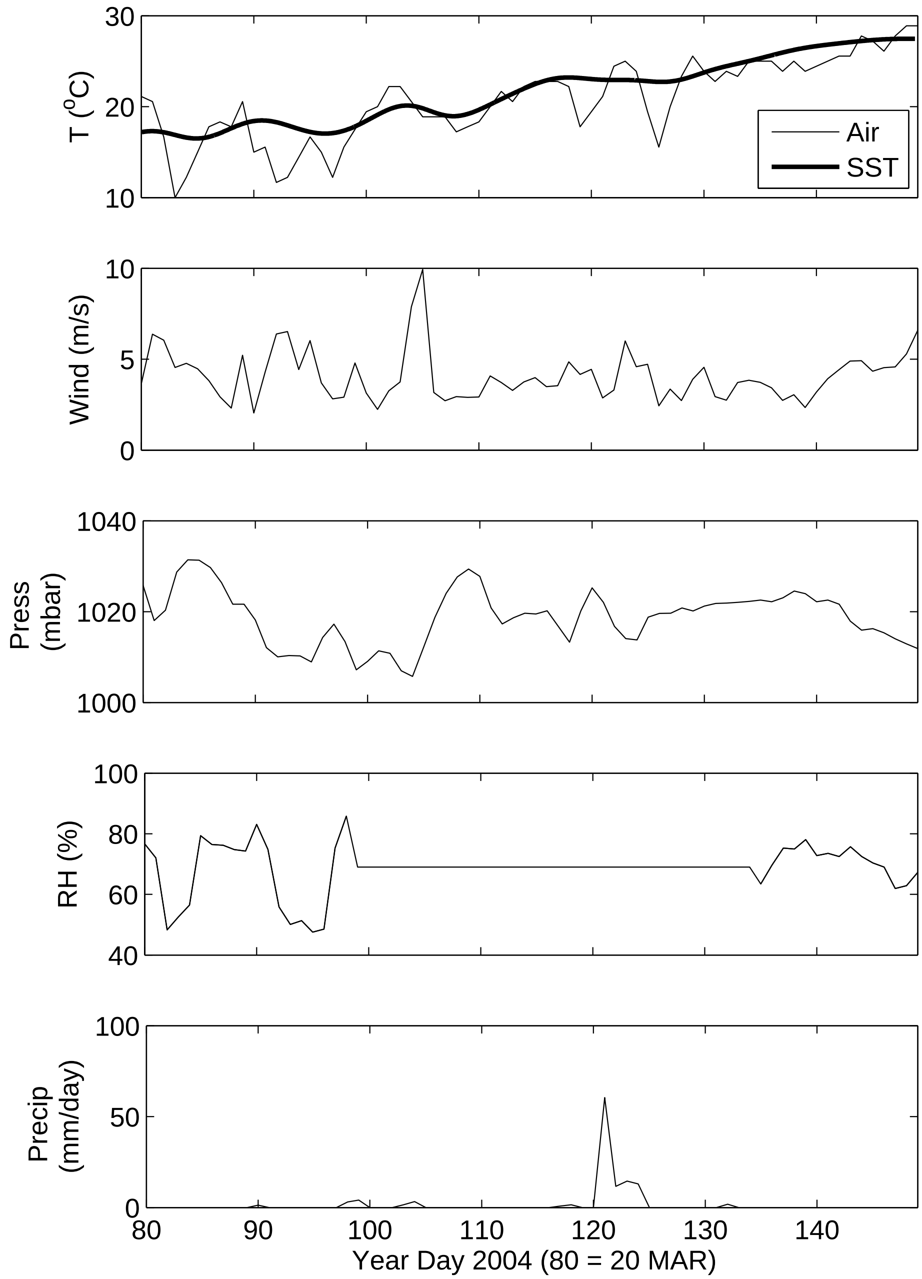

Figure 3.13: Daily averaged atmospheric (from the Marsh Landing weather station) and oceanographic (from the DUP01 mooring) measurements showing air and sea surface temperature, wind speed, atmospheric pressure, relative humidity and precipitation during the DUPLEX II experiment.

is not reported since there was no sustained up or down welling event as there was during the DUPLEX I experiment.

Figure 3.14 shows the computed daily averaged atmospheric heat fluxes which are dominated, as they were on an hourly time scale during DUPLEX I (see Figure 3.8), by short wave radiation as the major source term and latent heat as the major loss term, though during this period latent heat out is generally greater than short wave heat in. The net atmospheric heat flux is a loss during the first half of the experiment becoming neutral during the second half.

Constructing a daily averaged heat budget from the atmospheric and advective fluxes (see Figure 3.15) we show that residual tidal advection of heat accounts for 45% of the observed daily averaged heat storage while atmospheric fluxes account for 21% leaving 34% to be accounted for by unmeasured processes, which is approximately the same percentage as seen in the hourly scale budget at the same location during Duplex I (see Figure 3.8). As the residual of the cross channel velocity is negligibly small no estimate can be made of the cross channel temperature gradient for this deployment.

3.5 Discussion and Conclusions

The temperature-salinity diagrams and the heat budgets constructed for the Duplin River show a pronounced change in characteristics between the lower Duplin and the upper Duplin. The lower Duplin is characterized as having easy communication with Doboy Sound and relatively fewer side creeks carrying water through the upland marsh. The upper Duplin is somewhat isolated by the sinuous nature of the main channel and is surrounded by an extensive network of side creeks which flood and drain the marsh. The lower Duplin is also dominated by tidal processes with cool, salty water being brought in on each flood tide thus temporarily suppressing the along channel temperature gradient and mixing cool water up the channel. Short period temperature cycles are predominately at M2 tidal frequencies. In contrast, the upper Duplin is fresher and warmer reflecting the influence, presumably, of

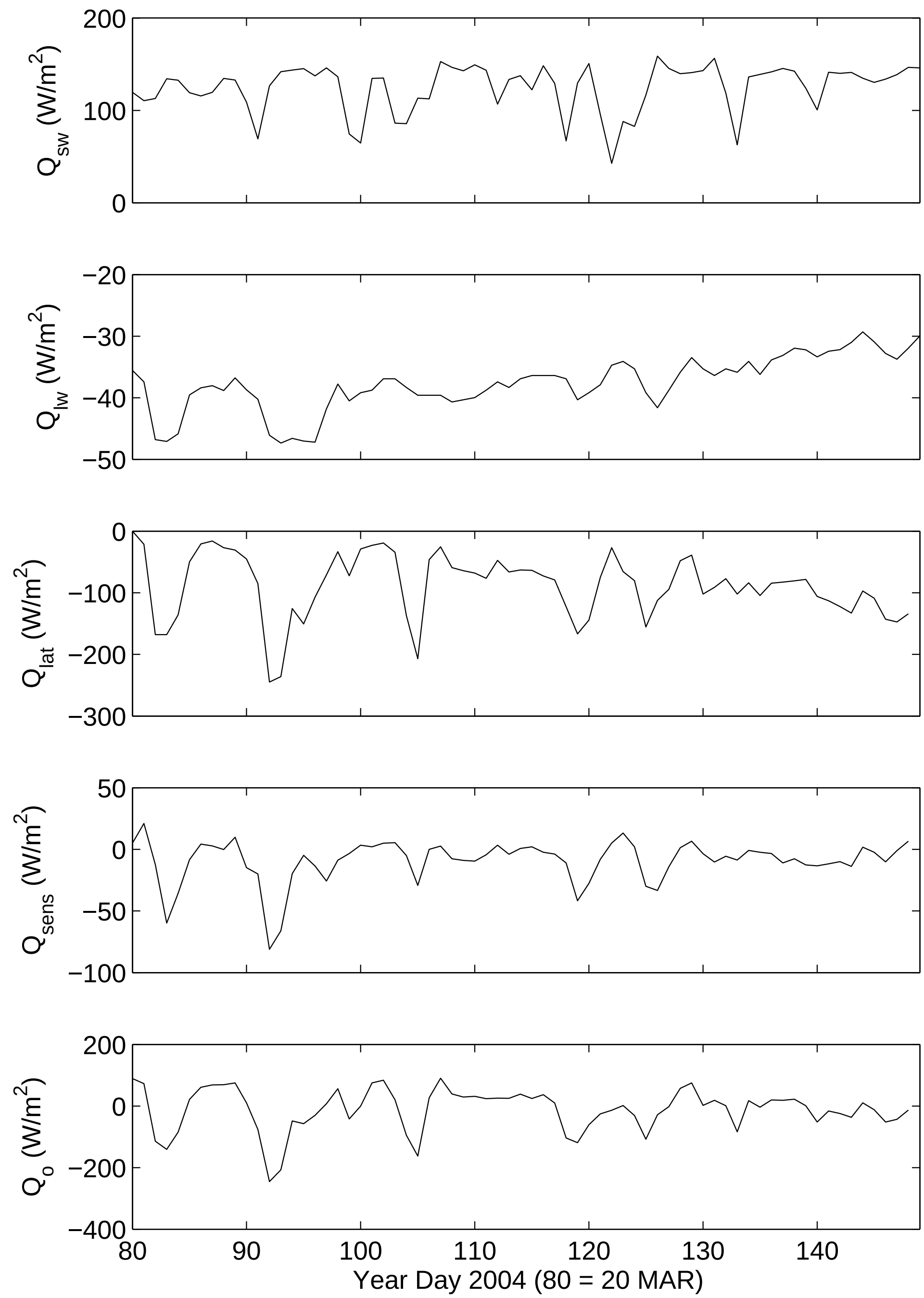

Figure 3.14: Calculated daily averaged atmospheric flux terms at the Marsh Landing weather station including shortwave, long wave, latent heat, sensible heat and rain heat fluxes into the water column during the DUPLEX II experiment. Net heating and cooling is shown as Q_0 in the bottom pane.

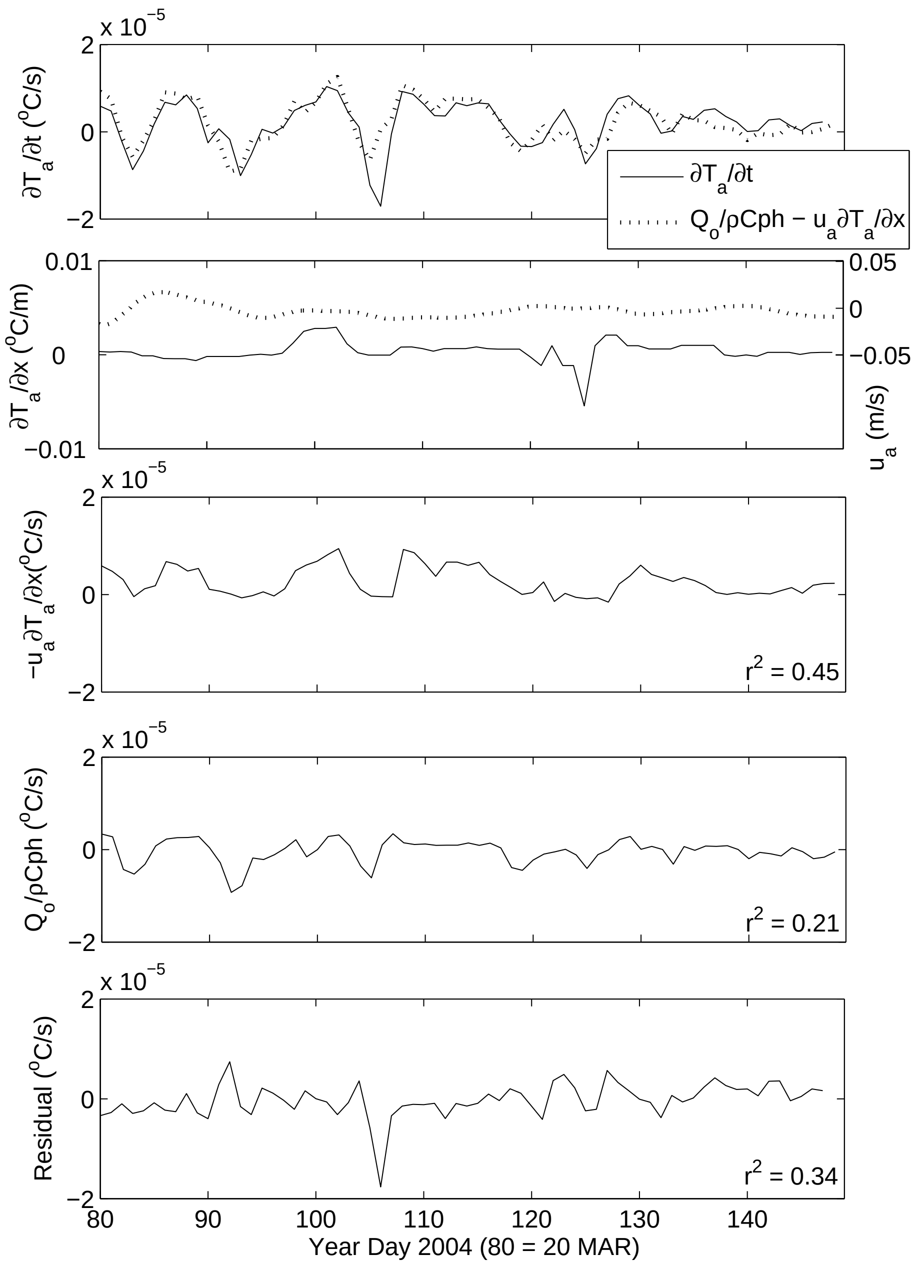

Figure 3.15: Daily averaged heat storage components at the lower Duplin (DUP01) mooring during the DUPLEX II experiment showing the measured heat storage along with advective and atmospheric fluxes and the unmeasured residual. r^2 values show the percentage of the measured storage attributable to each term.

ground water input (Ragotzkie and Bryson, 1955), the shallow nature of these waters and the greater extent of intertidal marshes and side creeks. It is isolated from the lower Duplin which attenuates the semi- diurnal tidal temperature signal and allows it to be overwhelmed by the diel S1 solar frequency temperature signal. This is in agreement with the observations of Hoguane et al. (1999) who described a similar transition between M2 and S1 temperature cycles in a mangrove swamp in Mozambique where part of the swamp was similarly isolated from direct tidal influences by a sill.

The boundaries of the lower and upper Duplin waters define the range of a third identified water mass in the middle Duplin which is strongly controlled by the fortnightly spring/neap cycle. On spring tide cool and salty water from Doboy Sound mixes in vigorously suppressing the along channel temperature gradient in the lower Duplin. At the same time the increased hydraulic head due to the large tidal range presumably pumps greater amounts of ground water out of the aquifer allowing fresh water to mix far down into the lower Duplin. On neap tide the decreased tidal energy mixes Doboy Sound water with that of the Duplin less vigorously thus allowing an along channel temperature gradient to be established further down the Duplin. Simultaneously less ground water is pumped into the system allowing higher salinity water to penetrate further into the Duplin. The middle water mass is strongly controlled by both the dilution and the cooling associated with ground water fluxes and its characteristics vary greatly between spring and neap tides.

Tidal advection of heat is a major factor in both the lower and upper Duplin accounting for 65% of the observed heat storage in the tidally dominated lower Duplin and a still significant 25% in the more isolated upper Duplin. The attenuation of tidal velocities in the upper Duplin combined with the inability of cool Doboy Sound water to penetrate that far serve to reduce the tidal variability in the upper waters but the strong along channel temperature gradient caused by the combination of increasingly shallow waters toward the head of the creek and the increase in the extent of intertidal marshes works to maintain a significant tidal signal even in these waters.

Direct atmospheric fluxes into the main channel play a minor role in controlling the temperature cycle in the Duplin accounting for a mere 2% of the observed temperature storage in the lower Duplin (see Figure 3.9) and 12% in the upper Duplin. However the presence of a strong S1 solar component in the temperature signal in the upper, and to a lesser extent the lower, Duplin shows that solar and atmospheric heat fluxes do play a major role in the Duplin heat budget through the diel heating and cooling of both the intertidal marsh and the shallow side creeks which cuts through it.

Synoptic scale meteorological events can play a strong role in determining water mass characteristics. Cooling due to precipitation, the attenuation of direct solar radiation and the increase in local winds associated with storm events can affect water temperature on an event time scale. Changes in offshore winds related to storm events and offshore wind climatology (Blanton et al., 1985), which are associated with upwelling or downwelling conditions, can affect temperature and water depth on even longer time scales.

The residual term needed to close the heat budget once tidal advective and direct atmospheric fluxes in the main channel are accounted for indicates the importance of the unmeasured or neglected terms in the heat budget equation. The largest of these terms is due to the lateral advection of heat across the side boundaries of the creek and into and out of the marsh and side creeks. Due to their shallow nature the small side creeks experience greater diel heating and cooling due to atmospheric heat fluxes than does the water in the main channel. This establishes a lateral temperature gradient, which interacts with tidal flows to transport heat into and out of the main channel of the Duplin at tidal frequencies. Similarly the vegetated mud flats of the intertidal marshes are subject to atmospheric heating and cooling when drained. Heat is then exchanged with the overlying water when the marsh is flooded, while it is also subject to atmospheric heat fluxes, and is mixed into both the main channel and the side creeks when the marsh drains (see, for example, Harrison and Phzacklea, 1985; Vugts and Zimmerman, 1985). This lateral heat transfer shows up in the main channel temperature signal at frequencies reflecting the solar, tidal semi-diurnal and higher order tidal harmonic frequencies. A strong spring/neap signal may be observed as well, reflecting the fortnightly modulation of tidal flows and of the percent inundation of the marsh at high tide, with spring high tides flooding the marsh for longer and with more water.

Approximate cross channel temperature gradients are computed based on a residual which agree fairly well with the limited data which exist quantifying this gradient. This lateral advection constitutes a very significant, though unmeasured, source of heat which accounts for 63% of the observed heat storage in the upper Duplin, where there are more extensive marshes and side creeks, and a still significant 33% in the lower Duplin which is bordered by more marsh hammocks, creekless upland marsh and mud flats along the channel sides. As the entire Duplin region is subject to similar atmospheric forcing the difference in both the percent contribution of these cross channel fluxes and, more importantly, of the magnitude of the signal itself is an indication of the relative ease with which a scalar quantity, which accumulates in the marsh, can be transferred to the main channel by tidal flows.

In addition to heat the intertidal marsh can also act as a source of sediment, carbon and other nutrients which enter the main channel through similar processes tied to tidal flows through the side creeks and the inundation and draining of the marsh (see, for example, Wolaver and Spurrier, 1988; Childers and Day, 1990a,b). On entering the main channel of the Duplin these substances and nutrients are advected and dispersed through the system by the same processes which largely control heat resulting in a similar zonation in the Duplin (Hanson and Snyder, 1980). Thus by observing the relative importance of the lateral advection of heat to the main channel temperature budget one can develop an understanding of the relative importance of the marsh in supplying sediment, carbon and other biogeochemical tracers to the main channel as well as their likely distribution along the channel. As the marsh appears fairly uniformly vegetated along the axis of the Duplin differences in export from the marsh to the main channel are likely to be due more to changes in morphology than in production and thus, like heat which is input into the marsh fairly evenly in all areas, sediment and nutrient fluxes from the marsh to the main channel will be controlled mainly by the prevalence of side creeks and the percent inundation of the marsh at high tide and should show similar geographic and temporal distributions.

Observing the heat budget on a tidally averaged scale to eliminate short period fluctuations and concentrate on seasonal processes reveals that direct atmospheric input is significantly more important in determining long term temperature trends in the lower Duplin. This effect accounts for 21% of the observed daily averaged heat storage in the lower Duplin during the 2004 spring warming with a concomitant decrease in the importance of residual along channel advection of heat. Interestingly the amount of heat storage attributable to unmeasured, and presumably lateral, processes was largely unchanged despite the change in both season and time scale.

The importance of lateral processes and marsh/creek interactions to the heat budget, on both hourly and seasonal scales, demonstrates the high importance of these intertidal areas in maintaining the physical, and by analogy the biogeochemical, characteristics of this class of marsh creek which serve as important conduits for the export of carbon (Cai et al., 2003; Wang and Cai, 2004) and other chemical signals to the coastal ocean as well as serving as habitat for, especially the larval stage, of many species. This has implications for coastal zone management and planning as the development of, or restriction of flow onto and off of, salt marshes and small tidal creeks could have a large impact on conditions in these tidal creeks and thus on export to the sounds and ultimately to the ocean.

3.6 Acknowledgments

This work was supported by the NSF (OCE-9982133) as part of the Georgia Coastal Ecosystems - Long Term Ecological Research (GCE-LTER) project (`http://gce-lter.marsci.uga.edu`). We are thankful to Dr. Jackson Blanton who played a critical role in the design of the Duplex I experiment. Thanks also go to the captains and crew of the R/V Savannah and R/V Spartina for their assistance in deploying and recovering moorings, to Julie Amft and Trent Moore of the Skidaway Institute of Oceanography for their assistance with the instrumentation and along channel surveys, to Ken Helm of the UGA Marine Institute for his assistance in maintaining the GCE moorings and to Dr. David Stooksbury and Dr. Pam Knox in the Office of the State Climatologist of Georgia for their assistance in locating and providing meteorological data from the Sapelo Island NWS co-op weather station. Finally we are grateful for the comments of two anonymous reviewers whose suggestions have contributed greatly to this paper.

Bibliography

Ayers, J. (1965). A late summer heat budget of Barnstable Harbor, Massachusetts. *Limnology and Oceanography*, 10:9–14.

Bernard, R., Davies, B., and Hodgson, A. (1988). Reproduction in a brackish-water mytilid: gametogenesis and embryonic development. *The Veliger*, 30:278–290.

Blanton, J., Lin, G., and Elston, S. (2002). Tidal current asymmetry in shallow estuaries and tidal creeks. *Continental Shelf Research*, 22:1731–1743.

Blanton, J., Schwing, F., Weber, A., Pietrafesa, L., and Hayes, D. (1985). Wind stress climatology in the South Atlantic Bight. In Atkinson, L., Menzel, D., and Bush, K., editors, *Oceanography of the Southeastern U.S. Continental Shelf*, pages 10–22. American Geophysical Union.

Boesch, D. and Turner, E. (1984). Dependence of fishery species on salt marshes: The role of food and refuge. *Estuaries*, 17(4):460–468.

Cai, W.-J., Wang, Z., and Wang, Y. (2003). The role of marsh-dominated heterotrophic continental margins in transport of CO2 between the atmosphere, the land-sea interface and the ocean. *Geophysical Research Letters*, 30(16):1849–1853.

Chant, R. (2002). Secondary circulation in a region of flow curvature: Relationship with tidal forcing and river discharge. *Journal of Geophysical Research*, 107(C9):3131–3142.

Childers, D. and Day, J. (1990a). Marsh-water column interactions in two Louisiana estuaries, I. Sediment dynamics. *Estuaries*, 13(4):393–403.

Childers, D. and Day, J. (1990b). Marsh-water column interactions in two Louisiana estuaries, II. Nutrient dynamics. *Estuaries*, 13(4):404–417.

Crabtree, S. and Kjerfve, B. (1978). Radiation balance over a salt marsh. *Boundary-Layer Meteorology*, 14:59–66.

Dai, T. and Wiegert, R. (1996). Estimation of the primary productivity of spartina alternaflora using a canopy model. *Ecography*, 19(4):410–423.

Dronkers, J. (1986). Tidal asymmetry and estuarine morphology. *Netherlands Journal of Sea Research*, 20:117–131.

Dyer, K. R. (1997). *Estuaries: A Physical Introduction*. John Wiley and Sons.

Evans, E., McGregor, G., and Petts, G. (1998). River energy budgets with special reference to river bed processes. *Hydrological Processes*, 12:575–595.

Fischer, H., List, E., Koh, R., Imberger, J., and Brooks, N. (1979). *Mixing in Inland and Coastal Waters*. Academic Press, Inc.

Hackney, C., Burbanck, W., and Hackney, O. (1976). Biological and physical dynamics of a Georgia tidal creek. *Chesapeake Science*, 17(4):271–280.

Hanson, R. and Snyder, J. (1980). Glucose exchanges in a salt-marsh estuary: Biological activity and chemical measurements. *Limnology and Oceanography*, 25(4):633–642.

Harrison, S. and Phzacklea, P. (1985). Seasonal changes in heat flux and heat storage in the intertidal mudflat of the Forth Estuary, Scotland. *Journal of Climatology*, 5:473–485.

Heilman, J., Heinsch, F., Cobos, D., and McInnes, K. (2000). Energy balance of a high marsh on the Texas Gulf Coast: Effect of water availability. *Journal of Geophysical Research*, 105(D17):22,371–22,377.

Hoguane, A., Hill, A., Simpson, J., and Bowers, D. (1999). Diurnal and tidal variations of temperature and salinity in the Ponta Rosa mangrove swamp, Mozambique. *Estuarine, Coastal and Shelf Science*, 49:251–264.

Hsu, S. A. (1988). *Coastal Meteorology*. Academic Press.

Hughes, C., Kalma, J., Binning, P., Willgoose, G., and Vertzonis, M. (2001). Estimating evapotranspiration for a temperate salt marsh, Newcastle, Australia. *Hydrological Processes*, 12:957–975.

Imberger, J., Berman, T., Christian, R., Sherr, E., Whitney, D., Pomeroy, L., Wiegert, R., and Wiebe, W. (1983). The influence of water motion on the distribution and transport of materials in a salt marsh estuary. *Limnology and Oceanography*, 28(2):201–214.

Jorgensen, C. (1990). *Bivalve Filter Feeding: hydrodynamics, bioenergetics, physiology and ecology*. Olsen and Olsen.

Kjerfve, B. (1973). Volume Transport, Salinity Distribution and Net Circulation in the Duplin Estuary, Georgia. Technical report, ERC-0273 Marine Institute, University of Georgia, Sapelo Island, Georgia.

Lahiri, K., Vallone, D., Gondi, S., Santoriello, C., and Dickmeis, T. (2005). Temperature regulates transcription in the zebrafish circadian clock. *PLoS Biology*, DOI: 10.1371/journal/pbio.0030351.

Mendenhall, W. and Sincich, T. (1994). *Statistics for Engineering and the Sciences, 4th Edition*, pages 625–633. Prentice Hall.

Millero, F., Perron, G., and Desnoyers, J. (1973). Heat capacity of seawater solutions from $5^o c$ to $35^o c$ and 0.5 to 22 percent chlorinity. *Journal of Geophysical Research*, 78:4499–4507.

Minello, T., Able, K., Weinstein, M., and Hays, C. (2003). Salt marshes as nurseries for nekton: Testing hypothesis on density, growth and survival through meta-analysis. *Marine Ecology Progress Series*, 249:39–59.

Newman, B., Papadopolous, I., Vorsatz, J., and Wooldridge, T. (2006). Influence of temperature on the larval development of Upogebia africana and U. capensis (Decapoda: Thalassinidae: Upogebiidae) in the laboratory. *Marine Ecology Progress Series*, 325:165–180.

Odum, E. and de la Cruz, A. (1967). Particulate organic detritus in a Georgia salt marsh-estuarine ecosystem. In Lauff, G., editor, *Estuaries*, pages 383–388. AAAS.

Perez-Domingues, R. and Holt, G. (2001). Effects of nursery environmental cycles on larval red drum (sciaenops ocellatus) growth and survival. *Fisheries Science*, 68(1):186–189.

Ragotzkie, R. and Bryson, R. (1955). Hydrography of the Duplin River, Sapelo Island, Georgia. *Bulletin of Marine Science of the Gulf and Caribbean*, 5:297–314.

Rattray, M. and Dworski, J. (1980). Comparison of methods for analysis of the transverse and vertical contributions to the longitudinal advective salt flux in estuaries. *Estuarine and Coastal Marine Science*, 11:515–536.

Reimold, R., Gallagher, J., Linthurst, R., and Pfeiffer, W. (1975). Detritus production in coastal Georgia salt marshes. In Cronin, L., editor, *Estuarine Research I*, pages 217–220. Academic Press.

Roegner, G. (2000). Transport of molluscan larvae through a shallow estuary. *Journal of Plankton Research*, 22(9):1779–1800.

Schwing, F. and Kjerfve, B. (1980). Longitudinal characterization of a tidal marsh creek separating two hydrographically distinct estuaries. *Estuaries*, 3(4):236–241.

Smith, N. (1983). A comparison of winter and summer temperature variations in a shallow bar-built estuary. *Estuaries*, 6(1):2–9.

Smith, N. (1985). The suitability of routine weather data for estimating local estuarine heat energy fluxes. *Estuaries*, 8(3):270–278.

Smith, S. (1988). Coefficients for sea surface wind stress, heat flux and wind profiles as a function of wind speed and temperature. *Journal of Geophysical Research*, 93:15,467–15,472.

Spurrier, J. and Kjerfve, B. (1988). Estimating the net flux of nutrients between a salt marsh and a tidal creek. *Estuaries*, 11(1):10–14.

Stevenson, J. and Niller, P. (1983). Upper ocean heat budget during the Hawaii-to-Tahiti shuttle experiment. *Journal of Physical Oceanography*, 13:1894–1907.

Turrell, W., Brown, J., and Simpson, J. (1996). Salt intrusion and secondary flow in a shallow, well-mixed estuary. *Estuarine, Coastal and Shelf Science*, 42:153–169.

Uncles, R., Bloomer, N., Frickers, P., Griffiths, M., Harris, C., Howland, R., Morris, A., Plummer, D., and Tappin, A. (2000). Seasonal variability of salinity, temperature, turbidity and suspended chlorophyll in the Tweed Estuary. *Science of the Total Environment*, 251-252:115–124.

Uncles, R. and Stephens, J. (2001). The annual cycle of temperature in a temperate estuary and associated heat fluxes to the coastal zone. *Journal of Sea Research*, 46(2):143–159.

Vaz, N., Dias, J., Leitao, P., and Martins, I. (2005). Horizontal patterns of water temperature and salinity in an estuarine tidal channel: Rio de Aveiro. *Ocean Dynamics*, 55:416–429.

Vernberg, F. (1993). Salt-marsh processes: A review. *Environmental Toxicology and Chemistry*, 12(12):2167–2193.

Vugts, H. and Zimmerman, J. (1985). Heat balance of a tidal flat area. *Netherlands Journal of Sea Research*, 19:1–14.

Wallace, J. and Hobbes, P. (1977). *Atmospheric Science: An Introductory Survey*. Academic Press.

Wang, Z. and Cai, W.-J. (2004). Carbon dioxide degassing and inorganic carbon export from a marsh dominated estuary (the Duplin River): A marsh CO2 pump. *Limnology and Oceanography*, 49(2):341–352.

Wolaver, T. and Spurrier, J. (1988). Carbon transport between a euhaline vegetated marsh in South Carolina and the adjacent tidal creek: contributions via tidal inundation, runoff and seepage. *Marine Ecology Progress Series*, 42:53–62.

Chapter 4

Salt Budget for a Shallow, Sinuous Salt Marsh Estuary

Abstract

An experimental study of the salt budget in the Duplin River, a tidal creek bordered by extensive intertidal salt marshes, was carried out in late summer of 2003 and spring of 2004 near Sapelo Island on the central Georgia coast in the southeastern U.S. The lower and upper tidal prisms of the Duplin are examined. In the lower tidal prism the salt budget is seen to be a balance between advective fluxes out of the creek, driven primarily by the export of fresh groundwater, and the tidal dispersion of salt into the creek, which is strongly regulated by the spring/neap cycle. In the upper Duplin the salinity gradient is seen to be small and reverses its sign on a fortnightly time scale. The advection of salt out due to groundwater export is shown to be a dominant term with the dispersion of salt small and variable. Despite the constant export of salt from the upper Duplin the mean salinity is seen to rise on spring tides, this is hypothesized to be due to the concentration of salt in the intertidal marshes on neap tide and its subsequent resuspension and export to the main creek channel with the greater marsh inundation of spring tide.

4.1 Introduction

Intertidal salt marshes are among the most productive ecosystems on the planet (Reimold et al., 1975), serving as habitat for numerous plant and animal species. The tidal creeks which cut through these marshes serve as both nursery and habitat for many species of aquatic animals of commercial and intrinsic value (Boesch and Turner, 1984; Minello et al., 2003) and productivity in the marsh exerts a strong influence on fisheries productivity (de la Cruz, 1973). The tidal creeks serve as the primary conduit through which marsh generated nutrients and material are transported to the coastal ocean (Ragotzkie and Bryson, 1955; Odum and de la Cruz, 1967) and the spatial and temporal distribution of their physical and biogeochemical characteristics, especially of salinity, strongly influence their productivity (Hackney et al., 1976; Underwood et al., 1998; Islam et al., 2006).

The flux of salt within a tidal creek is tied to several physical processes. The input of fresh groundwater into the creek tends to dilute the salt and, by driving the net outflow, to export it (Lewis, 1997; Dyer, 1997). The action of the tides tends to pump salt into the creek. The distilling and diluting effects of evaporation and precipitation, which can be significant in shallow waters, and the tidal inundation and draining of the intertidal marshes where salt may be concentrated in the sediment by evaporation and then resuspended during times of inundation or rainfall act as both a source and a sink of salt for the main channel.

The dispersive flux of salt through a tidal creek is the result of tidal processes, which are strongest near the mouth of the creek (Geyer and Signell, 1992). These along channel dispersive fluxes are tied to the interaction between tides, bathymetry and the intertidal marshes. This results in fluxes due to tidal correlations of depth, salinity and velocity. These fluxes can be modified by dispersion due to the interaction between vertical (Bowden, 1965) and lateral (Murray and Siripong, 1978; Rattray and Dworski, 1980) salinity variations with vertical and cross- channel shear. This is especially important in areas of high stratification or curvature in the main channel (Dyer, 1974). Tidal trapping, the effective along channel dispersion of salt due to interactions with marshes, side channels and embayments (Fischer et al., 1979), and salinity changes associated with lateral flows on and off of the marsh can also be important. These fluxes vary greatly on seasonal and spring/neap scales with changes in fresh water input and tidal energy, making them difficult to predict (see, for example, Banas et al., 2004; Medeiros and Kjerfve, 2005).

The objective of this study is to explore the relative importance of the various terms of the salt budget in the isolated upper region of a tidal creek which winds through an area of extensive intertidal marsh and compare that to the budget in the lower region, which enjoys more free communication with the coastal ocean and is bordered by less intertidal marsh area. This can then be compared to the heat budget conducted in the same region at the same time (McKay and Di Iorio, 2008) to develop an understanding of the dependence of the physical properties of the water of the main creek channel on interactions with the intertidal areas. Section 4.2 will develop the salt budget equation and discuss the physical meaning of the various terms. Section 4.3 will describe the experiment and data processing and Section 4.4 will discuss the measured salt budget. Finally Section 4.5 outlines the importance of the intertidal areas to the local salt budget and discusses implications for understanding the influence of the marsh on the local carbon and nutrient budgets as well.

4.2 Salt Budget Equation

A salt budget expresses the balance between the storage of salt in a volume and its flux through the bounds of that volume. For a differential volume, dx, dy, dz, in a tidal creek oriented such that x is aligned along the main axis of flow, and is positive toward the mouth of the creek (South), y is aligned cross channel and to the left of x (East), and z is the vertical, positive up, the salt budget may be expressed as,

$$\frac{\partial s}{\partial t} + \frac{\partial (us)}{\partial x} + \frac{\partial (vs)}{\partial y} + \frac{\partial (ws)}{\partial z} - \frac{s_s\,(E - P)}{h} = 0 \tag{4.1}$$

where s is salinity, t is time, u, v and w are the instantaneous velocities in the x, y and z direction respectively, s_s is the surface salinity, E and P are the rates of evaporation and precipitation, h is the water depth and molecular diffusion has been neglected (Dyer, 1997; Phillips, 1966).

If the Duplin can be regarded as vertically well mixed for salt during the deployment period, as will be discussed later, the interaction between stratification and shear is negligible, and a point measurement of salinity can be regarded as the vertical mean. In straight, narrow, shallow channels such as the Duplin, the vertical and cross-channel velocities (v and w) are small compared to the along channel velocity (u) and thus may be neglected in the salt budget. Lateral variations in along channel flow are also generally small, especially by comparison to vertical variations (Rattray and Dworski, 1980), and the center channel salt fluxes may be taken as largely representative for the creek. Neglecting turbulent fluctuations as small compared to tidal fluctuations, the instantaneous vertical mean of a quantity can be decomposed into its tidally averaged and tidally varying components such that

$$s = S + s_t \tag{4.2}$$

$$u = U + u_t \tag{4.3}$$

$$h = H + h_t \tag{4.4}$$

where the capitalized quantity is the tidal and depth mean and the subscript t denotes tidal deviations from this mean. Evaporation and precipitation are not similarly decomposed as they are not expected to have any tidal components.

Simplifying Equation (4.1) to remove neglected terms, substituting the above decompositions into the advective and surface flux terms and depth integrating, we can write the depth integrated salt budget per unit width of the channel as,

$$\frac{\partial(sh)}{\partial t} + \frac{\partial}{\partial x}\left[\left(U + u_t\right)\left(S + s_t\right)\left(H + h_t\right)\right] - \left(S_s + s_{st}\right)\left(E - P\right) = 0 \tag{4.5}$$

Now integrating along channel from $x = 0$, at the head of the creek where the along channel salt fluxes are zero, to a downstream location x where the flux measurements are taken, multiplying out all terms and tidally averaging we can write the tidally averaged, depth integrated salt budget per unit width of the channel as

$$\frac{\partial\left(\overline{\tilde{s}\tilde{h}}L\right)}{\partial t} + HUS + H\overline{u_t s_t} + S\overline{h_t u_t} + U\overline{h_t s_t} + \overline{h_t u_t s_t} - S_s\left(\overline{E-P}\right)L = 0 \tag{4.6}$$

where a tilde represents a longitudinal average, L is the length of the main channel and an overline represents averaging over tidal scales.

Examining the various terms of (4.6), the first term, $\partial\left(\overline{\tilde{s}\tilde{h}}L\right)/\partial t$ is the tidally averaged, depth and along channel integrated storage of salt per unit width in the region of the creek upstream of the flux measurement, accounting for changes in salinity and storage volume.

The second term, HUS, represents the tidally averaged, depth integrated residual advection of salt into or out of the creek per unit width. This net advection term accounts for the effects of salt transport due to net freshwater discharge into the creek and/or changes in upstream storage volume. In general, the residual flux term is positive, indicating a net export of water tied to fresh water discharge, with deviations from this being tied to atmospheric events and averaging to zero over a long period.

The third term, $H\overline{u_t s_t}$, gives the net advection of salt due to the correlation between tidally varying velocity and salinity acting over the mean depth. This term will be maximum, when velocity and salinity are in phase such that maximum and minimum salinity occur at maximum flood and ebb velocity, and the term will be zero when these quantities are out of phase. The term will be negative, indicating a net upstream dispersion of salt, when the salinity gradient is positive, with saltier water toward the mouth of the creek, such that the flood tide brings in saltier water than ebb tide exports.

The fourth term, $S\overline{h_t u_t}$, is analogous to Stokes' Drift (Medeiros and Kjerfve, 2005). This term represents the effects of tidal wave transport on the mean salinity and is maximum when max ebb and flood occur at high and low water, when the tide shows characteristics of a progressive wave, and zero when max ebb and flood occur at mean water, as in the case of a standing tidal wave (Dyer, 1997).

The final double correlation term, $U\overline{h_t s_t}$, gives the net advection of salt due to the action of the residual advective flow on the correlation between tidally varying depth and salinity.

This term is maximum, when the two tidal quantities are in phase, when maximum and minimum salinity occur at maximum or minimum water depth, and goes to zero when they are out of phase, when maximum and minimum salinity occur at mean water. The term will be positive, indicating net dispersion of salt out of the creek, when maximum salinity occurs near high water.

The triple correlation is the tidal pumping term due to the correlation between all three tidally varying quantities. This term is maximum when all three are in phase, that is maximum and minimum salinity occurring at high and low water on a progressive tidal wave, and goes to zero when any two quantities are out of phase. This term is generally negative, indicating a net dispersion of salt into the creek, and is often the dominant tidal dispersive term (Kjerfve, 1986).

The final term then represents the concentration and dilution of salt due to evaporation and precipitation at the surface of the main creek channel. It does not account for the concentration of salt in the marsh and side creeks due to evaporation and evapotranspiration, which will be discussed in a later section.

4.2.1 Salinity

Salinity in the study was measured according to the practical salinity scale, as a function of conductivity, temperature and pressure, and, as such, is unitless. In order to express salt fluxes in a meaningful fashion this practical salinity must be converted into an absolute salinity from which a mass of salt can be determined. The nature of the relation between practical salinity and absolute salinity is the subject of much of the work of the SCOR/IAPSO Working Group 127 on the 'Equation of State and Thermodynamics of Seawater'. Millero et al. (2008) have developed a relation between practical salinity and a newly defined reference salinity, being the absolute salinity of standard Atlantic surface water. In this formulation the absolute salinity of Atlantic surface water, which we take as a reasonable approximation of the water of the Duplin and Doboy Sound, is given as 35/35.16504 g kg^{-1} times the practical salinity. Multiplying the absolute salinity then by the density of seawater in kg m^{-3}, as calculated using the 1983 UNESCO equation (Fofonoff and Millard, 1983), which is also currently under revision, yields a salinity in g m^{-3} which allows for meaningful salt flux calculations to be made.

4.2.2 Salt Fluxes Due to Evaporation and Precipitation

Evaporation and precipitation are not limited to the main channel of the creek but also occur in the many shallow side creeks and in the intertidal marsh area when it is flooded. The salt, which is concentrated or diluted, in the side creeks is mixed back across the side boundaries of the main channel on ebb tide thus affecting the local salt budget. In the intertidal areas salt can be concentrated in the soil and porewater through evapotranspiration, and then through runoff from precipitation or by being resuspended into the overlying water during times of tidal inundation, become transported into the main channel when the marsh drains.

Evapotranspiration (E_T) is the loss of water from a wetted area due to both direct evaporation (E_M) of surface water, which is shaded by the marsh vegetation, and the transpiration (T) of water vapor due to vegetation, such that

$$E_T = E_M + T \tag{4.7}$$

Working in temperate intertidal salt marshes in Newcastle, Australia, Hughes et al. (2001) showed how the actual evapotranspiration rate, measured using eddy correlation methods, from a salt marsh is highly dependent on the nature of the vegetation, particularly on plant density, canopy height and leaf area, and can range from 50 to nearly 100% of the potential open water evaporation rate (E). Working in an area similar to the Duplin, on the Chesapeake Bay, Hussey and Odum (1992) showed that for a salt marsh, vegetated with low density, short canopy *Spartina alterniflora* (with a Leaf Area Index (LAI) ranging from 0.1 to 0.89), as is found over much of the Duplin marsh area, lysimeter measured evapotranspiration rates were not significantly different from measured open water evaporation rates. Thus a reasonable upper bound for for evapotranspiration can be established as being equal to the potential open water evaporation rate in the neighboring channel such that $E_T = E$.

It is not possible to predict the destination of the salt concentrated in the marsh on any given tide, whether it is concentrated in the sediment and pore water or mixed back into the main channel. However, since the salinity in the marsh is not increasing without bound it can be assumed to reach some sort of quasi-steady state such that the long term, tidal mean salt flux from the marsh and side creeks into the main channel can be approximated as

$$-S_s\overline{(E_T - P)\,A_m} \tag{4.8}$$

where A_m is the flooded area of the marsh, which is a function of tidal height. Combining this with the concentration term for the main creek channel itself, the total transport of salt into the creek due to evaporation and precipitation in the main channel and evapotranspiration and precipitation in the marsh can be estimated as

$$-S_s\left[\overline{(E - P)}A_c + \overline{(E_T - P)\,A_m}\right] \tag{4.9}$$

where A_c is the total surface area of the main creek channel. This relation gives the salt transport into the entire volume of the creek, not simply per unit width, and allows the establishment of the relative importance of evaporative and precipitative fluxes on the overall salt budget. Normalizing this term then by the mean width of the channel in the area of interest it can be used in the salt budget given by Equation (4.6).

4.3 Methods

The salt budget experiment in the Duplin River was part of the DUPLEX I experiment, conducted from August 11 through September 23, 2003, which has been previously described in Section 3.3 and shown in Figure 3.1. As in the heat budget experiment, the salt budget concentrates on the lower and upper Duplin regions as characterized by the DUP01 and 03 moorings respectively. At each of these mooring locations a Sontek 300 kHz acoustic Doppler profiler was deployed on a bottom mount mooring at center channel, in the thalweg with a mean depth of 6.5 m, with Seabird Microcat CTDs deployed at the bottom, on the mooring frame, and the surface, on an adjacent dock at the side of the channel (Marsh Landing and Hunt Dock respectively). The Microcats sampled conductivity, temperature and depth every twelve minutes while the ADPs pinged continuously at 2 Hz and logged averaged velocity profiles, with 0.2 m depth bins, every twelve minutes, coinciding with the Microcat samples.

From each 12 minute averaged velocity profile from the ADP the first depth bin above the transducer head and the bin containing the water surface were removed to eliminate ringing near the transducer and surface reflections. All depth bins were then cleaned to remove spikes, caused by spurious values in the single ping data, by replacing any value more than five standard deviations away from the three hour rolling mean for that depth bin with the average of the values immediately before and after it. The horizontal velocities were then rotated into their along channel and cross channel components. The lowest good velocity bin was centered 1.15 m above the bottom while the top bin was centered approximately 0.3 m below the surface, the precise location being a function of the exact water surface location. To resolve the surface and bottom velocities each profile was extrapolated upwards to the surface, such that there was zero shear at the surface, and downwards to the bottom, assuming a log layer profile. This profile was then depth averaged.

The bottom Microcat data at each mooring was unreliable almost from the beginning of the deployment, presumably due to plugging of the conductivity cell in these highly turbid and biologically active waters. The surface Microcat data was cleaned of spurious data points by filtering out all points more than five standard deviations away from the local mean of a three hour moving average with that point being replaced by an interpolation of the neighboring data.

For the purposes of calculating the salt fluxes, the measured practical salinity was converted to absolute salinity using the method described in Section 4.2.1. For the evaporative and precipitative flux estimates, the instantaneous surface area of the Duplin main channel was estimated as the product of the channel width and length as measured from a NOAA chart of the region. A high resolution digital elevation model of the intertidal areas of the Duplin has been created by Blanton et al. (2007) which allows the estimation of the surface area of the flooded marsh as a function of measured tidal height.

The tidally varying water depth, salinity and depth averaged along-channel velocity were filtered with a 40 hour, third order Butterworth low pass filter (Roberts and Roberts, 1978), run forwards and backwards for zero phase distortion, to extract the subtidal mean. This mean was then subtracted from the original signal to extract the tidal variations. While the Butterworth filter, as a recursive filter, is lossless and does not erode data from the ends of the time series as does a non-recursive filter (such as the Lanczos-cosine filter), ringing distorts the data at the beginning and end of the filtered output. This ringing requires the removal of data at the ends comparable to that lost using a non-recursive filter (Emery and Thompson, 2004). A subjective decision is required to recognize the difference between the 'good' and 'bad' data near the ends. In this case 48 hours worth of data were discarded at each end due to ringing, slightly more than would have been lost with a non-recursive filter. Despite this slightly greater data loss the Butterworth filter has a nearly square response and produces no phase shift and so is preferred over most alternatives.

4.4 Results

4.4.1 Vertical and Lateral Salinity Variations

A comparison of the surface salinity data with the bottom data, for those periods when the bottom Microcat appears to be functioning, shows that both mooring sites are essentially well mixed for salt for the entire time of the deployment, with the exception of brief periods of less than half an hour at slack low water when the DUP01 mooring experiences stratification as, apparently, a layer of fresh water overlies the water column. This structure exists just after slack water and is destroyed once flood tide commences. As has been previously shown for temperature stratification (McKay and Di Iorio, 2008), the fact that this stratification only occurs near slack water makes it out of phase with the velocity and thus it has a negligible contribution to the along channel salt fluxes. Neglecting this brief period of stratification, the observed difference between surface and bottom salinity is low and variable giving the appearance of noise. At all times it is below the accuracy of the instrument of 0.002 on the practical salinity scale (calculated from the reported instrument accuracy of 0.002 °C and 0.0003 S cm^{-1} taken from Seabird datasheets).

At both mooring sites, the bottom Microcats were located in the thalweg, at approximately center channel, while the surface Microcats were mounted on the neighboring dock and thus their difference captures both the vertical and lateral salinity variability. As the differences between the center/bottom and side/surface salinity measurements were below the accuracy of the instrument, with the exception at DUP01 previously noted, we can reasonably conclude that there is no significant lateral salinity variability at either mooring site and thus the Duplin can be considered to be sectionally homogeneous at both mooring sites during the experiment.

As was shown in Section 2.4 there is little cross-channel variability in u velocity in the Duplin when channel curvature is small. The small width of the Duplin combined with the generally straight channel in the region of both moorings reduces the lateral variability of along channel flow (Rattray and Dworski, 1980), as well as the secondary flows due to curvature and Coriolis, such that the center channel salt fluxes may be taken as representative for the section.

4.4.2 Evaporation and Precipitation

In the shallow waters of the Duplin near the end of summer, when evaporation is near its annual maximum and rain showers are common, the concentration and dilution of salt due to evaporation and precipitation could be a significant term in the local salt budget.

Calculation of these fluxes over the surface of the main channel is a straight- forward procedure. Precipitation was measured directly at the Marsh Landing weather station during the experiment. The evaporative flux of water is estimated from observations of air and water temperature, relative humidity, atmospheric pressure and wind speed using the method of Fairall et al. (1996), developed for the Tropical Ocean Global Atmosphere Coupled Ocean Atmosphere Response Experiment (TOGA COARE). This method is implemented in the MATLAB Air- Sea Toolbox developed by Bob Beardsley and Rich Pawlowicz (`www.sea-mat.whoi.edu`). It has been modified to give a more accurate representation of the latent heat of vaporization and of the density of these waters, which are measurably fresher than standard seawater, thus bringing it back in line with the TOGA COARE code. The open water evaporation rate is calculated as

$$E = \frac{Q_{lat}\Delta t}{L_E \rho} \tag{4.10}$$

where Q_{lat} is the latent heat flux at the water surface, shown in Figures 3.9 and 3.10 from McKay and Di Iorio (2008), Δt is the time between observations, L_E is the latent heat of vaporization and ρ is the density of the water. The Air-Sea Toolbox routine, EP.m, was modified such that the value of L_E is taken as $(2.501 - 0.00237T) \times 10^6$ W m^{-2} (taken from the hfbulktc.m routine, which more accurately reflects the original TOGA COARE code base and where T is the sea surface temperature) instead of using the constant 2.5×10^6 W m^{-2}. ρ is calculated using the 1983 UNESCO equation (Fofonoff and Millard, 1983) instead of being taken as a constant of 1025 kg m^{-3}, which is too high for these measurably diluted waters.

The two panes of Figure 4.1 show the water fluxes due to evaporation and precipitation during the DUPLEX I experiment; the heavy line shows the average evaporation rate; precipitation is episodic and its averaged value is negligible. The average evaporation rate varies between approximately 2 and 8.5 mm d^{-1} which is in the expected range for evaporation rates in this region (P. Knox - personal communication).

For the purpose of calculating the effect of salt concentration on the local salt budget in the upper and lower Duplin, the upper and lower tidal prisms, the boundaries of which were defined by the approximate tidal excursion distance of 4 km (Ragotzkie and Bryson, 1955), were examined along with all of the intertidal basins which drain into them as determined

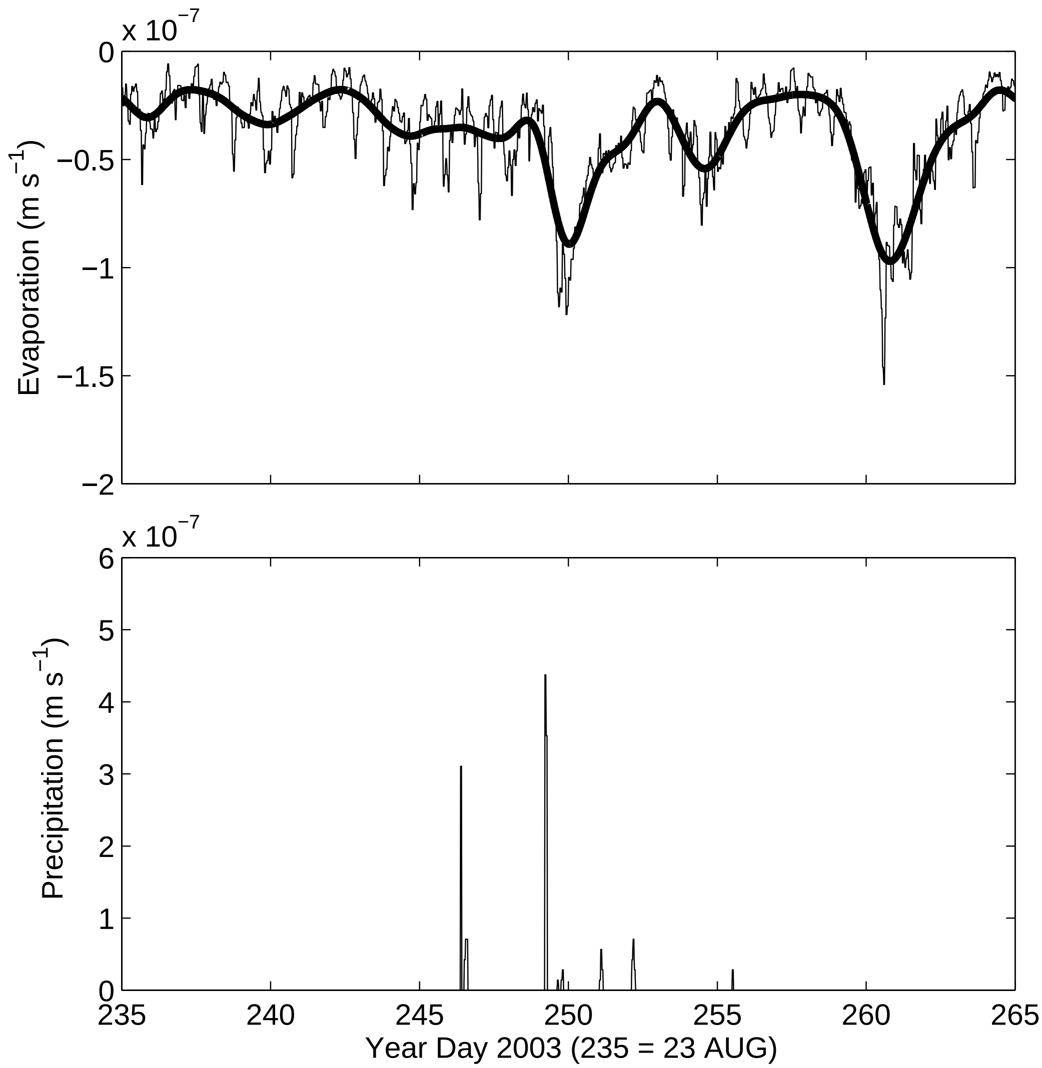

Figure 4.1: Fluxes of water per unit area due to evaporation and precipitation in the Duplin River basin during DUPLEX I. The heavy line shows averaged evaporation; averaged precipitation is negligible.

by Blanton et al. (2007). According to Figure 4.2, the lower Duplin was determined to drain basins 1–2 and 14–17 while the upper Duplin drains basins 4–8. Through measurements taken from a NOAA chart of the region the approximate main channel surface area of the lower Duplin was determined to be 1×10^6 m^2 while the equivalent area in the upper tidal prism was much less at 9x10^4 m^2, reflective of a mean width of around 22 m in the upper prism compared to 250 m in the lower tidal prism. From Blanton et al. (2007) the marsh drainage basins for the upper and lower Duplin region were identified and hypsometric curves were constructed, as shown in Figure 4.3.

Assuming that the marsh and side creeks are in steady state, the tidally averaged transport of salt into each tidal prism of the Duplin can be estimated using Equation 4.9. The upper panes of Figure 4.4 show the estimated extent of flooded area, both intertidal and in the main channel of the creek, as a function of time. Both tidal and spring/neap variability can be observed. As can be seen in Figure 4.3 the peak flooded area is greater in the lower Duplin than in the upper, however a greater extent of the marsh floods earlier in the upper Duplin than the lower, owing to the greater communication between the main channel and the marsh due to the large number of small side creeks. Thus much of the upper Duplin marsh is flooded for longer than the lower Duplin marshes; this will have implications to the relative evapotranspiration rates between the two prisms.

The lower panes of Figure 4.4 show the calculated salt transport into each tidal prism due to main channel evaporation (thin line) and marsh evapotranspiration (thick line). Main channel open water evaporation dominates in the lower Duplin, accounting for, on average, five times greater salt flux than can be attributed to the marsh. Marsh evapotranspiration is slightly higher in the upper Duplin than in the lower but main channel evaporation is much lower, owing to the narrower nature of the channel, with evapotranspiration there averaging 3 to 5 times higher than main channel evaporation.

Making the assumption that the salt coming out of the marsh mixes uniformly across the width of the main channel, these fluxes can be normalized by the channel width at each

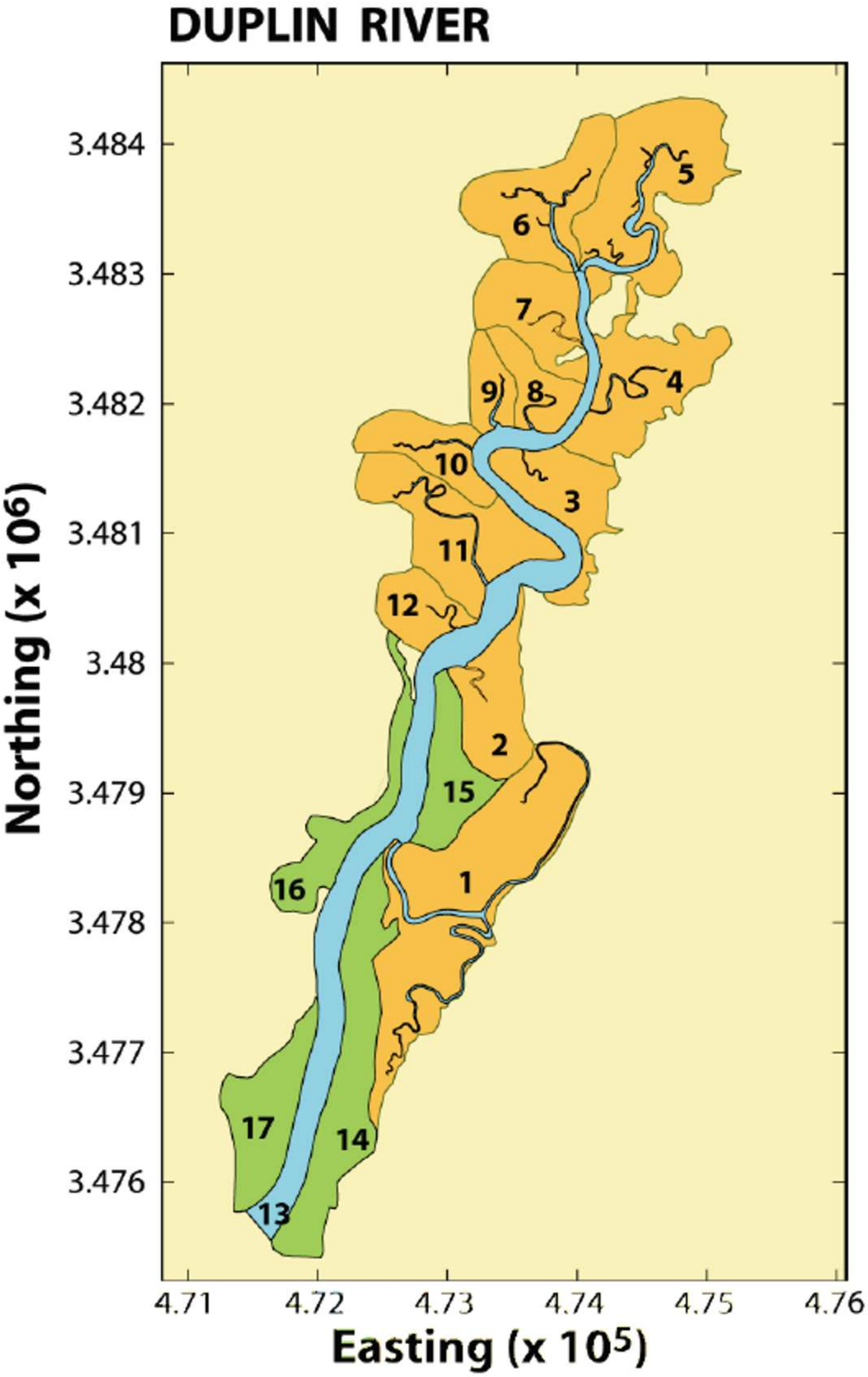

Figure 4.2: Intertidal basins in the Duplin, from Blanton et al. (2007).

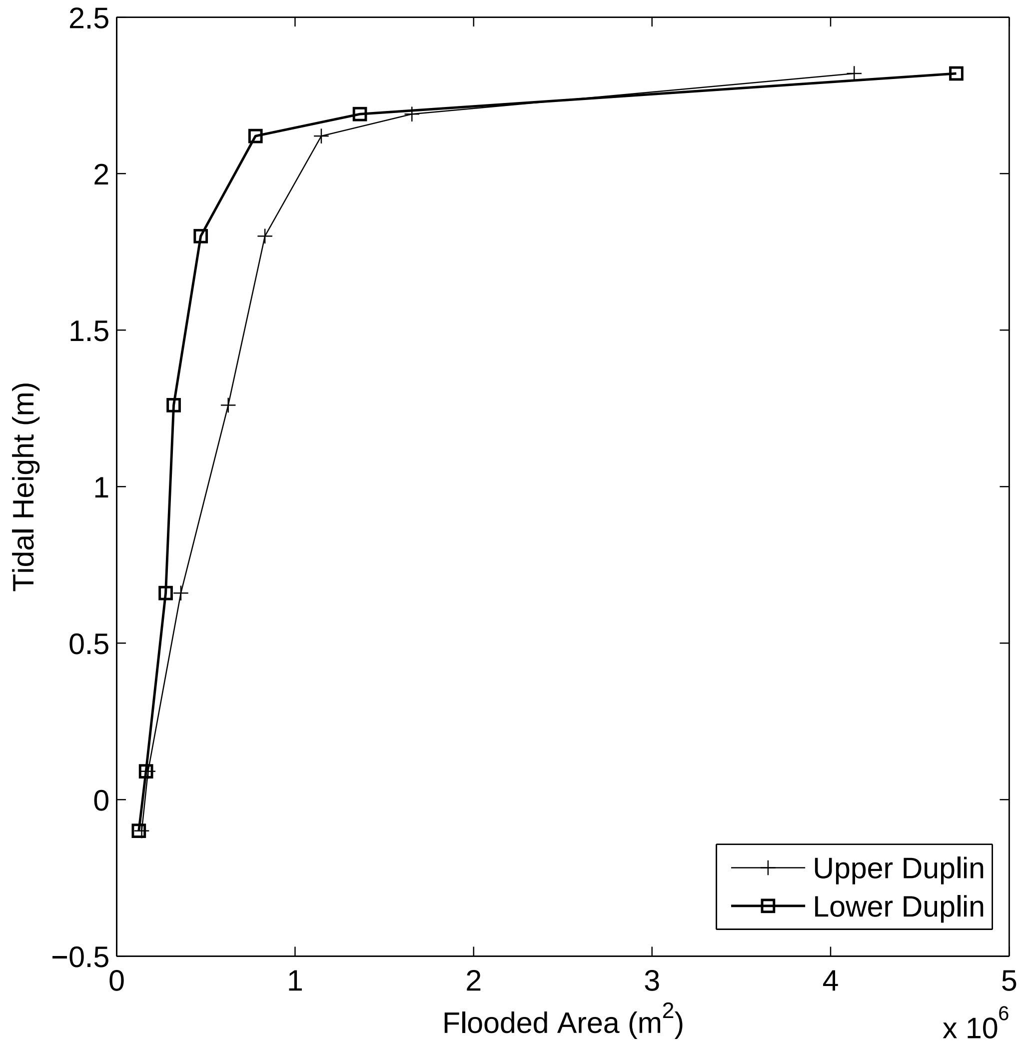

Figure 4.3: Hypsometric curves for the intertidal areas of the upper and lower Duplin compiled from Blanton et al. (2007).

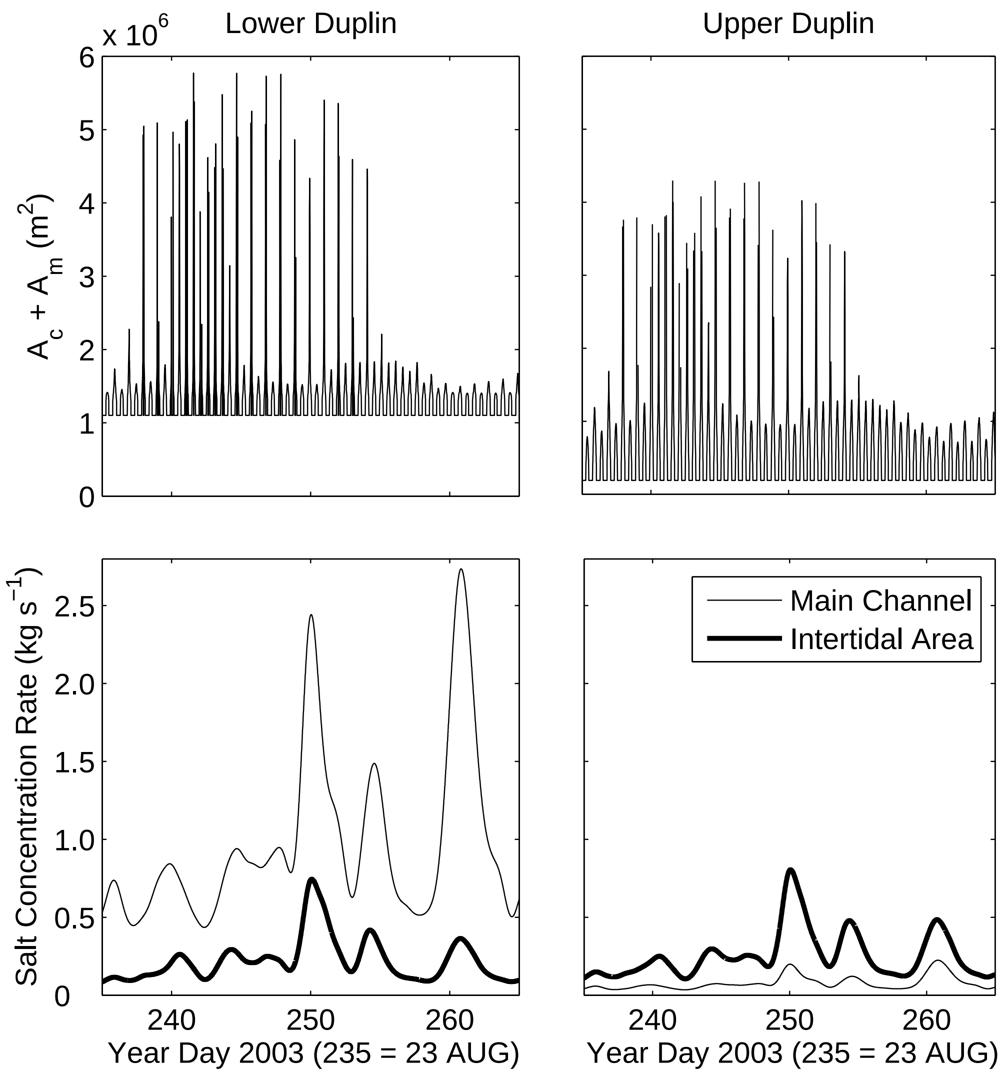

Figure 4.4: Total flooded area (intertidal and main channel) in the upper and lower tidal prisms of the Duplin during DUPLEX I. The lower panes shows tidally averaged salt fluxes into the Duplin due to main channel evaporation and to evapotranspiration in the marsh.

mooring location to get the total salt flux per unit width needed for the salt budget equation (4.6). This is shown in Figure 4.5.

4.4.3 Lower Duplin Salt Fluxes

Figure 4.6 shows the depth averaged along channel velocity, depth and salinity at DUP01 during the DUPLEX I experiment; each one decomposed into tidally varying (thin line) and tidally averaged (thick line) terms. In the upper pane the tidal mean velocity, U, can be seen to be very low compared to the tidal velocity, with U on the order of 1 cm s^{-1}. The tidally varying velocity ranges as high as 1.2 m s^{-1} on a strong spring ebb to less than 0.5 m s^{-1} on a weak neap ebb. A pronounced tidal asymmetry can be observed with a short strong ebb being followed by a weaker, but longer, flood. Unequal semi-diurnal tides are observed as a stronger flood/ebb pair is followed immediately by a weaker pair. A strong spring/neap cycle in velocity is apparent.

The second pane shows the tidal and residual depth during the experiment. The tidal depth shows a similar pattern to the tidal velocity with a strong spring/neap modulation in tidal range and with the unequal semi-diurnal tides reflected in the pattern of a higher high tide being followed by a lower high tide – this pattern is not as evident in low tides as they vary more smoothly with the spring/neap cycle. A half-meter increase in mean water depth is seen between year day (YD) 248 and 250. This is tied to the beginning of a Nor'Easter event as winds at the offshore monitoring buoy swing around from the southeast to the northeast and intensified, causing downwelling conditions on the coast, which forces oceanic water onshore increasing both the mean water depth and salinity (see Figure 3.7). After the Nor'Easter event begins to subside the offshore winds calm but continue from the northeast showing the annual switch in the regional wind climatology from summer conditions to what has been designated as Mariner's Fall (Blanton et al., 1985). A similar, though smaller, event occurs again around YD 260 as northeasterly winds again increase and are associated with another increase in mean water depth and salinity.

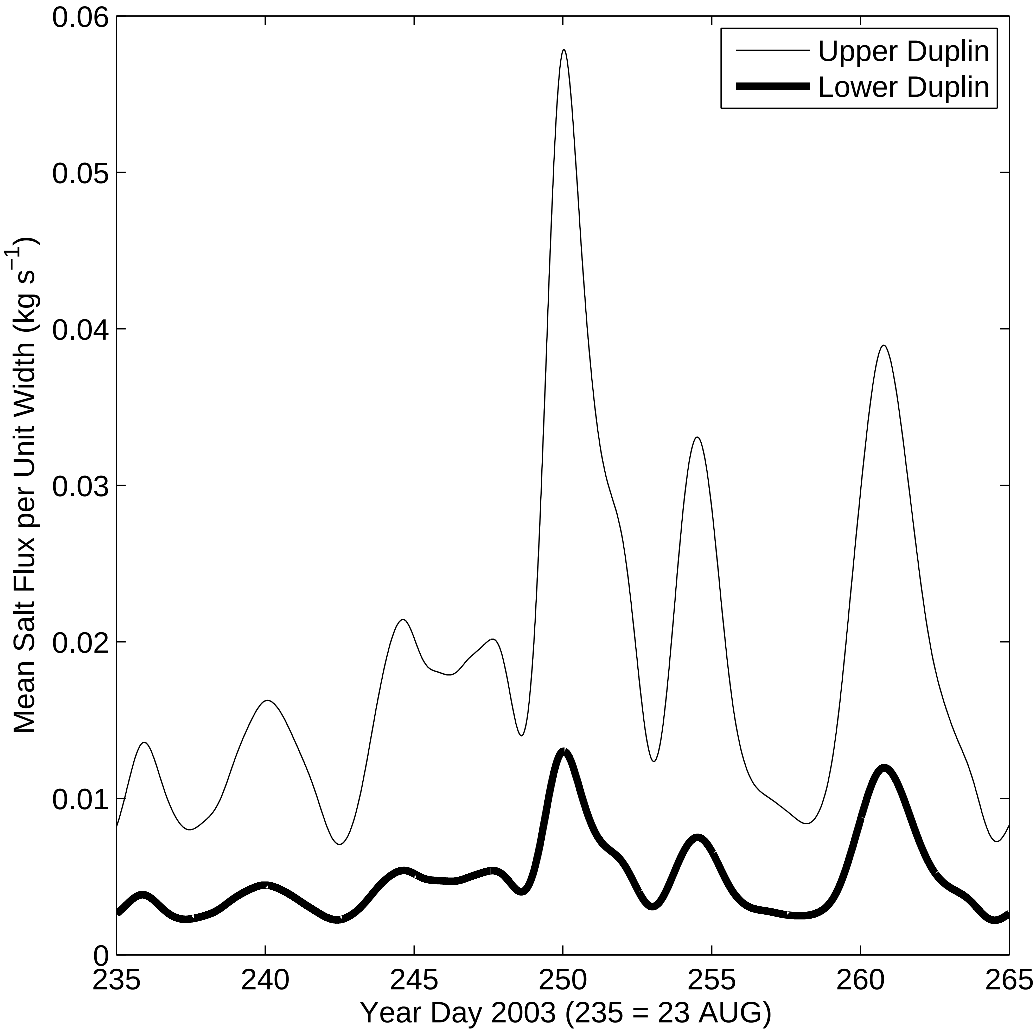

Figure 4.5: Total salt flux per unit width due to evaporation and precipitation in the main channel and the intertidal areas.

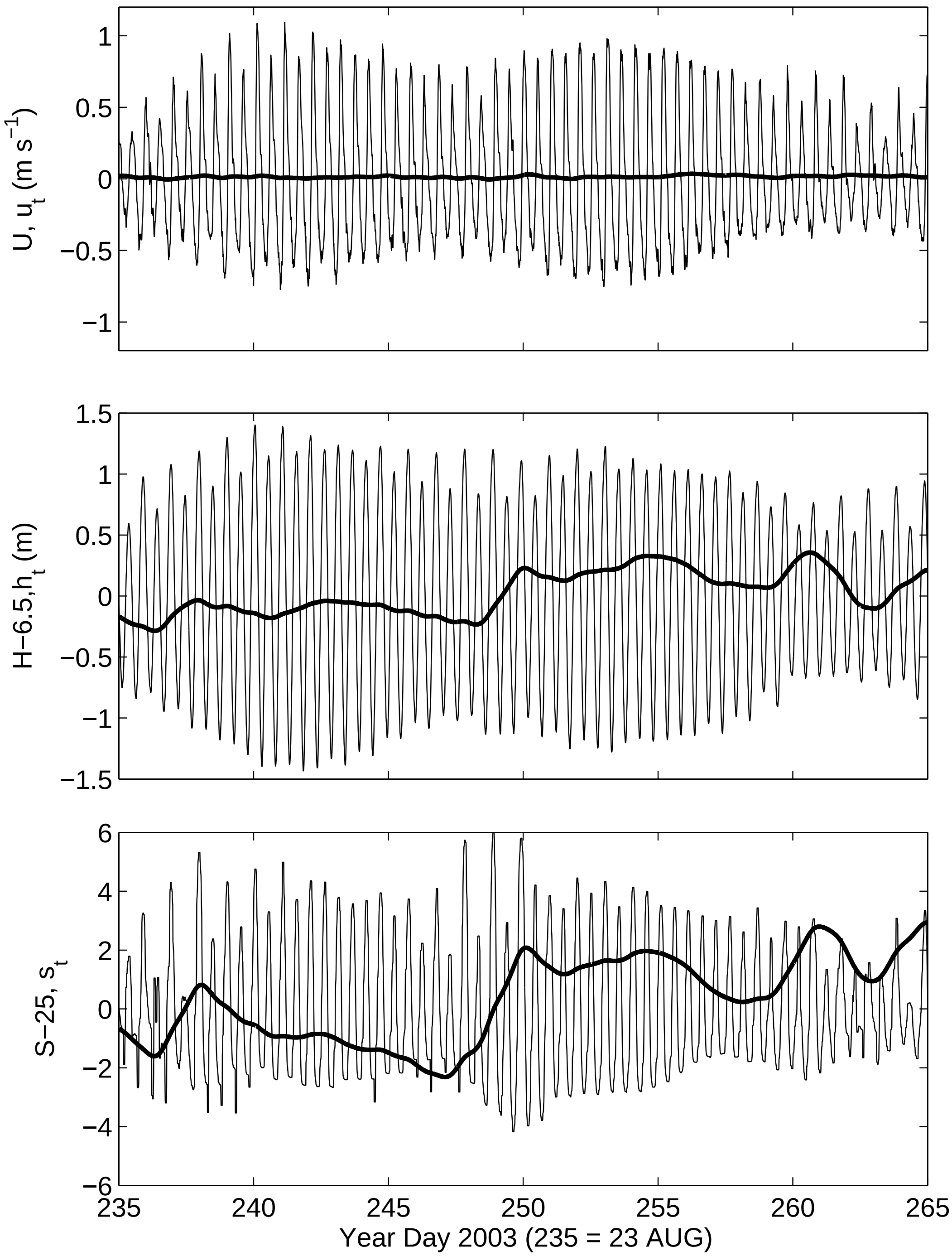

Figure 4.6: Depth averaged along channel velocity (upper pane), water depth (middle pane) and surface salinity (lower pane) at the DUP01 mooring. The heavy lines indicate 40 hour low pass filtered values.

The lower pane shows the tidal and residual salinity during the experiment. As with depth and velocity, unequal semi-diurnal tides can be seen as a small low/high salinity pair is followed by a larger pair, though the spring/neap cycle is less pronounced. An increase in mean salinity can be seen between YD 248 and 250 and again around YD 260, as was noted previously for depth.

Figure 4.7 shows phase diagrams of the double correlations used in Equation (4.6) at the DUP01 mooring during the DUPLEX I experiment, with times of peak spring and neap tide highlighted with red and green respectively. The upper pane shows the correlation between tidally varying salinity and velocity. This correlation shows mixed characteristics. Times of maximum and minimum salinity are centered about times of slack water. However these periods persist until close to time of maximum ebb and flood as well. This results in a variable dispersive term which changes sign through the tidal cycle. On spring tide a brief period of rapid freshening can be observed shortly after slack low water. This is believed to be due to a pulse of fresh groundwater entering the lower Duplin from Doboy Sound.

The second pane shows the correlation between tidally varying depth and velocity. This correlation is strongly affected by the presence of the intertidal marsh, which can store a large quantity of water with little change in center channel depth, and presents a character which is mixed between a standing and a progressive wave (Dyer, 1997). On flood, maximum velocity occurs near maximum water depth, indicating that the tide has the characteristics of a progressive wave and the marsh has been flooded. However, on ebb, maximum velocity occurs slightly above mean depth, indicating that the marsh has drained and the tide has the characteristic of a standing wave. This is variable on the spring/neap cycle with neap tides showing even more characteristics of a standing wave on ebb. This will result in a dispersive term with strong spring/neap variability.

The bottom pane of Figure 4.7 shows the correlation between the tidally varying depth and salinity. These terms are highly correlated, with high salinity occurring at high water and low salinity at low water. This strong correlation will result in a dispersive flux into the

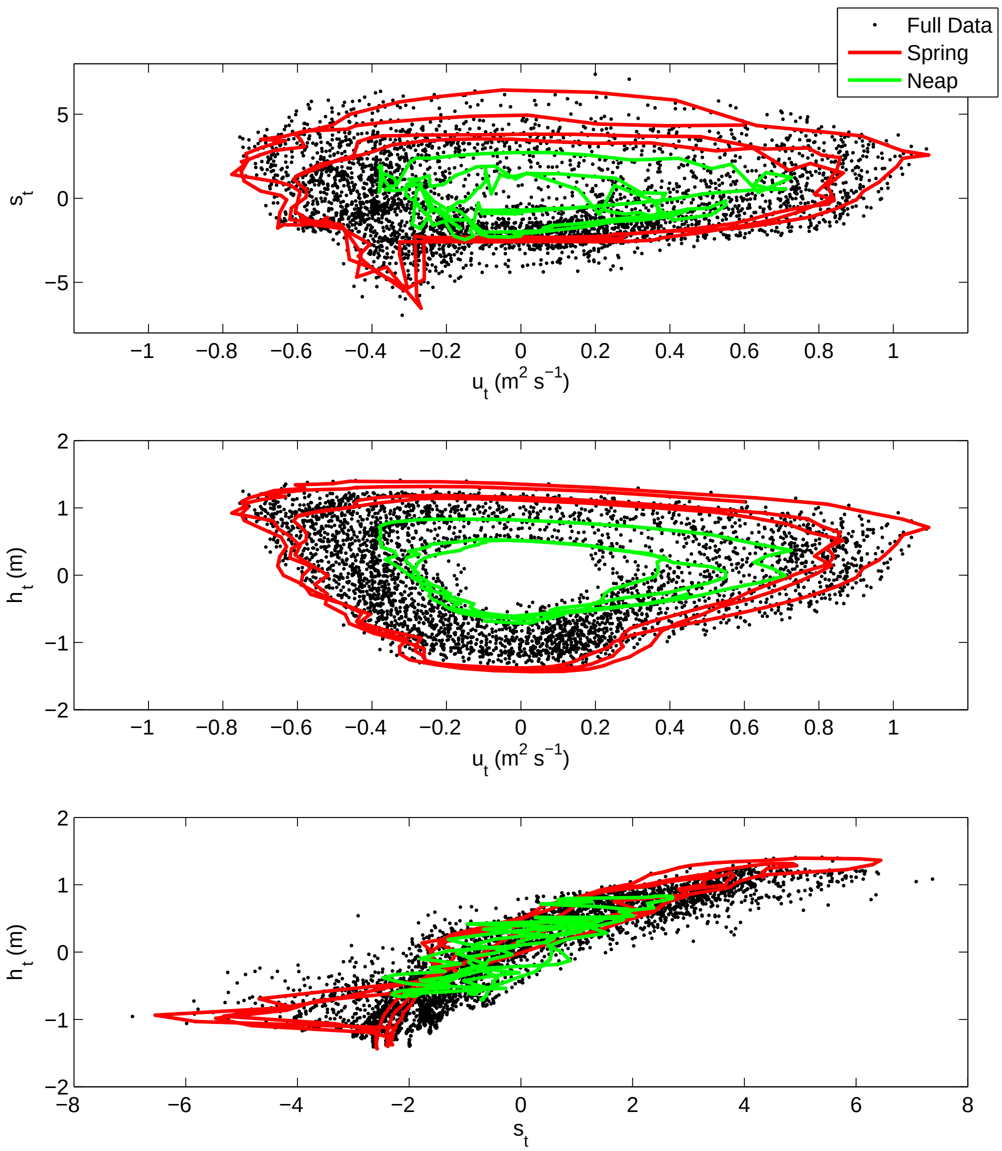

Figure 4.7: Phase diagrams of the correlations between tidally varying velocity, practical salinity and depth at the DUP01 mooring.

Duplin, but one which is attenuated by being multiplied by the very low residual outflow U. The short- lived freshening on the spring tide at the start of flood, as noted above, is also evident here.

The triple correlation is not plotted, but is represented by the three orthogonal views in the double correlation plots. Its magnitude is low owing to the opposing nature of the $\overline{u_t s_t}$ and the $\overline{u_t h_t}$ correlations.

The salinity gradient in the lower Duplin can be calculated, on the basis of along channel advection of salt such that $\partial S/\partial x = (-1/U)\partial S/\partial t$, and is shown in Figure 4.8, plotted in terms of salinity per meter. This term is always positive, reflecting that the mouth of the creek is always saltier than the upper regions of the lower Duplin, and varies between 4.5 and 9×10^{-4} g kg^{-1} m^{-1}.

Figure 4.9 then shows the calculated tidal dispersive and advective fluxes in the lower Duplin. The upper pane shows the tidal dispersive components. The largest component is the $S\overline{u_t h_t}$ flux which represents a net flux of salt into the Duplin tied to the progressive nature of the tidal wave on flood and the standing nature of the same wave on ebb (dashed line). The next largest component is the $H\overline{u_t s_t}$ flux, reflecting the mixed characteristics of the velocity-salinity correlation which causes it to change signs on a spring/neap cycle (dotted line). The other terms, including the tidal pumping triple correlation term, are low and the net tidal dispersion is shown as a thick solid line.

The net advective (thin solid line) and tidal fluxes (dashed line) are plotted in the lower pane along with their sum (thick solid line). These represent the total flux of salt into and out of the Duplin. This is highly variable in magnitude and sign, and is dominated by the advective flux term. Whatever spring/neap variability is present is overwhelmed by the residual flux variations tied to the offshore forcing.

As can be seen from Figures 4.5 and 4.9 the salt fluxes due to evaporation and precipitation, even when including the extensive intertidal areas, are a minor factor in the lower Duplin salt budget. Figure 4.10 shows a plot of the estimated storage of salt per unit

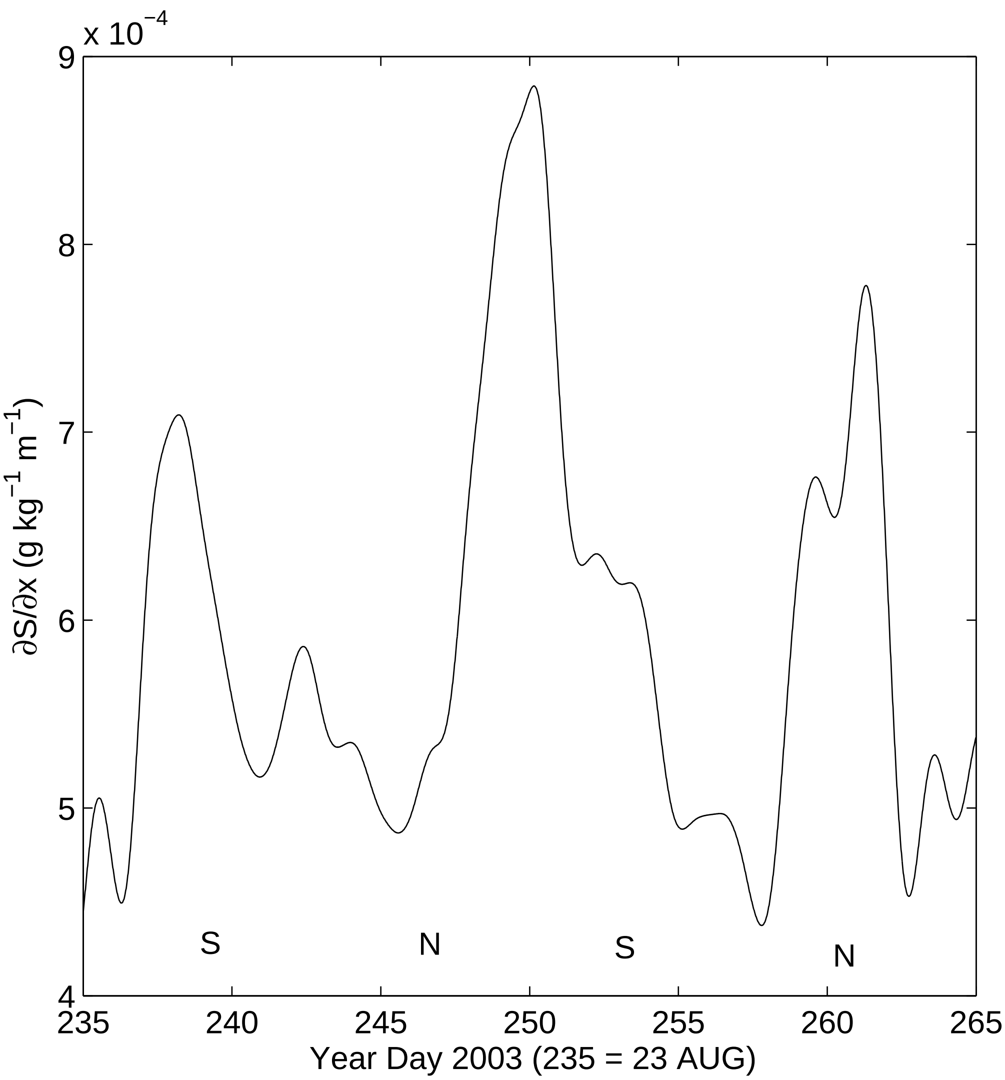

Figure 4.8: The along channel salinity gradient at the DUP01 mooring.

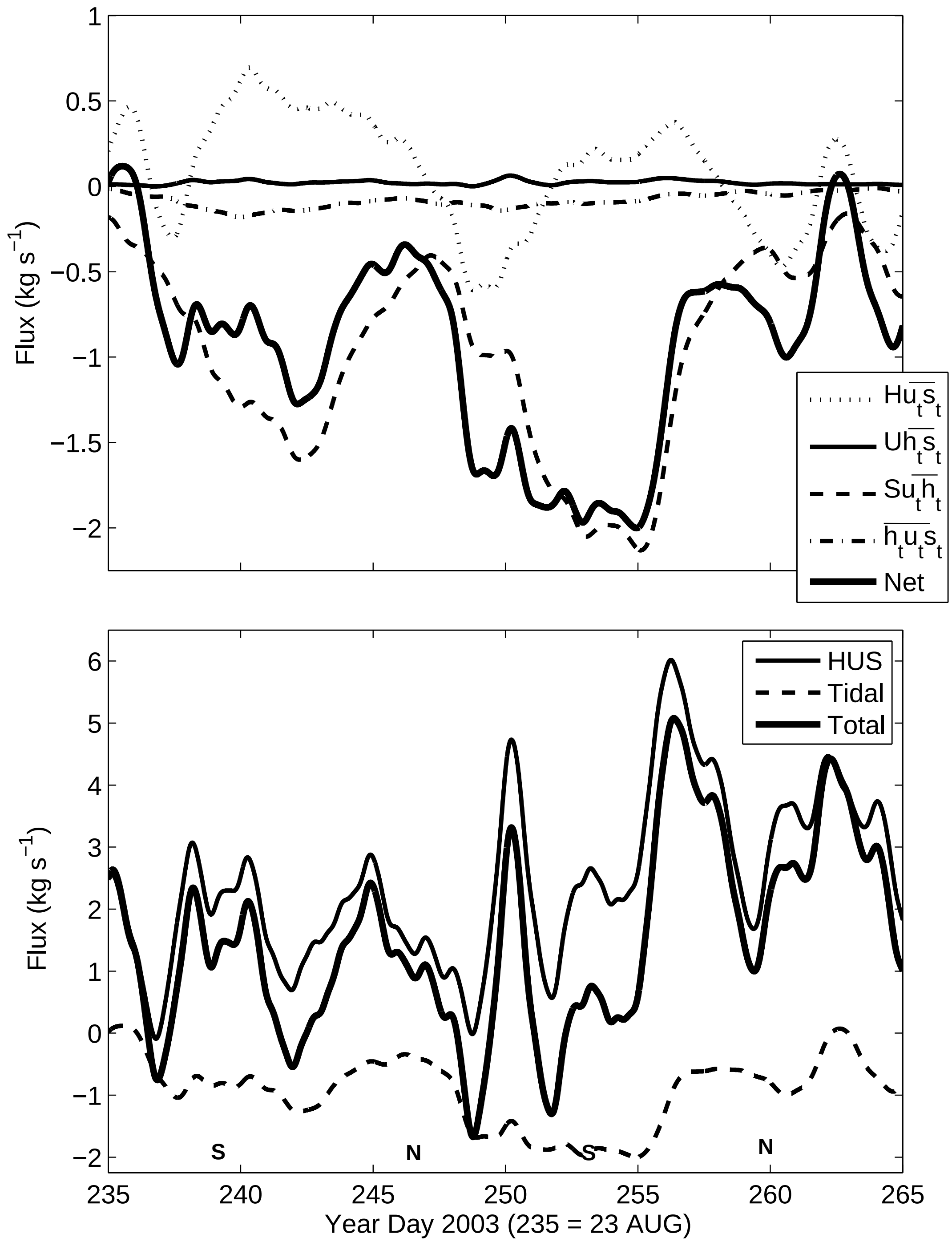

Figure 4.9: Tidal salt flux constituents at the DUP01 mooring (upper pane) along with the net salt flux due to tidal and residual transport (lower pane). Times of peak spring and neap tide are indicated by the S and N labels.

width in the lower Duplin tidal prism $(\partial\left(\widetilde{\overline{sh}}L\right)/\partial t)$ along with the negative of the net along channel advective and dispersive flux. Both the sign and shapes of the curves correlate reasonably well until YD 250. After YD 250, presumably, the relaxation of the system after the onshore transport due to the Nor'Easter brings salt into the system from the intertidal areas, accounting for the discrepancy between the observed storage and the along channel salt fluxes.

4.4.4 Upper Duplin Salt Fluxes

Figure 4.11 shows the depth averaged along channel velocity, depth and salinity at DUP03 during the DUPLEX I experiment, each decomposed into tidally varying (thin line) and tidally averaged (thick line) terms. In the upper pane the tidal mean velocity, U, can be seen to be very low compared to the tidal velocity, though higher than in the lower Duplin, on the order of 3 cm s^{-1}, which could be due to a larger amount of fresh water flux entering the Duplin upstream of this mooring and pointing to the much smaller cross-sectional area at this location. The tidally varying velocity ranges from as high as 0.7 m s^{-1} on a strong spring ebb to less than 0.4 m s^{-1} on a weak neap ebb, in all cases much less than in the lower Duplin, reflecting the dissipation of tidal energy as the tidal waves moves through the shallow and sinuous channel. A pronounced tidal asymmetry can be observed with a short strong ebb being followed by a weaker, but longer, flood; a semi-diurnal tidal inequality, observed as a stronger flood/ebb pair followed immediately by a weaker pair is also observed. A strong spring/neap cycle in velocity is also apparent.

The second pane shows the tidal and residual depth during the experiment. The tidal depth shows a similar pattern to the lower channel depth with the same spring/neap cycle and semi-diurnal asymmetry. As in the lower Duplin a half meter increase in mean water depth is seen between YD 248 and 250 with no appreciable phase lag between the two events, indicating that the mean water level adjusted nearly instantaneously throughout the system, as previously described.

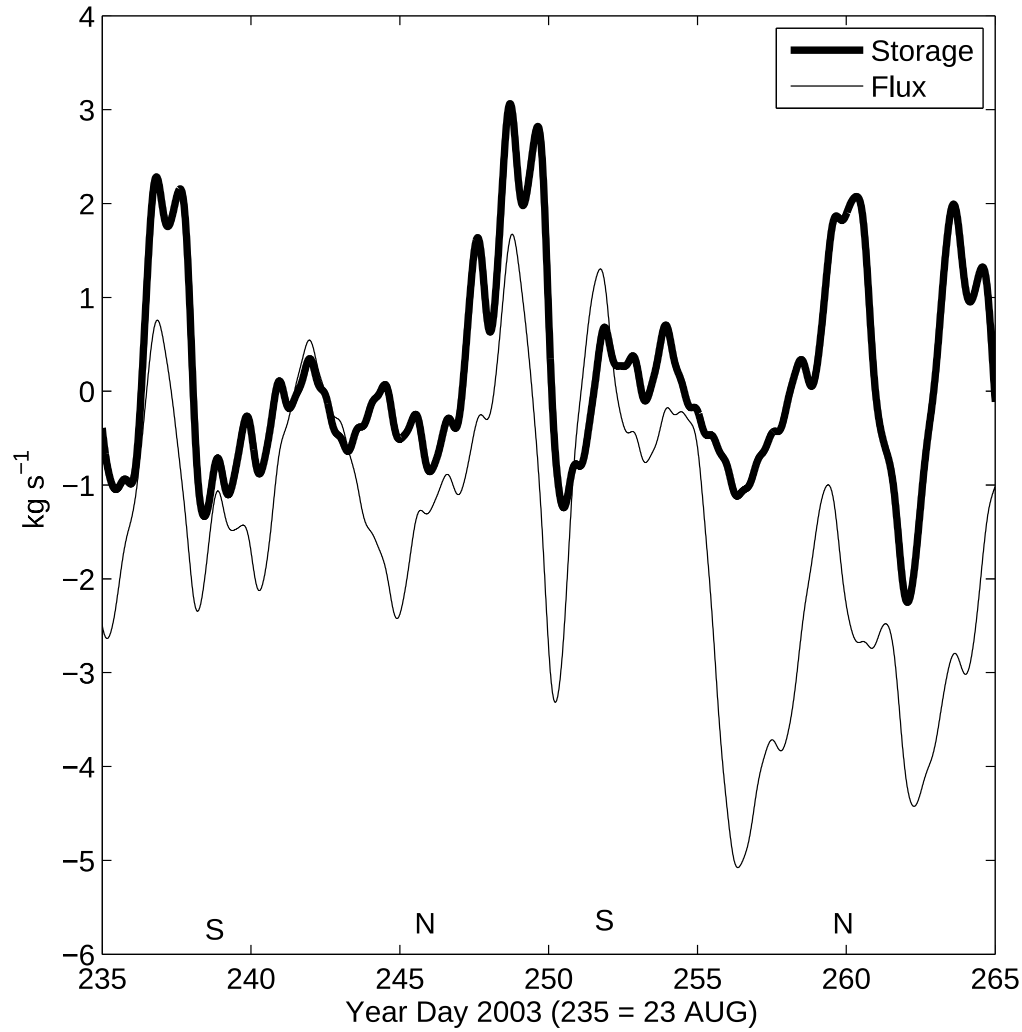

Figure 4.10: Tidally averaged salt storage $(\partial\left(\overline{\widetilde{s}h}L\right)/\partial t)$ in the lower tidal prism of the Duplin and the negative of the along channel salt fluxes past the DUP01 mooring.

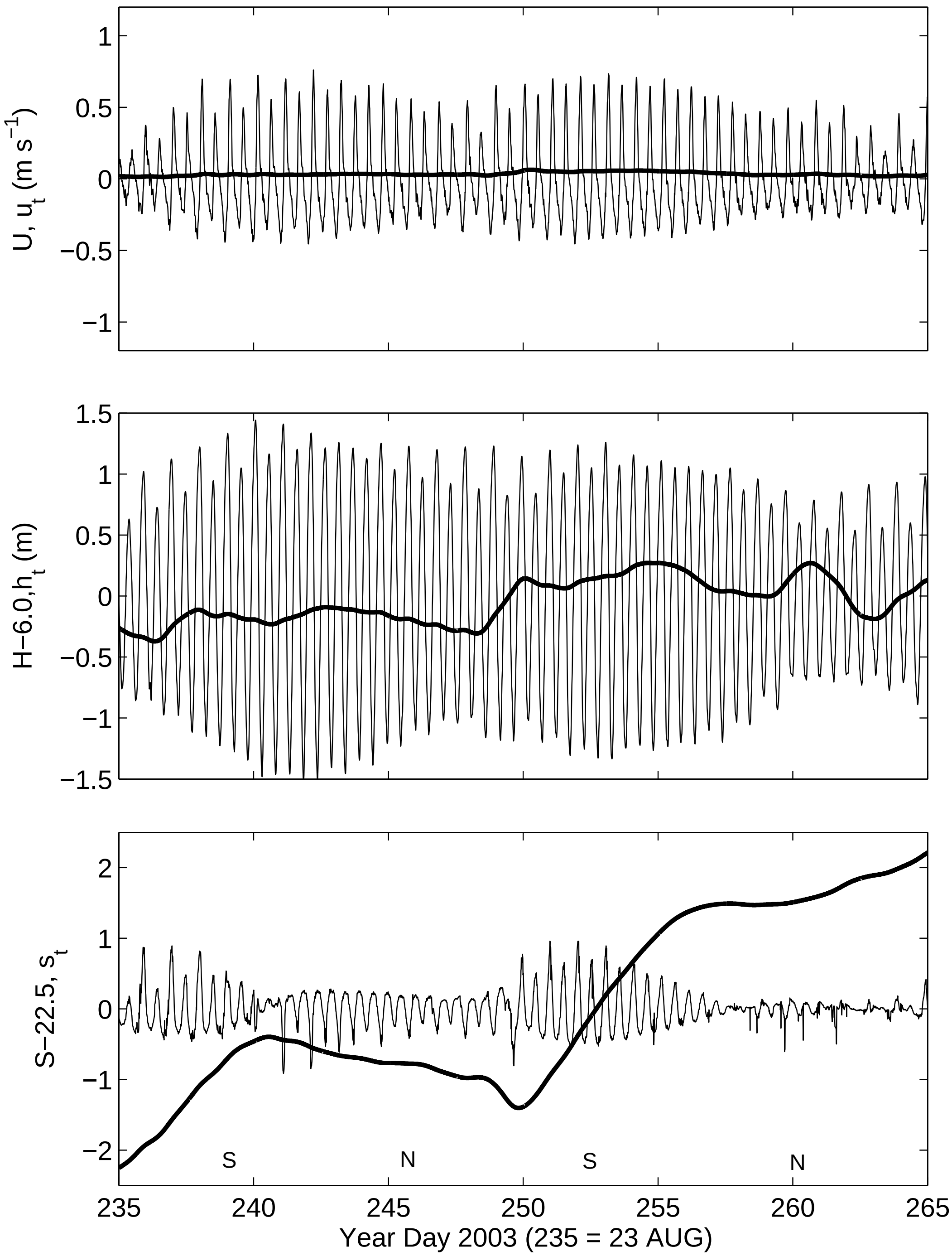

Figure 4.11: Along channel velocity, water depth and practical salinity at the DUP03 mooring. The heavy lines indicate 40 hour low pass filtered values.

The lower pane shows the tidal and residual practical salinity during the experiment. Tidal salinity variation is very low and an unusual pattern can be observed: during early spring tide a flooding tide brings increased salinity and an ebbing tide brings decreased salinity, followed by a transition period just after peak spring tide when tidal salinity variation is nearly negligible; then during a much longer neap tide, a flooding tide brings in lower salinity water and an ebbing tide higher salinity water. At the beginning of the next spring tide the regime abruptly transitions back to the early spring tide regime and begins the pattern again. An increase in mean salinity can be seen between YD 248 and 250 and around YD 260 as was noted previously in the lower Duplin.

Figure 4.12 shows phase diagrams of the double correlations in Equation (4.6) at the DUP03 mooring during the DUPLEX I experiment with peak spring and neap tides indicated. The upper pane shows the correlation between tidally varying salinity and velocity. This correlation shows mixed characteristics, similar to those seen in the lower Duplin, but with much lower tidal salinity variability. This will result in a dispersive term which alternates in sign and is very small.

The second pane shows the correlation between tidally varying depth and velocity. As in the lower Duplin this correlation is strongly affected by the presence of the intertidal marsh, showing characteristics of a progressive wave on flood and a standing wave on ebb. As before this will be the dominant salt flux term representing a net flux in, though reduced due to the lower mean salinity in the upper Duplin.

The bottom pane then shows the correlation between the tidally varying depth and salinity. This term shows an unusual pattern as the correlation reverses in sign on a spring/neap cycle. On early spring tide, flood tide brings in higher salinity water while ebb tide brings in lower salinity water; this forms the arm of the ‘X’ pattern running from lower left to upper right, and indicates a positive salinity gradient. On neap tide this pattern is reversed forming the arm, which runs from lower right to upper left, indicating that

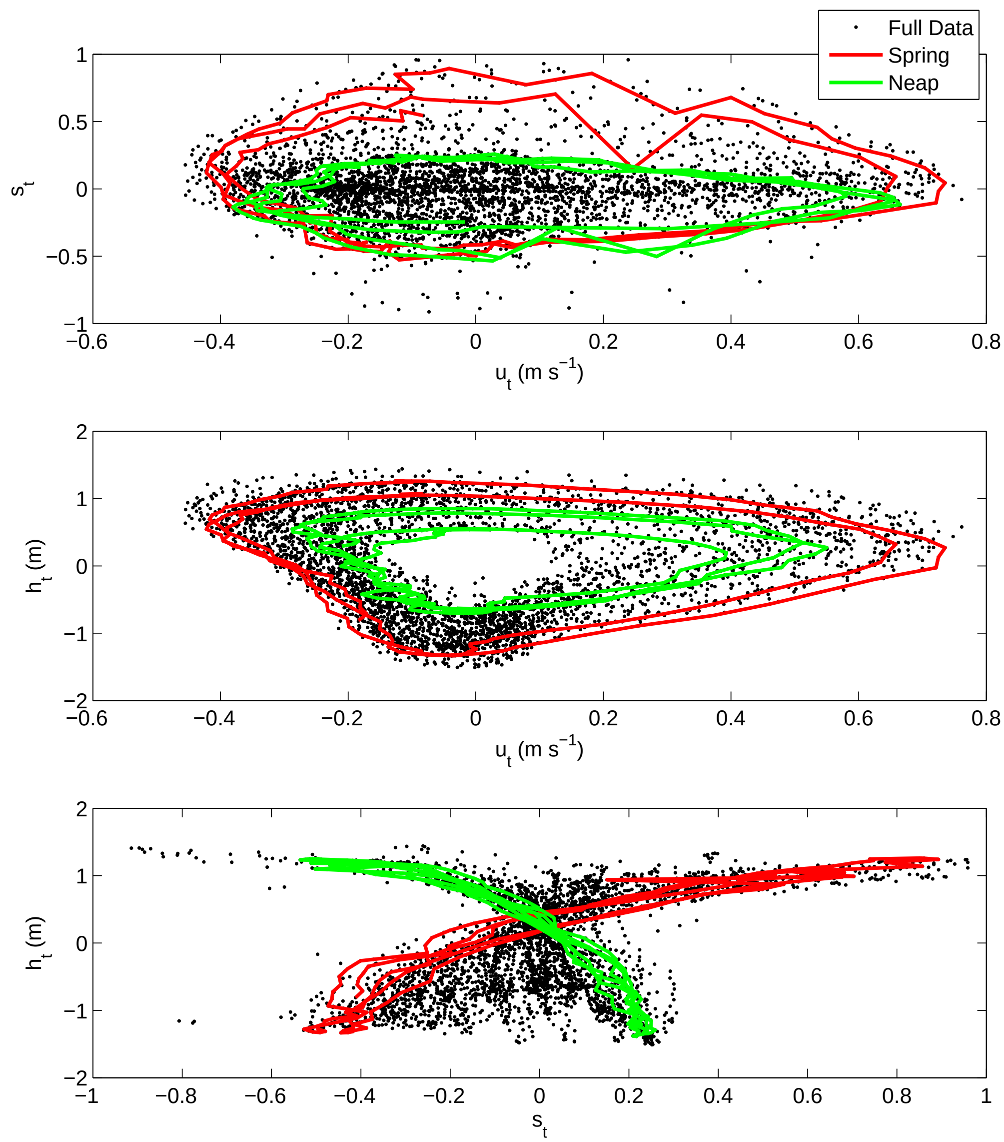

Figure 4.12: Phase diagrams of the correlations between tidally varying velocity, practical salinity and area at the DUP03 mooring.

the salinity gradient has reversed. The scatter in the lower region is due to the transition between these periods.

As before the triple correlation is not plotted, due to the difficulty of visualizing the correlation in three dimensional space, but is low owing to the opposing nature of the $\overline{u_t s_t}$ and the $\overline{u_t h_t}$ correlations.

The salinity gradient in the upper Duplin is shown in Figure 4.13. This term reverses with the spring/neap cycle varying from -1.25 to 2.5×10^{-4} g kg^{-1} m^{-1} reflecting the reversible nature of the upper Duplin estuary as the interaction between tidal energy in the lower Duplin pushing salty Doboy Sound water up and presumably fresh groundwater entering and diluting the middle Duplin water plays out on a fortnightly cycle, as will be discussed.

Figure 4.14 shows the tidal dispersive and advective fluxes in the upper Duplin. The upper pane shows the tidal dispersive components. The largest component, as before, is the $S\overline{u_t h_t}$ flux (dashed line) which represents a net flux of salt into the Duplin tied to the progressive nature of the tidal wave on flood and the standing nature of the same wave on ebb. This component shows the same spring/neap variability as in the lower Duplin, but is much smaller reflecting the lower mean salinity in the upper Duplin as well as the decrease of the velocity-depth correlation tied to the greater extent of intertidal areas. The term is maximum on spring tide when the positive salinity gradient is maximum and goes to near zero on neap tide as the salinity gradient goes to zero and then reverses sign. All other components are smaller.

The net advective (thin line) and tidal (dotted line) fluxes are plotted in the lower pane along with their sum (thick line), which represents the total flux of salt into and out of the Duplin. This term is consistently out of the Duplin and is dominated by the advective flux term. In contrast to the lower Duplin a spring/neap signal is observable and the net salt flux is always out of the Duplin. This does not fit well at all with the observed mean salinity trends in the upper Duplin, as shown in Figure 4.11, indicating that poorly constrained salinity fluxes outside of the main channel are important in these waters.

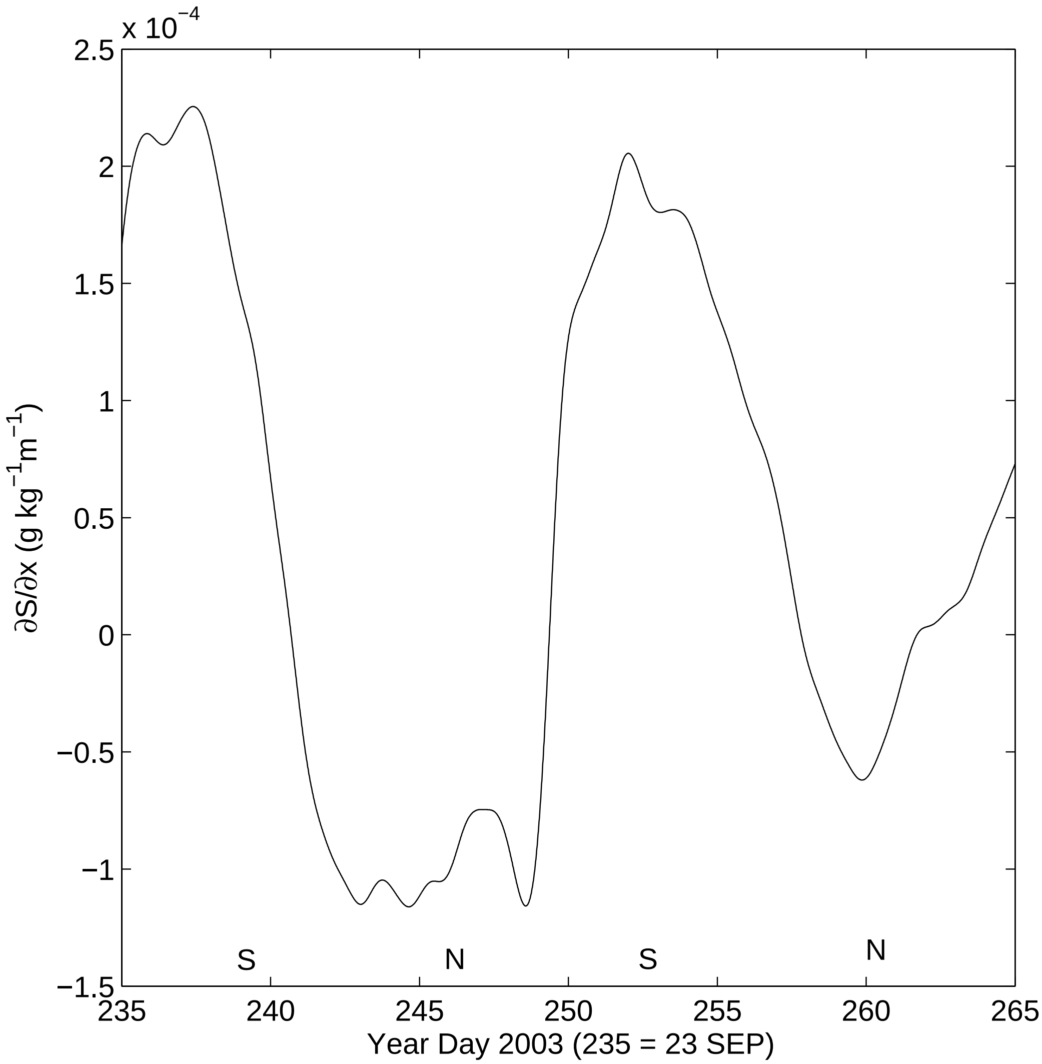

Figure 4.13: The along channel salinity gradient at the DUP03 mooring.

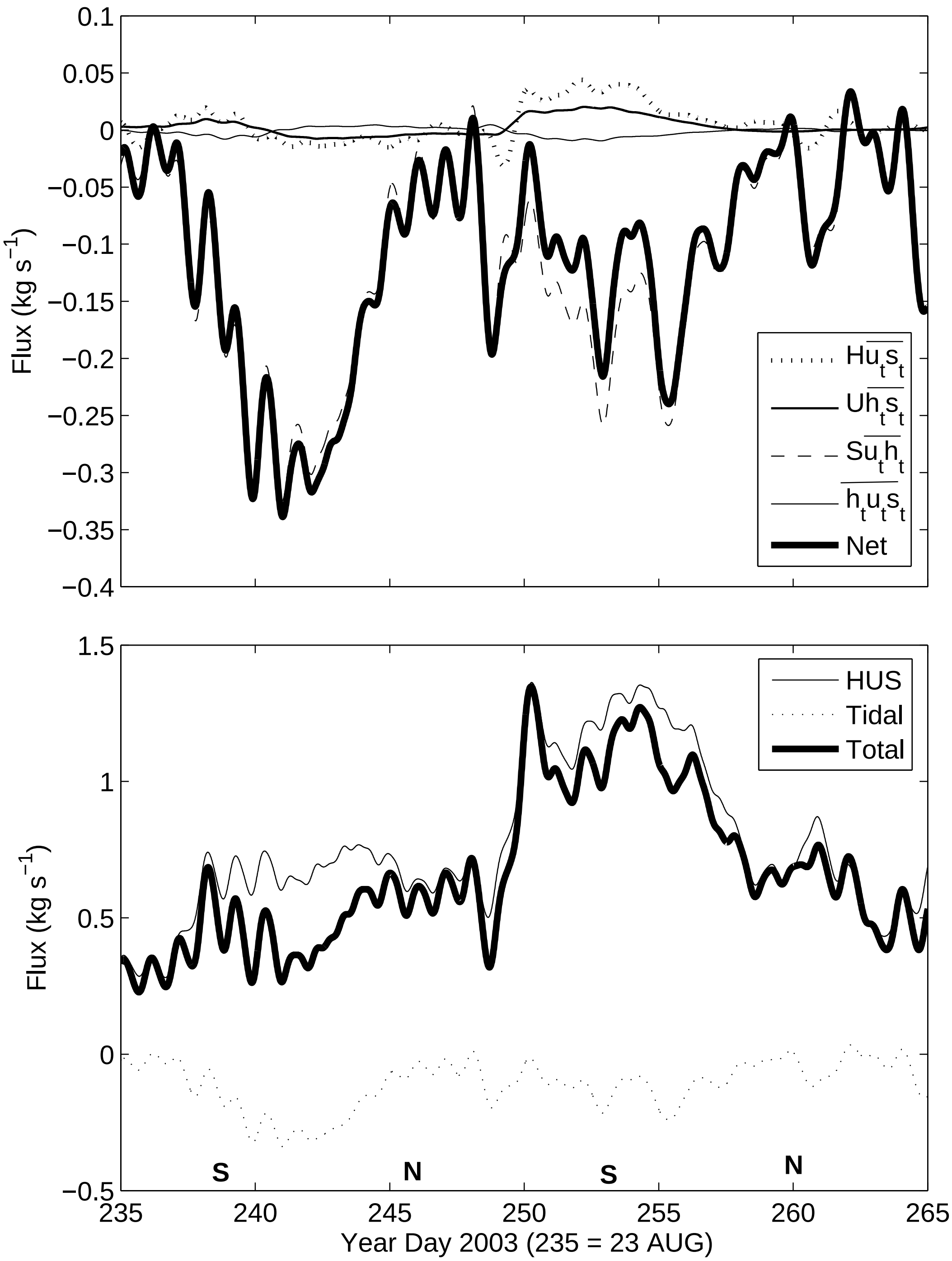

Figure 4.14: Tidal salt flux constituents at the DUP03 mooring (upper pane) along with the net salt flux due to tidal and residual transport (lower pane). Times of peak spring and neap tide are indicated by the S and N labels.

As can be seen from Figures 4.5 and 4.14 the salt fluxes due to evaporation and precipitation are a minor factor in the upper Duplin salt budget, even when accounting for the greater ratio of intertidal area to main channel area than in the lower Duplin. Figure 4.15 shows a plot of the calculated storage of salt in the upper Duplin tidal prism $(\partial\big(\overline{\overline{s}h}L\big)/\partial t)$ along with the net along channel advective and dispersive flux. Neither the sign nor the shape of the curves correspond well indicating that the sum of along channel advection and dispersion of salt and steady state concentration of salt due to evaporation in the main channel and the intertidal areas is insufficient to determine the local salt budget.

4.5 Discussion and Conclusions

In this paper we have presented measurements of the factors affecting the salt budget in a shallow, sinuous salt marsh estuary, the Duplin River, which is typical of a common class of such creeks in the marshes of the South Atlantic Bight. The salt flux in these creeks is controlled by an interplay between the input of fresh groundwater into the creek, derived primarily from aquifers beneath the adjacent barrier islands, the high tidal energy, tied to the large tidal range in the middle of the South Atlantic Bight, the dissipation of that tidal energy due to the shallow and sinuous nature of the creek channel, the influence of the intertidal marshes in distorting the tidal wave, evaporation in the main channel and evapotranspiration in the intertidal marsh.

The lower Duplin is characterized by its easy communication with Doboy Sound and its water is characteristically salty. Tidal processes mix this water in, over the 4 km length of the tidal excursion distance, establishing a strong along channel salinity gradient as this salty water mixes with the fresher water mass centered in the middle Duplin. This fresher water is presumably influenced by the fresh groundwater flux in and upstream of this region. Frictional distortion of the tidal wave due to the intertidal marsh areas results in a tidal wave which appears progressive on flood but that shows characteristics of a standing wave on ebb. There is very little stratification in this region, as the waters stay well mixed. The

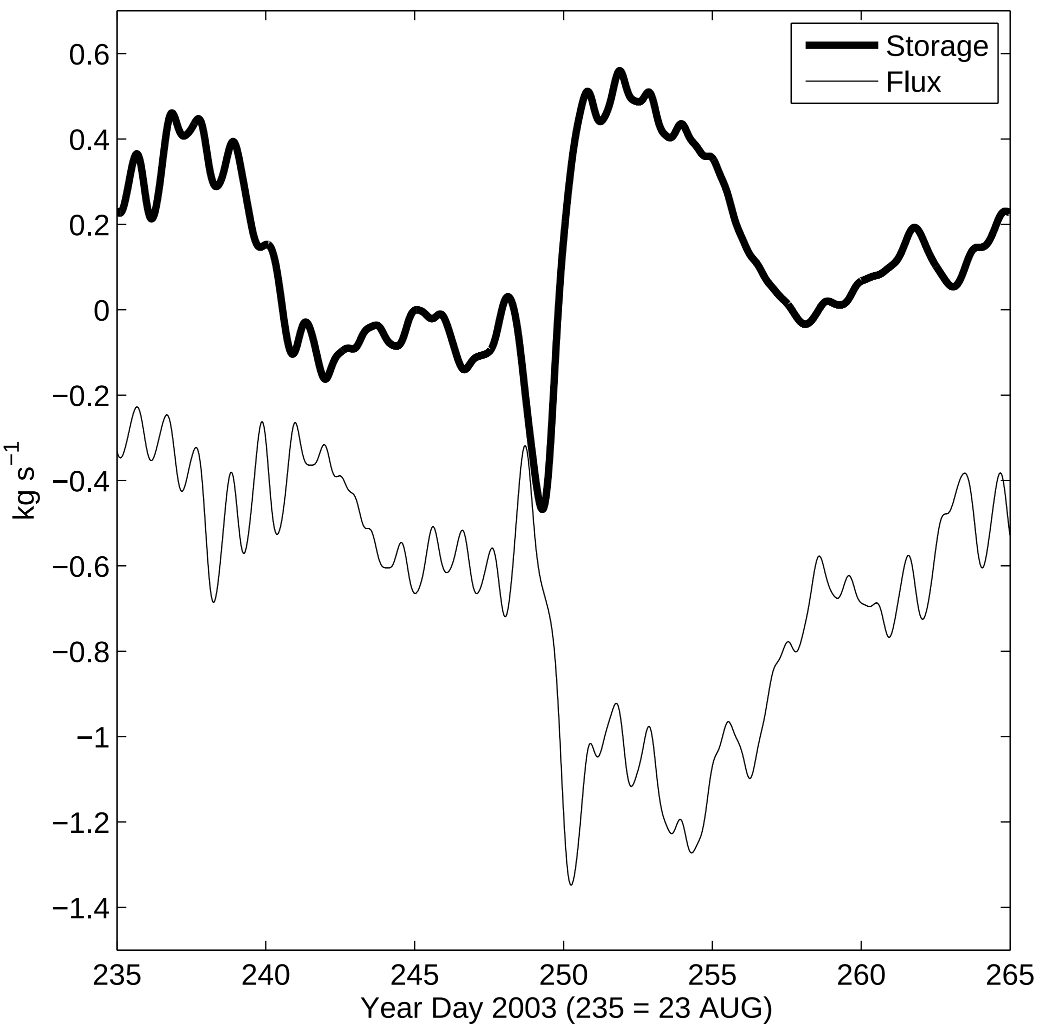

Figure 4.15: Tidally averaged salt storage $(\partial\left(\overline{\widetilde{s}\widetilde{h}}L\right)/\partial t)$ in the upper tidal prism of the Duplin and the negative of the along channel salt fluxes past the DUP03 mooring.

main contributor to tidal dispersion is the tidal wave transport that results in a net tidal flux of salt into the creek. This is generally opposed by the residual advection of salt out of the creek tied to the interplay between fresh groundwater input upstream and forcing due to offshore wind events. This residual advection is due to groundwater export, which varies with the spring/neap cycle, but is overwhelmed by the transport due to offshore forcing during this experiment.

While difficulties in making accurate measurements and in estimating upstream salt storage make it problematic to attempt to exactly correlate observed salt fluxes with trends in observed salinity (Simpson et al., 2001), the general form of the curves is instructive. In the lower Duplin the measured salt fluxes due to advective and dispersive processes agree in shape and sign with estimated salt storage in the lower Duplin tidal prism for most of the deployment period. The deviations from this agreement, especially around YD 260 when the shapes agree but the signs do not, point to the importance of poorly constrained, and here unmeasured, processes to the local salt budget. These include along channel salt dispersion due to tidal trapping, to transport across the upper bound of the tidal prism and to the intertidal marsh's role in sequestering and releasing salt tied to marsh inundation. The steady state concentration of salt due to evaporation in the main channel and evapotranspiration in the marsh is shown to be insignificant to the local salt budget but the marsh may act to store salt and release it in episodic events tied to the increased inundation due to high spring tides and increases in mean water depth due to offshore forcing.

The upper Duplin is somewhat isolated from the lower Duplin and Doboy Sound by the sinuous nature of the main channel which serves to dissipate the energy of the tidal wave as it progresses up the creek. These waters are characteristically fresh, with a low along channel salinity gradient, reflecting the influence of the broadly distributed fresh groundwater flux into this region which results in a very small tidal salinity range. As in the lower Duplin, frictional effects distort the tidal wave while also significantly attenuating the tidal velocity. Tidal dispersive processes are dominated by the tidal wave transport, but this term is significantly lower than in the lower Duplin, reflecting the effect of the attenuated tidal velocity, and of the variable nature of the salinity gradient here. The net advection of water, per unit width, out of the creek is much higher than in the lower reaches. This reflects the much smaller cross-sectional area of the creek here while indicating that a larger portion of the total fresh groundwater input occurs above the DUP03 mooring. While offshore forcing is still important, and seen here in a change in the mean water depth, a strong spring/neap cycle, which is not seen in the lower Duplin advection, is observable here presumably showing the change in groundwater pumping with the changing hydraulic head due to spring/neap variations in tidal range.

The salinity gradient in the upper Duplin is low and variable, being positive on early spring tide as high tidal energy mixes salty Doboy Sound water into the middle Duplin and establishes a normal estuarine salinity gradient throughout the entire Duplin River basin. On neap tide it is believed that the influence of fresh groundwater input in the middle region of the Duplin, combined with lower penetration of salt from the lower Duplin into these waters, establishes a weaker negative along channel salinity gradient in the upper Duplin, which persists until the start of the next spring tide. As reversing estuaries are known (see, for example, Valle-Levinson and Bosley, 2003) they generally reverse on seasonal time scales rather than with a fortnightly period making the upper Duplin fairly unique in this respect.

The steady state flux of salt into the upper Duplin due to evaporation in the marsh and main channel is much higher than in the lower Duplin, as the ratio of the area of the flooded marsh to the main channel surface area is much higher, however it is still an insignificant term in the local salt budget.

Unlike in the lower Duplin, the measured salt fluxes through the channel do not correlate well at all, either in trend or sign, with the observed salinity trends in the upper Duplin. A constant net outflux of salt is observed despite a general trend of steady or rising salinity in these waters. As the main periods of mean salinity increase in the upper Duplin are on spring tides, when the marsh is more fully inundated than on neap tide, it is hypothesized that salt is concentrated in the marsh and is sequestered in the sediment and pore water on neap tide only to be resuspended and enter the main channel of the estuary on spring tide, thus explaining the impulsive nature of the salinity increase.

This apparently increased dependence of upper Duplin salinity on marsh interactions, as compared to the lower Duplin, agrees with previous observations from heat budget measurements during the same deployment (McKay and Di Iorio, 2008). Main channel heating in the upper Duplin was shown to be more dependent on marsh interactions than was similar heating in the lower Duplin.

A third water mass exists in the middle Duplin which was not measured during the experiment. This mass is highly variable and its properties are regulated by the fortnightly spring/neap cycle. On spring tide salty water from Doboy Sound mixes in while at the same time the increased hydraulic head due to the large tidal range presumably pumps greater amounts of ground water out of the aquifer. This allows fresh water to mix down into the lower Duplin establishing a strong salinity gradient in these waters. Increased salt penetration into the upper Duplin establishes a positive salinity gradient throughout the entire Duplin River basin. On neap tide the decreased tidal energy mixes salty Doboy Sound water in less vigorously while simultaneously less ground water is pumped into the system. Higher salinity water penetrates further into the middle Duplin establishing a still positive but less strong salinity gradient in the lower Duplin. This higher salinity water does not mix past the boundaries of the middle Duplin, while fresh water input into the middle Duplin does mix into the upper Duplin, thus reversing the sign of the salinity gradient and creating a negative estuary in the upper Duplin.

This work shows the importance of the intertidal marsh and of fresh water input (presumably from groundwater) to the salt budget in a tidal creek. The importance of the marsh and its side creeks to constraining the salt budget is apparent and further work should be done to better measure these poorly understood processes. As the intertidal marsh also serves an important source of sediment, carbon and nutrients to the main channel (see, for example, Wolaver and Spurrier, 1988; Childers and Day, 1990a,b; Cai et al., 2003; Wang and Cai, 2004) an understanding of the spatial and temporal variations in the relative importance of the marsh to the salt budget, especially the spring/neap variability and the relative importance of the marsh to the upper and lower Duplin, can serve to inform research into the influence of the marsh on the budget of other substances of concern.

4.6 Acknowledgments

This work was supported by the NSF (OCE-9982133) as part of the Georgia Coastal Ecosystems - Long Term Ecological Research (GCE-LTER) project (`http://gce-lter.marsci.uga.edu`). We are thankful to Dr. Jackson Blanton who played a critical role in the design of the Duplex I experiment. Thanks also go to the captains and crew of the R/V Savannah and R/V Spartina for their assistance in deploying and recovering moorings, to Julie Amft and Trent Moore of the Skidaway Institute of Oceanography for their assistance with the instrumentation and along channel surveys, to Ken Helm of the UGA Marine Institute for his assistance in maintaining the GCE moorings and finally to Dr. Pam Knox, the assistant state climatologist of Georgia, for her assistance in providing information on evaporation rates for the Georgia coast.

Bibliography

Banas, N., Hickey, B., and MacCready, P. (2004). Dynamics of Willapa Bay, Washington: A highly unsteady, partially mixed estuary. *Journal of Physical Oceanography*, 24:2413–2427.

Blanton, J., Andrade, F., Adelaide-Ferreira, M., and Amft, J. (2007). A digital elevation model of the duplin river intertidal area. Technical report, Final report submitted to the GCE-LTER Program, University of Georgia.

Blanton, J., Schwing, F., Weber, A., Pietrafesa, L., and Hayes, D. (1985). Wind stress climatology in the South Atlantic Bight. In Atkinson, L., Menzel, D., and Bush, K., editors, *Oceanography of the Southeastern U.S. Continental Shelf*, pages 10–22. American Geophysical Union.

Boesch, D. and Turner, E. (1984). Dependence of fishery species on salt marshes: The role of food and refuge. *Estuaries*, 17(4):460–468.

Bowden, K. (1965). Horizontal mixing in the sea due to a shearing current. *Journal of Fluid Mechanics*, 21(2):83–95.

Cai, W.-J., Wang, Z., and Wang, Y. (2003). The role of marsh-dominated heterotrophic continental margins in transport of CO2 between the atmosphere, the land-sea interface and the ocean. *Geophysical Research Letters*, 30(16):1849–1853.

Childers, D. and Day, J. (1990a). Marsh-water column interactions in two Louisiana estuaries, I. Sediment dynamics. *Estuaries*, 13(4):393–403.

Childers, D. and Day, J. (1990b). Marsh-water column interactions in two Louisiana estuaries, II. Nutrient dynamics. *Estuaries*, 13(4):404–417.

de la Cruz, A. (1973). The role of tidal marshes in the productivity of coastal waters. *The Association of Southeastern Biologists Bulletin*, 20:147–156.

Dyer, K. (1974). The salt balance in stratified estuaries. *Estuarine and Coastal Marine Science*, 2:273–281.

Dyer, K. R. (1997). *Estuaries: A Physical Introduction*. John Wiley and Sons.

Emery, W. and Thompson, R. (2004). *Data Analysis Methods in Physical Oceanography: Second and Revised Edition*. Elsevier.

Fairall, C., Bradley, E., Rogers, D., Edson, J., and Young, G. (1996). Bulk parameterization of air-sea fluxes for tropical ocean-global atmosphere coupled-ocean atmosphere response experiment. *Journal of Geophysical Research*, 101:3747–3764.

Fischer, H., List, E., Koh, R., Imberger, J., and Brooks, N. (1979). *Mixing in Inland and Coastal Waters*. Academic Press, Inc.

Fofonoff, P. and Millard, R. (1983). Algorithms for computation of fundamental properties of seawater. Technical Report 44, UNESCO Technical Paper in Marine Science.

Geyer, W. and Signell, R. (1992). A reassessment of the role of tidal dispersion in estuaries and bays. *Estuaries*, 15(2):97–108.

Hackney, C., Burbanck, W., and Hackney, O. (1976). Biological and physical dynamics of a Georgia tidal creek. *Chesapeake Science*, 17(4):271–280.

Hughes, C., Kalma, J., Binning, P., Willgoose, G., and Vertzonis, M. (2001). Estimating evapotranspiration for a temperate salt marsh, Newcastle, Australia. *Hydrological Processes*, 12:957–975.

Hussey, B. and Odum, W. (1992). Evapotranspiration in tidal marshes. *Estuaries*, 27:59–67.

Islam, M., Hibino, M., and Tanaka, M. (2006). Distribution and diets of larval and juvenile fishes : Influence of salinity gradient and turbidity maximum in a temperate estuary in upper Ariake Bay, Japan. *Estuarine, Coastal and Shelf Science*, 68(1-2):62–74.

Kjerfve, B. (1986). Circulation and salt flux in a well mixed estuary. In van de Kreeke, J., editor, *Physcis of Shallow Estuaries and Bays*, pages 22–29. Springer Verlag: Berlin.

Lewis, R. (1997). *Dispersion in Estuaries and Coastal Waters*. John Wiley and Sons.

McKay, P. and Di Iorio, D. (2008). Heat budget for a shallow, sinuous salt marsh estuary. *Continental Shelf Research, in press*.

Medeiros, C. and Kjerfve, B. (2005). Longitudinal salt and sediment fluxes in a tropical estuary: Itimaraca, Brazil. *Journal of Coastal Research*, 21:751–758.

Millero, F., Feistal, R., Wright, D., and McDougall, T. (2008). The composition of standard seawater and the of the reference-composition salinity scale. *Deep Sea Research I*, 55:50–72.

Minello, T., Able, K., Weinstein, M., and Hays, C. (2003). Salt marshes as nurseries for nekton: Testing hypothesis on density, growth and survival through meta-analysis. *Marine Ecology Progress Series*, 249:39–59.

Murray, S. and Siripong, A. (1978). Role of lateral gradients and longitudinal dispersion in the salt balance of a shallow, well-mixed estuary. In Kjerfve, B., editor, *Estuarine Transport Processes*, pages 204–214. University of South Carolina Press.

Odum, E. and de la Cruz, A. (1967). Particulate organic detritus in a Georgia salt marsh-estuarine ecosystem. In Lauff, G., editor, *Estuaries*, pages 383–388. AAAS.

Phillips, D. (1966). *The Dynamics of the Upper Ocean*. Cambridge University Press.

Ragotzkie, R. and Bryson, R. (1955). Hydrography of the Duplin River, Sapelo Island, Georgia. *Bulletin of Marine Science of the Gulf and Caribbean*, 5:297–314.

Rattray, M. and Dworski, J. (1980). Comparison of methods for analysis of the transverse and vertical contributions to the longitudinal advective salt flux in estuaries. *Estuarine and Coastal Marine Science*, 11:515–536.

Reimold, R., Gallagher, J., Linthurst, R., and Pfeiffer, W. (1975). Detritus production in coastal Georgia salt marshes. In Cronin, L., editor, *Estuarine Research I*, pages 217–220. Academic Press.

Roberts, J. and Roberts, T. (1978). Use of the butterworth low pass filter for oceanographic data. *Journal of Geophysical Research*, 83:5510–5514.

Simpson, J., Vennell, R., and Souza, A. (2001). The salt fluxes in a tidally energetic estuary. *Estuarine, Coastal and Shelf Science*, 52:131–142.

Underwood, G., Phillips, J., and Saunders, K. (1998). Distribution of estuarine benthic diatom species along salinity and nutrient gradients. *European Journal of Phycology*, 33:173–183.

Valle-Levinson, A. and Bosley, K. (2003). Reversing circulation patterns in a tropical estuary. *Journal of Geophysical Research*, 108:3331–3356.

Wang, Z. and Cai, W.-J. (2004). Carbon dioxide degassing and inorganic carbon export from a marsh dominated estuary (the Duplin River): A marsh CO2 pump. *Limnology and Oceanography*, 49(2):341–352.

Wolaver, T. and Spurrier, J. (1988). Carbon transport between a euhaline vegetated marsh in South Carolina and the adjacent tidal creek: contributions via tidal inundation, runoff and seepage. *Marine Ecology Progress Series*, 42:53–62.

Chapter 5

The Cycle of Vertical and Horizontal Mixing in a Tidal Creek[1]

[1]Submitted to *Estuarine, Coastal and Shelf Science*, 5/1/2008.

Abstract

An experimental study of vertical and horizontal mixing near the mouth of the Duplin River, a tidal creek bordered by extensive intertidal salt marshes near Sapelo Island on the central Georgia coast in the southeastern US, was carried out over several spring/neap cycles in September and October of 2005. Vertical mixing is shown to be modulated on both M4 and fortnightly frequencies with turbulent stresses being generated near the bed and propagating into the water column on periods of max flood and ebb and being significantly greater on spring tide than on neap. Horizontal mixing is driven by tidal dispersion, which is also modulated by the fortnightly spring/neap cycle. Net export of salt from the lower Duplin is shown to be due to residual advection modified by upstream tidal pumping which exhibits a pulsating character with net export taking place for a short period on spring tide followed by a longer period of net import of salt. Analogies are drawn for the use of salt as a tracer for the export of marsh derived sediment as well as carbon and other nutrients to the coastal ocean.

5.1 Introduction

Efforts to understand the nature of the transfer of materials and dissolved substances across the land-ocean boundary and into the coastal ocean must necessarily focus on the estuaries and tidal creeks where such fluxes are concentrated. Since the early work on estuarine dynamics (see for example, Pritchard, 1952, 1954; Hansen and Rattray, 1965) vertical mixing, largely driven by bottom stress, surface stress and internally generated turbulence, has been known to be an important control on the flux of dissolved substances through its action on vertical stratification. More recently the spring-neap cycle, with its attendant modulation of tidal energy, has come to be appreciated as an important control on this vertical mixing itself (see for example, Peters, 1997; Chant, 2002; Simpson et al., 2005; Chant et al., 2007).

Longitudinal fluxes are the result of both advective and dispersive processes (Dyer, 1997), with the advective fluxes due, primarily, to fresh water input at the head and the dispersive fluxes due to tidal processes, and thus maximum near the mouth of an estuary or tidal creek (Geyer and Signell, 1992). These longitudinal fluxes can vary greatly on seasonal and spring/neap time scales and with changes in fresh water input and tidal energy making them difficult to predict (see for example, Banas et al., 2004; Medeiros and Kjerfve, 2005).

This paper presents the results of a mooring experiment conducted over several spring/neap cycles in September and October of 2005 near the mouth of the Duplin River, a salt marsh tidal creek on the central Georgia coast, which was intended to quantify the influence of the spring/neap cycle on both vertical mixing and longitudinal tidal dispersion.

In this paper, Section 5.2 will discuss the physical mechanisms of vertical and horizontal mixing and dispersion in estuaries, Section 5.3 outlines the details of the experiment and data processing, Section 5.4 shows the measured mixing and dispersion results and, finally, Section 5.5 will discuss implications for a better physical understanding of mixing in a tidal creek and export to the coastal ocean.

5.2 Estuarine Mixing

5.2.1 Vertical Mixing

In a sheared flow, vertical mixing results from both internally generated turbulence and turbulence generated by friction and stress at the top and bottom boundaries. As will be discussed later for the Duplin River, in a vertically well mixed system, Abraham (1980) showed that bottom boundary turbulence is dominant, except at slack water, with maximum mixing occurring near the bottom and extending upwards into the water column. Near slack water, when there is little to no bottom friction, internally generated turbulence becomes important and mixing is more broadly distributed through the water column.

It is common to treat turbulent mixing as a gradient process parameterized against the mean velocity shear as a turbulent eddy viscosity, N_z, and eddy diffusivity, K_z, (with units of m^2 s^{-1}) such that,

$$-\langle u'w' \rangle = N_z \frac{\partial \langle u \rangle}{\partial z}, \tag{5.1}$$

$$-\langle w's' \rangle = K_z \frac{\partial \langle s \rangle}{\partial z}, \tag{5.2}$$

where u and w are the along channel and vertical velocities respectively, s is the salinity, brackets $\langle\ \rangle$ represent a time averaged quantity and primed values represent the turbulent fluctuations from the time average (Dyer, 1997).

In vertically well mixed and homogeneous water, the eddy viscosity and diffusivity are nearly equal and $K_z \approx N_z$. In the presence of stratification, vertical mixing has to act against a density gradient and both the eddy viscosity and diffusivity are reduced. However, as momentum is transferred more readily than mass in such a case, K_z is attenuated less than is N_z (Dyer, 1997).

5.2.2 Horizontal Mixing

Along channel horizontal mixing in an estuary is a result of the sum of several processes on widely distributed spatial and temporal scales: from turbulent to tidal and fortnightly scales. Similar to vertical mixing, the turbulent stresses given by the $-\langle u'u'\rangle$ and $-\langle u's'\rangle$ correlations give rise to horizontal eddy viscosity, N_x, and diffusivity, K_x, parameters which are generally on the same order as their vertical mixing analogues. Bowden (1965) showed how the interaction between stratification and shear in both the mean flow and the tidally oscillating flow can give rise to horizontal shear dispersion which can, depending on the strength of the stratification, be several orders of magnitude greater than the corresponding turbulent diffusion (Lewis, 1997).

The interaction between estuarine tides, bathymetry and irregularities at the channel edge can result in tidal dispersive fluxes due to tidal pumping, cross channel shear dispersion and tidal trapping (Fischer et al., 1979). Of these three mechanisms tidal pumping, the generally upstream net transport due to correlations between tidal depth, velocity and salinity, is usually dominant. The presence of vertical shear and stratification (Bowden, 1965) and a generally much smaller effect of lateral shear and salinity variability (Rattray and Dworski, 1980) can act to modulate this tidal pumping mechanism, especially in areas of high stratification or curvature in the main tidal channel (Dyer, 1974). Irregularities in the channel edge, side creeks, and intertidal flats contribute to along channel dispersion by holding water with which they are inundated on flood and not releasing it back into the main channel at the corresponding stage of ebb, effectively trapping the water and then mixing it back into a potentially dissimilar water mass on subsequent ebb tides (Fischer et al., 1979).

Similar to vertical mixing, it is common to parameterize each of these horizontal mixing processes against the along channel salinity gradient as a diffusivity K_x (with units of m^2 s^{-1}). A total K_x can then be defined as the sum of the K_x values due to turbulent, shear and tidal dispersion which accounts for the effect of all three of these processes.

5.3 Methods

5.3.1 Location and Conditions

The study site presented here is near the mouth of the Duplin River, a tidal creek located in the marshes of the Sapelo Island National Estuarine Research Reserve on the central Georgia coast in the southeastern U.S. (see Figure 5.1). The Duplin is approximately 13 km long and varies from less than 1 m wide at its head in the intertidal marsh to 250 m wide at its mouth. It connects with Doboy Sound, which in turn is connected to the coastal Atlantic Ocean. With an estimated tidal excursion of 4 km (Ragotzkie and Bryson, 1955) it is believed to have three tidal prisms. The upper reaches of the Duplin wind through extensive intertidal marshes characterized by mud flats, vegetated primarily with *Spartina alterniflora,* and cut by a network of side creeks and channels of varying sizes, while the lower reaches consist of a straight and wide channel with few side creeks bordered by more upland, marsh hammocks and creekless marsh.

The mean depth along the thalweg in the lower Duplin is approximately 6.5 m. The drainage area of the intertidal marsh is approximately 12 km^2 (Blanton et al., 2007). Tides are predominantly semi-diurnal with a range of 1-3 m on neap and spring tide respectively. Along channel tidal velocities show an ebb dominance of flow that is a common characteristic of this class of salt marsh estuary (Dronkers, 1986; Dyer, 1997; Blanton et al., 2002) with depth averaged maximum flood velocities in the lower reaches being less than 1 m s^{-1} on spring tide while the corresponding maximum ebb can reach 1.2 m s^{-1}.

Despite the lack of surface freshwater input there is a significant, though unmeasured, submarine groundwater input (Ragotzkie and Bryson, 1955) which establishes an along channel salinity gradient in the lower reaches which can be as much as 10 or more (as measured using the Practical Salinity Scale) over the length of the lower tidal prism. Upstream of this lower prism the waters are generally well mixed along channel and the salinity gradient, when present, is small and variable. There is significant tidal salinity variation in the lower

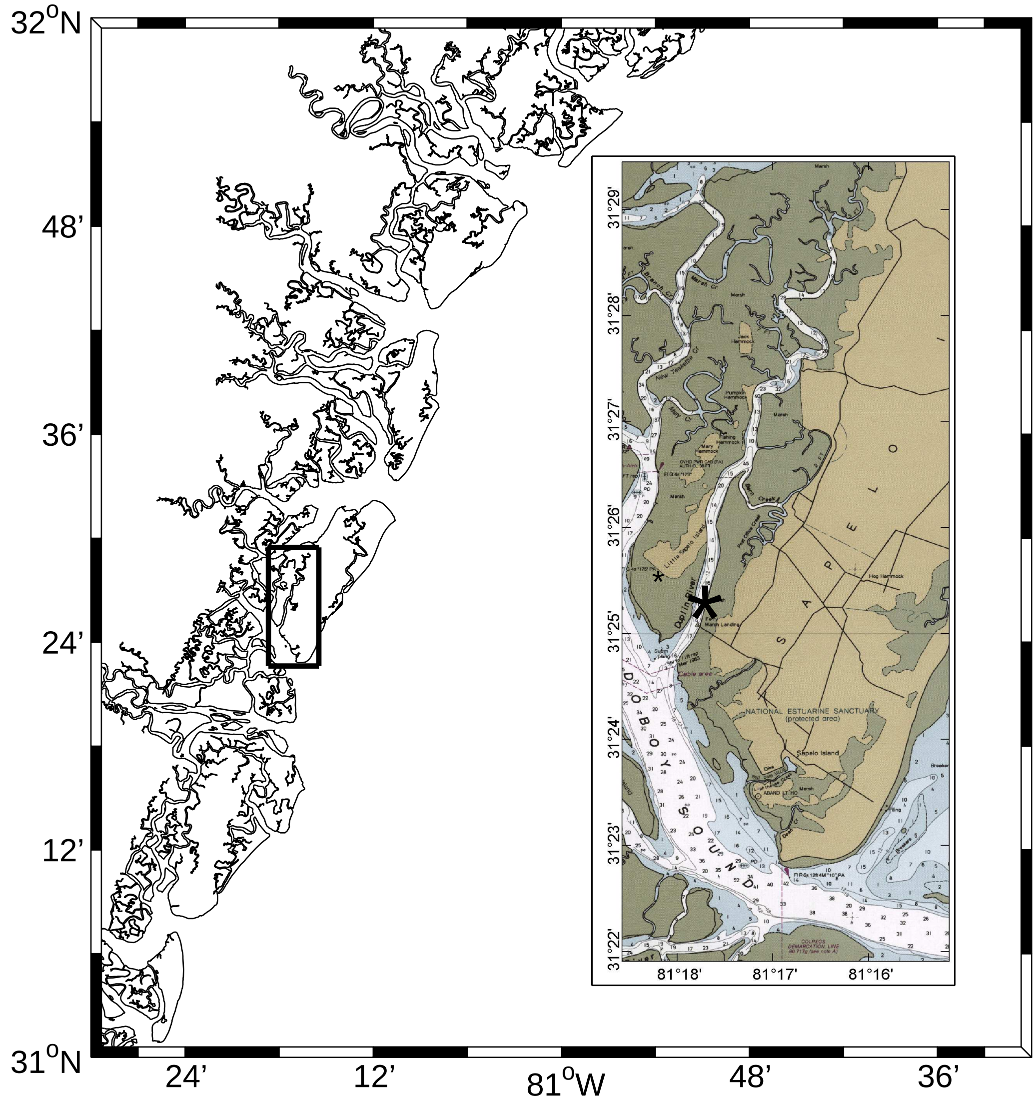

Figure 5.1: Chart showing the study area on the central Georgia coast. The black asterisk on the inset chart shows the ADCP mooring location in the lower Duplin River

reaches of the Duplin as water from Doboy Sound (influenced by the Altamaha River) is advected in (Kjerfve, 1973). While there are occasional periods of stratification in the lower Duplin believed to be related to changes in Altamaha River discharge, groundwater input, precipitation and oceanic forcing, it is generally vertically and laterally well mixed at all times. The location is not subject to any wave action beyond locally generated chop.

Meteorological conditions during the deployment were typical for the region (see Figure 5.2), which was in the middle of a prolonged drought. Winds were variable and generally less than 6 m s^{-1}, though reaching as high as 11 m s^{-1} during rain events, as measured at 10 m height at the weather station immediately adjacent to the deployment location. Sporadic rain showers were observed from 1–7 October and again on 22 and 25 October. Some of the decrease in mean salinity from year day (YD) 278–281 (as will be shown) is likely attributable to this rain event, however this period also corresponds with the spring tide, which is believed to increase fresh groundwater flux into the channel.

The mean properties of the Duplin have been previously reported on (see, for example, Ragotzkie and Bryson, 1955; Kjerfve, 1973; Imberger et al., 1983) but this is the first study to look at both horizontal and vertical mixing simultaneously in this system.

5.3.2 Instrumentation

The field experiment to measure the various mixing processes in the lower Duplin River was carried out over a 34 day period from 28 September to 31 October 2005 and covered two spring and two neap tides, ending shortly before a third spring tide. The experiment was designed to simultaneously measure vertical and horizontal mixing processes at the mouth of the Duplin accounting for the effects of the tidal interaction between salty Doboy Sound water advected in on flood and fresher upper/middle Duplin River water advected down on ebb, and of the fortnightly variations in tidal energy tied to the spring/neap cycle. Figure 5.1 shows a hydrographic chart of the study area on the Georgia coast as well as the location of the deployment site.

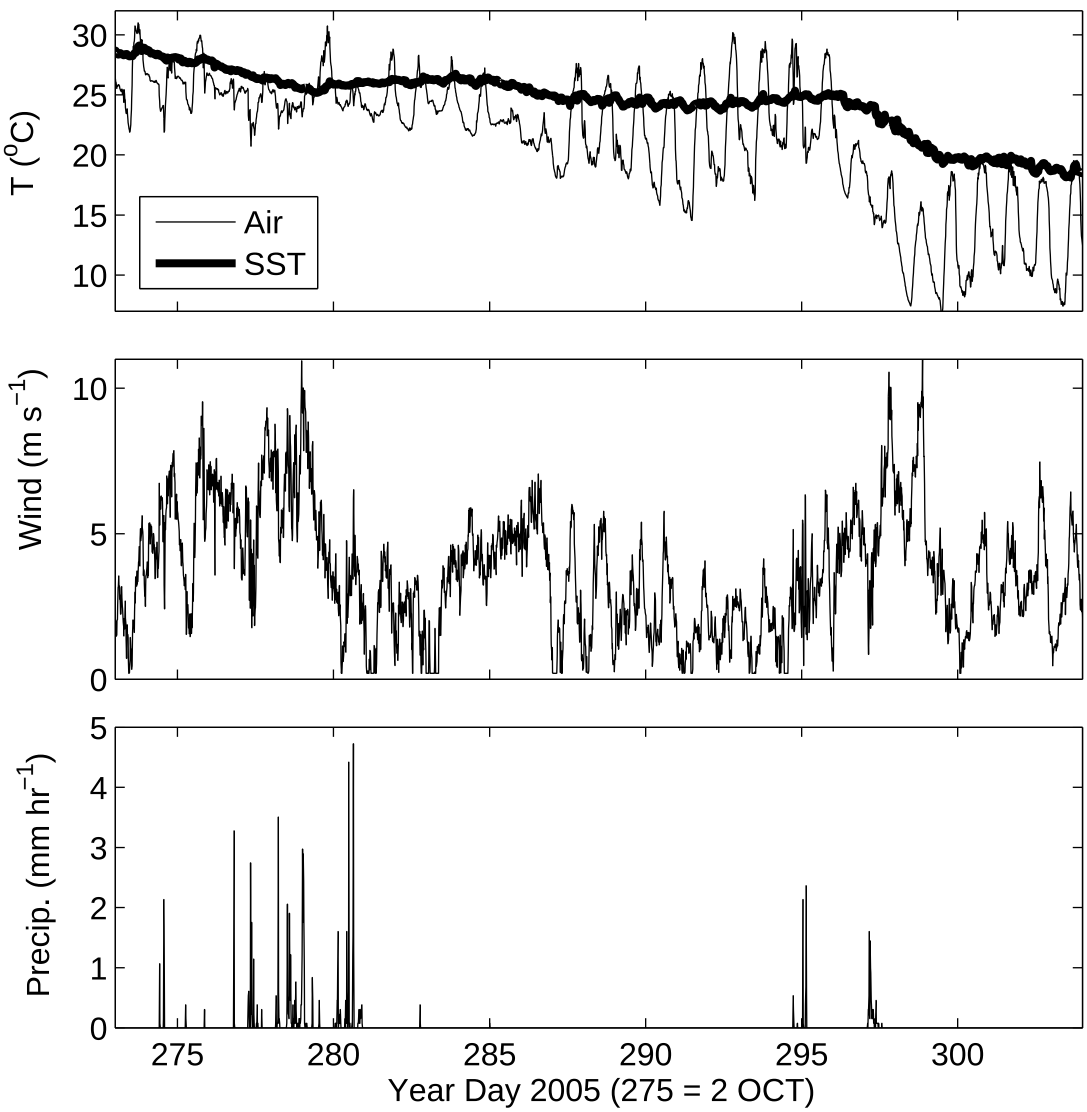

Figure 5.2: Air and water temperature, wind speed and precipitation rate at the Marsh Landing weather station immediately adjacent to the mooring location.

The instrument package was deployed during the September 2005 Georgia Coastal Ecosystems - Long Term Ecological Research (GCE-LTER) survey cruise with the R/V Savannah. A 4 beam 1200 kHz RDI Workhorse broadband ADCP was deployed on a heavy custom built pyramidal bottom mount mooring frame in the center of the channel in water with a mean depth of approximately 6.5 m. The ADCP operated in burst mode, sampling current velocity profiles at 2 Hz for 5 minutes every 30 minutes, and logged every ping in beam coordinate mode with 0.25 me depth bins. The first sample was centered 1.0 m above bottom. The 1-2 beam pair was aligned along the main axis of the channel. Seabird Microcat conductivity-temperature-depth (CTD) meters were moored at the surface, approximately 0.5 m beneath a tethered float, and bottom. Both sampled at 15 minute intervals.

Compass and pitch/roll sensors show that during this deployment the instrument's heading changed 0.5° over 34 days while pitch and roll started out at less than 3 and 1.5° respectively from the vertical with both settling to just over 1° over the first 10 days of the deployment and remaining constant for the rest of the deployment. While stress estimates are very sensitive to instrument alignment with the vertical, Lu and Lueck (1999) showed that errors in the stress estimate will be small for such small deviations. All time references were logged in UTC. Our coordinate system adheres to the estuarine convention such that x is the along channel direction and is positive out of the creek.

5.3.3 Salinity Data

The bottom Microcat salinity data became unreliable, due to biofouling of the sensor, on the fifth day of the deployment. Prior to this instrument failure, the surface and bottom measurements indicated that the system was vertically well mixed for both temperature and salinity at all times with the differences showing a random distribution and being below the noise threshold of each sensor. As this agrees with the authors' observations during two previous mooring experiments at this location in the Duplin River (McKay and Di Iorio, 2008) we have chosen to treat the surface values as being indicative of the entire water column. While the rain events likely introduced some short-lived stratification to the water column we were not able to measure this due to the failure of the bottom S. In all sections to come salinity will be reported as a unitless quantity in accordance to the practical salinity scale.

5.3.4 Vertical Mixing

For each beam, the velocity data at the top and bottom depth bins were deleted, to remove both surface noise and ringing near the transducer. Each beam was then further processed by removing all ping data with a PG (percent good) of less than 90% as reported by the internal diagnostics of the ADCP. For an ADCP logging every ping this is a measure of the echo strength of the returned signal. This resulted in the removal of one complete five minute ensemble on year day (YD) 289 as well as the removal of scattered other values, generally near the surface, which constituted less than 0.1% of the data. With the exception of the removed ensemble, deleted bins were replaced with a linear interpolation between the values in the bins above and below. Similarly, for each depth bin values were rejected which were three or more standard deviations away from the ensemble average and replaced with an interpolated value. This removed a similarly small amount of the data.

Along channel and cross channel velocities were calculated from the individual pings as

$$u = \frac{B_2 - B_1}{2\sin\theta} \tag{5.3}$$

$$v = \frac{B_4 - B_3}{2\sin\theta} \tag{5.4}$$

(Di Iorio and Gargett, 2005) where u is the along channel velocity, v the cross channel velocity, B is the along beam velocity for each beam, the 1-2 beam pair is aligned with the channel, the 3-4 beam pair is aligned cross-channel and θ is the beam angle (20° for the RDI ADCP used). The instantaneous u and v velocities were then averaged for each five minute ensemble to get the mean flow. To resolve the surface and bottom flows each velocity profile was extrapolated to the surface by assuming zero shear over a distance of 0.5m, and extrapolated to the bottom assuming a log layer profile over a 1.5 m distance.

Since the work of Lohrman et al. (1990), as elaborated by Stacey et al. (1999) and Lu and Lueck (1999), it has become common to estimate vertical eddy viscosity, and hence diffusivity of momentum, using a four beam, high frequency broadband acoustic Doppler current profiler (ADCP). This method, known as the variance method, allows the direct estimation of the Reynolds stress, $\tau_x/\rho = -\langle u'w' \rangle$, by comparing the velocity variances of opposing pairs of beams. This stress is determined using the relation

$$-\langle u'w' \rangle = \frac{\left\langle B_{2f}^2 \right\rangle - \left\langle B_{1f}^2 \right\rangle}{2\sin 2\theta} \tag{5.5}$$

(Di Iorio and Gargett, 2005) where $\left\langle B_{1f}^2 \right\rangle = \langle B_1^2 \rangle - \langle B_1 \rangle^2$, B_1 is the velocity along the beam one direction and the subscript f implies fluctuations. $\left\langle B_{2f}^2 \right\rangle$ is similarly defined but opposite from beam one. The time varying stress can then be estimated throughout the water column and parameterized against the observed vertical velocity gradient and thus N_z can be estimated using Equation (5.1). Noting that the system is well mixed and vertically homogeneous K_z is known as well.

This method requires the flow to be horizontally homogeneous such that there is no variation in the turbulent statistics over the separation distance between corresponding bins in each beam pair (Lu and Lueck, 1999). This condition is met by our deployment location being in the middle of the channel in a region of nearly constant cross-section. The sampling rate of 2 Hz and vertical bin size of 0.25 m allows us to resolve the smaller eddies in the flow which are involved in vertical momentum transfer (Rippeth et al., 2002). The 5 minute ensemble time represents a compromise between concerns of instrument battery life, the need for a statistically significant sample size and the need for quasi-stationary conditions during the sample period. Sampling for 5 minutes at 2 Hz provided a statistically significant 600 samples per ensemble while the 5 minute ensemble time, in a flow dominated by semi-diurnal and longer variability, was short enough to insure quasi-stationary conditions during the entire record.

Stress profiles were calculated for each ping in the record and then averaged for each five minute ensemble to give one stress profile for each half hourly sampling period. The statistical reliability of the Reynolds stress estimates increases with the square root of the number of samples per ensemble according to the relation given by Williams and Simpson (2004)

$$\sigma_R^2 = \frac{\gamma\left(\sigma_N^2 - \left\langle B_{if}^2\right\rangle\right)^2}{M\sin^2 2\theta} \tag{5.6}$$

where σ_R^2 is the mean squared variability of the Reynolds stress estimate, γ is a factor depending on the covariance of the individual velocity values, σ_N is the instrument noise level, $\left\langle B_{if}^2\right\rangle$ the mean square value of the turbulent fluctuations and M is the number of samples per ensemble.

From Equation(5.6) we can estimate a threshold value for detectable stress by examining low flow, when B_{if} goes to zero and γ to one, and taking a value for instrument noise of $\sigma_N = 0.017$ m s^{-1} from the instrument manufacturer. This then gives an approximate minimum measurable stress τ/ρ=2x10^{-5} m^2 s^{-2}.

To estimate the vertical eddy diffusivity, K_z, it is necessary to parameterize $-\langle u'w'\rangle$ against the vertical shear in the along channel velocity, $\partial\langle u\rangle/\partial z$, in the region where stresses are resolved by the ADCP. As small variations in $\langle u\rangle$ between depth bins can cause large swings in the value of $\partial\langle u\rangle/\partial z$, as calculated using numerical differentiation techniques, each velocity profile was smoothed by fitting with a polynomial and the gradient taken by differentiating that polynomial. As the shape of the velocity profile changes through the tidal cycle from being nearly linear to showing slight curvature, each profile was fit with both first and second order polynomials; the fit with the highest r^2 value was selected for the differentiation. The velocity profile was generally linear with a maximum at the surface.

Vertical mixing time during the tidal cycle can be estimated from low pass filtered values for depth averaged K_z, such that K_z is considered stationary within each tidal period, as

$$t = \frac{\overline{h}^2}{8\overline{\widehat{K}}_z} \tag{5.7}$$

(Lewis, 1997) where t is the approximate time for complete vertical mixing, in seconds, $\overline{h}$ the tidal mean water depth and $\overline{\widehat{K}}z$ the tidal and depth averaged eddy diffusivity. This estimated mixing time is based on the estimated time required for a concentrated substance in the middle of the water column to assume a Gaussian concentration distribution with depth.

5.3.5 Horizontal Mixing

As can be seen in Figure 5.1, our deployment is in an area with a straight channel with few side creeks or irregularities, reducing the importance of tidal trapping to along channel dispersion in this region. Further, previous work has shown little lateral variability in salinity and, as will be discussed, the mooring site can be regarded as generally unstratified thus allowing both the vertical and lateral shear contributions to along channel dispersion to be neglected. Since dispersion due to tidal processes is very much greater than that due to turbulent stresses, the latter may be neglected as well and along channel dispersion in these waters may be seen as primarily the result of tidal processes.

Following the work of Hansen (1965), as modified by Medeiros and Kjerfve (2005), and noting that the Duplin is vertically well mixed for salt, the depth integrated along channel flux of salt, or any conservative scalar, per unit width past the mooring along the centerline of the Duplin River, $F(t)$, is given by

$$F(t) = h(t)\widehat{u}(t)s(t) \tag{5.8}$$

where $h(t)$ is the tidally varying depth, $\widehat{u}(t) = 1/h\int_{-h}^{0} u(z,t)dz$, is the depth averaged along channel velocity and $s(t)$ is the salinity, which is held to be constant with depth.

We decompose the time varying quantities into their tidal mean (capitalized) and tidal deviations from that mean (subscripted t) such that

$$h(t) = H + h_t \tag{5.9}$$

$$\widehat{u}(t) = \widehat{U} + \widehat{u_t} \tag{5.10}$$

$$s(t) = S + s_t \tag{5.11}$$

From this point on, in the interest of simplicity and consistency of notation, we will drop the $\widehat{}$ denoting the depth average of u with the understanding that all references to the u velocity in reference to tidal dispersion refer to the depth averaged velocity. Now substituting (5.9 - 5.11) into (5.8), expanding terms and averaging over a tidal cycle we can write that

$$\overline{F} = HUS + H\overline{u_t s_t} + U\overline{h_t s_t} + S\overline{h_t u_t} + \overline{h_t u_t s_t} \tag{5.12}$$

where the overline represents a tidally averaged quantity.

Considering the right hand side of Equation (5.12), the first term, HUS, represents the advection of salt due to tidally averaged residual flows reflecting changes in freshwater discharge, mean depth and offshore forcing. The remaining terms account for the longitudinal tidal dispersive transport due to correlations between tidally varying quantities. After normalizing the tidal dispersive terms by the tidal mean water depth, H, they can be parameterized against the tidal mean along channel salinity gradient, $\partial S/\partial x$, to obtain an effective along channel tidal mean dispersion coefficient, K_x, which parameterizes the dominant along channel dispersive processes in the Duplin.

5.4 Results

5.4.1 Mean Flow

The upper pane of Figure 5.3 shows the depth distribution of the along channel velocity u, positive on ebb, at the mooring during a 14 day spring-neap-spring transition toward the beginning of the experiment. Along channel velocity profiles are generally linear with a minimum near the bed and a maximum near the surface. The second pane shows the depth averaged along channel velocity, $\widehat{u}$, during this same period. This term varies strongly with the spring/neap cycle and shows the ebb dominance of flow which is a common characteristic of this class of salt marsh estuary (Dronkers, 1986; Dyer, 1997; Blanton et al., 2002).

The entire period of observation is shown in Figure 5.4, separated into residual (40 hour low pass filtered) and tidal components. The upper pane shows the depth averaged

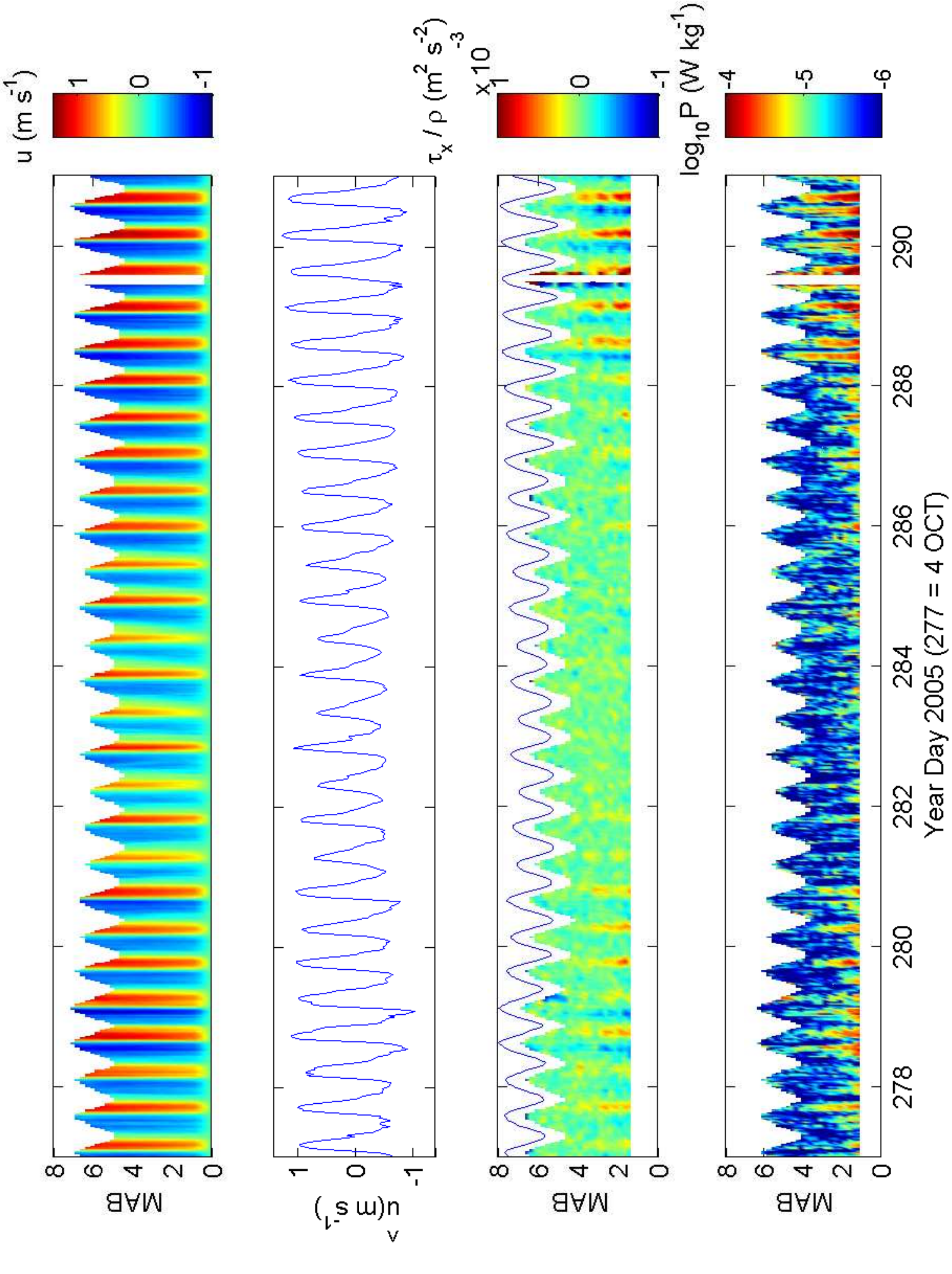

Figure 5.3: Along channel velocity u, depth averaged along channel velocity $\widehat{u}$,Reynold's stresses τ_x/ρ and turbulent kinetic energy production ($\log_{10}$P) during spring-neap-spring period from year day 277 to year day 291

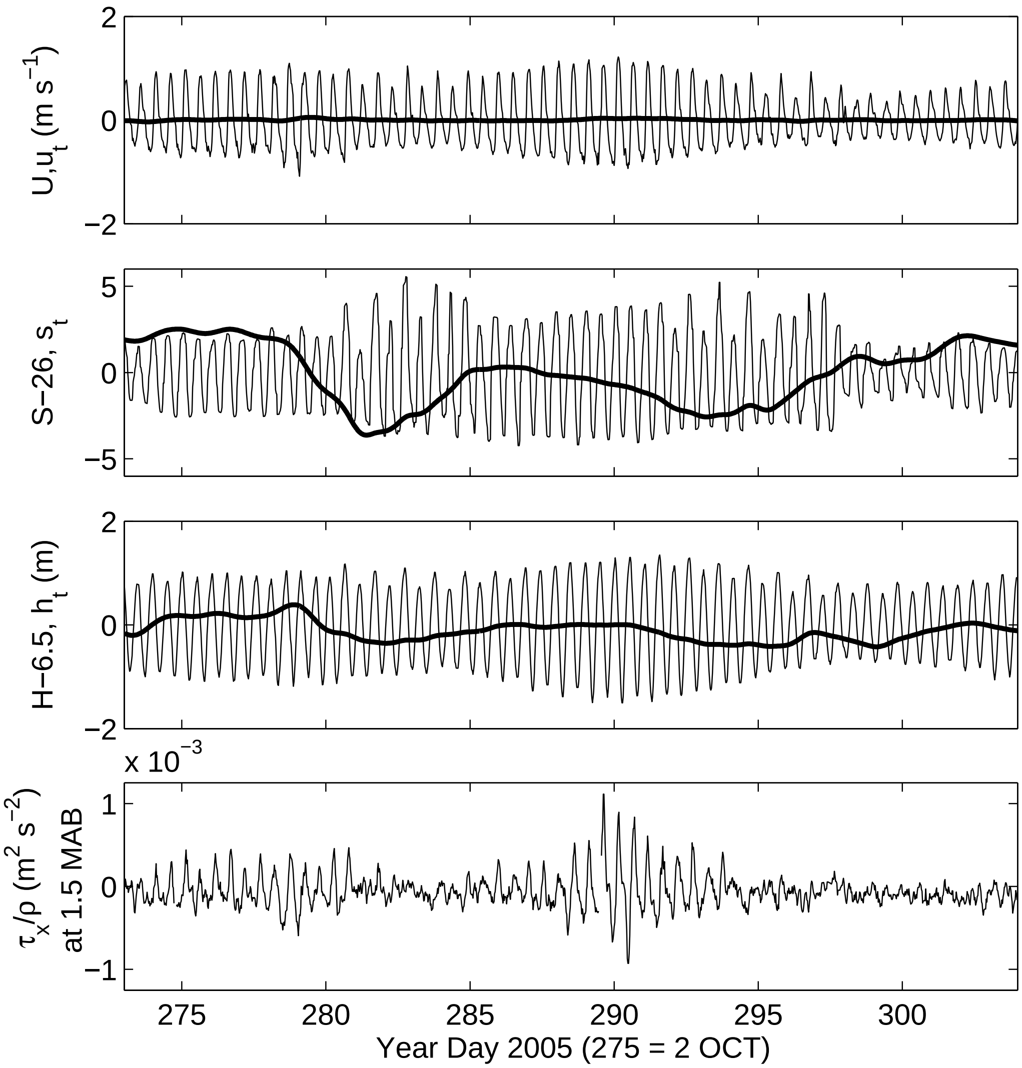

Figure 5.4: Depth averaged along channel velocity, surface salinity and center channel water depth, all decomposed into tidal and residual components. The heavy lines represent a 40 hour low passed tidal average of the relevant quantity. The Reynolds stress, τ_x/ρ, at 1.5 MAB is shown during the entire deployment period in the bottom pane.

quantities for the along channel flow. Surface salinity, which is taken as representative of the entire water column, is in the second pane with center channel depth shown in the third pane. In all three panes the heavy line represents the 40h low passed tidal average, with the mean salinity and depth removed where appropriate. A strong spring/neap cycle can be seen in both along channel tidal velocity and tidal depth variation with strong spring ebb flows peaking as high as 1.2 m s^{-1} while weak neap ebb flows are as slow as half of that, and a tidal depth range from 1 meter on neap to 3 meters on spring tide. Further, a marked semi-diurnal tidal asymmetry can be observed, most prominently at neap tide, with a strong flood/ebb pair being followed by a weaker one. This is especially pronounced during the second, smaller, neap tide. The flow is ebb dominant, showing a shorter, stronger ebb which contrasts with a longer but weaker flood. This is due to frictional distortion of the tide, caused by interactions between the main channel and the intertidal areas, which can be expressed by the relationship between the M2 and M4 tidal constituents (Dyer, 1997). Salinity varies throughout the experiment with a tidal salinity range of between 5 and 7 and a mean salinity varying between 23 and 28.

5.4.2 Stresses and TKE Production

In the third pane of Figure 5.3 we show the stress ($\tau_x/\rho = -\langle u'w' \rangle$) through the water column during the first spring-neap-spring period. Maximum stresses originate near the bed and propagate upwards into the water column decreasing in the upper layers. The periods of highest stress are found during the spring tide centered around max flood and ebb when the stresses reach as high as $\pm\ 1.2\times10^{-3}$ m^2 s^{-2} near the bed and show an M4 distribution. There is a pronounced tidal asymmetry in the stress production. Peak values are near the bed being lower on flood than ebb and with the stresses on ebb penetrating significantly further into the water column than on flood, due to peak ebb velocities being much higher, though of shorter duration, than flood. At neap tide there is greatly decreased stress production on max ebb and flood with consequently less penetration of the stress into the water column.

Near slack water, at both spring and neap tides, stress production is uniformly low and patchy throughout the water column as bed shear becomes low and the low production from internally generated turbulence dominates (Abraham, 1980).

The bottom pane of Figure 5.3 shows the turbulent kinetic energy production calculated as $P = -\langle u'w'\rangle\,\partial\langle u\rangle/\partial z$ and plotted on a logarithmic scale. As the system is vertically well mixed for both temperature and salinity the seawater density is constant with depth and thus the TKE production mirrors the stress distribution being concentrated on spring tide and showing an M4 frequency distribution. Peak TKE production is approximately 5×10^{-4} W kg^{-1} decreasing upwards into the water column. In the absence of buoyancy fluxes and turbulent transport, TKE production could balance the dissipation of TKE.

The bottom pane of Figure 5.4 shows a time series of τ_x/ρ in the lowest good bin, centered 1.5 m above bottom (MAB), for the entire deployment period. Both fortnightly and semi-diurnal variability in stress production are clearly visible with peak stresses during spring tides being much higher than during neap tides, when they are very low, and with the peak stresses during the second spring tide being more than double those during the first. Semi-diurnal variability is seen in that peak positive, ebb tide, stresses are significantly higher than peak negative, flood tide, stresses due to the asymmetry in ebb and flood velocities. Cross channel stresses, $\tau_y/\rho = -\langle v'w'\rangle$, are not shown in these plots as they are uniformly low, owing to the low cross channel velocity.

Our measurement of near bed stress, near the top of the constant stress layer, is compared to an estimate of bottom stress computed using the quadratic drag law, such that

$$\tau_b = \rho C_D\,|u_b|\,u_b, \tag{5.13}$$

where τ_b is the bottom stress, C_D is a constant bottom drag coefficient and u_b is the along channel velocity at 1.0 MAB extrapolated from the measured velocity profile assuming a log layer below the lowest measured bin at 1.5 MAB.

Figure 5.5 shows measured near bed stress, τ_b/ρ, plotted against the calculated bed stress $C_D|u_b|u_b$. The bottom drag coefficient C_D has a value of 3.35x10^{-3} which is obtained from a

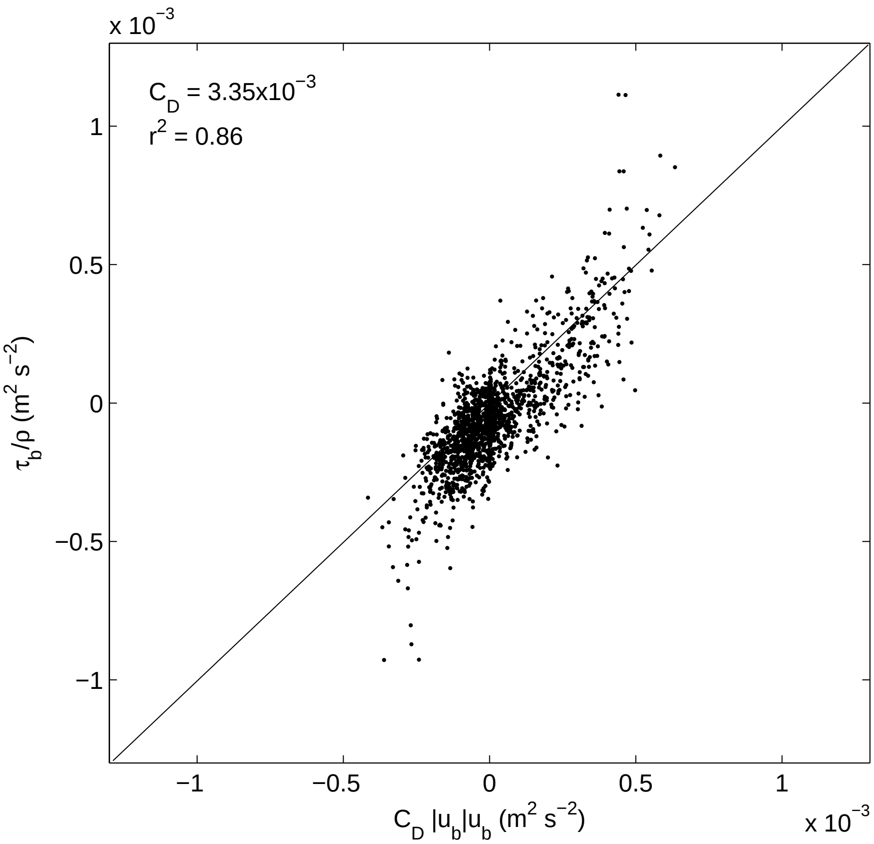

Figure 5.5: Plot of the relation between measured stress (τ_b/ρ) and the bottom stress predicted by the quadratic drag law ($C_D|u_b|u_b$). The line shows the 1:1 correspondence. Regression between the measured stresses and $|u_b|u_b$ gives an r^2 value of 0.86 with a slope, and thus drag coefficient, of 3.35x10^{-}3.

linear regression of τ_b/ρ versus $|u_b|u_b$, which has a regression coefficient, r^2, of 0.86. This value is within the range given by Soulsby (1990) for a mud bed and close to the value determined by Geyer et al. (2000) using the same technique for a similar bed in the Hudson River. The 1:1 correspondence is shown by the solid line. The plot shows fair correspondence in low to mid-velocities but shows that the quadratic drag law underpredicts the stress at max ebb and flood on spring tide.

5.4.3 Vertical Eddy Diffusivity

Vertical eddy viscosity, K_z, is calculated by parameterizing the stress, τ_x/ρ, against the vertical shear, $\partial\langle u\rangle/\partial z$. The top pane of Figure 5.6 shows depth normalized hourly velocity profiles from max flood to max ebb on October 18 (YD 291) at the peak of the strong second spring tide. The velocity profiles can be seen to be nearly linear through the portion of the water column resolved by the ADCP with little curvature, and thus nearly constant shear as the log layer occurs below the lowest ADCP bin. Given this profile, parameterizing the stresses, which are greatest at the bottom and decrease with height above bed (see Figure 5.3), against a nearly constant shear, $\partial\langle u\rangle/\partial z$, results in a K_z profile with depth which rather than having the classic parabolic shape follows a near linear distribution with depth. What parabolic shape there is to the K_z profile will occur below the lowest measured ADCP bin. While stresses are lower on flood than on ebb, shear is less on flood than on ebb. This results in high values for vertical eddy viscosity penetrating further upwards into the water column than they do on ebb.

Significant stresses are mainly generated around the time of max flood and ebb at spring tide and these will thus be the times of the greatest vertical mixing. The bottom pane of Figure 5.6 shows depth normalized profiles of the calculated values of K_z at the times of max flood and ebb at the peak of the two spring tides. As with the stresses, the values are greatest near the bed with values of 1.2×10^{-2} m^2 s^{-1} rapidly decreasing with height above bottom to near zero close to the surface. Flood and ebb values are similar and both follow

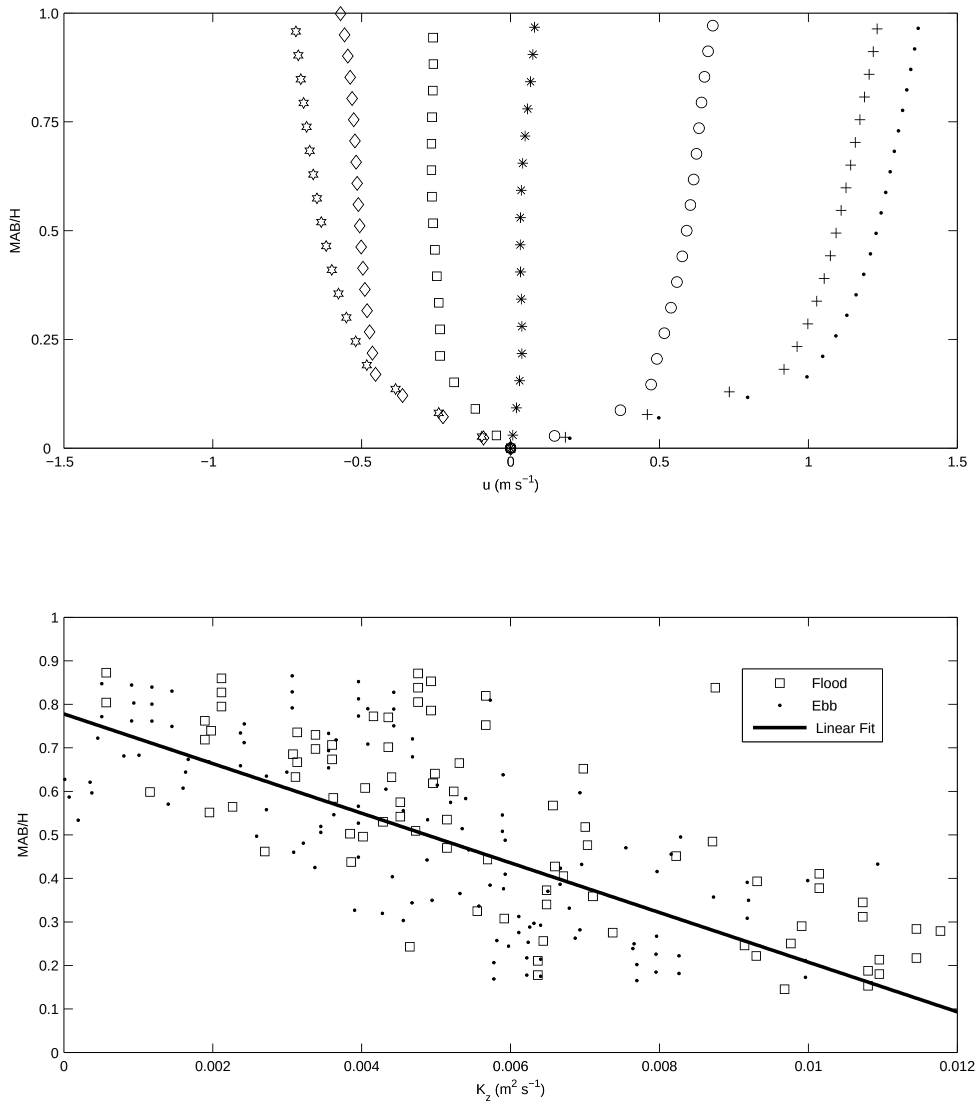

Figure 5.6: Profiles of along channel velocity through one tidal cycle from max ebb to max flood on YD 291 (upper pane). The lower pane shows profiles of K_z at max ebb and max flood, during the times of significant stress generation on spring tide. Depths are normalized with respect to channel depth. The linear fit in the lower pane has an r^2 of 0.81.

the plotted least squares linear fit, which has an r^2 value of 0.81. The spread in the values is concentrated in the mid water region where deviations from a linear velocity profile are most likely to occur.

Neap tide stresses are similarly concentrated around times of max flood and ebb but, as can be seen in Figure 5.3, the periods of significant stress generation are much shorter than on spring tide and the high stress region does not penetrate nearly as far up into the water column. Outside of the times and regions of high stress the stresses are low, patchy and variable and do not present a well defined profile.

As substances mix through the water column they experience the entire vertical range of mixing energy. This range can be parameterized as an effective depth averaged $\widehat{K}_z$ which is shown in the upper pane of Figure 5.7. Both tidal and fortnightly variability are apparent with values fluctuating strongly during the tidal cycle tied to the generation of stress at the bed. $\widehat{K}_z$ shows M4 variability tied to the four periods of max flood and ebb during each lunar day. The mean value of $\widehat{K}_z$, shown by the heavy line as a 40 h low pass filtered value, varies on a fortnightly time scale being highest on spring tides, centered around YD 277 and 290, in the range of $4 - 6 \times 10^{-3}$ m^2 s^{-1} and lowest on neap tide, being half to a third of the spring tide values. Even the low values, however, represent significant vertical mixing in this shallow system (Lewis, 1997).

Equation (5.7) allows us to calculate the approximate time for complete vertical mixing during a tidal period as a function of the mean water depth and the tidal mean, depth averaged value of K_z. This is shown in the bottom pane of Figure 5.7 plotted in minutes. Even at its slowest, complete vertical mixing is achieved in slightly over one hour and at spring tide takes as little as 20 minutes. This is very much less than the tidal period and supports our conclusion that the lower Duplin stays well mixed at all times unless acted upon by an outside influence.

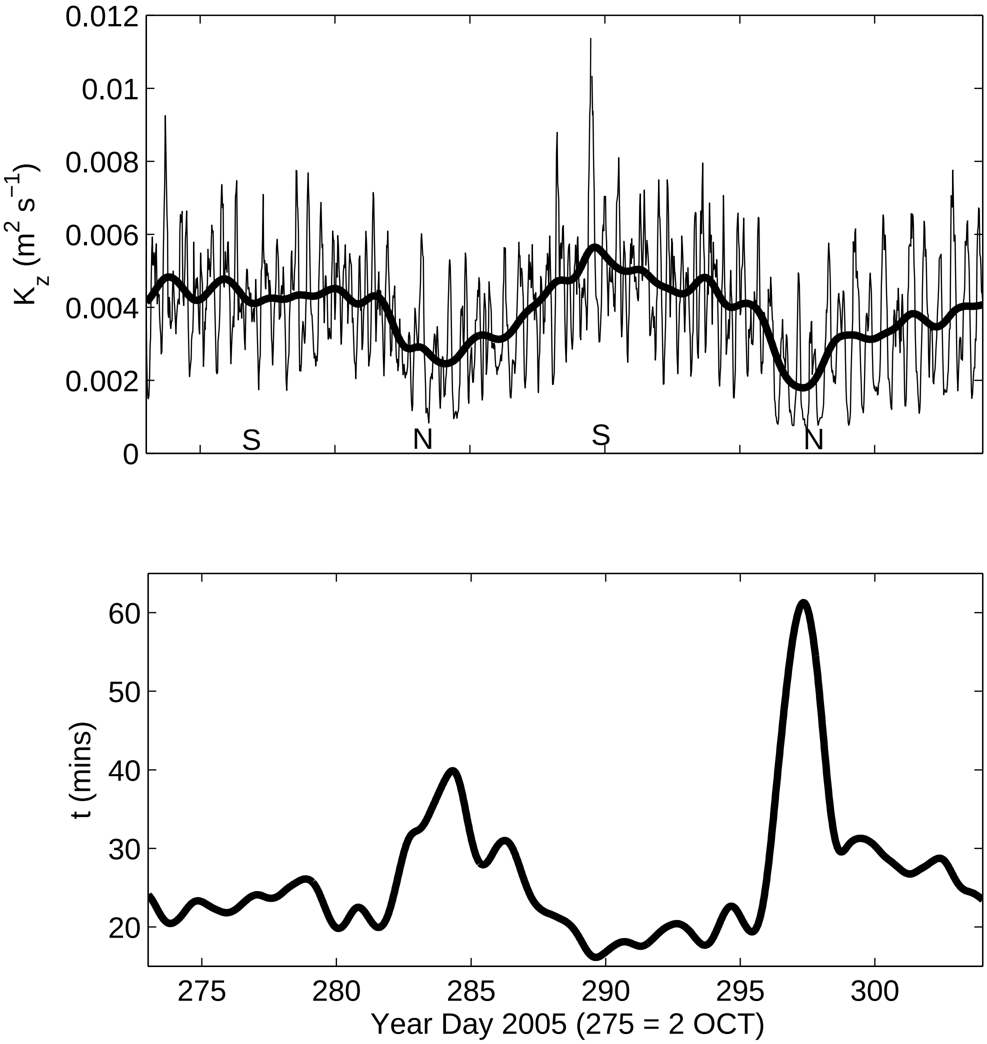

Figure 5.7: Time series of depth averaged vertical eddy diffusivity ($\widehat{K}_z$) and vertical mixing time (t) during the deployment period. The heavy lines indicate 40 hour low pass tidal averaged values. S and N label times of spring and neap tide respectively

5.4.4 Horizontal Mixing

While the rain events during the deployment period could serve to create stratification, thus potentially modifying the along channel salt fluxes, the vertical mixing caused by tidal stress serves to homogenize the water column. When vertical mixing is vigorous and the mean vertical turnover time is very much less than the tidal period (as has been shown) Lewis (1997) showed that the along channel dispersion coefficient in a tidal channel due to both steady state and tidal shear can be estimated as

$$K_{xs} = \frac{u_s^2 h^2}{30K_z} + \frac{U_s^2 H^2}{60K_z}, \tag{5.14}$$

where the mean and tidal velocity have a nearly linear profile with depth (as has been shown) and have values of u_s and U_s respectively at the surface.

The maximum estimated magnitudes of the tidally averaged along channel dispersive coefficients due to stratification acting on shear in both the residual and tidally oscillating flow can be estimated from this relationship. K_x due to stratification acting on the shear in the residual flow ranges from 0.01 m^2s^{-1} on spring tide to 0.03 m^2s^{-1} on neap tide. Similarly K_x due to stratification acting on shear in the tidally oscillating flow ranges from 18 m^2 s^{-1} on spring tide to 21 m^2 s^{-1} on neap tide. As these values are very much lower, as will be shown, than the K_x term due to depth averaged tidal processes, the effects of possible stratification are judged to be a minor player in the long term salt budget during this experiment.

The dominant driver of along channel horizontal dispersion is then not turbulence or shear but the tidal correlations, which acts much more slowly but with greater energy and on larger scales than do turbulent and shear processes. The upper pane of Figure 5.8 shows a time series of the various tidal correlation terms in Equation (5.12) as well as their net sum (thick solid line). The largest of these tidal correlation terms is the salt flux into the Duplin due to the correlation between tidal velocity and depth (dashed line). The deeper water on the weaker but longer flood allows more salt to flow in than the shallow waters on the stronger but shorter ebb allow out. The next largest term is a net flux out due to

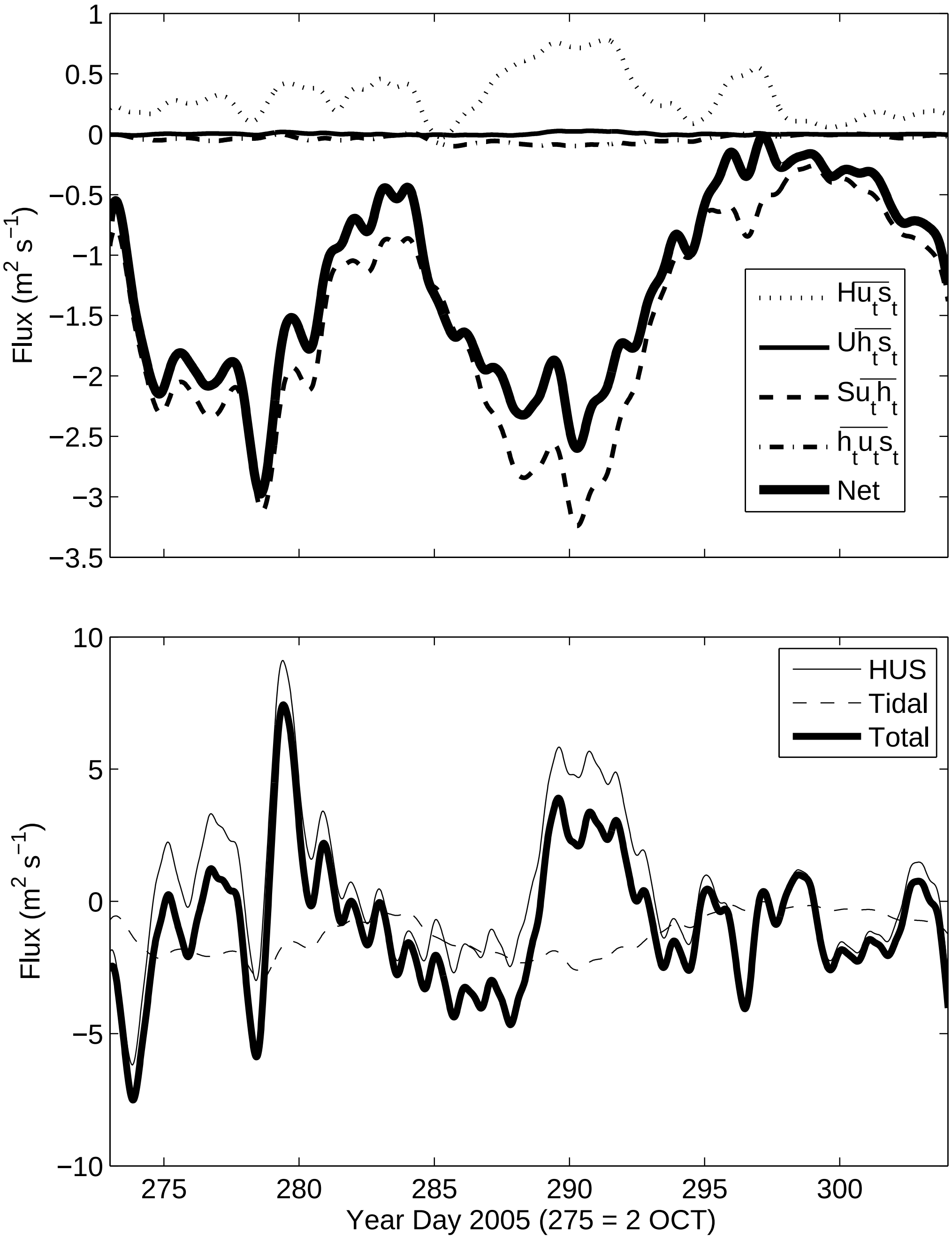

Figure 5.8: Time series of center channel salt flux components during the deployment period. The upper pane shows the various tidal constituents while the lower pane compares tidal and net advective fluxes.

the correlation between velocity and salinity (dotted line) caused by the higher ebb tide velocity exporting salt which has been mixed in on flood. Both of these terms show a strong spring/neap modulation with each approaching zero on neap tide and being greatest on spring. Of the remaining terms the correlation between depth and salinity (thin line) is negated by being multiplied by the very low mean velocity, on the order of ± 1 cm s^{-1}, and the triple correlation is similarly small. The net tidal flux is shown by the heavy line as a net flux of salt into the Duplin, where it follows the same strong spring/neap modulation as do its components.

The lower pane shows the tidal dispersive term (dashed line) along with the flux of salt due to residual advection (thin solid line) and the change in mean water depth tied to changes in storage volume. Despite the low residual velocity the residual advective term is much greater than the tidal pumping term due to the high value of the mean salinity compared to its tidal fluctuations. Net advection varies strongly on a spring/neap cycle showing a pulse-like export of salt on spring tides followed by a weaker, but longer, period of import of salt on neap tides. This pattern, which has been observed before in well mixed to partially stratified estuaries (see for example Nunes and Lennon, 1987; Bowen and Geyer, 2003) is believed here to be due to variations in the flux of fresh groundwater into the upper/middle Duplin caused by changes in the tidal range on the spring/neap cycle. On neap tide, when tidal range is small, little fresh groundwater is pumped into the upper/middle Duplin and thus little pressure is exerted on water in the lower Duplin and residual advection nears zero. Tidal pumping then brings salt into the lower Duplin and the salinity in this region increases. With the increased tidal range at spring tide, more fresh groundwater is pumped into the upper/middle Duplin which then flows down to the lower Duplin. Residual advection increases as this freshwater mass forces saltier water out of the lower Duplin and salinity decreases as it mixes into the lower Duplin water mass. Tidal dispersion of salt into the lower Duplin increases with the increased tidal energy but it is not enough to overcome the diluting effects of the fresh groundwater. When compared to lower Duplin salinity in the second pane of Figure 5.4 the net flux can be seen to closely correlate with changes in the mean salinity in the lower Duplin. The sharp, but short term, decrease in salinity around YD 280 as well as the lesser, but longer lasting, decrease around YD 290 both correlate with spring tide induced net export as shown in the lower pane of Figure 5.8 while the slow recovery periods correlate with the low net influx of salt on neap tide.

To get a net along channel dispersion coefficient for the lower Duplin we normalize the net tidal pumping term by the mean water depth and then parameterize it against the along channel residual salinity gradient, $\partial S/\partial x$, as is shown in Figure 5.9. The upper pane shows the depth normalized net tidal pumping term from Figure 5.8 while the second pane shows the along channel residual salinity gradient, calculated from the tidally averaged along channel advection of salt past the mooring as $\partial S/\partial x = (-1/U)\partial S/\partial t$. The salinity gradient is positive, showing saltier water toward the mouth of the Duplin, with its greatest value on neap tide as decreased tidal energy pumps less salt into the upper reaches of the creek. Parameterizing the depth normed net tidal pumping flux against the salinity gradient gives a value for the along channel tidal dispersion coefficient K_x. This is shown in the bottom pane and varies strongly on a fortnightly cycle from near 1000 m^2 s^{-1} on spring tide to close to zero on neap tide.

The long term mean of the K_x term is approximately 500 m^2 s^{-1}, which is significantly higher than the value of 300 m^2 s^{-1} predicted by the steady state theory of MacCready (2004). This is likely due both to the non-steady state nature of the estuary and the wide range of tidal energy on the spring/neap cycle.

5.5 Discussion and Conclusions

We have presented measurements near the mouth of a small and generally vertically well mixed tidal creek, the Duplin River, which serves as the main conduit between Doboy Sound and the intertidal marshes of the Sapelo Island National Estuarine Research Reserve. These measurements directly resolve the vertical velocity structure through most of the 6.5 m

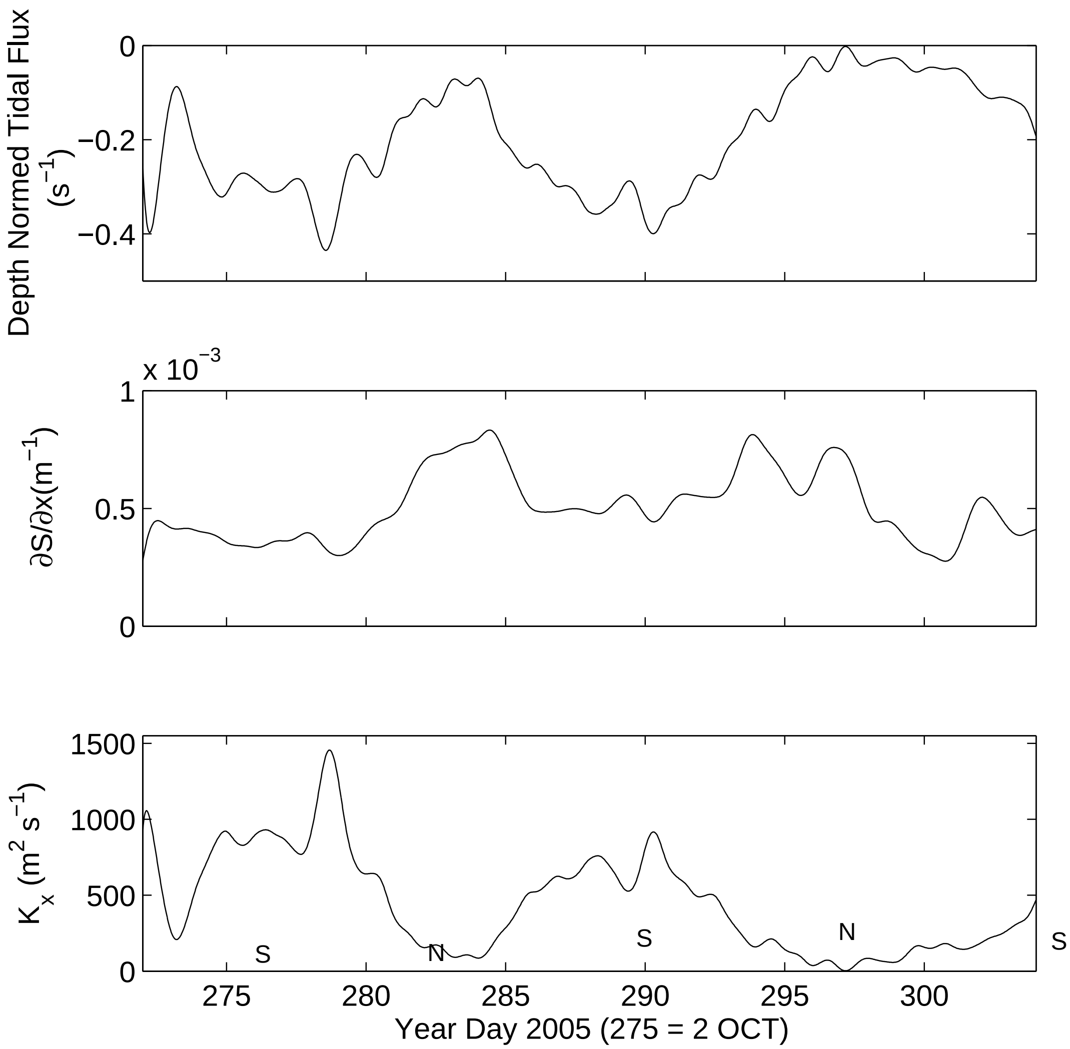

Figure 5.9: Time series of net center channel tidal salt fluxes normalized by mean depth, the along channel salinity gradient and the resultant along channel dispersive coefficient (K_x) during the deployment period

mean water depth of the lower Duplin as well as allow the estimation, through the variance method, of the stresses which give rise to vertical mixing. Through salt budget methods we also quantify the along channel tidal dispersion. Spanning a 34 day period, consisting of two spring and two neap tides along with the transitions between these tides, our measurements resolve the wide range of time scales, from turbulent, to tidal and fortnightly, which influence the mixing in these waters.

Estimates of the vertical turbulent stress, τ_x/ρ, show modulation on both tidal and fortnightly frequencies with maximum stress being generated near the bed on max flood and ebb at spring tide and penetrating high into the water column while neap tide stresses are weaker and concentrated near the bottom. Internally generated turbulence plays a larger role near times of slack water with stresses being more broadly distributed through the water column. Near bottom stress estimates agree fairly well with the predicted stresses from the quadratic drag model at all times except during maximum ebb and flood on spring tides. Geyer et al. (2000) have observed similar underprediction of stress by the quadratic model, when compared to stress both from measurement and a momentum stress model, at times of high flow, suggesting that the dynamics of the stress-velocity relationship change at high velocities. This has implications for modeling similar systems, suggesting that a simple quadratic drag model may be sufficient to model stresses at all but the highest velocities, such as occur for only a few hours per month at max flood and ebb on spring tide.

Due to the nearly linear profile of velocity with depth and the constant density, turbulent kinetic energy production closely mirrors the temporal and spatial distribution of stresses with high production through the water column at peak flood and ebb on spring tide and lower, though still significant, production at other times. Given the vertically well mixed nature of the water column the Richardson number is always much less than 0.25. Because of this lack of buoyancy effects we expect that turbulent production will be balanced by viscous dissipation. The estimated time for complete vertical mixing varies from 20 - 30 minutes on spring tide to 40 - 60 minutes on neap tide and is at all time very much less than the tidal period, thus insuring that the water column stays well mixed at all times during the deployment.

Tidal dispersive fluxes are, by nature, tidally averaged so we can not comment on intertidal variability and time scales. These fluxes show a strong spring/neap cycle with maximum upstream dispersive fluxes being found at spring tide while neap tide fluxes approach zero. The upstream flux due to the correlation between the tidally varying depth and velocity is the primary driver of along channel dispersion, but it is somewhat counterbalanced by an opposing dispersive flux due to the correlation between tidally varying velocity and salinity. These dispersive salt fluxes are generally overwhelmed by the net advective flux of salt due to the residual flow in or out of the creek. Residual flows in this environment can be tied to changes in groundwater input and oceanic forcing from meteorological events.

The net water flux is generally out at spring tide. The increased tidal range on spring tide increases the hydraulic head acting on the aquifer increasing the groundwater flux into the middle and upper Duplin (Schultz and Ruppel, 2002). This increases the downstream pressure gradient and thus increases the net outflow of water. On neap tide, groundwater input into the upper and middle Duplin decreases and tidal pumping, no longer opposed as strongly by residual export, brings salt in from Doboy Sound.

The total salt flux due to tidal dispersive and advective fluxes correlates well with the trends in lower Duplin salinity during the deployment period. Examining the net horizontal flux, it becomes apparent that the Duplin shows a net export of salt for a brief period on spring tide which is followed by a longer period of either net import or near neutral conditions. Salt export is then in a pulsating pattern tied to the fortnightly spring/neap tidal frequency.

The intertidal marsh which borders the Duplin serves as a source of sediment, carbon and nutrients which enter the main channel through the side creeks and through the inundation and draining of the marsh (see, for example, Wolaver and Spurrier, 1988; Childers and Day, 1990a,b; Cai et al., 2003; Wang and Cai, 2004). On entering the main channel of the Duplin these substances and nutrients are transported, mixed and dispersed through the creek by the same processes which largely control salinity resulting in a similar zonation in the Duplin (Hanson and Snyder, 1980). While dissolved materials entering the lower Duplin will be exported on every ebb tide the majority of the marsh-creak interaction occurs in the upper and middle Duplin (McKay and Di Iorio, 2008) and thus the concentration of dissolved and suspended sediment and nutrients will be greatest in this region. These substances will then be transported to the lower Duplin by the residual advective flow which is modulated on a spring/neap cycle. As the Duplin serves as the primary linkage between the intertidal marshes near Sapelo Island and the waters of Doboy Sound, and thus the Atlantic Ocean, the export of marsh derived carbon and other nutrients will follow a similar pattern to salt, accumulating in the upper and middle Duplin on neap tide and being exported to the coastal ocean in pulses at spring tide.

5.6 Acknowledgments

This work was supported by the NSF (OCE-9982133) as part of the Georgia Coastal Ecosystems – Long Term Ecological Research (GCE-LTER) project (`http://gce-lter.marsci.uga.edu`). Thanks also go to the captain and crew of the R/V Savannah for their assistance in deploying and recovering moorings and to Ken Helm of the UGA Marine Institute for his assistance in maintaining the moorings.

Bibliography

Abraham, G. (1980). On internally generated estuarine turbulence. In Carstens, T. and McClimans, T., editors, *Second international symposium on stratified flows*, pages 344–363. AIHR.

Banas, N., Hickey, B., and MacCready, P. (2004). Dynamics of Willapa Bay, Washington: A highly unsteady, partially mixed estuary. *Journal of Physical Oceanography*, 24:2413–2427.

Blanton, J., Andrade, F., Adelaide-Ferreira, M., and Amft, J. (2007). A digital elevation model of the duplin river intertidal area. Technical report, Final report submitted to the GCE-LTER Program, University of Georgia.

Blanton, J., Lin, G., and Elston, S. (2002). Tidal current asymmetry in shallow estuaries and tidal creeks. *Continental Shelf Research*, 22:1731–1743.

Bowden, K. (1965). Horizontal mixing in the sea due to a shearing current. *Journal of Fluid Mechanics*, 21(2):83–95.

Bowen, M. and Geyer, R. (2003). Salt transport and the time dependent salt balance of a partially stratified estuary. *Journal of Geophysical Research*, 108:27:1–15.

Cai, W.-J., Wang, Z., and Wang, Y. (2003). The role of marsh-dominated heterotrophic continental margins in transport of CO2 between the atmosphere, the land-sea interface and the ocean. *Geophysical Research Letters*, 30(16):1849–1853.

Chant, R. (2002). Secondary circulation in a region of flow curvature: Relationship with tidal forcing and river discharge. *Journal of Geophysical Research*, 107(C9):3131–3142.

Chant, R., Geyer, R., Houghton, R., Hunter, E., and Lerczak, J. (2007). Estuarine boundary layer mixing processes: Insights from dye experiments. *Journal of Physical Oceanography*, 25:1859–1877.

Childers, D. and Day, J. (1990a). Marsh-water column interactions in two Louisiana estuaries, I. Sediment dynamics. *Estuaries*, 13(4):393–403.

Childers, D. and Day, J. (1990b). Marsh-water column interactions in two Louisiana estuaries, II. Nutrient dynamics. *Estuaries*, 13(4):404–417.

Di Iorio, D. and Gargett, A. (2005). *Sounds in the Sea: From Ocean Acoustics to Acoustical Oceanography*, pages 500–517. Cambridge University Press.

Dronkers, J. (1986). Tidal asymmetry and estuarine morphology. *Netherlands Journal of Sea Research*, 20:117–131.

Dyer, K. (1974). The salt balance in stratified estuaries. *Estuarine and Coastal Marine Science*, 2:273–281.

Dyer, K. R. (1997). *Estuaries: A Physical Introduction*. John Wiley and Sons.

Fischer, H., List, E., Koh, R., Imberger, J., and Brooks, N. (1979). *Mixing in Inland and Coastal Waters*. Academic Press, Inc.

Geyer, W. and Signell, R. (1992). A reassessment of the role of tidal dispersion in estuaries and bays. *Estuaries*, 15(2):97–108.

Geyer, W., Trowbridge, J., and Bowen, M. (2000). The dynamics of a partially mixed estuary. *Journal of Physical Oceanography*, 30:2035–2048.

Hansen, D. (1965). Currents and mixing in the Columbia River estuary. In *Transaction of the Joint Conference of the Marine Technologocal Society and the American Society of Limnology and Oceanography*, pages 943–955.

Hansen, D. and Rattray, M. (1965). Gravitational circulation in straits and estuaries. *Journal of Marine Research*, 23:104–122.

Hanson, R. and Snyder, J. (1980). Glucose exchanges in a salt-marsh estuary: Biological activity and chemical measurements. *Limnology and Oceanography*, 25(4):633–642.

Imberger, J., Berman, T., Christian, R., Sherr, E., Whitney, D., Pomeroy, L., Wiegert, R., and Wiebe, W. (1983). The influence of water motion on the distribution and transport of materials in a salt marsh estuary. *Limnology and Oceanography*, 28(2):201–214.

Kjerfve, B. (1973). Volume Transport, Salinity Distribution and Net Circulation in the Duplin Estuary, Georgia. Technical report, ERC-0273 Marine Institute, University of Georgia, Sapelo Island, Georgia.

Lewis, R. (1997). *Dispersion in Estuaries and Coastal Waters*. John Wiley and Sons.

Lohrman, A., Hackett, B., and Roed, L. (1990). High resolution measurements of turbulence, velocity, and stress uding a pulse-to-pulse coherent SONAR. *Journal of Atmospheric and Oceanic Technology*, 7:19–37.

Lu, Y. and Lueck, R. (1999). Using a broadband ADCP in a tidal channel. Part II:Turbulence. *Journal of Atmospheric and Oceanic Technology*, 16:1568–1579.

MacCready, P. (2004). Toward a unified theory of tidally-averaged estuarine salinity structure. *Estuaries*, 27(4):561–570.

McKay, P. and Di Iorio, D. (2008). Heat budget for a shallow, sinuous salt marsh estuary. *Continental Shelf Research, in press*.

Medeiros, C. and Kjerfve, B. (2005). Longitudinal salt and sediment fluxes in a tropical estuary: Itimaraca, Brazil. *Journal of Coastal Research*, 21:751–758.

Nunes, R. and Lennon, G. (1987). Episodic stratification and gravity currents in a marine environment of modulated turbulence. *Journal of Geophysical Research*, 92:5465–5480.

Peters, H. (1997). Observations of stratified turbulent mixing in an estuary: Neap-to-spring variations during high river flow. *Estuarine, Coastal and Shelf Science*, 45:69–88.

Pritchard, D. (1952). Estuarine hydrography. *Advances in Geophysics*, 1:242–280.

Pritchard, D. (1954). A study of the salt balance in a coastal plain estuary. *Journal of Marine Research*, 13:133–144.

Ragotzkie, R. and Bryson, R. (1955). Hydrography of the Duplin River, Sapelo Island, Georgia. *Bulletin of Marine Science of the Gulf and Caribbean*, 5:297–314.

Rattray, M. and Dworski, J. (1980). Comparison of methods for analysis of the transverse and vertical contributions to the longitudinal advective salt flux in estuaries. *Estuarine and Coastal Marine Science*, 11:515–536.

Rippeth, T., Williams, E., and Simpson, J. (2002). Reynolds stress and turbulent energy production in a tidal channel. *Journal of Physical Oceanography*, 32:1242–1251.

Schultz, G. and Ruppel, C. (2002). Constraints on hydraulic parameters and implications for groundwater flux across the upland-estuary interface. *Journal of Hydrology*, 260:255–269.

Simpson, J., Williams, E., Brasseur, L., and Brubaker, J. (2005). The impact of tidal straining on the cycle of turbulence in a partially stratified estuary. *Continental Shelf Research*, 25:51–64.

Soulsby, R. (1990). *The Sea*, volume 9 of *Ocean Engineering Series*, pages 523–566. John Wiley and Sons.

Stacey, M., Monismith, S., and Burau, J. (1999). Measurements of Reynolds stress profiles in unstratified tidal flow. *Journal of Geophysical Research*, 104:10933–10949.

Wang, Z. and Cai, W.-J. (2004). Carbon dioxide degassing and inorganic carbon export from a marsh dominated estuary (the Duplin River): A marsh CO2 pump. *Limnology and Oceanography*, 49(2):341–352.

Williams, E. and Simpson, J. (2004). Uncertainties in estimates of Reynolds stress and TKE production rate using the ADCP variance method. *Journal of Atmospheric and Oceanic Technology*, 21:347–357.

Wolaver, T. and Spurrier, J. (1988). Carbon transport between a euhaline vegetated marsh in South Carolina and the adjacent tidal creek: contributions via tidal inundation, runoff and seepage. *Marine Ecology Progress Series*, 42:53–62.

Chapter 6

Discussion and Conclusions

6.1 Summary of Findings

A multi-year study has been conducted of the physical processes which regulate the distribution and cycle of temperature and salinity in the Duplin River, a salt marsh tidal creek in the Sapelo Island National Estuarine Research Reserve on the central Georgia coast. The results obtained have allowed an understanding of the structure of the three water masses in the Duplin as well as the relative importance of the physical processes which maintain those water masses.

6.1.1 Duplin River Water Masses and Characteristics

Temperature-Salinity diagrams of the Duplin at both spring and neap tide in August of 2003 show the Duplin to be divided into three water masses (see Figure 3.4). The location of these three masses is shown in Figure 6.1. The lower water mass, indicated in red, corresponds to the lower tidal prism described by Ragotzkie and Bryson (1955). This water is directly influenced by the water of Doboy Sound and is cool and salty during all of the measurement periods. This salty water mixes up the Duplin, driven by tidal dispersion, which is largely tied to the transport caused by the distorting effect of the marsh on the tidal wave. A strong salinity gradient is established in the lower Duplin as this salty water mixes with the fresher water advecting down from upstream.

Immediately upstream is the water of the middle Duplin, indicated in blue on Figure 6.1. This water is fresher, indicating the likely influence of fresh groundwater input into this region. Its temperature varies on a spring/neap cycle, being warmer than the lower Duplin on neap tide and as cool as the lower Duplin on spring tide. The salinity gradient in, and upstream, of the middle Duplin is very low resulting in very little upstream salt transport due to tidal processes. The middle Duplin is fresher on neap tide than on spring, a fact believed to be tied to the interplay between groundwater pumping into the middle Duplin and the input of salt tied to tidal pumping from the lower Duplin along with the release of salt previously sequestered in the marsh. This results in a salinity gradient between the

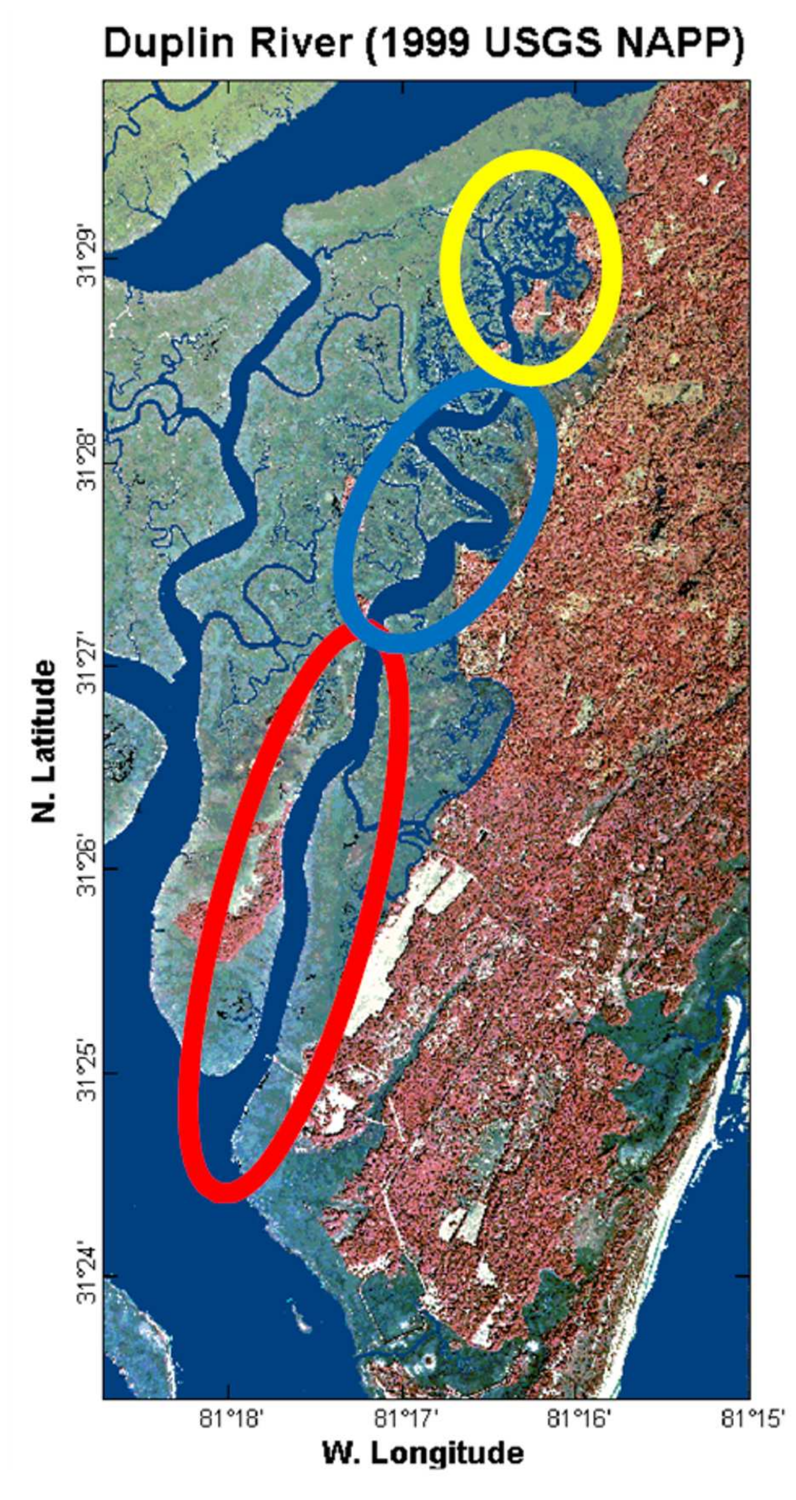

Figure 6.1: Approximate locations of the three water masses present in the Duplin River. Red indicates the lower Duplin water mass, blue the muddle Duplin and yellow the upper Duplin.

middle and upper Duplin, which changes sign on a fortnightly cycle making this region of the Duplin a reversing estuary.

The upper reaches of the Duplin define a third water mass which is warm and fresh, reflecting the influence of heating tied to the water's easy communication with the intertidal marsh and, presumably, the diluting effects of fresh groundwater input. While no direct measurements of groundwater input throughout the Duplin are available, point measurements have been made, particularly in the upper Duplin (Moses Hammock) and the lower edge of the middle Duplin (Barn Creek) indicating that significant amounts of groundwater do flow through the interface between the upland and the marsh (Schultz and Ruppel, 2002).

The middle and upper Duplin water masses are isolated from the lower Duplin by the sinuous nature of the channel, which dissipates tidal energy, and by the very low along channel salinity gradient which blocks tidal dispersion. This has been observed by Imberger et al. (1983) who noted that there was little communication between the water of the upper Duplin and that of the lower.

The characteristics of these water masses are likely to change over time in a manner tied to changes in groundwater input, meteorological conditions and the influence of the Altamaha River on Doboy Sound. The waters of the upper Duplin, which are warmer than the lower Duplin during late summer and fall, can be cooler than the lower Duplin in winter and early spring. This reflects the greater heat loss to the atmosphere this water experiences in the intertidal marsh and the shallow nature of these waters. Data from long term moorings of Seabird Microcat CTDs in the upper Duplin and Doboy sound from 2003 through 2006 indicate that the temperatures in Doboy Sound and the upper Duplin converge in late fall and stay similar until the spring warming begins. During this time the upper Duplin is sporadically cooler than Doboy Sound.

The salinity regime is also known to change in ways likely tied both to changes in groundwater input and the influence of the Altamaha River on Doboy Sound salinity. Kjerfve (1973), working in August 1969, observed a similar salinity distribution in the Duplin as has been described here. The head was even more dilute with salinities nearing 18 on the practical salinity scale. However Imberger et al. (1983), working in June and July 1977, reported a salinity which was nearly constant along the length of the Duplin except when disturbed by rain events which dramatically lowered upper Duplin salinity, which then quickly recovered. It seems likely that the diluting effect of fresh ground water, which serves to maintain the diluted nature of the upper and middle Duplin, was reduced during this period. Data from the long term moorings of Seabird Microcat CTDs in the upper Duplin and Doboy sound indicate that the upper Duplin is always fresher than Doboy Sound during the 2003-2006 time period; but, as the region was in a drought there was little effect of Altamaha River water. It is likely that when Altamaha River discharge is especially high Doboy Sound could become fresher than the Duplin resulting in the creek taking on the characteristics of a negative estuary along its entire length.

Vertical mixing has been shown to be vigorous and acts to homogenize the water column, eliminating stratification during these experiments. However, stratification has been noted by past researchers including Kjerfve (1973). This could be caused by a number of environmental factors including an increase in Doboy Sound salinity tied to changes in Altamaha River flow or offshore forcing, a change in middle and upper Duplin salinity tied to changes in fresh groundwater input, either of which could contribute to strain induced periodic stratification, or the input of fresh water tied to rain events.

The ease of communication between Duplin water and the intertidal marshes is tied to the number of small creeks and embayments which cut through the marsh. This helps to explain both the greater heating in the upper Duplin and the greater freshwater input in the upper and middle Duplin, as these regions have more small creeks than does the lower Duplin region, which is largely devoid of them. Increased communication with the marsh will cause increased exchange of properties and substances with the marsh surface including salt, as evapotranspiration removes water from the marsh surface but leaves behind salt.

6.1.2 A Box Model of Subtidal Processes in the Duplin River

Despite the increasingly common use of sophisticated hydrodynamic models to understand estuarine processes (see for example Levasseur et al., 2007; Sousa and Dias, 2007), box models still enjoy wide popularity for their relative ease of setup and use and can provide valuable insight into estuarine physics. Models based on salt budget techniques are often used to estimate residence time and flushing (see for example Miller and McPherson, 1991; Hagy et al., 2000). Models using salt, water volume and other tracers are used to estimate freshwater discharge, including groundwater, (Crusius et al., 2005; Garvine and Whitney, 2006). While many, if not most, box models are based on an assumption of steady-state they can often be modified to account for changing conditions in estuaries which are not in a steady-state (see for example Li et al., 1999; Hagy et al., 2000).

Model Design

A simple three box model of subtidal processes in the Duplin has been created to allow a better understanding of the influence of the unmeasured groundwater and salinity inputs to maintaining the characteristics of the Duplin River, especially in the completely unmeasured middle Duplin water mass. Figure 6.2 shows a schematic layout of the model. Box 1 encloses the water of the upper Duplin, from its head to the top of the sinuous middle region. This water is fresher than Doboy Sound water and is influenced by interactions with the marsh and by groundwater. Box two encloses the water of the middle Duplin from the top of the sinuous mid-region to the maximum extent of the salinity intrusion from Doboy Sound. This water is also fresh showing the influence of groundwater input and interactions with the intertidal marsh. The third box encloses the water of the lower Duplin, from the upper extent of the tidal excursion to the outlet and connection with Doboy Sound. This water is salty, showing the influence of Doboy Sound.

The model implements both a water volume and a salt budget in order to derive an estimate of the unmeasured groundwater input and the unmeasured salt input due to inter-

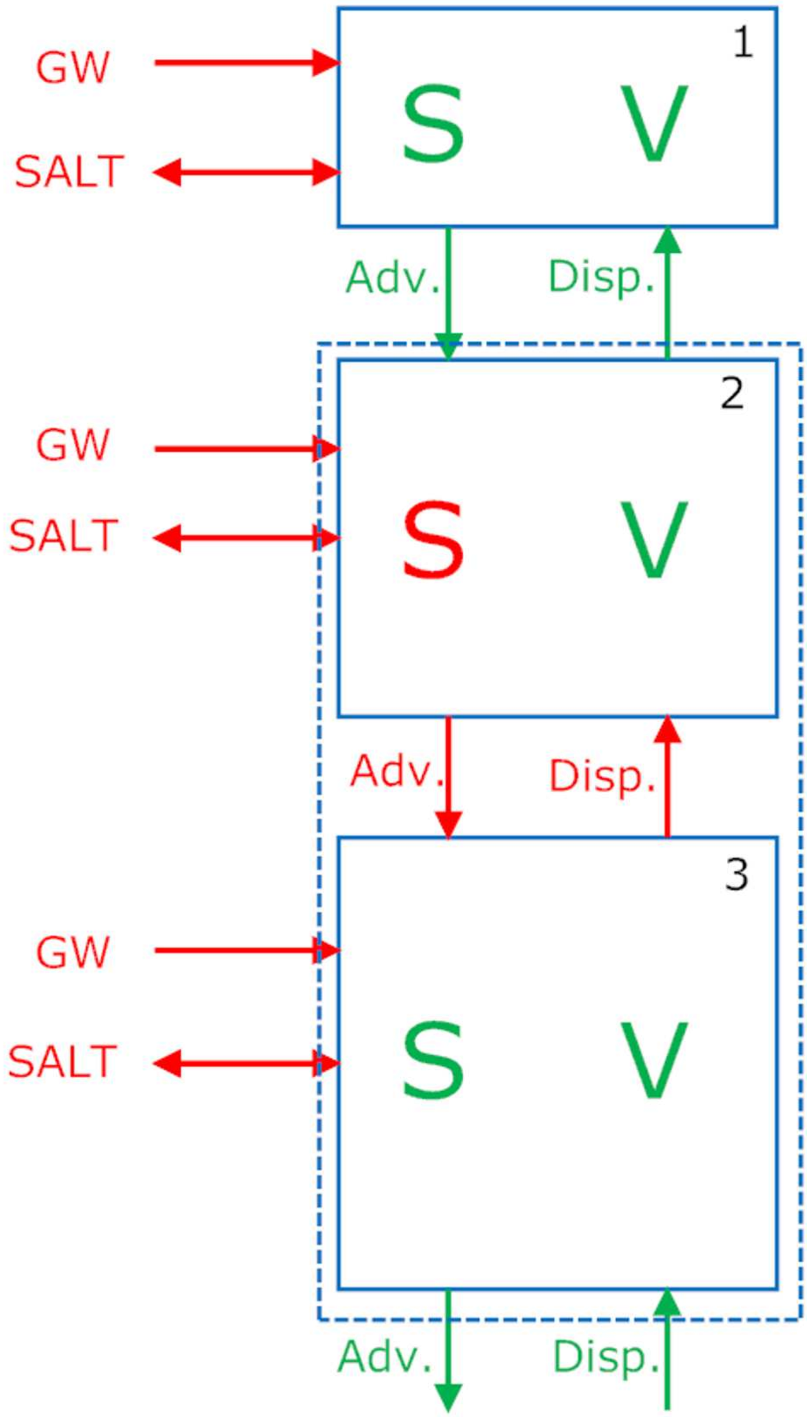

Figure 6.2: Schematic of the three box Dublin River subtidal model. Quantities in green are measured while red indicates unknown processes.

actions with the intertidal marsh, which can include salt storage in and release from the marsh, transport due to tidal trapping, and other unmeasured processes. The model requires measurements of salinity and water volume within each box as well as the residual transport rate into and out of each box, and the rate of tidal dispersive salt transport into and out of each box. Figure 6.2 shows each of these inputs with quantities in green being known and quantities in red being unknown. The effects of evaporation and precipitation in the main channel are neglected as they have previously been shown to be small (see Section 4.4.2).

In its general form, the water budget for the middle box is written as

$$\frac{\partial V}{\partial t} = Adv.(1-2) + Adv.(2-3) + GW \tag{6.1}$$

where V is the subtidally varying storage volume of box 2, $Adv.(1-2)$ is the rate of advection of water from box 1 to box 2, $Adv.(2-3)$ is the rate of advection of water out of box 2 and into box 3 and GW is the groundwater input into box 2.

A set of seven cross-sections were surveyed along the axis of the Duplin at the start of the DUPLEX experiment in August 2003 using the echosounder of the R/V Gannet. These surveyed sections allow the estimation of the cross-sectional area of the Duplin at the boundaries of the three boxes as a function of tidally averaged depth. Interpolating between these surveyed cross-sections and taking channel lengths from hydrographic charts of the Duplin, an estimate of the storage volume of each box, as a function of tidally averaged depth, can also be made. While there are a number of approximations of creek bathymetry required to make these estimates, the fact that the variation in tidally averaged depth generally occurs in a straight sided portion of the channel cross-section simplifies the geometry and allows a fairly accurate estimate of $\partial V/\partial t$ to be made. The advective water fluxes are calculated as the product of the tidally averaged along channel velocity, U, and the cross-sectional area.

Following the method for Equation)6.1), the salt budget for the middle box is,

$$\frac{\partial V\rho S}{\partial t} = Adv.(1-2) + Adv.(2-3) + Disp.(2-1) + Disp.(3-2) + SALT \tag{6.2}$$

where $V\rho S$ is the mass of salt contained in the box, expressed in kg (following the method of Section 4.2.1 to convert from Practical Salinity to salt mass), $Adv.(1-2)$ is the rate of advection of salt, in kg s^{-1} from box 1 into box 2, $ADV.(2-3)$ is advection between box 2 and 3, $Disp.(2-1)$ is the rate of salt transport from box 2 to box 1 by tidal dispersion, $Disp,(3-2)$ the same from box 3 to 2 and $SALT$ is the input of salt into box 2 due to unmeasured processes, including marsh interactions. All quantities are calculated as positive into a box and negative out of a box.

Model Results

The model was evaluated over a 14 day period from YD 235 to YD 248 (23 AUG to 5 SEP) 2003 at the start of the DUPLEX experiment. This period was selected to cover an entire neap-spring-neap cycle when the Duplin was densely instrumented and when there was little storage volume change due to offshore forcing, which could mask the groundwater and salinity signals. During this period salinity, temperature and flow velocity were measured in boxes 1 and 3 and tidal dispersive transport was calculated (see Section 4.4) for each of these boxes. No measurements were taken in box 2 and no measurements are available of groundwater input or of the unknown salt fluxes into any box.

Following equation (6.1), a similar equation for the water volume budget of the upper Duplin (box 1), can be expressed as,

$$\frac{\partial V1}{\partial t} = Adv.(1-2) + GW \tag{6.3}$$

In the absence of surface water input into box 1, this equation states that the change in water volume storage must be accounted for by groundwater input and flow between boxes 1 and 2. These terms are shown in Figure 6.3. The volume storage (shown in the upper pane) is calculated from the time rate of change of the residual height of water. The measured residual advection of water is always out of box 1 as shown in the middle pane. After starting around 2 m^3 s^{-1} it increases to around 4 m^3 s^{-1} and stays fairly constant through the remainder of the neap-spring-neap cycle. As the storage volume changes little over this period, the net

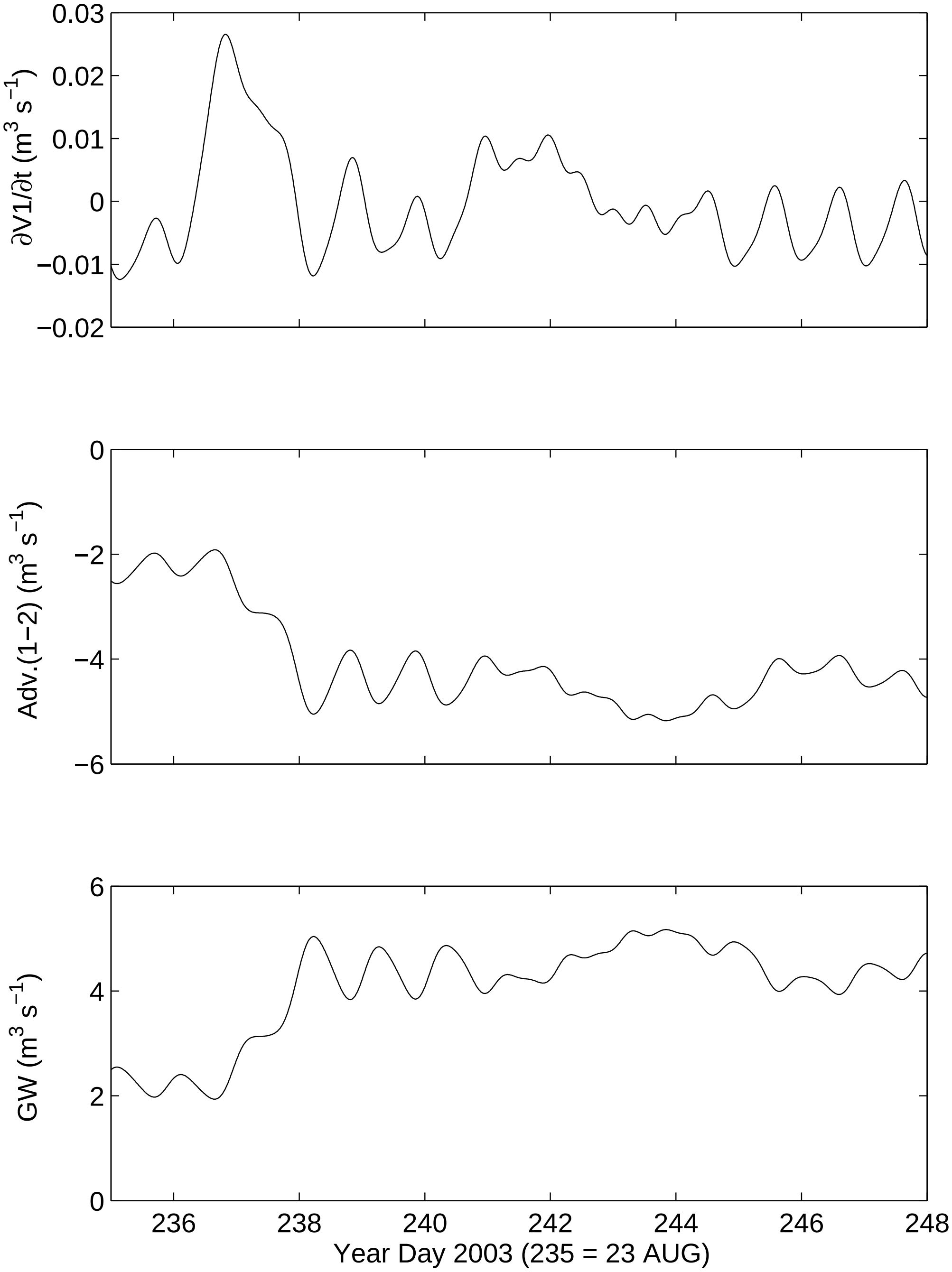

Figure 6.3: Water budget for the upper Duplin (box 1). Storage is balanced by measured advection and estimated groundwater input.

advection out must be balanced by groundwater input as there was no precipitation during this time.

Following equation (6.2), a similar equation for the salt budget in box 1 can be expressed as

$$\frac{\partial V1\rho S1}{\partial t} = Adv.(1-2) + Disp.(2-1) + SALT \tag{6.4}$$

This shows that the rate of change of the salt mass in box 1 is accounted for by the rate at which salt goes out through advection and the rate it comes in through dispersion and unmeasured processes ($SALT$). Since salt dispersion in the upper Duplin has been shown to be a very minor term in the salt budget (see Section 4.4) it may be neglected. The resultant salt budget is shown in Figure 6.4. As with water, there is little salt storage after the first few days and the system reaches a quasi steady-state where the along channel salt export of between 80 and 100 kg s^{-1} is balanced by an equivalent salt input. This input presumably comes from the release of salt stored in the marsh, salt transport due to tidal trapping and salt in the groundwater input.

While the balance between these fluxes is unknown, certain bounds can be assigned to them. The groundwater flowing in is of an unknown salinity, but it is generally less than the salinity of the creek. Water which floods the marsh at high tide either returns, minus a loss due to evaporation, as a surface flow or else sinks into the marsh sediment where it mixes with the porewater. This additional water exerts hydrostatic pressure on the porewater thus forcing it into the creek channel (Jahnke et al., 2002). The salinity of this subsurface water is unknown but can be assumed to be at least as salty as the creek water.

In order to estimate the range of probable groundwater salinities, the salt flux due to surface exchange with the marsh and subsurface recirculation is estimated for salinities 25 and 40 on the practical salinity scale. The volume of water exchanged is estimated from the hypsometric curves of (Blanton et al., 2007) and the potential evaporative loss calculated in section 4.4.2. The time averaged flux of water out of the marsh and into the creek due to surface drainage and recirculation through the sediment can be estimated by tidally

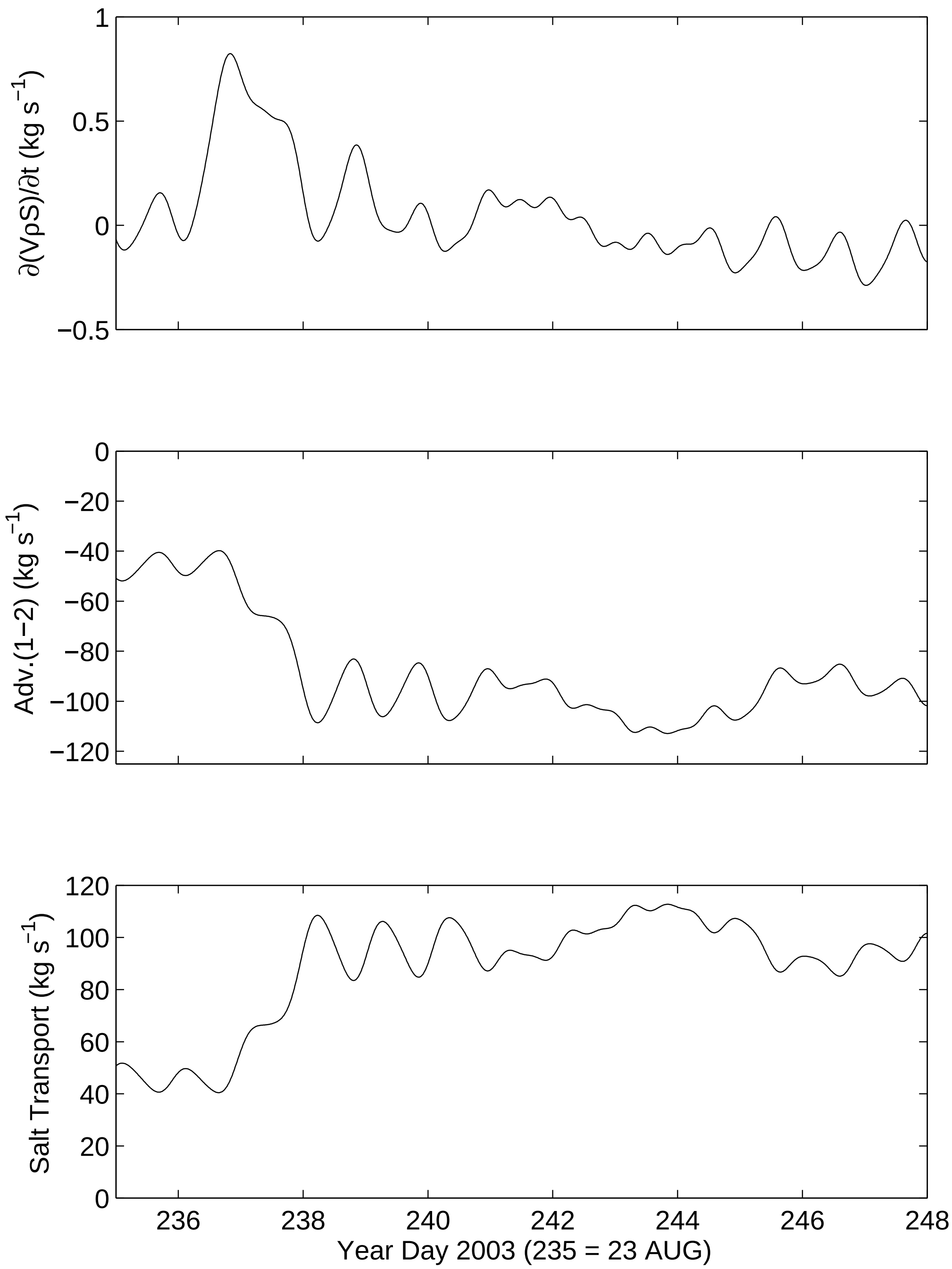

Figure 6.4: Salt budget for the upper Duplin, box 1. Storage is balanced by measured advection and estimated salt input from unmeasured sources.

averaging the time varying volume of water on the marsh minus the evaporative flux out assuming that the marsh water table is in long term steady-state Jahnke et al. (2002). Multiplying this flux by an assumed salinity results in a salt flux from the marsh to the creek. Subtracting this from the calculated total salt flux (shown in Figure 6.4) and dividing by the estimated groundwater flux gives an approximate groundwater salinity. The results of these calculations are shown in Figure 6.5.

The upper pane of Figure 6.5 shows the total rate of transport of salt into the upper Duplin due to both groundwater and marsh interactions. Taking the time varying volume of water on the marsh, as a function of tidal height, accounting for evaporative loss and tidally averaging to get the steady state flux of water out of the marsh due to surface drainage and pressure driven pore water fluxes, a time varying marsh-creek water flux can be calculated which has an average value of 0.54 $m^3\ s^{-1}$. Based on this curve, the salt flux out of the marsh is depicted in the middle pane for returned water salinities of 25 (blue line) and 40 (red line) on the practical salinity scale. The lower pane then shows the calculated groundwater salinity for each case. Since the volume of water recirculating through the marsh is a small percentage of the estimated groundwater input, modeled groundwater salinity is not sensitive to marshwater salinity and remains around the salinity of the creek for both cases.

The middle Duplin (box 2), presents a problem in that no instruments were deployed there and thus neither salinity nor temperature (needed for water density) nor flow velocity were measured and thus the box is unsolvable as-is. However, noting the very low along channel salinity gradient shown in the TS diagrams in Figure 3.4 and also in Figure 4.13, the salinity for box 2 can be taken to be approximately equal to that in box 1, at least for this level of model. Further, from the along channel temperature gradient, which can be estimated from the TS diagrams in Figure 3.4, an approximate temperature can be estimated for box 2, thus allowing the water density to be calculated. The bounds of box 2 were chosen such that the lower bound is upstream of the tidal excursion distance in the lower Duplin and thus the along channel salinity gradient is low there. As a result the tidal dispersion of salt

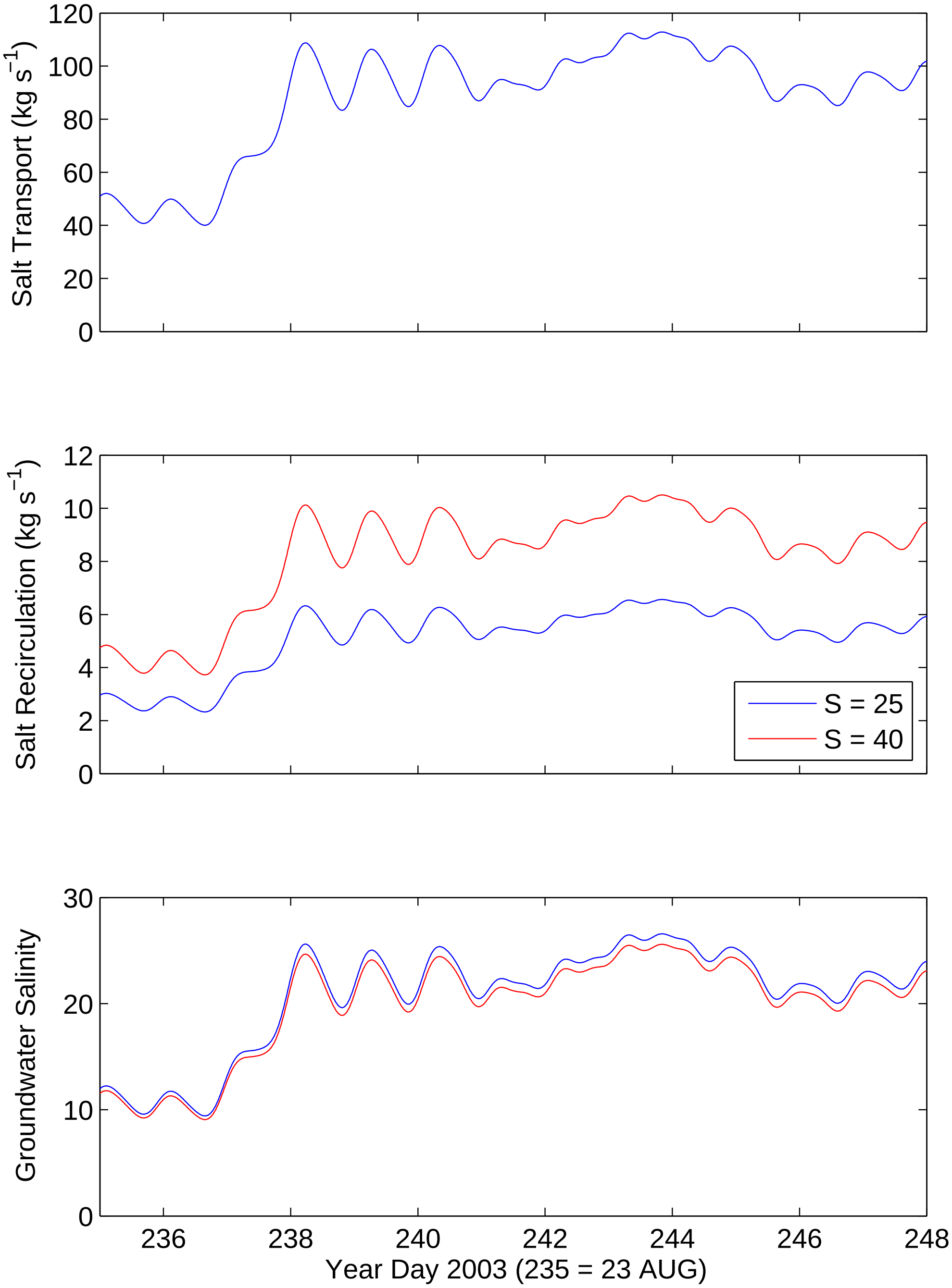

Figure 6.5: Sensitivity of modeled groundwater salinity to changes in modeled recirculated marsh/porewater salinity. The blue line shows salt fluxes due to marsh return water with a salinity of 25 and the red line of 40. The lower pane shows groundwater salinity associated with the two cases.

from box 1 into box 2 is low and can be neglected. It will further be assumed, on the basis of the fact that the upper and middle Duplin waters are significantly fresher than those of the lower Duplin, that a large majority of the groundwater input into the Duplin River occurs in these two boxes and thus groundwater input into the lower Duplin will be assumed to be close to zero.

With this final assumption, the advective flux of water out of the middle Duplin and into the lower Duplin can be assumed to be equal to the measured flux from the lower Duplin to Doboy Sound minus any storage in the lower Duplin. Box 2 then becomes solvable. The water budget of Equation (6.1) is then a good approximation and expresses that the change in water storage in box 2 is related to the difference in the volume of water coming in from both the upper Duplin and from groundwater input and the water flowing out into the lower Duplin. This is shown in Figure 6.6. Storage is low and the input of water from the upper Duplin is fairly constant around 4 m^3 s^{-1}. The flow of water from box 2 to box 3 is more variable, fluctuating between 0 and 15 m^3 s^{-1}. This is balanced by a variable groundwater flux which shows an apparent negative flux around YD 237, which is likely tied to inaccuracies in the model, and several periods of around 10 m^3 s^{-1}. There is no apparent spring/neap periodicity to this cycle.

No such approximation, as was made with groundwater, can be made in regards to the relative values of the unmeasured salt input into the middle and lower Duplin boxes. Thus in order to solve the salt budget in this region, boxes 2 and 3 must be combined into a single box. This is shown by the dotted box in Figure 6.2. This budget is given by

$$\frac{\partial V(2+3)\rho S}{\partial t} = Adv.(1-2) + Adv.(3-Doboy) + Disp.(3-Doboy) + SALT \tag{6.5}$$

which shows that storage of salt in the combined middle and lower Duplin box is a balance between salt advected down from the upper Duplin, salt exported to Doboy Sound, salt dispersed into the lower Duplin from Doboy Sound and unmeasured salt input, which can not be separated into middle and lower Duplin components without additional measurements.

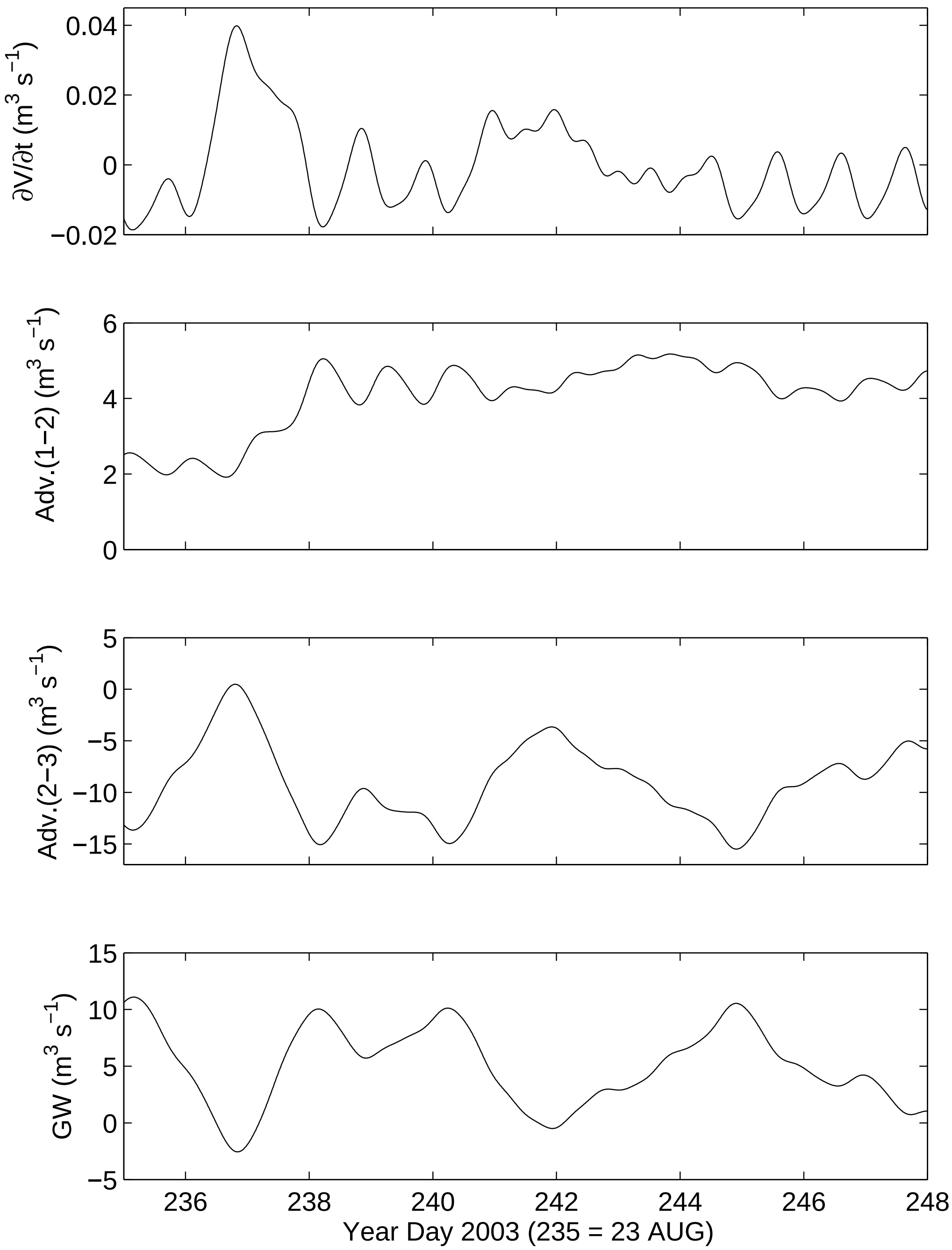

Figure 6.6: Water budget for the middle Duplin (box 2). Storage is balanced by measured advection and estimated salt input from unmeasured sources.

The salt budget in this box is then shown in Figure 6.7 with the storage shown in the upper pane. Salt input from the upper Duplin is fairly steady at around 100 kg s^{-1} while net salt export to Doboy sound fluctuates and changes sign as the relative magnitude of residual export and tidal dispersive import changes. Unmeasured salt fluxes vary between 200 and -150 kg s^{-1} but do not appear to show any spring/neap periodicity.

Analysis

The model was evaluated over a 14 day neap-spring-neap period during which there was little storage volume change which would serve to mask a groundwater or salinity signal. Processes in the upper and lower Duplin, boxes 1 and 3, were measured but had to be inferred in order to constrain the model for the middle Duplin, box 2.

The results for the upper Duplin (box 1) are instructive. The small nature of this box and the simple dynamics give us some confidence in these results. Groundwater input is seen to be fairly constant, after the first few days, at around 4 m^3 s^{-1} and this input is the driver of the net water export, which reaches as high as 3 cm s^{-1} in this region. A similarly constant input of salt, around 100 kg s^{-1}, is observed as well, replacing the salt exported by the net outflow. Periods of increased salt storage, without concurrent increases in groundwater flux, are likely due to salt export from the marsh into the main channel as well as other tidal dispersive transport mechanisms, like tidal trapping.

The evaluation of the results of the model of the middle and lower Duplin is more difficult. The combined lack of measurements in the middle Duplin and the larger storage volume in the lower Duplin increases the likelihood of error. It is likely true that most, though not all, of the groundwater input into the combined middle and lower Duplin region comes into the middle Duplin and varies on the order of 0 to 10 m^3 s^{-1} during this period. That gives it an average of approximately 1.5 times the estimated input into the upper Duplin. This agrees with the theory that the neap tide freshening of the middle Duplin relative to the upper Duplin is related to groundwater input in this area. Total groundwater input into the entire

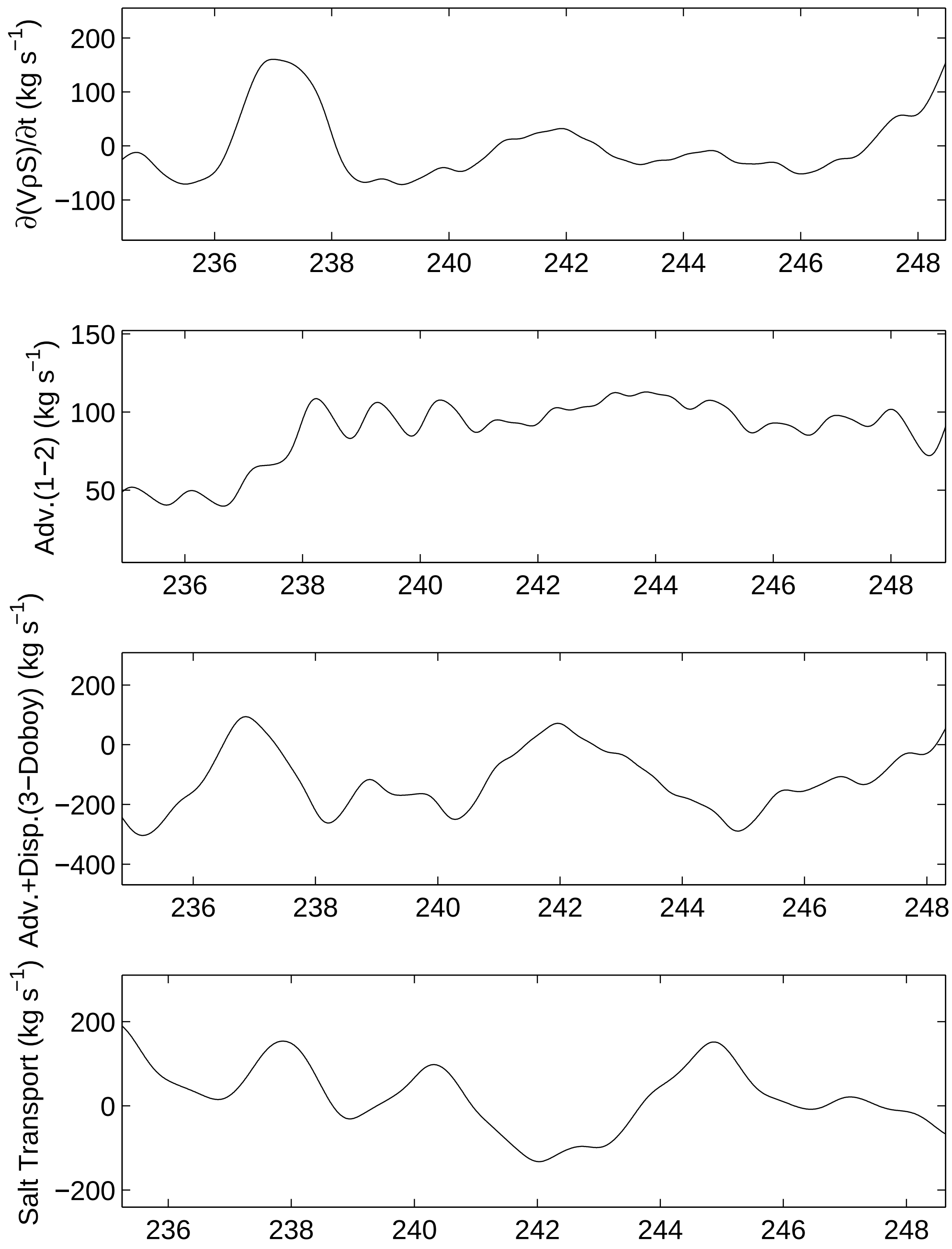

Figure 6.7: Salt budget for the combined middle and lower Duplin (boxes 2 and 3). Storage is balanced by measured advection and estimated salt input from unmeasured sources.

Duplin is estimated to range as high as 15 m^3 s^{-1} with no apparent spring/neap variability during this modeled period. Unmeasured salt fluxes into the combined middle and lower Duplin box are shown to vary between +200 and -150 kg s^{-1} reflecting the interplay between salt export and the tidal dispersion of salt into the creek, as well as the possible storage and release of salt in the marsh or variations in groundwater salinity. The exact cause can not be extracted from this model.

The results from this model should be regarded as order of magnitude estimates only. The lack of measurements in the middle Duplin, along with the lack of independent measurements of groundwater fluxes and marsh salinity, combined with potential errors in the storage volume estimates, can all introduce errors in the numbers. However as their signs and magnitudes make sense, especially in the upper Duplin, it is likely that they represent a good first order approximation of these unmeasured processes in the Duplin River.

No direct measurements of the volume of groundwater input into any region of the Duplin have been made. Some estimates are available in similar systems (Crusius et al., 2005) however the extreme variability in conditions between even apparently similar systems makes them impossible to compare.

6.2 Recommendations for Future Work

While a basis for understanding the physical characteristics of the Duplin River has been established there is significant work to be done to get at the poorly constrained processes which can play a major role. Several questions remain unanswered and future work should be undertaken to investigate them.

The reversing salinity gradient between the middle and upper Duplin indicates that there is a regular salinity change taking place in the middle Duplin region which is tied to the spring/neap cycle. This process is potentially important to understanding the nature of this region yet it has not been adequately measured. While the DUPLEX I experiment did include both an ADCP and a Microcat near the junction between the lower and middle

Duplin, these were poorly placed in a scour hole in a region of high curvature, and the Microcat fouled within days of deployment. Thus no good time series of flow or salinity and temperature data exists for any portion of this region. Instrumenting the middle Duplin, preferably near the middle of the water mass in the vicinity of Lumber Landing, should be a priority for future investigations. Measurements of flow and salinity in this region will allow the above presented box model to be more fully constrained resulting in a much more accurate estimate of groundwater input into this region.

While it is likely that the upper Duplin was unstratified at all times during these experiments, some observations indicate that the lower Duplin is occasionally stratified. This is likely tied to changes in groundwater input, local meteorological forcing, especially from rainwater runoff, and offshore forcing transporting oceanic water onshore. Long term surface and bottom Microcat moorings should be established in each of the three Duplin River water masses in hopes of capturing one or more of these stratification events to measure their strength and duration and their distribution along channel.

Similarly the long term characteristics of the water masses are still unclear. The analysis presented here holds for late summer conditions in 2003 and 2005 and spring of 2004. Seasonal and interannual variations in conditions are likely to have an impact on the water mass structure. A network of temperature and salinity mooring needs to be established along the channel of the Duplin to allow this seasonal and interannual variability to be captured. While the GCE-LTER project maintains Microcat CTD moorings in Doboy Sound (GCE6) and the upper Duplin (GCE10), they do not provide enough spatial resolution. Six Microcats, at least, spaced along the axis would capture the conditions and necessary gradients in each of the three water masses.

This work strongly suggests that interactions between the main channel and the marsh play a role in regulating main channel properties, but our measurements do not allow the determination of the mechanisms by which these interaction occur. Accordingly an experiment should be planned to investigate this process in at least the upper, and preferably as well the lower Duplin River.

An atmospheric flux tower erected in the marsh would allow the direct measurement of heat (and gas) fluxes into and out of the marsh as well as the measurement of the actual evapotranspiration rate. Preliminary contact has been made with Professor Monique Leclerc in the Department of Crop and Soil Sciences at the UGA Griffin campus for collaborative work and deployment of such a tower. Instruments should be placed in the marsh soil itself to measure porewater temperature and salinity along a line from the tower to the nearest creek edge. An understanding of these characteristics, combined with an estimate of the volume of water overlying the marsh on flood, will allow an estimate to be made of the flux of salt and heat from the marsh into the creek body.

Groundwater is apparently a major driver of upper and middle Duplin characteristics. While water budgets can be instructive in estimating groundwater fluxes over broad regions they can not identify individual seeps or accurately describe the water characteristics. Ongoing work by Professor Samantha Joye has focused on a number of fixed sites, primarily in the upper Duplin on Moses Hammock. Future mooring campaigns should be coordinated with this work in an effort to locate the major sources of the groundwater input into the upper and middle Duplin and to develop better estimates of the fluxes and their variability with time.

The work we have done so far paints a broad picture of the Duplin, showing its basic outline and describing the environmental factors which influence it. Future work will enable us to fill in the details; to develop more quantitative estimates of the importance of the marsh and of groundwater to defining the water mass structure. It will allow us to understand the Duplin as a constantly changing system, not just on tidal and fortnightly scales, but through the seasons and the years (for climate change purposes), and to better define those characteristics which remain constant and those which are variable. In the end a detailed portrait can be developed describing one of a very large class of such tidal creeks, which are both common and important parts of the Georgia coastal landscape.

Bibliography

Blanton, J., Andrade, F., Adelaide-Ferreira, M., and Amft, J. (2007). A digital elevation model of the duplin river intertidal area. Technical report, Final report submitted to the GCE-LTER Program, University of Georgia.

Crusius, J., Koopmans, D., Bratton, J., Charette, M., Kroeger, K., Henderson, P., Ryckman, L., Halloran, K., and Colman, J. (2005). Submarine groundwater discharge to a small estuary estimated from radon and salinity measurements and a box model. *Biogeosciences*, 2:141–157.

Garvine, R. and Whitney, M. (2006). An estuarine box model of freshwater delivery to the coastal ocean for use in climate models. *Journal of Marine Research*, 64:173–194.

Hagy, J., Sanford, L., and Boynton, W. (2000). Estimation of net physical transport and hydraulic resistance times for a coastal plain estuary using box models. *Estuaries*, 23:328–340.

Imberger, J., Berman, T., Christian, R., Sherr, E., Whitney, D., Pomeroy, L., Wiegert, R., and Wiebe, W. (1983). The influence of water motion on the distribution and transport of materials in a salt marsh estuary. *Limnology and Oceanography*, 28(2):201–214.

Jahnke, R., Alexander, C., and Kostka, J. (2002). Advective pore water input of nutrients to the satilla river estuary, georgia, usa. *Estuarine, Coastal and Shelf Science*, 56:641–653.

Kjerfve, B. (1973). Volume Transport, Salinity Distribution and Net Circulation in the Duplin Estuary, Georgia. Technical report, ERC-0273 Marine Institute, University of Georgia, Sapelo Island, Georgia.

Levasseur, A., Shi, L., Wells, N., Purdie, D., and Kelly-Gerreyn, B. (2007). A three-dimensional hydrodynamic model of estuarine circulation with an application to southampton water, uk. *Estuarine, Coastal and Shelf Science*, 73:753–767.

Li, M., Gargett, A., and Denman, K. (1999). Seasonal and interannual variability of estuarine circulation in a box model of the strait of georgia and juan de fuca strait. *Atmosphere-Ocean*, 37:1–19.

Miller, R. and McPherson, B. (1991). Estimating estuarine flushing and residence times in charlotte harbor, florida, via salt balance and a box model. *Limnology and Oceanography*, 36:602–612.

Ragotzkie, R. and Bryson, R. (1955). Hydrography of the Duplin River, Sapelo Island, Georgia. *Bulletin of Marine Science of the Gulf and Caribbean*, 5:297–314.

Schultz, G. and Ruppel, C. (2002). Constraints on hydraulic parameters and implications for groundwater flux across the upland-estuary interface. *Journal of Hydrology*, 260:255–269.

Sousa, M. and Dias, J. (2007). Hydrodynamic model calibration for a mesotidal lagoon: the case of ria de aveiro (portugal). *Journal of Coastal Research*, SI50:1075–1080.

Appendix A

The MATLAB Air-Sea Toolkit

The MATLAB Air-Sea Toolbox (`www.sea-mat.whoi.edu`) was developed by Bob Beardsley and Rich Pawlowicz to aid in the computation of heat fluxes across the ocean surface. In this work a number of its routines have been employed to calculate various surface heat flux components. Results of these calculations are reported in Chapter 3. These routines, packaged as a collection of MATLAB m-files, implement a number of different bulk formulae which will be described below.

A.1 Short Wave Heat Flux

The heat flux due to shortwave (solar) radiation at the ocean's surface is computed, using the swhf.m routine, as a function of measured short wave radiation and the calculated albedo. The albedo is calculated using the method of Payne (1972) by comparing the measured shortwave radiation to the no-atmosphere value calculated from sun angle. With the calculated albedo, the shortwave heat flux is calculated as

$$Q_{sw} = (1 - \alpha)\, dsw \tag{A.1}$$

where α is the calculated albedo and dsw the measured downward shortwave radiation.

A.2 Long Wave Heat Flux

With downward longwave radiation unmeasured, the net heat flux due to longwave radiation from the ocean or the atmosphere is computed, using the blwhf.m routine using measured air and sea surface temperature, relative humidity and a cloudiness correction factor. The routine uses the method of Berliand and Berliand (1952), as described by Fung et al. (1984), such that

$$Q_{lw} = -E_{lw}kT_a^4\left(0.39 - 0.05e_a^{0.5}\right)F_c - 4E_{lw}kT_a^3\left(T_s - T_a\right) \tag{A.2}$$

where E_{lw} is the longwave emissivity of the ocean (taken from Dickey et al. (1994)), k is the Stefan-Boltzmann constant, T_a is the air temperature, e_a is the vapor pressure calculated from relative humidity and air temperature using relations from Gill (1982), F_c is a cloudiness correction factor calculated based on the method of Reed (1977) and T_s is the sea surface temperature.

A.3 Latent and Sensible Heat Fluxes

The latent heat flux due to evaporation and the sensible heat flux due to conduction are both computed using the hfbulktc.m routine. This routine implements a version of the code developed by Fairall et al. (1996) for the Tropical Ocean Global Atmosphere Coupled Ocean Atmosphere Response Experiment (TOGA COARE). Heat fluxes are calculated from measurements of wind speed, atmospheric pressure, relative humidity and air temperature, all measured at 10 m height, and sea surface temperature.

A.4 Heat Flux due to Precipitation

The heat flux due to precipitation is computed using the rain_flux.m routine. This routine calculates the momentum and heat flux due to precipitation following the method of Fairall et al. (1996) using measurements of wind speed, atmospheric pressure, relative humidity and air temperature, all measured at 10 m height, along with rain rate, sea surface temperature and salinity.

A.5 Sensitivity to Measurement Location

Data from the Marsh Landing weather station has been taken to be representative of data throughout the entire Duplin watershed. This could be problematic for two reasons. The Marsh Landing weather station is located approximately 10 km from the upper Duplin mooring site and conditions are not necessarily the same at both sites. Further, the weather station is not located in a pristine area - it is installed on a concrete pad located at the edge of an asphalt parking lot.

Smith (1985), working with data from both local and remote stations, showed that while daily differences in accumulated solar radiation could be significant across distances of this scale, the accumulated differences averages to close to zero over a period of 21 days or more. The major difference in conditions was found to be related to wind speed, which has the most effect when wind speeds are either low or else show a large amount of variability.

Asaeda et al. (1996) have demonstrated the effect of heat storage in pavement materials on properties of the lower atmosphere. At maximum, hot asphalt was shown to release as much as an extra 150 W m^{-2} of longwave radiation and contribute another 200 W m^{-2} in sensible heat transport compared to bare earth. This can potentially have a significant effect on measured air temperature at the 10 m height of the weather station.

A series of numerical experiments was run to estimate the sensitivity of the calculated surface heat fluxes to potential errors in measured wind speed and air temperature. Atmospheric pressure and humidity measurements were judged to not be as sensitive to the potential sources of error and so were regarded as essentially correct. Of the five surface heat flux terms shown in Figure 3.8, shortwave radiation is not a function of wind speed and air temperature, and cooling due to precipitation is seen to be insignificant to the local heat budget. The remaining terms, longwave radiation and latent and sensible heat, are all functions of air temperature and the latent and sensible heat fluxes are functions of wind speed as well.

Figure A.1 shows the calculated heat fluxes due to longwave radiation, latent and sensible heat during the DUPLEX I experiment. The blue line represents the baseline calculation with

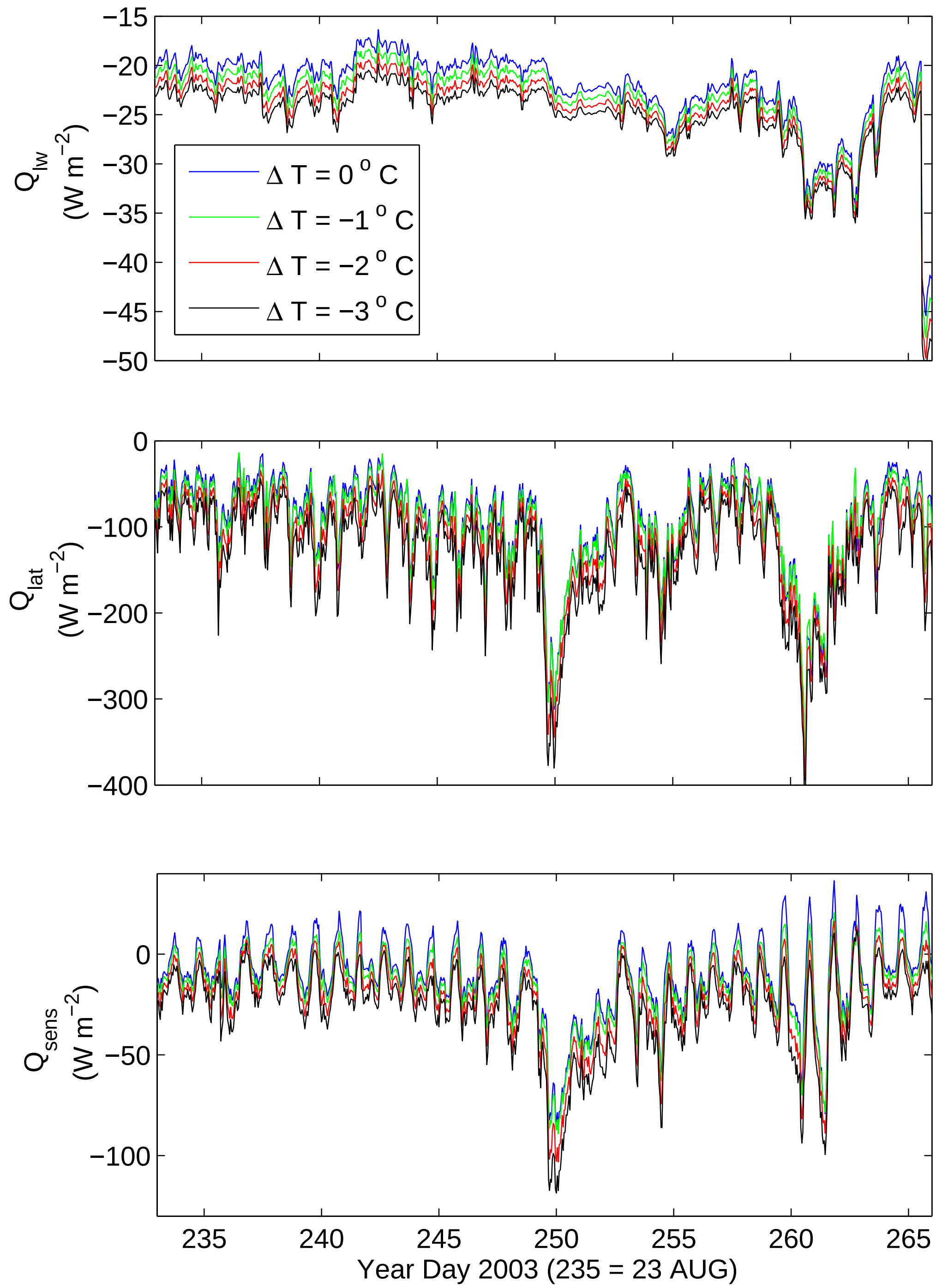

Figure A.1: Calculated surface heat fluxes due to longwave radiation and latent and sensible heat losses during the DUPLEX I deployment. The colored lines show the effect of lowering the measured air temperature by up to 3 °C.

air temperature as measured at the Marsh Landing weather station. The green line shows the effect of lowering air temperature by 1 °C, the red by 2 and the black by 3. The most sensitive, as far as a percentage of the signal, is the heat flux due to longwave radiation where the increased flux out averages 23% for a 3 °C reduction in air temperature. However the magnitude of the change is far greater for latent and sensible heat. For a 3 °C reduction in measured air temperature, the longwave radiative heat flux out increased, on average, by 4 W m^{-2} while latent heat loss increased by 28 W m^{-2} and sensible heat loss increased by 16 W m^{-2} on average.

While the wind speed measured at Marsh Landing can be taken as correct for the DUP 01 mooring, located immediately adjacent, the sheltered nature of the upper Duplin mooring is such that wind speed could be greatly reduced. Figure A.2 shows the impact of reducing wind speed to 50% of measured wind speed and to zero on the calculated latent and sensible heat fluxes. A 50% reduction in wind speed reduces latent heat loss by an average of 54% and an elimination of the wind reduces this term by, on average, 86%, reducing it almost to zero. The sensible heat flux is similarly attenuated by an average of 49% with a halving of wind speed. When the wind speed is reduced to zero sensible heat loss is reduced by, on average, 61% while the periods of sensible heat gain are completely eliminated.

While the effect of the modeled temperature change on the net surface heat flux is minor, the effect of reducing wind speed to zero is potentially major. On average this would cause a reduction in latent heat loss, the major heat loss term, of 67 W m^{-2} and a maximum reduction, during high wind periods, of 344 W m^{-2}. This would increase direct atmospheric heating of the water column during the entire deployment but its major effect would be a reduction in the major cooling associated with wind events, especially the one centered around YD 250. However, as the direct atmospheric signal in the heat budget is low, even a major decrease in latent heat loss, especially if it is primarily tied to sporadic wind events, will not substantially change the heat budget in these waters. Considering the case where air temperature is constrained to the measured temperature, and wind speed in the upper

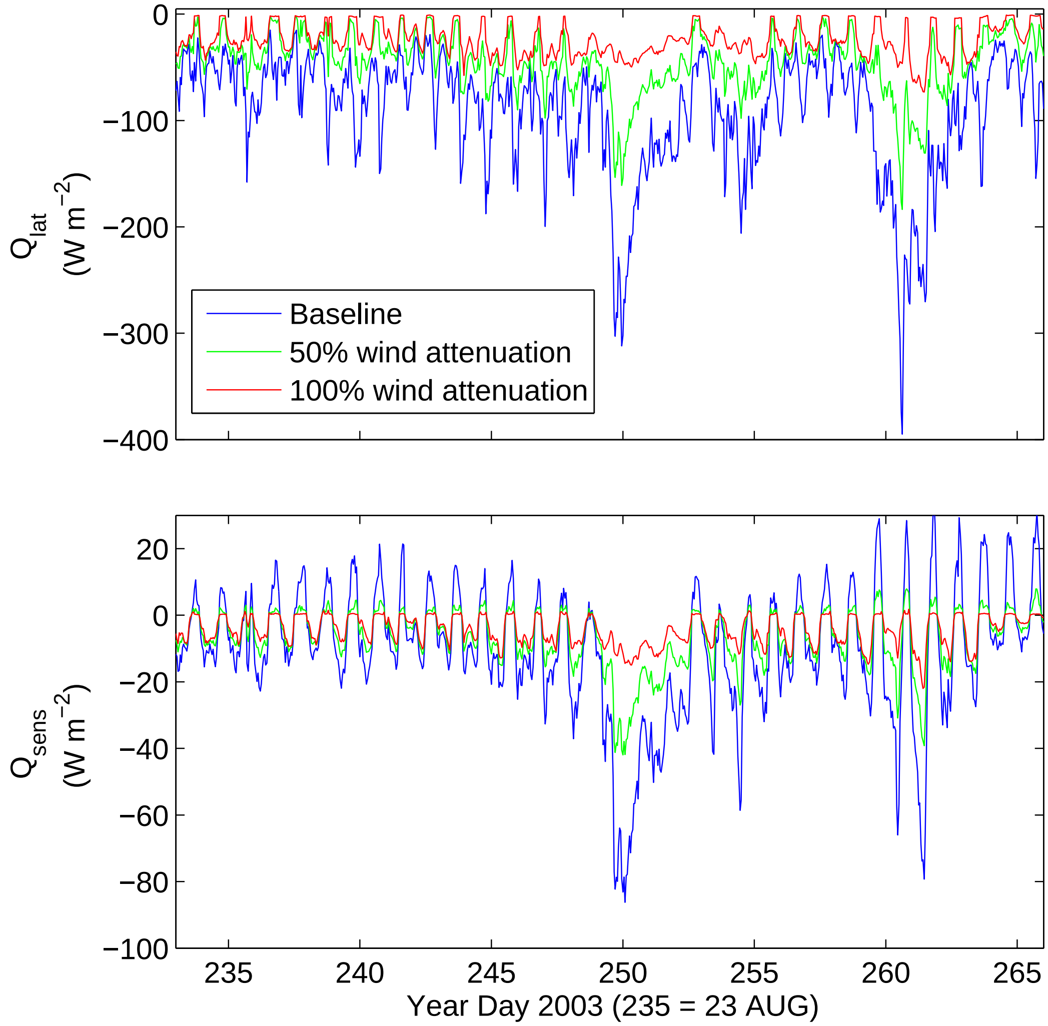

Figure A.2: Calculated surface heat fluxes due to longwave radiation and latent and sensible heat losses during the DUPLEX I deployment. The colored lines show the effect of attenuating the wind by 50% and 100%

Duplin is assumed to be zero, the net atmospheric heat flux term Q_0 is increased to 13.5% of the observed heat storage - up from 12% in the original heat budget.

It is apparent then that some effort should be undertaken to better quantify the difference in wind speed between the lower Duplin, which is exposed to winds from the Atlantic through Doboy Sound, and the more sheltered water of the upper Duplin. Regardless, these sensitivity results show that any atmospheric differences will probably not make any major impact on the heat budget in the upper Duplin.

Bibliography

Asaeda, T., Ca, V., and Wake, A. (1996). Heat storage of pavement and its effect on the lower atmosphere. *Atmospheric Environment*, 30:413–427.

Berliand, M. and Berliand, T. (1952). Measurement of the effective radiation of the earth with varying cloud amounts (in russian). *lzv. Akad. Nauk SSSR Set. Geofiz.*, 1.

Dickey, T., Manov, D., Weller, R., and Siegel, D. (1994). Determination of longwave heat flux at the air-sea interface using measurements from buoy platforms. *Journal of Atmospheric and Oceanic Technology*, 11:1057–1079.

Fairall, C., Bradley, E., Rogers, D., Edson, J., and Young, G. (1996). Bulk parameterization of air-sea fluxes for tropical ocean-global atmosphere coupled-ocean atmosphere response experiment. *Journal of Geophysical Research*, 101:3747–3764.

Fung, I., Harrison, D., and Lacis, A. (1984). On the variability of the net longwave radiation at the ocean surface. *Reviews of Geophysics*, 22:177–193.

Gill, A. (1982). *Atmosphere-Ocean Dynamics*. Academic Press.

Payne, R. (1972). Albedo of the sea surface. *Journal of the Atmospheric Sciences*, 29:959–970.

Reed, R. (1977). On estimating insolation over the ocean. *Journal of Physical Oceanography*, 7:482–485.

Smith, N. (1985). The suitability of routine weather data for estimating local estuarine heat energy fluxes. *Estuaries*, 8(3):270–278.